Zhenju Chuang

Experimental and Numerical Investigation of Speed Loss due to Seakeeping and Maneuvering

Doctoral Thesis

Zhenju Chuang

NTNU – Trondheim
Norwegian University of
Science and Technology
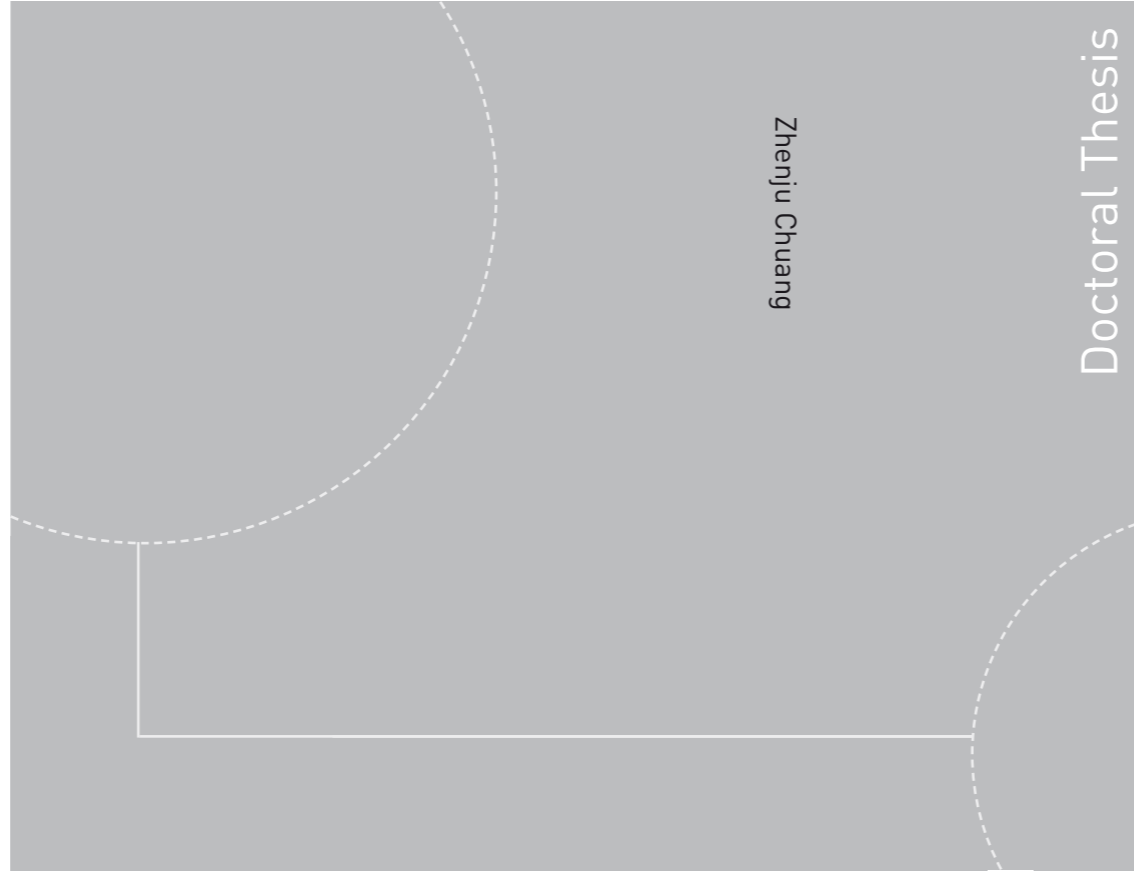
NTNU

Zhenju Chuang

Experimental and Numerical Investigation of Speed Loss due to Seakeeping and Maneuvering

Undertittel på avhandlingen

Thesis for the degree of philosophiae doctor

Trondheim, June 2013

Norwegian University of Science and Technology
Faculty of Engineering Science and Technology
Department of Marine Technology

NTNU – Trondheim
Norwegian University of
Science and Technology

Abstract

Accurate prediction of the real voyaging speed for ocean-going vessels in the actual weather condition is important for the expanding shipping industry. Ship owners are always aiming at achieving the highest profit, so delivering the goods to the destination within the designed schedule time is of great concern. At the same time, the increasing attention on environmental issues as well as increasing fuel price have put more pressure on optimizing the ship design with respect to energy efficiency. Also, accurate prediction of the real attainable speed will greatly improve the sea margin prediction. From these respects, the research work on speed loss study is important and necessary. Speed loss is usually categorized as voluntary or involuntary. Voluntary speed loss is when the ship master actively reduces the ship speed to avoid slamming, propeller racing, excessive ship motion or other effects that might cause danger or severe discomfort. Voluntary speed loss is subjective and relies on ship master's experience. Different ship masters can have quite different actions to the same circumstance based on their ability to estimate the potential danger. Involuntary speed loss is due to added resistance from waves, wind, current and reduced thrust and efficiency due to waves and other changes in operational conditions. Involuntary speed loss is in focus in this thesis work. In order to investigate the nature of speed reduction in the real environment, integrated knowledge about resistance, propulsion, ship machinery, seakeeping, automatic control and maneuvering are required. This thesis takes advantage of model tests and a numerical simulation tool based on simplified modular concept to investigate the nature of speed reduction in seakeeping and maneuvering conditions.

A series of experiments were carried out on a model of 8000 DWT tanker in the large towing tank and ocean basin at Marine Technology Center in Trondheim, Norway. The model was self-propelled and mainly running in moderate long wave conditions. For speed loss in head sea conditions, three different bow shapes were tested in order to investigate the influence of added wave resistance. Due to the practical difficulty of applying towrope force to balance the frictional resistance coefficient difference between model scale and full scale ship, a method is proposed in this thesis to make compensation for the frictional resistance difference and predict speed loss of the ships when propeller is working at 'ship propulsion point'. Test results show that a conventional bow with bulb and flare gave least calm water resistance, while a bow without bulb and flare gave the least total resistance in the tested wave conditions. That means

bulb can have positive influence on calm water resistance and negative effect on added wave resistance. Reduction of speed loss in waves up to order of 10% can be gained by relatively minor changes to the bow shape of a vessel. Another two tests for speed loss in zigzag maneuvering in head waves and speed loss in oblique waves were carried out in the towing tank and ocean basin respectively. Speed loss when doing zigzag maneuvering in waves is due to yawing, added wave resistance and loss of thrust due to steering; while for speed loss in oblique waves is due to added wave resistance and loss of thrust due to steering. For the test of speed loss in oblique waves, towrope force is added by an air fan. Due to limitation of basin length, converged speed is not always achieved during the tests due to the large mass of the model. A converged speed prediction method is proposed which can be used to correct the non-converged tests results. This method is carefully verified and can give good prediction of attainable speed in waves. However, this method is sensitive to the selection of thrust deduction factor in waves. Also how much speed loss due to added wave resistance and due to steering is pointed out. Speed loss due to added wave resistance and steering is of the same magnitude in head sea and bow sea conditions. While for beam sea, speed loss due to steering is dominating.

Numerical simulation work was carried out in order to make comparisons with experimental results. Comparable calculations were performed in the frequency domain tool *ShipX* and in the time-domain tool *Vessel Simulator*. Ship motion is calculated by linear strip theory and added wave resistance in head sea is calculated by the method developed by Gerritsma and Beukelman and the Direct Pressure Integration method. Wave resistance in other than head sea condition in surge, sway and yaw directions is calculated by the method proposed by Loukakis and Sclavounos, which is an extension of the Gerritsma and Beukelman method to other than head sea. For the speed loss in head sea condition, both frequency domain calculations using *ShipX* and time domain calculations using *Vessel Simulator* were carried out. It is concluded that both methods can give a good prediction of speed loss in moderate sea conditions. For the cases that steering effect has to be taken into account, time domain simulation is a preferable method. Generally speaking, numerical results can give a good correlation with model test data. Based on the good validation of the numerical tool, further numerical investigations were carried out to compare the speed loss characteristics between conventional propeller-rudder system and azimuth thrusters. The results showed that conventional propeller-rudder system has better speed keeping ability than azimuth thrusters. That is because in the conventional propeller-rudder system propeller force is not decomposed by the rudder angle and also conventional propeller-rudder system has higher ratio of longitudinal thrust force/transverse thrust force than azimuth thrusters within the working steering angle range.

In the end, recommendations to ITTC procedures to predict speed loss and power increase in irregular waves and sea margin were proposed. A method to predict 'ship propulsion point' from the self-propulsion test carried out at 'model propulsion point' is specified in this thesis. This method will greatly improve the procedures to predict power increase in irregular waves from model tests in regular waves. Also another suggestion is proposed that when evaluating power increase in irregular waves and sea margin prediction, thrust deduction due to ventilation and steering effect should be taken into account in addition to thrust diminution factor.

Acknowledgements

It would have been impossible to finish my PhD work without the help and assistance of many people.

Most of all, I would like to express my sincerely gratitude to my supervisor, Prof. Sverre Steen. Thank him for providing me the PhD opportunity to perform this work in Norway. During the past years, I learned a lot from his broad professional knowledge, innovative thinking, positive attitudes, novel ideas, and extensive experience. His supervision work exists in each sentence and fig in this thesis. Without his patient and consistent guidance, the present work would not have been possible. He is always trying his best to help every one of his PhD candidates and Post docs. I am so lucky to be one of them.

Next I would like to thank the persons who helped me a lot during my PhD study. I would like to deeply thank Dariusz Fathi, Edvard Ringen, Tor Einar Berg, Jingzhe Jin, and Leif Aarseth for discussing the theoretical problems and using the software. I am also grateful to the people at Marintek who helped me with the model tests, among them I would especially like to mention Sverre Anders Alterskjær. I want to express my deeply grateful to Luca Savio, Hamid Amini, Suzanne Ruth Hutchison for answering my questions about propulsion systems.

I would like to thank Professor Odd M. Faltinsen, who lectured me about the advanced topics of Hydrodynamics. I also wish to thank the help from Professor Torgeir Moan, who interviewed me in China and recommended me to my direct supervisor Prof. Sverre Steen.

I am grateful to all my friends who make my life meaningful and interesting in Norway. It is impossible to name them all here, but deeply in my heart. Among them, I would like to mention Dr. Huirong Jia, Dr. Jingzhe Jin and Marit Irene Kvittem. They are always there whenever I need help. I am deeply appreciated.

Last, but definitely not least, I would like to thank my family for their continued encouragement and unconditional support throughout the years, especially my parents. Most of all, I am deeply grateful to my dear husband Li Zhou. He has very strong mind and never say give up for whatever difficulties we met. His love and continuous confidence in me and my work have carried me through the hard times in my life. Through this work, I also wish to express love to my little son Lukas Haozhe Zhou.

Zhenju Chuang

February, 4th, 2013.

Trondheim, Norway

Table of Contents

List of Appended Papers

The core of this thesis is constituted by Papers 1-5 which are included in Appendix A.

Paper 1:

Prediction of Speed Loss of a Ship in Waves

Zhenju Chuang, Sverre Steen

Published in Second International Symposium on Marine Propulsors, smp'11, Hamburg, Germany, June 2011

Paper 2:

Experimental and Numerical Study of Stem Shape Influence on Speed Loss in Waves

Zhenju Chuang, Sverre Steen

Published in Ship Technology Research, Volume 59, No. 2, pp. 4-17, April 2012 (a)

Paper 3:

Speed loss due to seakeeping and maneuvering in zigzag motion

Zhenju Chuang, Sverre Steen

Published in Ocean Engineering, Volume 48, pp. 38–46, July 2012 (b)

Paper 4:

Speed loss of a vessel sailing in oblique waves

Zhenju Chuang, Sverre Steen

Published in Ocean Engineering 64(2013)88–99

Paper 5:

Measurement of speed loss due to waves

Sverre Steen, Zhenju Chuang

Published in Third International Symposium on Marine Propulsors, smp'13, Launceston, Tasmania, Australia, May 2013

Chapter 1 Introduction

1.1 Background and motivation

The new framework of the global economy has stimulated and expanded the shipbuilding and shipping industry. Simultaneously, environmental concern and a constant increase in the price of fuels have put more pressure and demands on designers to minimize the energy consumption, maximize the protection of the marine environment and maximize the efficiency and economy of maritime operations. This leads to the research on the speed loss and power increase of a ship in a seaway. Fig. 1.1 gives the impression of an ocean-going vessel sailing in the sea.

Most studies of performance of an ocean-going vessel are based primarily on the calm water resistance of the ship hull without considering the real weather condition prevailing on the route that the ship is designed to operate. This calm water resistance is used as a first estimation of the power required to drive the ship in a seaway. An allowance is added to this value of the resistance to consider the effect of the environment on ship behavior. This quantity is called "Sea Margin" or "Power Margin", which is to determine the additional power to be installed above the calm water power requirements to account for various environmental conditions encountered in service, such as wind, waves, hull and propeller fouling and increase of roughness due to ageing (ITTC-Recommended procedures and Guidelines 7.5-02-03-01.5, 2008). The value of the Sea Margin is usually stated at the design stage by the ship owner or ship designer (often 15-30% of the ship calm water power), based on experience of similar ships sailing on the same route or tradition to take environmental effects into account (Perez, 2007). This rough and empirical method usually results in designs that are too heavy, too costly, and not optimally efficient. Worse still, is that in some cases this result in ship or propulsion units that are insufficiently strong or powerful, leading to a ship that cannot fulfill its original designed schedule. Also, accurate speed loss calculation in a seaway enables optimization of a ship design for a given route or trade. So it is important to have efficient and reliable methods to predict the real attainable speeds for ocean-going vessels.

Fig. 1.1 Vessel sailing in seaway (http://fishwrecked.com/image/me-work-bass-straight)

Also in recent years, there is an increasing interest in optimizing steering system of ship in a seaway. Larger ships are increasingly using azimuth propulsion instead of traditional propeller and rudder system due to its better low-speed maneuverability, compact design, reduced noise, low vibration, and in some cases also improved energy-saving effects. Fig. 1.2 shows an azimuth thruster installing at the ship stern. On the other hand, azimuth propulsion tends to make the ship more course–unstable. So the directional stability of the vessel equipped with azimuth steering system needs further investigation. All in all, the concept of using azimuth thrusters as main propulsion device in ships is relatively new and relatively little hydrodynamic knowledge has yet been collected (Amini, 2011).

When it comes to sea conditions, the hydrodynamic behavior of a propulsor becomes more complicated. The change of propulsor behavior can be caused by several phenomena. For the extreme sea conditions with large wave induced ship motions in heave and pitch, the propeller can come out of water and lose effective disc area, and thereby lose thrust. When a propeller blade comes out of water, the thrust is zero and it will take some time to build it up again after is has submerged into water, called Wagner effect. Also when propeller is working close to the free surface, additional wave motion will be set up by the propeller and lead to reduced thrust. The above three factors has already been well studied by Faltinsen et al. (1980) by introducing a thrust diminution factor. When a propeller operates at high load and low speed close to the water surface, air might be drawn into the propeller. This phenomenon is usually called ventilation. Propeller ventilation leads to a sudden large loss of thrust and torque, which might lead to propeller racing and possibly damaging dynamic loads, as well as noise and vibrations. Propeller ventilation has been studied by Fleischer (1973) and later by Koushan (2006a, 2006b,

2006c, 2007a, and 2007b), Califano and Steen (2011a, 2011b) and others. Effects of propeller out of water and ventilation are not included in the propulsion models in this thesis, since speed loss in moderate sea states are studied.
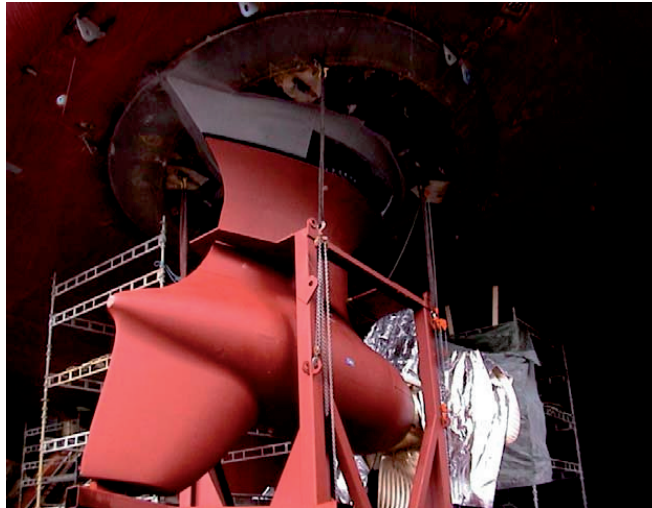
Fig. 1.2 Azimuthing pulling propeller designed by Rolls Royce Marine (Vartdal, 2008)

Although there have been many studies of wave loads on ships, propulsion system behavior and so on, there are a limited number of publications about speed reduction in the real weather conditions. In order to study speed loss of an ocean going ship, integrated knowledge about resistance, propulsion, ship machinery, seakeeping, automatic control and maneuvering are required. All the aspects have to be considered together to understand the real behavior of a ship during seakeeping and maneuvering conditions, which is regarded as the major challenge of this work.

1.2 Speed loss in seakeeping and maneuvering

Speed loss of a ship can be regarded as voluntary or involuntary (Faltinsen et al. 1980). Voluntary speed loss is that when the ship encounters dangerous heavy sea conditions, the ship master will voluntarily reduce the ship speed in order to avoid slamming, propeller racing and excessive ship motion. The decision that one master will take under specific circumstances is subjective and will depend on experience and ability to properly estimate the potential danger

(Prpic-Orsic and Faltinsen, 2012). This kind of speed loss is presently not included in this paper, but ought to be considered in the future.

Involuntary speed loss is due to added resistance from wave, wind, current, as well as reduction of propulsive efficiency caused by waves and increased resistance and reduced thrust force in the heading direction due to steering. If the power from the propulsion system is kept constant, resistance increase from the environment and also reduced thrust force due to steering will break the balance between the original calm water resistance and thrust force. Then, vessel speed will drop correspondingly until the new balance point is reached by the calm water resistance, added resistance from environmental conditions and the new thrust force. Fig.1.3 shows the speed reduction process after encountering incoming waves.

Fig. 1.3 speed loss due to increased added wave resistance

This thesis is focusing on the involuntary speed loss and how to precisely estimating the speed drop value due to seakeeping and maneuvering. This speed loss is mainly depending on:

- Ship hull form

- Calm water speed

- Environmental condition

- Maneuvering behavior

- Propulsion power

- Thrust loss factors (such as ventilation)

- Automatic control

4

1.3 Literature review

The literature study is divided into four parts: speed loss and power increase; seakeeping and maneuvering combination; added wave resistance evaluation; and propulsion system behavior for steering in waves.
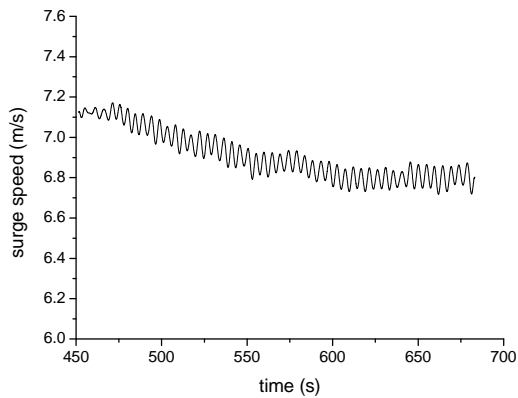
Speed loss and power increase

In order to investigate the speed loss of a vessel in a seaway, researchers need the knowledge about seakeeping, maneuvering, propulsion system, autopilot control and also machinery dynamics. Based on the literature study, it is found that not many works goes directly into speed loss of a vessel under real navigation condition.

Van Berlekom et al. (1975) carried out a project about the speed loss due to wind and sea of a bulk carrier with big superstructure and conventional rudder-propeller propulsion system. They categorized the resistance in additional to calm water resistance as wind resistance of the ship's above water parts, wind and wave inducing yawing resistance, rudder resistance and resistance caused by wind induced waves. During the numerical simulation, hydrodynamic coefficients obtained from PMM tests were used and wind coefficients are determined through wind tunnel tests. They present the relation between speed drop and the sum of additional resistance. They also set up the criterion for how to decide speed loss. If the sum of the additional resistance is larger than zero, then it implies speed loss. Speed increase means that the additional resistance is smaller than zero. In their work, incoming wave influence is neglected.

Journee (1976a) developed a computer program to calculate the speed and behavior of a ship in seaway. Both wind and waves were taken into consideration. In the numerical simulation part, he took advantage of empirical formulas for still water resistance, wind resistance, added wave resistance and also wake fraction and thrust deduction factor from thruster part. All of the work is focusing on head sea condition. He pointed out that added resistance due to waves is the largest part of the total resistance. Of course, this is depending on the ship's length and the sea spectrum tested, as well as the size of the superstructure. Later in Journee's next report the same year (1976b), he showed a comparison between this numerical tool and model tests. Good agreement was shown in head sea conditions.

Kwon (2008) presented simpler and easier empirical formulas to predict the speed loss due to wind and sea for vessels with block coefficient ranging from 0.55 to 0.85 within Froude number from 0.05 to 0.3. Wind coefficients are taken from Van Berlekom's (1981) wind tunnel tests. Wave added resistance is calculated by Maruo's (1960) formula, which is based on the conservation of energy and momentum. The weather direction problem has been solved by introducing weather direction reduction factors developed by Aertssen (1969).

Grimstad (2009) studied the added resistance increase and speed loss due to steering for a course unstable ship. Neglecting the influence of incoming waves, she quantified the added resistance due to steering, yawing and extra distance for zigzag maneuvering. Both pulling and pushing azimuth thrusters were analyzed in her case. She pointed out that yawing gives a larger contribution than steering in most cases.

Prpic-Orsic and Faltinsen (2012) developed a time domain numerical model to predict the speed loss of a vessel in irregular sea. They also extended this research by implementing the ventilating propeller model by Smogeli (2006) in severe sea conditions. Their work covered the estimation of CO_2 emission from a containership on the Northern North Atlantic route, which was based on the mean speed drop, constant engine power and fuel consumption. Speed loss in oblique wave conditions with vessel heading varied from 0 degree to 180 degree were also presented in their work. But their numerical model lacks verification.

Seakeeping-maneuvering combination

The combined seakeeping and maneuvering study plays a key role in evaluating the speed reduction and power increase of a vessel sailing in the real sea condition. Traditionally, the maneuverability of a vessel is evaluated in calm water. However, this is not a practical condition, since ocean-going vessels are mostly maneuvering in different wave conditions.

McCreight (1986) presented a nonlinear maneuvering model in waves where the first order radiation loads were evaluated in a body-fixed coordinate system by using an appropriate filter technique, which was implemented in the time domain.

Bailey et al. (1997) proposed a unified mathematical model including maneuvering and seakeeping to simulate the ship steering behavior in waves. This unified theory allowed extraction of the traditional theories of seakeeping in waves and maneuvers in calm water assuming suitable forms of the fluid actions. The most important point in his mathematical model is considering the relationship between maneuvering derivatives and seakeeping coefficients with encounter frequency variations. Impulse response functions and convolution integral formulations were taken to describe the transient effect of fluid actions. Later, Bailey et al. (2000) implemented this unified mathematical model with reference in the time domain simulation of a Mariner ship type maneuvering in a seaway. The prediction of zigzag maneuver in head and following seas emphasized the sensitivity of maneuvering due to the presence of surface waves. However, their simulation is able to produce the trends as observed in experiments. But it is very difficult to repeat their model due to the complicated coupling effect of maneuvering derivatives and seakeeping coefficients.

Munif and Umeda (2000) predicted the roll motion and capsizing of a moderate-speed ship in astern waves by a modular-type maneuvering mathematical model including heave and pitch

effects. Their results show that the effect of heave and pitch motions on the ship maneuvering can be significant when the wave steepness becomes larger.

Umeda and Hashimoto (2002) utilized a four-degree-of-freedom numerical model with dense grids of control parameters and the sudden-change concept to intensively explore nonlinear ship motions in following and quartering seas. This model can successfully explain the capsizing phenomena qualitatively, but overestimates the danger of capsizing quantitatively.

Fang et al. (2005) developed a simplified six degrees of freedom mathematical model to present the two container ship's behavior during turning circle maneuver in waves. All hydrodynamic coefficients are time varying with encounter frequency and calculated by strip theory. He showed that the effect of nonlinear terms for maneuvering derivatives is significant and cannot be neglected.

Ayaz et al. (2005) took advantage of an existing coupled non-linear six-degree-of-freedom model (Ayaz et al. 2001) to simulate the maneuvering and seakeeping behavior of an azimuth pod-driven vessel. Their attention were paid to investigating the directional stability and course keeping ability of pod-driven ships, as well as the effect of large pod induced heel angles to the turning and ship motions in waves.

Ayaz et al. (2006) attempted to develop a numerical tool for addressing ship motion in astern seas. Their model is a coupled non-linear six-DOF model with frequency dependent coefficients, incorporating memory effects and random waves. Due to the difficulty of applying strip theory to this low encounter frequency problem in following sea, they took advantage of Ohkusu's (1986) study, which is focusing on taking into account the effects of waves resulting from the disturbance of the incident waves by the ship. Those waves are supposed to be of higher order than the incident waves. The numerical results indicate that the inclusion of frequency coefficients definitely affects the accuracy of the prediction. In order to enhance further the numerical model and obtain useful information on motion coupling, extensive captive and free running model tests should be carried out in the future.

Carrica et al. (2008) applied URANS analysis to study the ship motions and speed variation during a broaching event of a ship in irregular quartering seas. An autopilot was implemented to control heading and speed. The most important finding is that the autopilot causes the ship to be in an adverse dynamic condition at the beginning of the broaching process, and thus is partially responsible for the occurrence of the broaching event. But this conclusion is based on a significantly simplified propeller model whose thrust and torque is not dependent on the local flow field near the propeller, but only on the average velocity of the ship. Side force from the propulsion system was also neglected. So a more advanced propeller model is probably needed to achieve more meaningful results.

Skejic and Faltinsen (2008) applied a two time scales concept to solve the combined seakeeping and maneuvering problem. In this method the linear wave induced motions of a ship are assumed to occur on a more rapidly varying time scale than the maneuvering. The wave frequency problem is affected by the slowly varying maneuvering. On the other hand, the effect of the seakeeping on the maneuvering analysis is in term of slowly varying mean second order wave loads that occur for the changing ship speed and wave heading. Later, Skejic and Berg (2010) implemented this unified seakeeping and maneuvering theory into ship-to-ship operations. Faltinsen (2011) verified this theory with CFD and model tests results. Satisfactory agreement between this numerical simulations and experiments of the trajectory of a containership in a turning maneuver in regular waves is demonstrated. However, this method is challenged when the encounter frequency is low, for example in following sea condition. When the encounter frequency is small, seakeeping and maneuvering problems needs to be solved simultaneously.

Fathi et al. (2009) developed a time domain simulation tool *Vessel Simulator* to solve this seakeeping and maneuvering combination problem. Resistances from calm water in the longitudinal direction and the cross flow drag are pre-calculated for different speeds; All the forces from waves, wind, and current as well as from the propulsion system are pre-calculated for different vessel speeds, headings and frequencies (for wave condition). When the simulation process is started in the time domain, the real value of all the forces are found by interpolation in the input dataset. Time series of the vessel position, speed, acceleration as well as forces were all available. But it has to be pointed out that (some of the) propulsion systems like pod model lack validation. The thrust and torque of the propeller is calculated based on a set of Fourier expansions of thrust and torque coefficients for a general propeller model. Then pod effect is added based on a very limited model tests to make compensation for the difference between pod thruster and conventional propeller. Further validation of the propulsor model should be carried out.

Added wave resistance evaluation

Added wave resistance is important for evaluating ship performance and propeller loading in real sea states. Based on the literature study, many researchers make efforts in this subject and make great contributions.

Maruo (1957) developed a formula which is based on the conservation of energy and momentum to evaluate the added resistance. The ship hull is represented by a singularity distribution and the wave field velocity potential consists of a superposition of the regular incoming field and the disturbance by the hull form. A control volume is chosen around the ship and then energy and momentum balance is derived within the control volume. However, this

method does not take the diffraction effect into account and overestimate the added resistance at low frequency (Fang and Chen, 2006).

Gerritsma and Beukelman (1972) proposed another radiated energy method to calculate the added resistance in long waves. The method equates the work of added resistance to the energy contained in the damping waves radiated away from the ship. Ship motion is derived from strip theory. But this method does not give satisfactory results in other than head sea.

Fujii and Takahashi (1975) expanded Maruo's formula by considering added resistance in short waves. They modified the empirical formula by Havelock (1940) by taking the ship speed and draught into account. The added resistance was divided into the part induced by wave diffraction and the part by ship motion.

Faltinsen et al. (1980) derived an asymptotic equation to calculate the added resistance of conventional displacement vessels in short waves. Their formula is remarkable in taking into account the interaction of diffraction waves with steady current around the hull. However, there are still some limitations of this method. It is only valid for moderate Froude number, blunt bow and under the assumption that the ship has to have vertical sides in the water line.

Faltinsen et al. (1980) showed a method to obtain added resistance by direct pressure integration over the instantaneous position of the wetted surface. Moreover, this method takes the effect of sway, roll, yaw and other anti-symmetric flow effects into consideration. But this method is quite sensitive to the bow shape of the stem (Chuang and Steen, 2012(a)).

Steen and Faltinsen (1998) carried out model test to measure the added resistance in small sea states. Five displacement models with different bow profiles and waterline were tested. They pointed out that the main experimental error comes from the stability of short waves. The results were used to verify Faltinsen's asymptotic formula (1980). They showed that this formula underestimates the added resistance in short waves, especially for slender bows with flare.

Kashiwagi et al. (2009) evaluated the added resistance with the modified version of Maruo's approach, using the enhanced unified theory (ETU). ETU can capture the 3D effect and forward speed effect which are usually ignored in strip theory. However, this method still shows large deficiency when compared with model test data in the condition when the ship is sailing with forward speed in short waves.

Guo and Steen (2011) took advantage of CFD tools to evaluate the added resistance of KVLCC2 tanker in short waves. They tested three eddy viscosity models with free surface and got good agreement with experimental data. However, CFD is still considered to be too complicated and time-consuming to be a practical tool for determining added resistance due to waves.

Kim and Kim (2010) adopted a higher order, B-spline Rankine panel method in time domain for the numerical calculation of added resistance, which is evaluated directly by integrating the second-order pressure on the body. Neumann-Kelvin and double-body linearization of the free surface are tested. The results show that added resistance with Neumann-Kelvin linearization has better accuracy at high Froude number and for slender bodies, while the double-body method is good at low Froude number and wide displacement ships with low Froude number.

Studies of the propulsion system during seakeeping and maneuvering

Applying accurate thrust from propulsion system is very important for evaluating the ship speeds in waves. Moreover, loss of propulsive efficiency, reduced thrust due to interaction with the wave induced ship motion will also contribute to the power increase and speed drop. Several researchers have already pointed out relationships between propeller characteristics and the loading change due to waves.

Van Sluijs (1972) carried out propulsion experiments in a seakeeping basin. The main attention was given to the powering characteristics in waves, in particular with regard to the fluctuation of torque and thrust in waves. He concluded that the power characteristics does not necessary coincide with maximum ship motion. Moreover, mean thrust, torque and revolutions increase, required to maintain speed in a seaway, can be assumed to be proportional to the square of the wave height.

Faltinsen et al. (1980) pointed out that the propulsion factors based on resistance and propulsion tests in waves is traditionally done by fitting data into a conventional open water propeller diagram, found using a deeply submerged propeller in calm water. They argued that this is physically wrong since open water propeller diagrams depend also on the submergence. So when the propeller is working close to the free surface, the thrust must be corrected by a thrust loss coefficient which takes into account the steady wave motion created by the propeller, loss of disk area and Wagner effect.

Lee (1983) made some effort on the propulsive performance in seaway. Based on self-propulsion model tests in regular waves, he pointed out that added thrust, torque and number of revolutions of propellers in waves has their peaks when the ship motions are severe, showing the close resemblance with the added resistance. He also showed that the propulsion factors vary remarkably in the region of the ratio of wave length to ship length $\lambda/L=1\sim1.5$, where the ship motions are mostly pronounced, and tend to the still water values with the increase of λ/L. The conclusion derived from model tests agrees well with Yamazaki and Nakatake's (1978) numerical results where they represent the ship hull by distributing sources and doublets at the ship mean position of oscillations, and propeller is replaced by bound vortices which are distributed on the disk located at its mean position and by the free vortices of constant pitch.

Belibassakis (2009) examined the effects of the ship wave-induced vertical oscillatory motion on the modification of propeller's operational characteristics (force, torque and efficiency). Nonlinear BEM method (Belibassakis and Politis, 1998, 2002) was used for propeller study. Added wave resistance was obtained by strip theory (Salvesen et al. 1970) and radiated energy method (Loukakis and Sclavounos, 1978) in his work. His numerical method showed good agreement with the full scale tests data on thrust and torque.

Another interesting subject is that the introduction of the azimuthing pod drives into service on large commercial ships has brought many benefits in wide range of areas covering maneuvering, hull space saving for extra passengers and cargo, noise and vibration and so on.

Reichel (2007) focused on the maneuvering in calm water of a gas carrier model with an azimuthing podded propulsor. Steering forces were measured with the different range of advance coefficients and deflection angles, where fixed vessel speed was set in each single test without taking wave effect into account.

Ayaz et al. (2005) took advantage of an existing coupled non-linear six-degree-of-freedom model to simulate the maneuvering and seakeeping behavior of an azimuthing pod-driven vessel. His attention was paid to roll and pitch motion of the vessel in different sea states and the large steering forces created by pod drives to roll motion in heavy seas. Later, Ayaz et al (2006) carried out model tests to validate the numerical results. Good agreements were got between model test and numerical results on simulating parametric rolling behavior.

Woodward et al. (2003) studied if the IMO maneuvering criterion is applicable for pod-driven ship. A dedicated numerical tool is also developed. Tested maneuvers were including turning circle, zigzag and stopping ability. The study reaches the definitive conclusion that the criterion provides equivalent information about the maneuvering response of pod-driven ship as for conventionally propelled ships and can thus be applied directly.

Liu et al. (2009) investigated propulsive dynamics of a podded propulsor unit in steering motion at fixed azimuth angles numerically, ignoring the influence of the hull effect on the thruster.

However, the research on the azimuth thruster during seakeeping and maneuvering condition is limited.

1.4 Objective and scope of the present work

The objective of this PhD work is to investigate the speed loss of ocean-going vessels in seakeeping and maneuvering conditions. Experiments were carried out in different wave conditions with the ship model of a new 8000 DWT tanker which was developed by Rolls-Royce Marine. The ship model was self-propelled and steered with twin AZP120 thrusters. Numerical

simulations based on the modular concept to integrate ship, wave and propulsion system together were also done in order to make comparisons with the model test results.

The main components of the study can be specified as:

- Speed loss in head sea conditions along straight line course with three different bow shapes

Model tests in the towing tank were carried out with a completely free ship model. The model was self propelled and self steered with twin AZP 120 thrusters with constant power supply. Three different bow shapes were tested in order to study the effect of ship bow shape influence on added wave resistance. Due to the practical difficulty to apply towrope force, the tests were carried out without towrope force to correct for the higher frictional resistance coefficient in model scale than in full scale, and a method was proposed and verified to compensate for the model test defect.

Numerical approaches were carried out in both frequency domain and time domain in this head sea condition with straight line course. Different methods to calculate added resistance were used. Change of propulsive efficiency in waves depending on whether towrope force is used or not was investigated. The relationship between bow shape and power saving was also discussed.

- Speed loss in zigzag maneuvering in head sea

Speed loss during 10/2 zigzag maneuvering in head sea conditions were investigated both by model test and numerical simulations. Added resistance in this condition can be categorized as added wave resistance, added resistance due to yawing and added resistance due to steering. Thrust forces in longitudinal direction and transverse direction during maneuvering condition were all presented in this thesis. How much the wave influenced the finally attainable speed and overshoot angle was also discussed.

- Speed loss in oblique waves

Speed loss in other than head sea with heading angles being 30, 60, 90 and 150 degrees were investigated both experimentally and numerically. A method was proposed in this part of the work to predict the attainable speed in oblique waves based on tests where converged speed was not reached. This converged speed prediction method is verified in this thesis. Different initial speeds were studied. Moreover, how much added wave resistance and loss of thrust due to steering contributed to the whole vessel speed loss were shown in this part of work.

- Prediction of sea margin and speed loss in irregular waves

  Predictions of sea margin and speed loss in irregular waves are discussed. A method is suggested to predict 'ship propulsion point' from 'model propulsion point'. Also a recommendation to ITTC recommended procedures and guidelines to predict sea margin and power increase in irregular waves is proposed. That is applying a thrust deduction factor that includes the effects of seakeeping and maneuvering instead of the calm water value. Moreover, how to calculate speed loss due to wind is specified.

- Also comparisons between conventional rudder-propeller system and azimuth thruster on their ability to keep the vessel running at the designed speed are investigated in this thesis.

1.5 Structure of the thesis

This thesis is organized as paper collection based on the articles reproduced in Appendix A, which summarizes the main aspects of the work.

Chapter 2 presents the experimental study of the speed loss during seakeeping and maneuvering conditions. Three different kinds of model tests were carried out. They are: Speed loss in head sea conditions with straight line course; Speed reduction during 10/2 zigzag maneuvers in calm water and in different head sea conditions; Speed loss in other than head sea.

Chapter 3 is about numerical simulation of speed loss using the three combinations of seakeeping and maneuvering conditions.

Chapter 4 specifies the procedures for calculating speed loss and power increase in irregular waves and predicting sea margin. Also how to include wind force is given.

Chapter 5 summarizes the conclusions, main contributions of this thesis and recommendations for the future work.

Appendix A includes the papers 1-5 including two conference papers and three journal papers. The papers are:

I. Chuang. Z., Steen, S. 'Prediction of Speed Loss of a Ship in Waves'. SMP'11, Hamburg, Germany, 2011.

II. Chuang. Z., Steen, S. 'Experimental and Numerical Study of Stem Shape Influence on Speed Loss in Waves', Ship Technology Research. VOL. 59, NO. 2, pp: 4-17, April 2012 (a).

III. Chuang. Z., Steen, S. 'Speed loss due to seakeeping and maneuvering in zigzag motion', Ocean Engineering 48, pp. 38–46, 2012 (b).

IV. Chuang. Z., Steen, S. 'Speed loss of a vessel sailing in oblique waves'. Accepted for publication in Ocean Engineering.

V. Steen, S., Chuang. Z. 'Measurement of speed loss due to waves'. Accepted for presentation at SMP' 13, Launceston, Tasmania, Australia, 6-8th May, 2013.

Appendix B shows comparisons between conventional rudder-propeller system and azimuth thruster on the ability to keep the vessel running at the designed speed. This part was added as an appendix, since it isn't sufficiently extensive for a separate publication, and doesn't fit in elsewhere.

Declaration of authorship: In all the above papers (except paper 5), the first author performed the numerical simulations, planned the experiments, attended all the tests, analyzed the results, and wrote the papers under the supervision of Professor Sverre Steen. Prof. Sverre Steen has contributed to the ideas of the papers, comments on the results and commented on all the papers. Prof. Sverre Steen wrote paper 5 based largely on the results of the work of the second author. The experiments were carried out with the professional assistance by the technicians at MARINTEK.

Chapter 2 Experimental Approaches

This chapter describes the experimental methodology used in the present research work. The content in this chapter is mainly divided into three parts: speed loss in head sea conditions with straight line course; speed loss in 10/2 zigzag maneuvers in different wave conditions; and speed loss in oblique waves.

2.1 Speed loss in head sea conditions

2.1.1 Model description

Speed loss tests in head sea were carried out in the large towing tank ($L \times B \times D = 260m \times 10m \times 5m$) at The Marine Technology Centre. A model of a new 8000 DWT tanker was applied, which was developed by Rolls-Royce Marine, Ship Technology – Merchant. The model has wide transom stern and was self-propelled by twin AZP 120 model thrusters, as shown in Fig. 2.1 and Fig. 2.2.
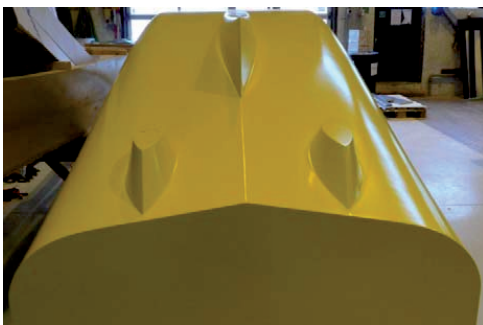
Fig. 2.1 Model stern   Fig. 2.2 Thruster arrangement

In order to investigate how much bow shape can influence the added wave resistance, three different bow shapes were used during the tests. Model A (Fig. 2.3, with Marintek series number: M2943A) has conventional bow with flare and bulb. Model B (Fig. 2.4, with Marintek series number: M2946A) has vertical stem with very little flare and bulb, and model C (Fig. 2.5, with Marintek series number: M2947A) has vertical stem with very little flare and without bulb. All these three models have the same waterline contour at the design loading condition. The body plan of model A is presented in Fig. 2.6. The main dimensions of Model A are listed in

Table 2.1. For model B and model C, slight differences in L_{OA}, ∇ and C_B are observed from model A, but very small. The main characteristics of the thrusters are shown in Table 2.2 and open water characteristics are presented in Fig.2.7.
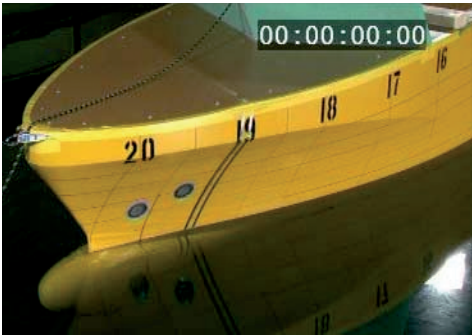
Fig. 2.3 Stem shape of model A
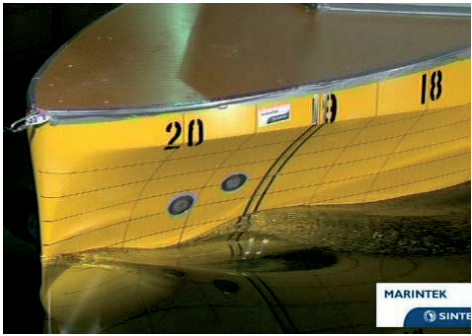
Fig. 2.4 Stem shape of model B
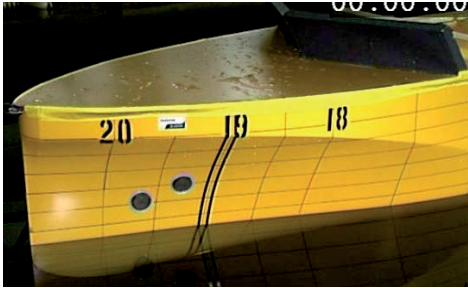
Fig. 2.5 Stem shape of model C
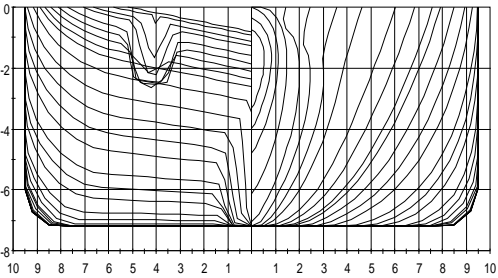
Fig. 2.6 The body plan of model A

Table 2.1 The main particulars of the 8000 DWT tanker

	Unit	Ship	Model (A)
Scale		1	16.57
L_{OA}	[m]	118.336	7.142
Lpp	[m]	113.2	6.832
D	[m]	15	0.905
B	[m]	19	1.147
T	[m]	7.2	0.435
∇	[m^3]	11546.4	2.538
C_B	[-]	0.7456	0.7456

Table 2.2 Main particulars of the thrusters

	Unit	Ship	Model
Scale		1	16.57
Propeller diameter	[mm]	3300	199.15
Pitch	[-]	1.2	1.2
Blade area ratio	[-]	0.435	0.435
Number of blades	[-]	4	4
Number of thrusters	2		
Rotation direction	Inwards		
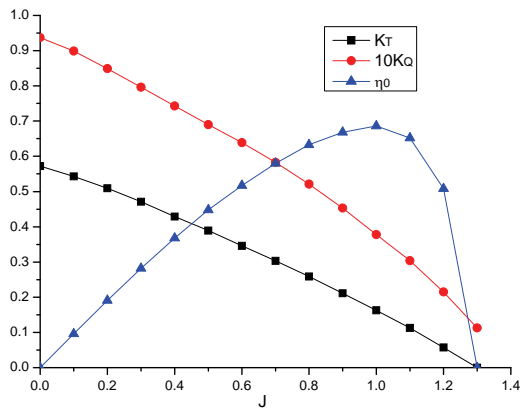
Fig. 2.7 Open water diagram of the thruster

2.1.2 Experiment set up

Before the model was installed in the towing tank, eight regular waves with different heights and periods were carefully calibrated. Both long waves ($\lambda/L>0.5$) and short waves ($\lambda/L<0.5$) were included as specified in Table 2.3. Long waves are of major interest for the objectives of our work. Due to the instability of short waves and since there will not be significant ship motions induced by short waves, just one short wave was selected. Waves were generated by a wave generator which is installed on one end of the tank; on the other end of the tank, a wave beach absorbing the wave energy is installed.

A towing carriage was used to carry the amplifiers and data acquisition system. The ship model is completely free, and self-propelled and steered by twin azimuth thrusters. Cables were used to connect the model and carriage to transfer signals and provide power to the thruster motors. Also two ropes were used to connect the vessel at the tip of stem and stern to the front and back bridge. The function of the two ropes is to tow the model to the right position when needed. During testing, the ropes are slack. Three wave probes were used during the tests. The first one is located in the middle of a small fixed carriage located 10 meters away from the wave maker, which is used to measure the undisturbed wave; the second was mounted on the carriage in front of the vessel to measure the encountered waves; the third one was mounted on the model at the propeller position to measure the wave elevation relative to the ship at the propeller position. A Qualisys optical position measurement system with eight cameras mounted on the carriage was used to measure the position of the model in all six degrees of freedom. Speed relative to the carriage is obtained by derivation of the position. Total velocity is found from the measured carriage speed plus the speed measured relative to the carriage. A track controller was adopted on the model in order to keep it running along the centerline of the towing tank to minimize wall effect. The track controller set up a control point on the ship which was a bit ahead of the forward perpendicular to ensure a stable control. A track point, located on the desired track at a distance of 20 meters forward the centre of gravity in front of the control point, was used to calculate the course to steer. The cross track error was calculated by finding the deviation of the ship control point from the track. The course to steer was calculated based on this error. Another control system was applied on the propulsion system to keep the power supplied to the thruster constant during each test. The set up of the test is shown in Fig. 2.8. The electric power supplied to each of the thrusters is given in Fig. 2.9.

Fig. 2.8 Set-up of the test

Table 2.3 Wave conditions in model tests

	H(m)	T(s)	Fn	L_{pp}/λ
Regular waves	0.12	1.35	0.212	2.4
	0.12	1.84	0.212	1.29
	0.12	2.09	0.212	1
	0.06	2.38	0.212	0.77
	0.12	2.38	0.212	0.77
	0.24	2.38	0.212	0.77
	0.12	2.58	0.212	0.66
	0.12	3.07	0.212	0.46
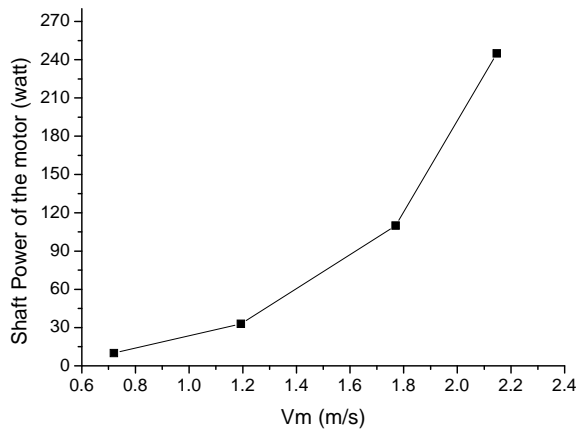
Fig. 2.9 Shaft power of the motor to each of the thrusters

2.1.3 Test procedures

Before testing in waves, model A was tested at designed speed (V_m=1.769 m/s) in calm water. The purpose of this was to find the required power to reach this speed in calm water. This power level was used in subsequent tests in waves to determine speed loss at constant power.

Then regular head waves as listed in Table 2.3 were created. The model was accelerated to the designed speed before the waves reached the model. When encountering the wave, the model speed dropped gradually until it eventually reached a converged attainable speed for the actual wave. Vessel speed, propeller thrust, unit thrust force in *x* and *y* direction, torque, RPM and six-degree of freedom motion at the center of gravity were all recorded as time series. During this procedure, the carriage speed has to be carefully controlled by the technician, in order to make sure the two ropes did not exert any force on the model.

The model was stopped using the ropes before running into the wave maker, and then it was towed back to the starting position. When the water in the tank became calm, another wave in table 2.3 was created and the process repeated. When all the waves were finished with model A, we repeated all the steps for model B and model C.

A list of the channels (variables) measured during the tests is shown in Table 2.4. This table also shows the derived (calculated) channels (variables) computed in real time from the measured channels.

Table 2.4 List of measured and calculated channels

	Description of channels	Unit	Measured/ Calculated	Sampling frequency [Hz]	Filtered frequency [Hz]
WAVE	wave elevation in front of ship model	[m]	Measured	200	20
	wave elevation relative to the tank	[m]	Measured	200	20
	Wave elevation relative to the ship – at the propeller position, both sides	[m]	Measured	200	20
VESSEL	Vessel position (COG) relative to carriage in six DOF	[m]	Measured	25	
	Vessel speed relative to carriage	[m/s]	Calculated		
	Vessel yaw acceleration (rate gyro)	[m/s^2]	Calculated		
	Vertical acceleration, FP, COG, AP	[m/s^2]	Calculated		
Carriage	Carriage position	[m]	Measured	25	
	Carriage Speed	[m/s]	Calculated		
Two Thrusters	Unit thrust in X direction	[N]	Measured	200	20
	Unit thrust in Y direction	[N]	Measured	200	20
	Propeller force	[N]	Measured	200	20
	Torque	[N·M]	Measured	200	20
	Shaft speed	RPS	Measured	200	20
	Power	[W]	Calculated		
	Azimuth angle	[deg]	Measured	200	20

2.1.4 Data analysis

Ideally, attainable speed in waves can be directly obtained from the measurement. However, it has to be pointed out that since the model tests were performed at the model propulsion point, the results should be corrected to obtain a reliable estimation of the speed loss in full scale. This is discussed in the following.

Since frictional resistance in model scale is relatively larger than in full scale, a towrope force is needed to ensure that the model propeller is operating at the same relative loading condition as the ship propeller (ship propulsion point). Towrope force is usually applied by using a weight connected to a rope through a pulley system or by connecting the model to the carriage through a force transducer. A detailed description of the two methods to apply towrope force can be found in Paper 2. For the case studied in this thesis, towrope force can amount to more than 40% of the calm water resistance. Fig. 2.10 shows the trends of towrope force with model speed for model A.
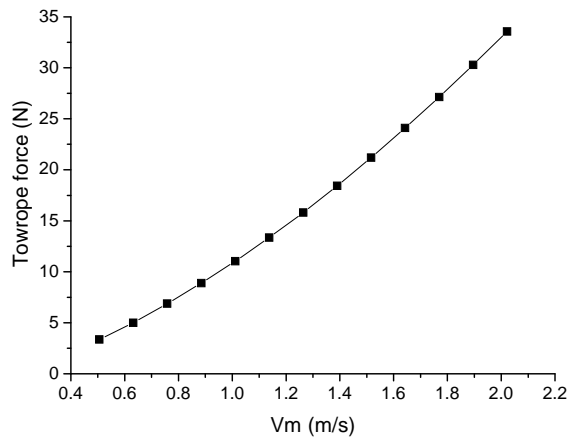
Fig. 2.10 Towrope force as function of model speed

However, for the completely free running model without connection to the carriage, it is difficult to apply a towrope force by the traditional methods as introduced in Paper 2. Applying an air fan which is mounted to the model on a load cell is a possible solution, but no suitable fan was available at the time the tests were performed.

Testing at the model scale propulsion point instead of the full scale propulsion point will definitely influence the finally attainable speed in waves, as it is shown in Paper 1. A correction method is proposed in this thesis to compensate for the lack of towrope in the experiment. A linear method was specified in Paper 1. This method is based on a numerical calculation of attainable speeds in waves for the conditions when towrope force is used or not. When the deviation between the two cases is calculated, the real converged speed in waves with corrected towrope force applied can be obtained. Later, this method was improved in Paper 2 by taking the nonlinearities into account. The comparisons between the two methods were presented in Paper 2.

2.1.5 Uncertainty analysis

It is important to keep in mind when performing all kinds of physical experiments that there is inherent uncertainty in all measured data. A test results is really just one example of the range of possible outcomes of the experiment (Aarsnes and Steen, 2008). In order to know how far the measured value is from the 'true' value, uncertainty analysis is necessary, since the 'true' value is generally unknown. The aim of the uncertainly analysis performed here is to give a quantitative evaluation of how reliable our measurements were.

Error is used for the difference between a measurement result and the 'true' value. Uncertainty is the statistical representation of error. Generally speaking, there are two types of errors, namely bias and precision. Bias is systematic error. Bias will not change with just repetitions of the tests with the same facility and set up, but it will be different if part or all the test facility changed. Calibration is the most effective way to reduce bias errors. Precision is also named random error, which is distributed in results. For example in the tests in this section, the measured attainable speed in waves can be influenced by many factors such as if the heading of the model was kept exactly in the 0 degree heading direction; if the thruster steering angle output was the same with repeated runs; if the water surface was calm enough before new waves created; if the model was running along the centerline of the towing tank to avoid tank wall effect to the minimum, and so on. A good way to evaluate precision error is by repeated measurements. However, in the field of ship hydrodynamics, the complexity and high cost of experiments do often not allow a satisfactory repetition of the tests (Zhu, Wu and Moan, 2011).

So the uncertainty analysis here is based on finding the precision limit from multiple time windows, instead of from repeated runs down the tank. The multiple time windows are created by shifting the start and end time forward 10 seconds for each new time window. Three different wave conditions were selected. a quantitative evaluation of how reliable the measured attainable speed in waves (V), starboard (SB) and port side (PS) propulsor thrust in longitudinal direction (F_X), in transverse direction (F_Y), torque (Q), revolutions (RPS), steering angle (θ) and power are analyzed.

The confidence interval is set to be 95%. Precision limit and uncertainty for a single run and for the mean are all given. The main difference between them is standard deviation for the former is calculated based on the equation (2.1); while for the later is obtained by applying equation (2.2).

$$S_x = \sqrt{\frac{1}{N-1}\sum_{j=1}^{N}(X_j - \overline{X})^2} \qquad (2.1)$$

$$S_{\overline{x}} = S_x / \sqrt{N} \qquad (2.2)$$

Where S_x is standard deviation; $S_{\overline{x}}$ is standard deviation for the mean; N is the number of time windows; $\overline{X}$ is the mean value for the variable X_j.

Table 2.5 Uncertainty analysis for the case with wave period T=2.383s, wave height H=0.06m

Number of time windows	10			
Length of each time window (s)	40			
Parameter	precision limit	Uncertainty	precision limit for the mean	Uncertainty for the mean
V (m/s)	0.0049	0.29 %	0.0015	0.09 %
F_X_SB	0.2085	0.45 %	0.0659	0.14 %
F_X_PS	0.2479	0.53 %	0.0784	0.17 %
F_Y_SB	0.5174	0.57%	0.1636	0.18%
F_Y_PS	0.5322	0.58%	0.1683	0.18%
Q_SB	0.0024	0.12 %	0.0007	0.039%
Q_PS	0.0042	0.23 %	0.0013	0.07%
RPS_SB	0.0163	0.16 %	0.0051	0.05%
RPS_PS	0.0147	0.15 %	0.0046	0.046%
θ_SB	0.0929	17.52%	0.0294	5.54%
θ_PS	0.0936	17.65%	0.0296	5.58%
Power_SB	0.0131	0.04%	0.0041	0.014%
Power_PS	0.0453	0.16%	0.0143	0.049%

Table 2.6 Uncertainty analysis for the case with wave period T=2.383s, wave height H=0.24m

Number of time windows	16			
Length of each time window (s)	60			
Parameter	precision limit	Uncertainty	precision limit for the mean	Uncertainty for the mean
V (m/s)	0.0266	2.45%	0.0067	0.61%
F_X_SB	0.4527	0.90%	0.1132	0.22%
F_X_PS	1.6033	3.16%	0.4008	0.79%
F_Y_SB	9.5854	9.15%	2.3964	2.29%
F_Y_PS	7.8803	7.52%	1.9701	1.88%
Q_SB	0.0146	0.71%	0.0036	0.18%
Q_PS	0.0206	1.04%	0.0052	0.26%
RPS_SB	0.0641	0.68%	0.0160	0.17%
RPS_PS	0.0570	0.61%	0.0142	0.15%
θ_SB	5.1615	62.23%	1.2904	15.56%
θ_PS	5.2163	62.89%	1.3041	15.72%
Power_SB	0.0085	0.028%	0.0021	0.007%
Power_PS	0.4282	1.49%	0.1071	0.37%

Table 2.7 Uncertainty analysis for the case with wave period T=3.07s, wave height H=0.12m

Number of time windows	16			
Length of each time window (s)	60			
Parameter	precision limit	Uncertainty	precision limit for the mean	Uncertainty for the mean
V (m/s)	0.0074	0.43%	0.0018	0.11%
F_X_SB	0.2706	0.60%	0.0677	0.15%
F_X_PS	0.3547	0.78%	0.0887	0.19%
F_Y_SB	1.6647	1.87%	0.4162	0.47%
F_Y_PS	1.0528	1.18%	0.2632	0.30%
Q_SB	0.0024	0.13%	0.0006	0.032%
Q_PS	0.0027	0.15%	0.0007	0.036%
RPS_SB	0.0137	0.13%	0.0034	0.033%
RPS_PS	0.0130	0.13%	0.0033	0.032%
θ_SB	0.3591	35.83%	0.0898	8.96%
θ_PS	0.3596	35.88%	0.0899	8.97%
Power_SB	0.0142	0.048%	0.0035	0.012%
Power_PS	0.0747	0.26%	0.0187	0.064%

Thrust force in transverse direction (T_Y) and steering angle (θ) are oscillating around their very small mean value, since autopilot control is used to keep the model running along straight line course. So when calculating the normalized uncertainty, the average value of T_Y and θ are replaced by the average of the total unit thrust force ($\sqrt{F_X^2 + F_Y^2}$) and the average value of the magnitude of each steering angle oscillation cycle respectively.

It is clearly seen that uncertainty for the case study in Table 2.6 are higher than the other two cases in V, T_Y and θ. For the severe sea condition reported in Table 2.6, a slowly varying component in speed was observed. So the average speed value in each time window will be influenced by this slowly varying component which leads to higher standard deviation and uncertainty. Bigger uncertainties for T_Y and θ in Table 2.6 are mainly attributed to more steering forces are needed in higher sea states in order to keep the model running along the designed straight line course.

2.2 Speed loss during zigzag maneuvers in waves

Model tests about speed loss in 10/2 zigzag maneuvers (10 degrees means azimuth steering angle and 2 degrees means heading change) were carried out with model A in the large towing tank in the Marine Technology Centre. The model was free and self-propelled and steered with

twin AZP 120 thrusters. Main dimensions of the vessel model and thrusters are described in Table 2.1 and Table 2.2. The same set up with the same measurements were used as described in section 2.1.2, except that the track controller is disabled in this case. Calm water speed for model A is 1.769m/s. Five regular waves were carefully calibrated before the tests started, as listed in Table 2.8 in model scale.

Table 2.8 Waves used for 10/2 zigzag maneuver tests

H (m)	T (s)	λ/L_{pp}
0.12	1.351	0.42
0.12	1.597	0.57
0.12	1.842	0.78
0.12	2.088	1
0.12	2.579	1.52

The speed loss during zigzag maneuvering in waves was categorized as being due to added wave resistance, and loss of thrust due to steering and due to yawing. In order to figure out this topic, four main steps were needed to complete the tests. Firstly, straight line course in calm water was tested as a basic reference, and the power required to reach a model speed of 1.769 m/s was determined. All subsequent tests were performed at this power level, using a controller as discussed above. No towrope force was applied - all tests were performed at model self-propulsion point. A track controller was used to ensure a stable straight line course in the approach to the zigzag. A small average azimuth angle (within 1 degree) was observed to starboard at this stage and this may be caused by a slight asymmetry of the hull model.

Secondly, 10/2 zigzag motion in calm water was considered. The model was accelerated to the design speed and then azimuth angle was set to 10 deg to port at first and reversed to starboard 10 deg when the vessel heading had turned 2 deg off the original heading. Then the ship would continue turning to port with decreasing rate and successively turning to starboard. These steps were repeated until the model reached the end of the tank or came too close to the tank walls. At most five overshoot angles were captured. Speed reduction due to loss of thrust due to steering and added resistance due to yawing can be obtained by the speed in the first step minus the speed achieved in this step.

After that, straight line course in waves was tested. This is similar to the tests described in section 2.1. In this condition, the speed drop relative to calm water can be attributed to added wave resistance.

Finally, zigzag motion in waves was considered. Speed drop in this case includes all the effects including added wave resistance, loss of thrust and yawing. The relationship between vessel speeds, overshoot angle, thrust force with different wave conditions was clear.

2.2.1 Uncertainty Analysis

No uncertainty analysis was performed particularly for this test series. It is reasonable to believe that the values for propeller forces and speed reported in section 2.1.5 are fairly representative.

2.3 Speed loss in oblique wave conditions

2.3.1 Model test set up

Model tests about speed reduction in oblique waves were done in the Ocean Basin at the Marine Technology Centre, using model A with the same propulsion system as specified in section 2.1. The effective dimensions of the ocean basin are 50 meters wide and 65 meters long. The false bottom was set at a depth of 4 meters. An XY-carriage shown in Fig. 2.11 was used to follow the model during the tests. The main carriage can be controlled moving along the longitudinal direction, while the sub-carriage which is connected underneath the main carriage can move back and forth along the transverse direction. Measuring amplifiers and data acquisition systems were installed on the sub-carriage, signal cables and power cables to the propulsor motor were collected in a bundle which went down to the model.
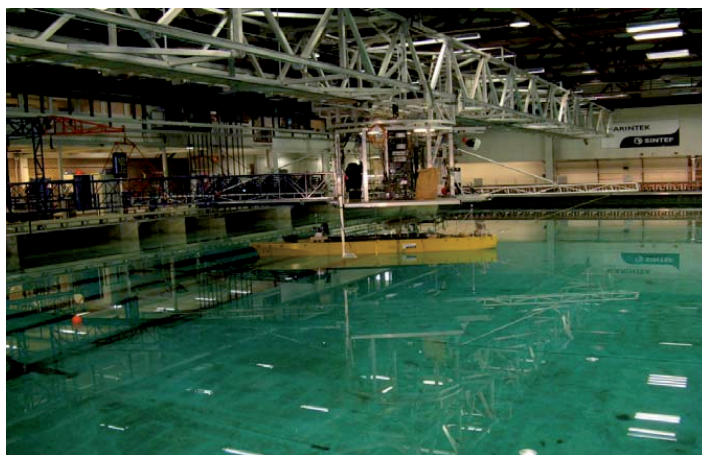

Fig. 2.11 Carriage system in Ocean Basin in Marintek

A double-flap wave maker (BM2) along the 50-meter side generates long crested waves. Along the 65-meter side, there is a multi-flap wave maker (BM3) consisting of 144 individually

controlled flaps. Wave absorption beaches are installed on the two opposite sides to minimize wave reflection. Towrope force was obtained here by applying an air fan that was blowing rearward, producing forward thrust. The fan was mounted on a load cell so that the thrust of the fan could be measured. However, since the air jet was blowing over the model there was a significant thrust loss of the fan, so that the effective fan force is only 0.67 times the measured fan force. This was found by additional tests which were carried out after completion of the test program. During these additional tests, the model was connected to the bank of the basin by a rope tied to its stern. Different revolutions of the fan were tested and the force measured by the load cell and the net force (force measured on the rope) were recorded to obtain the thrust loss factor. Specified data were shown in Table 2.9. The average thrust loss factor of the fan was found to equal 0.67, and this value is used in subsequent calculations and analyses. This means that the model was tested at a propulsion point between the model propulsion point and the correct full scale propulsion point.

Table 2.9 Thrust loss factor of the fan

RPS of the fan	T_1 (N)(force measured by the load cell)	T_2 (N) (Net thrust)	T_2/T_1
50	6.555	4.45	0.6789
66.12	11.9	7.955	0.6685
83.11	18.86	12.55	0.6654
100.3	27.51	18.48	0.6718
116.9	37.47	24.95	0.6659
133.4	49.47	33.42	0.6756

The position of the model in six degrees of freedom is measured by the optical position measurement system Ocus delivered by Qualisys. In this system, twenty-seven cameras were distributed mainly at the four corners of the basin. The cameras observe the position of the four reflective spherical markers mounted on masts on the model, which can be seen on the photo in Fig. 2.12. A marker must be seen by at least two cameras viewing from different directions to determine its position in space. In order to determine the pitch, roll and yaw angles of the model at least three markers must be viewed at any given time. The purpose of having four markers is to get redundancy, in case one marker is getting out of view of the cameras. Magnitude of standard deviation between true position and measured position is 1.3 mm, which both includes noise and systematic errors. Velocities were derived from the measured positions. The measured variables were as shown in Table 2.5. Sampling frequency for the position measurement is 25 HZ and all other channels are sampled at 200 HZ, with a low-pass filter with a cut-off frequency of 20 Hz.

Eight regular waves with different height and period were chosen in the model test. Four headings (30 degrees, 60 degrees, 90 degrees and 150 degrees) and two calm water speeds (V_m=1.769m/s and 1.191m/s) were tested. The combination between wave, heading and model speed are specified in Table 2.10 and 2.11.

Table 2.10 Calibrated waves in model scale

Wave No.	Wave maker	Wave type	H(m)	T(s)	λ/Lpp
1	BM2	REG	0.121	1.351	0.42
2	BM2	REG	0.121	1.842	0.78
3	BM2	REG	0.121	2.088	1
4	BM2	REG	0.121	2.383	1.3
5	BM2	REG	0.061	2.383	1.3
6	BM2	REG	0.242	2.383	1.3
7	BM2	REG	0.121	2.579	1.52
8	BM2	REG	0.121	3.071	2.15
9	BM3	REG	0.121	1.351	0.42
10	BM3	REG	0.121	1.842	0.78
11	BM3	REG	0.121	2.088	1
12	BM3	REG	0.121	2.383	1.3
13	BM3	REG	0.121	2.579	1.52

Table 2.11 Test conditions for all the runs

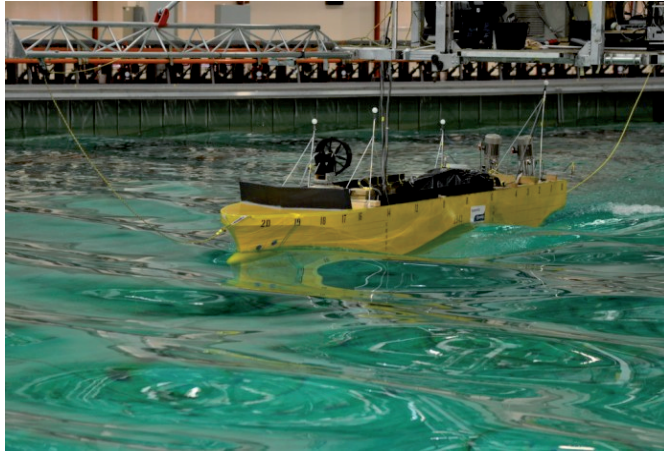| V_m (m/s)	Direction (deg)	Wave No.
1.769	30	1,2,3,4,5,6,7,8
	60	1,2,3,4,5,7,8
	90	9,10,11,13
	150	1,2,3,4,7,8
1.191	30	2,3,4,6,7
	60	2,3,4,7
	150	2,4

Fig. 2.12 Model A running in oblique waves in ocean basin (V_m=1.769m/s, H_m=0.121m, Heading 150deg)

2.3.2 Test procedure

For this displacement vessel with low resistance/weight-ratio, the speed will converge quite slowly when the resistance changes, so that a long distance is travelled before converged speed is reached. Since the size of the ocean basin is limited compared to this large model, special procedures were taken in order to reach converged speed:

Firstly, after the model being towed to the corner of the basin and set up with the correct heading direction (30 degrees heading comes first), a calm water run with design speed was executed. This was used as a basis for comparison and to find the correct power value for the thruster motors.

Then, a pre-calibrated wave was added. The propellers were started initially with a high power level to accelerate the model before the waves reached the model. When a pre-defined threshold speed was reached, the power was reduced automatically to the correct level. Then the model speed was approaching to the converged value from a higher or lower level. When the model was getting close to the end of the basin, the propellers were stopped and the model was stopped by tightening a rope from the carriage, connected to the stern of the model. The value of the pre-defined speed threshold is important for the ability to reach a converged speed. The threshold speed should be close to the converged speed, so some trial and error was needed to find the right threshold speed for each test condition.

When all the waves were finished at the first heading, the model was set to the next heading direction (60 degrees, 90 degrees, 150 degrees in sequence).

Then, the next model speed was carried out with the same procedures as specified above.

2.3.3 Data analysis

For the cases where the converged attainable speed is achieved in the tests, the value of the converged speed can be found by directly averaging the recorded speed within the effective time window. Effective time window (between 20 seconds to 30 seconds for different conditions) is chosen as close as to the end of the test before the model was towed to stop, so speed converging process with the smallest acceleration is captured. However, even when different threshold speeds were tested to try to get the attainable speeds in the model tests, still for 7 out of 36 runs converged speed was not obtained. Fig. 2.13 shows two examples of the not converged runs with still decreasing (Fig. 2.13 (a)) or increasing (Fig. 2.13 (b)) speed within the effective time window.

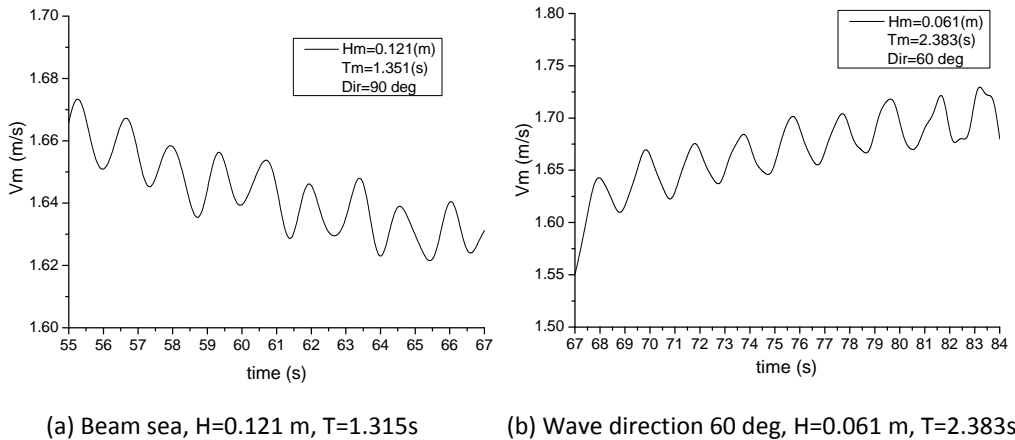(a) Beam sea, H=0.121 m, T=1.315s   (b) Wave direction 60 deg, H=0.061 m, T=2.383s

Fig. 2.13 Two examples of not converged speeds from model tests with initial speed 1.769 m/s

A converged speed prediction method is proposed in this thesis.

The method is based on the balance between resistance and thrust force. Two steps are necessary when applying this method to predict the converged speed. Firstly, applying an accurate thrust deduction factor in waves plays an important role here. Both the calm water thrust deduction and numerical thrust deduction is used. The numerical thrust deduction factor is found by solving the force balance equation by considering the inertial force, thrust force, effective towrope force and resistance from both calm water and incoming wave. Then, the finally converged speed is obtained by solving the equation with balanced thrust and resistance

31

by assuming acceleration of the vessel is zero. More details about this converged speed prediction method were specified in paper 4.

2.3.4 Uncertainty analysis

For uncertainty of the tests with speed loss prediction in oblique waves, the focus is put on the threshold speed selection which influences the final results accuracy directly. Threshold speed is chosen based on the experience to estimate the finally converged speed value.
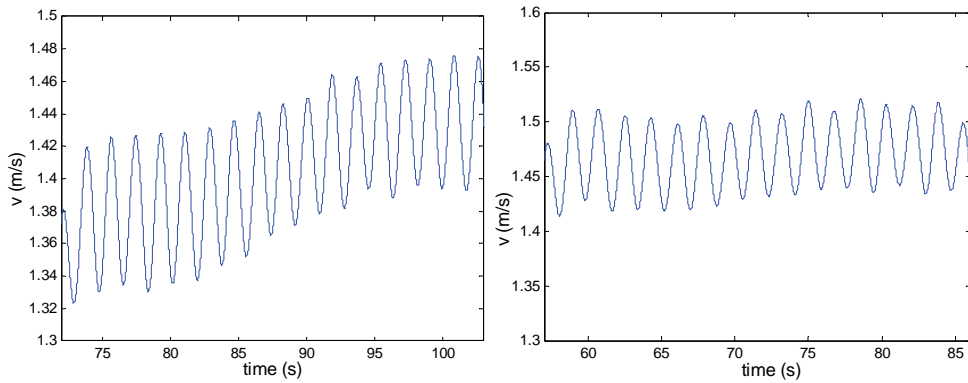
(a) Threshold speed is equal to 1.3 m/s   (b) Threshold speed is equal to 1.4 m/s

Fig. 2.14 Threshold speed influence on the converged speed for wave case with H=0.121m, T=2.383s, V_0=1.769m/s, heading 30 degrees
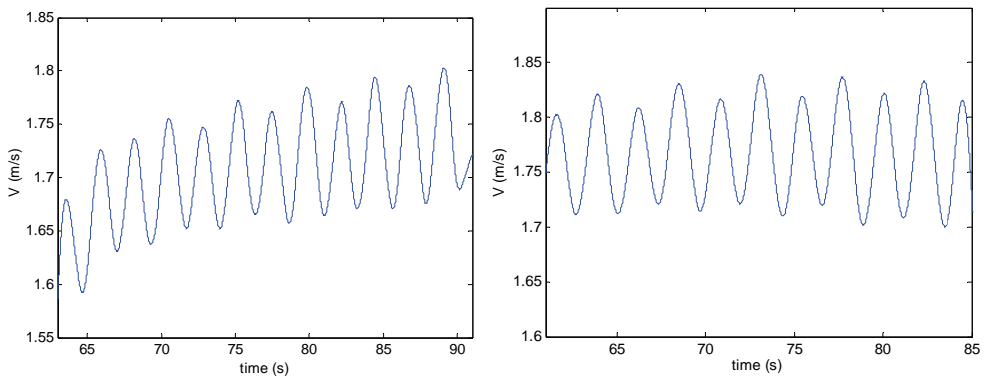
(a) Threshold speed is equal to 1.5 m/s   (b) Threshold speed is equal to 1.65 m/s

Fig. 2.15 Threshold speed influence on the converged speed for wave case with H=0.121m, T=3.071s, V_0=1.769m/s, heading 30 degrees

Fig. 2.14 and Fig. 2.15 show two examples of the relationship between threshold speed and its influence on the converged speed prediction. Threshold speeds were lower evaluated than the converged speed in the two examples, so the converged speed is being approached from lower speed range with increasing speed trend. For the case in Fig. 2.14 (a), the highest value of model speed is reached up to around 1.44 m/s with threshold speed set to be 1.3 m/s. The speed increased until the end of the test, due to bigger difference between threshold speed and the real converged speed value. Then, with a little higher value of the threshold speed being 1.4m/s (Fig. 2.14 (b)), well converged speed is captured with the average value to be 1.47 m/s. Fig. 2.15 presents the same phenomenon. When threshold speed was set to 0.15 m/s higher, converged speed was obtained. So it can be concluded that the smaller difference between threshold and 'real' converged speed value in waves, the less space and time is needed to arrive at the attainable speed during the test.

Both the two cases in Fig. 2.14 and Fig. 2.15 were being used in the validation of the converged speed prediction method which is proposed in Paper 4. The uncertainty introduced by threshold speed can be greatly reduced by the correction method. More details were shown in Paper 4.

2.4 Uncertainty analysis of thrust deduction

Presence of the propeller behind the ship will increase the resistance of the hull and hence lead to reduced thrust. Thrust deduction is usually determined by propulsion tests in calm water or by empirical formulas. The value of the thrust deduction is influenced by:

- ship speed
- hull form and loading condition of the hull (draught and trim)
- propeller loading condition
- thrusters arrangement
- (wave induced) ship motion
- steering

The top four factors have already been well studied by many researchers and they are widely well known knowledge, so no additional explanation is given here. For the influence of wave induced ship motion on thrust deduction, several researchers had already made some contributions. Nakamura and Naito (1977) carried out resistance and propulsion tests in waves in the tank of Osaka University. They obtained thrust deduction in different wave lengths at the same Froude number. Thrust deduction in wave shows considerable difference from the calm water thrust deduction value when the wave length to ship length ratio λ/L varies from 0.9 to 1.3. This is also the range of wave lengths where significant wave motion was induced. They also varied the wave height in the same wave length range with the vessel speed kept constant. Distinct change in thrust deduction with wave height was observed in their study. So it can be

concluded that thrust deduction has a strong relationship with wave induced wave motion. Similar work was also done by Yamazaki and Nakatake et al. (1978), Kadoi et al. (1986) and Bhattacharyya (1978). In this section, thrust deduction variation due to steering will be studied.

Thrust deduction derived from resistance and propulsion tests carried out in the towing tank at the Marine Technology Centre with two thrusters fixed to zero steering angle direction (Alterskjær, 2010) is shown in Fig. 2.16. It is seen that the thrust deduction increase quite significantly with speed.
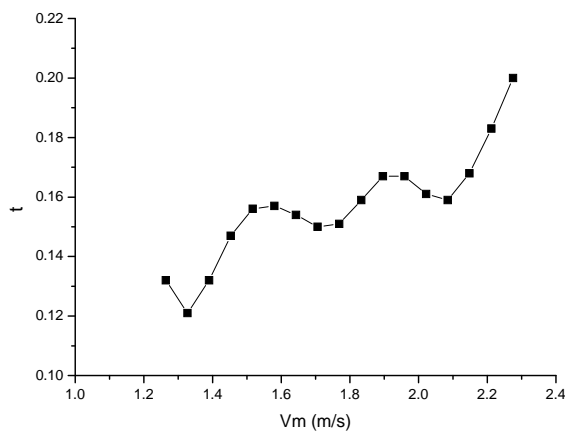

Fig. 2.16 Thrust deduction from resistance and propulsion tests in calm water with the case vessel studied in this thesis

When comes to propulsion tests in calm water with freely running model, proper azimuth angles are needed to balance the unsymmetrical effect of the hull and some disturbance from side directions in order to keep the vessel running along designed straight line course. Output steering angles are controlled by autopilot. Several calm water tests with straight line course from towing tank and from ocean basin are selected to investigate the effect of steering on thrust deduction, as given in Table 2.12.

Table 2.12 Difference in thrust deduction from propulsion tests and seakeeping tests

	V_m	F_x_SB	F_x_PS	RPS_SB	RPS_PS	Q_SB	Q_PS	F_Y_SB	F_Y_PS	θ_SB	θ_PS
No.\Unit	m/s	N	N	/s	/s	NM	NM	N	N	deg	deg
No.1	1.782	46.902	43.020	10.308	10.283	1.701	1.801	0.504	1.358	1.011	1.170
No.2	1.779	41.880	45.715	10.179	10.153	1.680	1.754	0.628	1.364	1.123	1.282
No.3	1.775	44.346	43.606	10.196	10.248	1.717	1.709	-5.175	3.433	0.027	-0.172
No.4	1.764	36.499	34.967	9.716	9.728	1.575	1.539	-5.044	3.545	-0.466	-0.672
No.5	1.767	35.925	34.953	9.726	9.768	1.465	1.456	-4.989	3.588	-0.149	-0.321
No.6	1.816	35.736	34.744	9.804	9.880	1.463	1.453	-5.895	2.803	0.085	-0.093
No.7	1.207	17.619	17.222	6.779	6.808	0.705	0.702	-3.394	0.666	0.287	0.199

...

F_D	R_{TM}	t	K_T_SB	K_T_PS	K_T_SB _owd	K_T_PS_ owd	K_Q_SB	K_Q_PS	K_Q_SB_o wd	K_Q_PS _owd	R_{TM}_co rr
N	N										N
0.000	69.400	0.228	0.281	0.259	0.261	0.260	0.051	0.054	0.053	0.052	76.344
0.000	70.480	0.195	0.257	0.282	0.257	0.256	0.052	0.054	0.052	0.052	74.368
0.000	70.051	0.204	0.273	0.265	0.259	0.261	0.053	0.052	0.052	0.052	74.672
27.465	69.477	0.285	0.248	0.236	0.243	0.243	0.053	0.052	0.050	0.050	79.075
26.756	69.302	0.275	0.244	0.234	0.242	0.244	0.049	0.049	0.050	0.050	78.103
28.000	74.378	0.211	0.240	0.227	0.235	0.238	0.049	0.048	0.049	0.049	78.598
14.336	33.708	0.308	0.248	0.236	0.245	0.247	0.049	0.048	0.050	0.051	39.918

Tests No.1 and No.2 were from calm water test before the zigzag test in waves in the towing tank (make reference to Paper 3). Tests No.3 to No.7 were from calm water tests done in the Ocean basin before oblique waves were created (make reference to Paper 4). No towrope forces were applied to tests No.1, No.2 and No.3. Variables like model speed (V_m), starboard (SB) and port side (PS) propulsor thrust in longitudinal direction (F_X), in transverse direction (F_Y), torque (Q), revolutions (RPS), steering angle (θ) and towrope force (F_D) were all obtained by the measurements during the tests. R_{TM} is calm water resistance which is taken from the original resistance tests (Alterskjær, 2010). Thrust deduction t is calculated by equation (2.3):

$$t = 1 - \frac{R_{TM} - F_D}{F_x\_SB + F_x\_PS} \tag{2.3}$$

Thrust deduction values calculated according to equation (2.3) are all higher than the thrust deduction from the propulsion test in Fig. 2.16. At testing speed V_m=1.76 m/s, t from the original propulsion test is 0.151; while from equation (2.3) are varying from 0.195 to 0.285 for the mentioned tests. For testing speed V_m=1.207 m/s, t from the original propulsion test is

around 0.13; while from equation (2.3) it is 0.308 for the test in the ocean basin. Before analyzing the reasons for the big difference, it is necessary to make sure the measured thrust is correct. This is done by comparing the measured thrust with the open water diagram (owd) (Fig. 2.7) of the thruster. K_T in Table 2.12 is calculated by $\sqrt{F_x^2 + F_Y^2} / (\rho_m n_m^2 D_m^4)$ and K_Q is calculated by $Q / (\rho_m n_m^2 D_m^5)$; while K_T_owd and K_Q_owd are found from open water character diagram by inserting the corresponding advance coefficient J-value, which is computed from the measured V_m, n_m and the wake fraction from the original propulsion tests. Small deviations were observed between K_T and K_T_owd, which will contribute maximum to 3 N for the difference between R_{TM} and R_{TM}_corr. Good agreement is shown between K_Q and K_Q_owd.

Then, the first reason to cause the discrepancy in thrust deduction is due to ship model resistance change. R_{TM}_corr in Table 2.12 is calculated by $(F_x\_SB + F_x\_PS) \cdot (1 - t_{pt}) + F_D$, here thrust deduction from propulsion test t_{pt} is used. R_{TM}_corr is larger than R_{TM} by several Newtons. R_{TM} is found using the original calm water resistance test which is carried out in the year of 2010. After that, the model had been used for a number of different tests during the past two years' time including a paint smear test, seakeeping tests with different bow shapes, small zigzag tests in the towing tank, and PMM forced motion tests and seakeeping-maneuvering test in oblique seas in ocean basin. Previous experience shows that resistance of hull models increase over time, mainly due to deterioration of the surface finish (repainting the model tend to reduce the resistance almost to original level). The paint smear test is particularly hard on the surface finish. Also, for the seakeeping-maneuvering test, the model had been equipped with bilge keels and additional masts and a screen on the fore deck, so additional air resistance also contributes to the increase of model resistance. Thus, it is quite likely that the resistance has increased relative to the original calm water test, and that this is partly explaining the thrust deduction difference.

Another reason is attributed to steering. For the freely running model, steering angles were oscillating around the 0 degree direction under the command from auto pilot control to balance the transverse disturbances. Transverse thrust component will reduce the thrust force in the longitudinal direction under the condition of constant power. It is clearly been seen from Table 2.12 that a significant F_Y exists in most of the cases. Also a steering thruster will also change the velocity profile of the after body and influence the wake fraction which consequently influence thrust deduction.

Chapter 3 Numerical methods

In order to achieve attainable speed in a seaway under maneuvering conditions, the force balance between resistance and thrust is needed. During the numerical simulation for this subject, work should go to calm water resistance and wave resistance in surge, sway and yaw direction, four-quadrant thrust force, autopilot control and ship machinery.

3.1 Ship motions

Accurate prediction of the ship motion is very important for added wave resistance calculation and also important for evaluating the vertical positions of the propeller. Here, STF strip theory (Salvesen et al. 1970) is used through the implementation in *ShipX Vessel Response* (Fathi and Hoff, 2008). Within this strip theory, the following main assumptions are made:

- Viscous effects are disregarded.
- The ship has long slender hull form, this means 3D effects were neglected.
- Vessel oscillatory motions are linear and harmonic.
- Encounter frequency is relatively high. This means the wave created by the ship's oscillation should have a wave length of the order of ship beam rather than ship length.
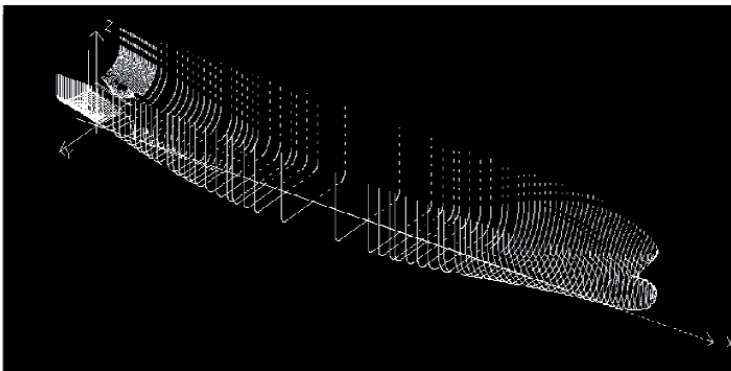- Ship has lateral symmetry.

Fig. 3.1 Strips of 8000 DWT tanker

The ship hull is presented by a series of strips as shown in Fig. 3.1. Since the hull has a bulb with flare at the bow and wetted transom stern, more strips were distributed at the bow and the stern. Fewer strips were needed at the middle section of the hull. 2D sectional added mass and damping is obtained by Frank close-fit source distribution method. The total hydrodynamic force and moment on the ship are obtained by integrating the sectional force calculated for every strip. The exciting loads, namely Froude-Kriloff and diffraction loads are solved through integration of the incident hydrodynamic pressure and Haskind-Hanaoka relationship respectively. Together with the hydrodynamic coefficient and wave exciting loads, the six degree of freedom ship motions are solved according to Newton 2nd law.

3.2 Wave resistance calculation

Added wave resistance plays an important role on speed loss in waves. In numerical simulations, several methods were applied to evaluate added resistance in different sea conditions. Added resistance in head sea conditions were calculated both by the radiated energy method (Gerritsma and Beukelman (1972)) and Direct Pressure Integration method (Faltinsen et al. (1980)). The results of Gerritsma and Beukelman method were presented in Paper 1 and Paper 2. Comparisons between the results obtained from Gerritsma and Beukelman method and Direct Pressure Integration method were shown in Paper 2. For the conditions other than head sea, Loukakis and Sclavounos (1978) is adopted for evaluating added wave resistance, transverse drift force and mean yaw moment. Relevant results were shown in Paper 3 and Paper 4.

3.2.1 Added resistance in head sea conditions

3.2.1.1 Radiated energy method

In head sea condition, added wave resistance is calculated by the method proposed by Gerritsma and Beukelman (1972). This method is based on the energy principle under the assumption that the energy in the radiated waves caused by the wave induced ship motions is equal to the work of added resistance. We consider regular head waves. The energy radiated during one wave encounter period T can be obtained by

$$P = \int_0^T \int_L b_{33} V_Z^2 dx_b dt \qquad (3.1)$$

Where L is ship length, b_{33} is sectional damping coefficient of the vertical motion of a section x_b, V_Z is the average vertical relative velocity of the water velocity in heave.

The damping coefficient can be defined as:

$$b_{33} = N' - V\frac{dm'}{dx_b}$$ (3.2)

where N' is 2D cross-sectional heave damping coefficient, and m' is the cross-sectional added mass.

Vertical relative velocity can be approximated by

$$V_Z = \dot{Z} - x_b\dot{\theta} + U\theta - \dot{\zeta}$$ (3.3)

Here, $\dot{Z}$ is the vessel vertical velocity, U is the ship forward speed, θ is the pitch angle, ζ' is the effective wave displacement for a cross-section. The value of ζ' is a correction to the Froude-Kryloff hypothesis which considers that the water pressure on the ship hull and the wave field is not disturbed by the ship. This correction affects the amplitude of the incident wave, and for deep water it can be calculated using

$$\zeta' = \zeta(1 - \frac{k}{y_w}\int_{-T}^{0} y_b e^{kz_b} dz_b)$$ (3.4)

Where k is wave number; (y_b, z_b) are the points of the section at x_b and y_w is the half width of the design waterline at section x_b. ζ is the wave amplitude without modification.

Since V_Z is an harmonic function of time with amplitude V_{Za} and frequency ω_e, so the mean value can be written as

$$P = \frac{\pi}{\omega_e}\int_L b_{33}V_Z^2 dx_b$$ (3.5)

The work being done by the added resistance R_{AW} is also given by:

$$P = R_{AW}(V+c)T_e = R_{AW}\lambda$$ (3.6)

So added resistance can be expressed as:

$$R_{AW} = \frac{\pi}{\omega_e\lambda}\int_L b_{33}V_Z^2 dx_b$$ (3.7)

This method works well when the ship relative vertical motion with respect to the water is important, as shown by equation (3.3) and (3.4). It means that this method can give a good prediction of added wave resistance in long waves. In short waves, when the ship oscillatory motion can be neglected, equation (3.7) cannot give satisfactory resistance prediction. For a

motionless ship with high speed, this method will underestimate the diffraction force and also fail to include the influence of viscous effects when the encounter frequency is high.

3.2.1.2 Direct pressure integration method

Added wave resistance in this thesis is also calculated by direct pressure integration (DPI) method which was developed by Faltinsen et al. (1980).

This theory assumes that the incident wave length is large relative to the cross-section dimensions. The diffraction potential is solved by the 'relative motion method', which implies that the wave length is large, three-dimensional effects can be neglected and the diffraction potential can be solved by the two-dimensional Laplace equation. This method expands the Bernoulli's equation to second order taking instantaneous ship motion and wetted hull surface into consideration and integrates the longitudinal component of the oscillating pressure over the wetted surface of the hull. Added resistance can be written as equation (3.8):

$$
\begin{aligned}
R_{AW} = & \int_c (-\frac{\rho g}{2}\overline{\zeta_r^{\,2}})n_1 ds - w_e^2 M\overline{\eta_3\eta_5} + w_e^2 M\overline{(\eta_2 - Z_G\eta_4)\eta_6} \\
& + \rho\int_{S_B}\overline{\{(\eta_2 + x\eta_6 - z\eta_4)\frac{\partial}{\partial y}(\frac{\partial\phi^{(1)}}{\partial t} + U\frac{\partial\phi^{(1)}}{\partial x})\Big|_m} \\
& + (\eta_3 - x\eta_5 + y\eta_4)\frac{\partial}{\partial z}(\frac{\partial\phi^{(1)}}{\partial t} + U\frac{\partial\phi^{(1)}}{\partial x})\Big|_m \\
& + \frac{1}{2}((\frac{\partial\phi^{(1)}}{\partial x})^2 + (\frac{\partial\phi^{(1)}}{\partial y})^2 + (\frac{\partial\phi^{(1)}}{\partial z})^2)\}n_1 ds
\end{aligned}
\tag{3.8}
$$

Where c is the water line curve; $\zeta_r = \zeta - (\eta_3 - x\eta_5 + y\eta_4)$ is the relative wave amplitude along the ship; ω_e is encounter frequency; $\phi^{(1)}$ is first order velocity potential; ζ_i (i=1, 2...6) is vessel displacement in six degree of freedom, which was obtained by Salvesen-Tuck-Faltinsen (STF) strip theory (Salvesen et al, 1970) ; S_B is the average wetted surface of the body; M is the ship mass and Z_G is the z-coordinate of the center of gravity of the ship; $\big|_m$ indicates that the variables should be evaluated on the average position of the wetted ship hull; the bar over the expressions indicates time-averaged values.

The pressure term $U\frac{\partial\phi}{\partial x}$ in equation (3.8) is calculated as follows. The total velocity potential ϕ is with the same expression as the equation shown in Faltinsen et al. (1980). But since the diffraction part of the total velocity potential is solved by the 'relative motion method' without

being solved explicitly. So this term can be calculated from the difference of the total velocity potential at the center of each panel in the longitudinal direction. This method is very sensitive to the ship shape and strip distribution along the hull. The results related to this DPI method are presented in Paper 2.

3.2.2 Added resistance in oblique sea conditions

For oblique waves, the wave resistance is calculated by the method proposed by Loukakis and Sclavounos (1978). As shown in Fig 3.2, the ship is moving along a predetermined direction along its x-axis with speed U. The waves are coming from a direction at angle β with propagating speed $\bar{C}$. Added wave resistance $\bar{R}_x$, transverse drift force $\bar{R}_y$ and mean yaw moment in surge, sway and yaw directions are composed of the mean second order wave force on a ship in oblique waves. These forces are calculated by the method proposed by Loukakis and Sclavounos (1978). This method is based on the extension of the method proposed by Gerritsma and Beukelman (1972) which is originally only for head waves.
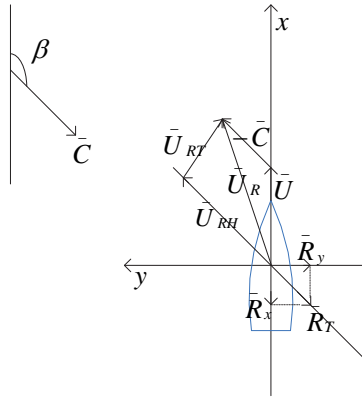

Fig. 3.2 Definition of heading direction and mean second order force

The G&B method is based on the energy principle under the assumption that radiated energy is equal to the work of added resistance done and the energy contained in the damping waves. And this energy relationship can be expressed by the equation (3.9).

$$(-R_x)(U-c)T = \frac{\pi}{\omega}\int_0^L (b_{33} - U\frac{da_{33}}{d\xi})|U_{RZ}|^2 \, d\xi \qquad (3.9)$$

Where ω and T are encounter frequency and encounter period of the wave, U_{RZ} is the vertical relative velocity of each ship section, a_{33} and b_{33} are two-dimensional sectional added mass and damping coefficients.

The left part of equation (3.9) corresponds to the work done on the fluid plus the amount of energy taken away from the direction of propagation of the incident wave and radiated all around the ship.

This approach can be extended to calculate the added resistance and drift force in oblique regular waves. It is known that if one considers a control surface fixed in space and surrounding the ship, the energy influx and efflux through it are equal when the contribution of the diffracted waves and ship generated waves are taken into consideration. The velocity of the ship relative to the fixed control surface is $U_R = U - c$ and can be resolved into U_{RH} and U_{RT} which are along and perpendicular to c respectively. The motion of the ship with U_{RT} does not make contribution to the mean horizontal force R_T, which consequently has the direction of the incident wave propagation. Then $(-R_T)U_{RH}$ shall represent the net energy given by the ship to the fluid $((-R_x)U)$ and the energy radiated all around the ship ($R_T c$). Then the left part of equation (3.9) can be rewritten as:

$$P = (-R_T)U_{RH} = (-R_T)(-c - U\cos\beta) \tag{3.10}$$

The final expressions which allow us to calculate the added resistance and drift force in oblique waves are:

$$(-R_T)(-c - U\cos\beta) = P_{35} + P_{26} + P_4 + 2P_{24} \tag{3.11}$$

$$\left|R_T\right| = \frac{k}{\omega}(P_{35} + P_{26} + P_4) + \frac{2k}{\omega}P_{24} \tag{3.12}$$

$$\left|R_x\right| = \left|R_T\cos\beta\right| \tag{3.13}$$

$$\left|R_y\right| = \left|R_T\sin\beta\right| \tag{3.14}$$

Where P_{35}, P_{26}, P_4, and P_{24} are energy radiated by ship heave-pitch motion, sway-yaw motion, roll motion and sway-roll motion during one encounter period. For an explanation on how to compute the P_{jk} terms see Loukakis and Sclavounos (1978).

3.3 Propulsion system study

Real behavior of propulsion system needs to be taken into consideration in an accurate manner when evaluating vessel speed deduction process. Since vessel speed is changing, propulsion point is changing correspondingly. Accurate evaluation of thrust, torque, RPS, efficiency and azimuth angle are needed in order to obtain the real attainable speed. Two numerical azimuth thruster models were applied in this thesis. One is four-quadrant numerical pod thruster model

(Ringen, 2010), based on a set of Fourier expansion of thrust and torque coefficients. This thruster was used for the numerical study in Paper 1, Paper 2 and Paper 3. Another is an empirical propulsion model based on model tests (Berg, 2002), which is applied in Paper 4. For all the cases studied in this thesis, thrusters were working within the first-quadrant condition.

3.3.1 Numerical azimuth thruster model

The four-quadrant propeller model is based on the work described by Strøm-Tejsen and Porter (1972). General analytical expression has been developed for the performance of an arbitrary propeller as functions of blade-area ratio, blade pitch setting and any combination of propeller rate and direction of revolution and ship speed and direction of motion. The first step in calculating the thrust and torque from the propeller is to calculate the advance velocity, ship drift angle and azimuth angle at the propeller position. Based on the revolutions and diameter, the hydrodynamic angle of advance can be obtained at radius 0.7R, as shown in equation (3.15).

$$\beta_i = \tan^{-1}(\frac{V_a}{0.7\pi nD}) \qquad (3.15)$$

Where β_i is hydrodynamic angle of advance, $V_a = \dfrac{V_x(1-w)}{nD}$ is advance velocity, n is propeller revolutions, D is propeller blade diameter, V_x is ship velocity in the longitudinal direction along the ship, w is wake fraction. Four quadrants of operation conditions are now defined as in Fig. 3.3, by the different combinations of advance velocity direction and propeller revolution direction:

Second quadrant $(90 \leq \beta_I < 180)$ $V_a \geq 0$ $n < 0$	First quadrant $(0 \leq \beta_I < 90)$ $V_a \geq 0$ $n \geq 0$
Third quadrant $(180 \leq \beta_I < 270)$ $V_a < 0$ $n < 0$	Fourth quadrant $(270 \leq \beta_I < 360)$ $V_a < 0$ $n \geq 0$

Fig. 3.3 Definition of four-quadrant propeller operation condition

The propeller thrust and torque coefficients are applied as function of hydrodynamic angle of advance in four quadrants. The non-dimensional thrust and torque coefficients C_T and C_Q are defined in equation (3.16) and (3.17):

$$C_T = \frac{T_a}{\frac{1}{2}\rho(V_a^2 + (0.7\omega R)^2)\frac{\pi}{4}D^2}$$ (3.16)

$$C_Q = \frac{Q_a}{\frac{1}{2}\rho(V_a^2 + (0.7\omega R)^2)\frac{\pi}{4}D^3}$$ (3.17)

The propeller thrust and torque are calculated based on a set of Fourier expansion of C_T and C_Q as shown is equation (3.18) and (3.19).

$$C_T(\beta) = \sum_{k=0}^{20}(A_T(k)\cos\beta k + B_T(k)\sin\beta k)$$ (3.18)

$$C_Q(\beta) = \sum_{k=0}^{20}(A_Q(k)\cos\beta k + B_Q(k)\sin\beta k)$$ (3.19)

The effect of the pod is included as a calculated drag force, based on the total ship velocity at propeller position, pod area and the drag coefficient. Neglecting the lift force effect of the pod is considered as a short-coming of the present propulsion model. The pod drag coefficient, which is based on model tests data, is applied as a function of pod angle and ship heading angle (Ringen, 2010). Interaction effects between propeller race and pod are not taken into account.

In time domain study, an electric engine model is selected here for the two thrusters. Gear ratio and shaft loss are included by editing engine-propeller gear ratio and mechanical efficiency. Also the total moment of inertia of the engine and propeller are considered in order to give the correct rate of change of engine revolutions.

3.3.1.1 Limitations and verification

It is important to be aware of the limitations of this model. Thrust and torque of the propeller is calculated based on a set of Fourier expansions of thrust and torque coefficients for a general propeller model as specified in section 3.3.1. In order to include the pod effect, a dataset of corrections were done based on model test to make compensation for the difference between pod thruster and conventional propeller on thrust force in longitudinal and side direction and yaw moment. Corrections were implemented for 360 degrees in 18 degrees step. Linear interpolation is performed in between data points. However, a very limited set of model tests

data were used for this case. So verification of this numerical model is considered to be necessary and important.

Verification of this numerical thruster model is done in calm water condition with vessel running at designed speed (14kn). In order to match this numerical thruster to the real model thruster, adjusting pitch ratio, blade area ratio and pod area are needed. In this thesis work, pitch ratio was tuned from 1.2 to 1.5; blade area ratio was increased from 0.435 to 0.5; wetted pod area was reduced from 23.34 m^2 to 15 m^2. Under these conditions, good agreement between numerical model and real thruster model was obtained with RPS_exp/RPS_Ringen=0.9923, Thrust_exp/Thrust_Ringen=1.014 (The subscript Rigen means the model implemented into *Vesim* by Ringen, 2010, refer to section 3.3.1). More results to show the agreement of the thrusters characteristics in waves are shown in Fig 3.4.

3.3.2 Empirically azimuth thruster model through model tests

Another empirically based propulsion model is applied to represent the forces from the thrusters in paper 4. The simulation model is based on a systematic series of open water tests with a model of the Azipull thruster (Berg, 2002), where advance number, azimuth angle and propeller pitch were varied systematically. The model tests reported by Berg (2002) were performed by MARINTEK, while the implementation of the propulsion model was done by Rolls-Royce Marine. The empirical propulsion model is interpolating in the model test results in tabular form to produce a propeller open water curve for the instantaneous value of pitch and azimuth angle. The propulsion model also contains a correction term to account for the flow straightening effect of the hull when the ship is turning. This model is used for the study to predict speed loss in oblique waves. More details were presented in Paper 4.

3.3.3 Comparisons of Kt for the three thruster models

Fig. 3.4 shows the thrust curve comparisons between the real model thruster used in the test and the two numerical thrusters. '*Kt_exp*' means the thrust curve of the model thruster which is obtained from the propulsion test; '*Kt_TD (Ringen)*' and '*Kt_TD (Berg)*' curves are obtained by the implementing the corresponding numerical model in time domain simulation (models description refer to section 3.3.1 and section 3.3.2); '*Kt_FD(exp)*' is obtained by directly using the '*Kt_exp*' curve in the frequency domain study of speed loss. The calculated points for *J* and *Kt* are obtained from their attainable speeds in waves respectively. It can be seen that the three thruster curves are generally in good agreement with each other. '*Kt_TD (Ringen)*' is slightly higher than '*Kt_exp*' for J<0.75. The deviation is increasing with decreasing of J. '*Kt_TD (Berg)*' is a little lower than '*Kt_exp*' for J<0.78. Since the '*Kt_exp*' curve is directly applied in the frequency domain calculations, very good agreement with '*Kt_FD(exp)*' curve is obtained, as expected.
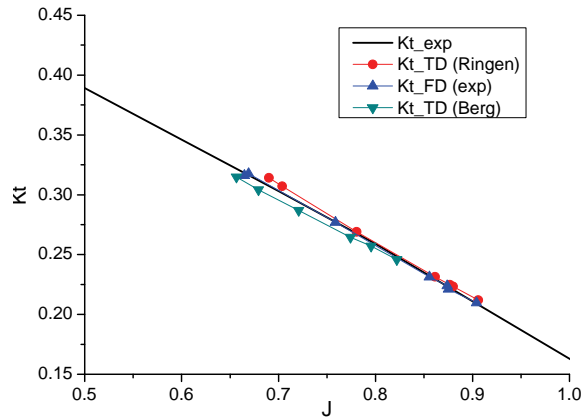
Fig. 3.4 Kt comparisons for the three thruster models

3.4 Speed loss in frequency domain

Speed loss in regular head sea condition with vessel running along a straight line without rudder angle can be simulated in the frequency domain. Results of such calculations are shown in Paper 1 and Paper 2. In the frequency domain simulation, an iterative procedure is utilized to predict the forward speed that gives equilibrium between thrust and resistance. The difference between the power prescribed and the power calculated is calculated first. The velocity is then reduced or increased according to the power difference, and power is calculated a second time. The velocity is iterated on until the propulsion power balance within a small margin. The main procedure is based on the computational algorithm (Berget et. al. 2009), shown in Fig. 3.5:
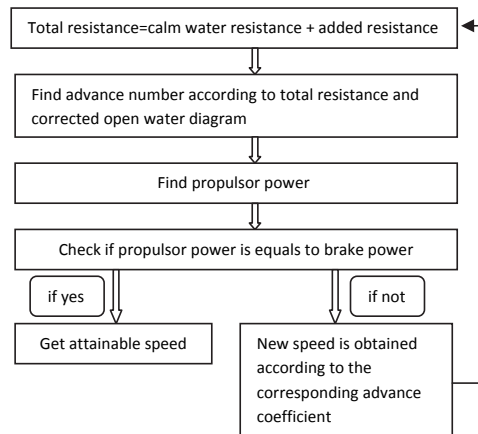

Fig. 3.5 Speed loss computational algorithm in the frequency domain

Provided the initial vessel speed input, the total resistance including the calm water resistance and the added resistance are calculated. Then based on calculated total resistance, the open water diagram is applied to find the corresponding torque and advance number. After that the delivered propulsion power is calculated by equation (3.20).

$$P_D(kw) = \frac{2\pi}{1000}\rho D^5 n^3 \frac{K_Q}{\eta_R} \tag{3.20}$$

At last one should check if the delivered propulsion power equals the power delivered to the propeller. If they are equal, the final attainable speed is obtained. Otherwise, one should recalculate the new speed according to the known corresponding advance number and upgrade the total resistance until the equilibrium point is found.

3.5 Speed loss in time domain

Speed reduction process of a ship during seakeeping and maneuvering condition can be simulated in the time domain. Calculations were performed by using the *Vessel simulator* (Vesim) (Fathi, et al. 2009). Relevant results were shown in Paper1 to Paper 4.

Three coordinate systems are used in Vesim. The first one is North-East-Down (NED) coordinate system. x_n-axis is directed towards north; y_n-axis is directed to east and z_n-axis pointed downwards to the center of the earth. This coordinate system is used to locate the vessel position.

The second coordinate system is body-fixed reference coordinate system, which is a frame moving with the hull. x_b is directed from aft to fore; y_b is directed to starboard and z_b is pointed downwards. This coordinate system is used to present the linear and angular velocities. The origin of the coordinate system is located at the center of gravity.
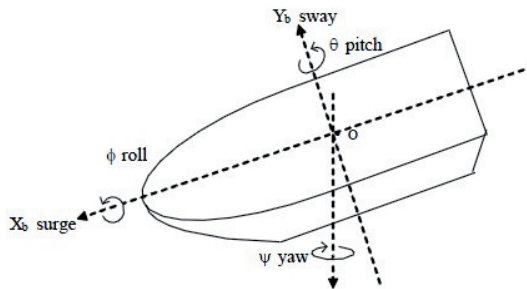

Fig. 3.6 Body-fixed coordinate system

The third coordinate system is applied to describe the positions on the vessel, which is used to specify for example thruster position on the vessel. This coordinate system is a left-hand

47

coordinate system with the origin at the intersection between the aft perpendicular, centerline and the base line. X-axis is pointing towards forward, y-axis directs starboard and z-axis is pointing upwards.

The equations of motion in six degrees of freedom were solved at each time step in body fixed coordinate system in full scale.

$$(M + A_{jk})\ddot{\eta}_j = \sum F_k \tag{3.21}$$

M is the mass of the body; A_{jk} is added mass in j-direction due to exciting force in k-direction; η_j is the position of the body in j-direction; $\sum F_k$ is the sum of all the external forces in k direction. In this thesis, the external forces from calm water resistance, incoming wave resistance and thrust from propulsion system are considered.

$$\sum F_k = F_{calm\_k} + F_{wave\_k} + F_{thrust\_k} \tag{3.22}$$

Added mass and damping are frequency dependent. However, in the time domain calculation, there are many excitation frequencies, for instance in a transient response. Thus, the radiation forces are calculated by means of a convolution integral using retardation (kernel) functions, to include the so-called 'memory effects'. Following the work by Cummins (1962), the radiation force in time domain is written as:

$$F = \int_0^t h(t - \tau)\dot{\eta}(\tau)d\tau \tag{3.23}$$

Where $h_{jk}(t)$ is retardation function, which can be evaluated by

$$h_{jk}(t) = -\frac{2}{\pi}\int_0^\infty w(A_{jk}(w) - A_{jk}(\infty))\sin wt dw \tag{3.24}$$

$$h_{jk}(t) = \frac{2}{\pi}\int_0^\infty (B_{jk}(w) - B_{jk}(\infty))\cos wt dw \tag{3.25}$$

Where $A_{jk}(\infty)$ and $B_{jk}(\infty)$ are added mass and damping matrix at infinite frequency. Calculation of $h_{jk}(t)$ requires information on the behavior of either A_{jk} or B_{jk} at all frequencies.

3.6 Preference on Speed loss calculation in frequency domain or in time domain

Two criteria are necessary for judging if speed loss investigation should be performed in the frequency domain or in the time domain.

- If speed loss process is of interest

In the cases that where only finally attainable speed in waves is of interest, both frequency domain and time domain can be applied. Difference between them is that only the mean values for speed, thrust and resistance (including calm water resistance and added wave resistance) are produced in a frequency domain study, while all the variables were found oscillating with encounter frequency in a time domain calculation. But if the same thrust and resistance curves are implemented, the same mean values will be achieved in the two methods in the same wave condition under the assumption that transient effect is not included. This has been shown in Paper 2.

However, the process of how the converged speed is achieved from designed speed can only been obtained from time domain study. Also time series of thrust and resistance only exist in time domain simulation.

- Transient phenomenon

Speed reduction due to transient environmental effect is best calculated in a time domain method. There are several scenarios in which we consider transient phenomena. One example is changing heading direction during maneuvering. This will cause continuously changing forces in surge, sway and yaw directions. Another example is propeller ventilation, which might happen in heavy sea states with severe ship motions, or when the ship is operating in very light displacement condition. Ventilation reduces the thrust, and the occurrence of ventilation is sudden and irregular. The effect of ventilation on achievable speed has been investigated by Prpic-Orsic and Faltinsen (2012). A third example is slamming or green water on deck, which excites highly transient ship motions. Due to their inherently non-linear and time dependent nature, numerical simulations should be carried out in the time domain.

Frequency domain method is suitable for calculating speed loss under steady state vessel motion and normal propeller behavior in moderate sea states. Computing speed loss in the frequency domain is much simpler and quicker to perform, so whenever a frequency domain method is considered sufficient, it is preferable over a time domain method.

Chapter 4 Prediction of sea margin and speed loss in irregular waves

This thesis is focusing on a study of speed loss in regular waves. However, since regular waves are hardly encountered outside the laboratory environment, the final aim must be to predict speed loss in realistic, irregular sea states during the typical maneuvers of ship operations. Such predictions are useful in many applications, for instance in the prediction of sea margin. However, time doesn't allow a detailed study of speed loss in irregular waves. This is left as a recommendation for further work. Only an outline of how such calculations can be done is given here, based on existing knowledge and knowledge obtained through the work on this thesis.

4.1 Prediction of power increase in irregular wave from model tests

4.1.1 Recommendation to ITTC procedure: Prediction of 'ship propulsion point' from 'model propulsion point'

Conducting self-propulsion tests in irregular waves is the most direct and simple way to get the power increase in actual sea states. However, this is not in general a satisfactory solution, since the results are restricted to a particular irregular wave condition which is impossible to generalize to other sea states. So in order to predict power increase in irregular waves, tests are often carried out in regular wave conditions to get transfer functions and then to predict power increase for the wanted irregular wave conditions using the transfer functions. Four different methods are proposed in the ITTC Recommended Procedure 7.5-02-07-02.2 (2008). They are:

- Direct Power Method. This method is based on the assumption that the mean increase in delivered power in regular waves is proportional to the square of wave amplitude. Mean increase in power in irregular waves is calculated from the power transfer functions measured in regular waves by the equation (4.1).

$$\delta P_M = 2\int_0^\infty \frac{\delta P(\omega)}{\varsigma_a^2} S(\omega)d\omega \qquad (4.1)$$

- Torque and Revolution Method (QNM). This method is based on the assumption that the mean increase in propeller torque and revolutions in regular waves are proportional to

the square of the wave amplitude. Mean increase in torque and revolution in irregular waves are calculated from the torque transfer function and the revolution transfer function in regular waves, see equations (4.2) and (4.3). Based on that, the mean increase in power in irregular waves is calculated by equation (4.4).

$$\delta Q_M = 2\int_0^\infty \frac{\delta Q(\omega)_M}{\varsigma_a^2} S(\omega)d\omega \tag{4.2}$$

$$\delta n_M = 2\int_0^\infty \frac{\delta n(\omega)_M}{\varsigma_a^2} S(\omega)d\omega \tag{4.3}$$

$$\delta P_M = 2\pi\{(Q_{SW} + \delta Q_M)(n_{SW} + \delta n_M) - Q_{SW}n_{SW}\} \tag{4.4}$$

- Thrust and Revolution Method (TNM). The assumption here is that the mean increase in propeller thrust and revolutions in regular waves are proportional to the square of wave amplitude. Mean increase in thrust in irregular waves is calculated from the thrust transfer function in regular waves, see equation (4.5). Mean increase in revolutions in irregular waves is calculated from the revolutions transfer function in regular waves, see equation (4.6). Based on that, the mean increase in power in irregular waves is calculated by equation (4.7).

$$\delta T_M = 2\int_0^\infty \frac{\delta T(\omega)_M}{\varsigma_a^2} S(\omega)d\omega \tag{4.5}$$

$$\delta n_M = 2\int_0^\infty \frac{\delta n(\omega)_M}{\varsigma_a^2} S(\omega)d\omega \tag{4.6}$$

$$\delta P_M = 2\pi\frac{K_Q}{J^3}\rho(1-w)^3V^3D^2 - P_{SW} \tag{4.7}$$

- Resistance and Thrust Identity Method (RTIM). In this method, added resistance transfer function is utilized to calculate mean increase in added resistance in regular waves, as shown in equation (4.8). Then based on the relationship between total resistance and thrust in equations (4.9) and (4.10), the increased power in irregular waves can be obtained by equation (4.11).

$$\delta R_M = 2\int_0^\infty \frac{\delta R(\omega)_M}{\varsigma_a^2} S(\omega)d\omega \tag{4.8}$$

$$R_M = R_{SW,M} + \delta R_M \tag{4.9}$$

$$T_M = \frac{R_M}{1 - t_{SW}} \qquad (4.10)$$

$$\delta P_M = 2\pi \frac{K_Q}{J^3} \rho (1-w)^3 V^3 D^2 - P_{SW} \qquad (4.11)$$

For equations (4.1) to (4.11), subscript M means mean value; SW means still water. P means delivered power; $S(\omega)$ means irregular wave spectrum; ω is wave circular frequency; ς_a is regular wave amplitude; T is propeller thrust; Q is propeller torque; n is propeller revolutions per second; t is thrust deduction; w is wake fraction; D is propeller diameter and V is ship model velocity.

For the above four methods, the Direct Power Method has advantages both in theory and in practical use. Since the assumption in the method that power increase in regular waves is proportional to the square of the wave amplitude is closer to reality than the assumptions in the other three methods it is expected that it will give better results. Also the Direct Power Method does not require knowledge of the particulars of the propeller. These advantages have already been pointed out in the ITTC Recommended Procedure 7.5-02-07-02.2 (2011).

However, for all the four methods above, self-propulsion tests in calm water and in regular waves should be carried out at 'ship propulsion point' instead of at 'model propulsion point'. This means tow-rope force should be used to make up for the frictional resistance coefficient difference between model scale and full scale ship. But applying towrope force to make the correction is difficult, time consuming and expensive. So an estimation method to get 'ship propulsion point' from 'model propulsion point' is an attractive alternative.

In this thesis, the suggested method to predict 'ship propulsion point' from 'model propulsion point' is specified as follows. The method has to be worked in cooperation with the method proposed in Paper 1 or Paper 2 to predict speed loss at 'ship propulsion point' when towrope force is not applied during the tests.

1. Model tests are carried out in calm water or in regular waves without applying towrope force with propeller working at 'model propulsion point'. When the designed speed V_m is obtained, the value of the delivered power P is recorded at the same time through the measurement of the torque and propeller speed.
2. By applying the method proposed in Paper 1 (linear) or Paper 2 (nonlinear), the attainable speed at the 'ship propulsion point' V_s is obtained at the same power value P.
3. Thrust force at 'ship propulsion point' with delivered power equal to P can be obtained by $T_S = P\eta_D/(V_S(1-t))$. Here η_D is propulsive efficiency and t is thrust deduction.
4. From thruster open water characteristics curve, the relationship between K_T and J are known. For example, it can be written as polynomial curve:

$$K_T = aJ^2 + bJ + c \tag{4.12}$$

Where a, b, c are regression coefficients.

$$K_T = T_S / (\rho n^2 D^4) \tag{4.13}$$

$$J = V_S / (nD) \tag{4.14}$$

5. Insert equations (4.13) and (4.14) into equation (4.12), the only unknown variable n can be found. So the ship propulsion point is obtained.

Note that in step 3, the thrust deduction fraction for the actual wave condition should be used.

4.1.2 Recommendation to ITTC procedure: Prediction of thrust deduction in waves

Another limitation in the ITTC procedure when predicting power increase in irregular waves based on model experiments in regular waves is that the thrust deduction in waves is taken to be the same value as in still water. As has already been discussed in this thesis in Chapter 3, Paper 4 and Paper 5, the thrust deduction in waves is not always the same as the calm water value. Significant difference between them was observed when the wave length was approaching ship length, with wave length divided by ship length varying from 0.9 to 1.3. Two methods to obtain thrust deduction factor in waves from model tests are suggested in this thesis:

1. Perform both resistance and propulsion test at same speed in the same wave conditions.

2. Perform the propulsion test at (at least) two different tow rope forces for the same speed and wave condition.

More details of the two methods are given in Paper 5.

4.2 Prediction of speed loss in irregular wave from numerical methods

Speed loss prediction in irregular waves is always done by assuming that the waves are a narrow banded process. It is then legitimate to cut the wave record into successive regular wave parts where each wave has a certain amplitude and frequency. Prpic-Orsic and Faltinsen (2012) followed the procedure proposed by Faltinsen et al. (1980) and divided the time series of irregular sea states into regular waves by locating the zero-upcrossing points. The time between two zero-upcrossing points is taken as wave period and the half distance between two maximum inside this time period is taken as wave amplitude. Ship motions, wave resistance and propeller performance can be calculated by only considering regular waves. This method can be used for any irregular sea state.

In order to calculate the thrust diminution factor β, narrow banded analysis can also be applied for the amplitude of relative motion. The relative motion can be described by the Rayleigh function. Details of how to do it can be found in Minsaas et al. (1983). This method was implemented into *ShipX Ship Speed and Powering* (Berget, et al. 2009) and *Vessel Simulator* (Fathi et al., 2009) to enable speed loss calculation in irregular waves in frequency domain and time domain respectively.

4.3 Prediction of sea margin

Sea margin can be defined as the margin which should be added to the estimation of the speed-power relationship for a newly built ship in ideal weather conditions to allow for the operation of the ship in realistic conditions. In practice this does not mean that the ship must meet full speed in all weather conditions, but that it can sustain its service (design) speed over a realistic percentage of conditions (ITTC recommended procedures and guidelines (7.5-02-03-01.5), 2008).

In order to calculate sea margin, speed and power relationships for the newly built condition and the supposed operation condition are all necessary. Resistance increase in the operating condition due to wave, wind, current, shallow water effect, displacement change and fouling effect on ship hull and propeller surface have all to be taken into consideration. Standard procedures to calculate sea margin are given in ITTC recommended procedures and guidelines (7.5-02-03-01.5, 2008).

Here some recommendations are made based on the work in this thesis. In the procedure of predicting self-propulsion characteristics, the effect of thrust and torque change in waves is considered by introducing a thrust diminution factor β as proposed by Faltinsen et al. (1980). The thrust diminution factor β includes the effects of out-of-water effect, wave pattern generated by the propeller when it is approaching the free surface and the Wagner effect to describe the dynamic effect of propeller blades coming out of water. However, other effects should also be considered when predicting sea margin since more complicated operating conditions than straight ahead without steering can be encountered by voyaging ships. Thrust deduction factor changes due to ventilation and due to maneuvering in waves are two important factors that should be taken into account. Propeller ventilation leads to a sudden large loss of thrust and torque, which might lead to propeller racing and possibly damaging dynamic loads, as well as noise and vibrations. Propeller ventilation has been studied by several researchers both experimentally and numerically such as Fleischer (1973), Koushan (2006a, 2006b, 2006c, 2007a, and 2007b), Califano and Steen (2011a, 2011b) and Smogeli (2006). Change of wake and thrust deduction factor due to seakeeping and maneuvering is also an effect that should be considered. Remarkable change of thrust deduction can happen when the ship encountering severe sea states or under heavy steering. For the cases studied in this thesis,

with a self-propelled model sailing along straight line course in waves, the thrust deduction factor reached up to two times the calm water value when the wave length approached the ship length. Even bigger change is expected to happen under bigger maneuvering operations. More details are given in this thesis Chapter 2, Paper 4 and Paper 5 to see the change of thrust deduction factor under seakeeping and maneuvering conditions. So, only applying the calm water thrust deduction to evaluate the sea margin is not really reasonable and satisfactory.

4.4 Wind force

In the work in this thesis, the effect of wind has not been taken into account. This is not because wind force is not important for the speed loss. Therefore, for the sake of completeness, a description of how the effect of wind can be included in speed loss estimation, using the established methods found in the literature, is given.

4.4.1 Definition of wind force

The resistance increase due to wind can be calculated according to the ITTC recommended procedures and guidelines (7.5-04-01-01.2, 2005), as outlined in the following.

$$R_{AA} = \frac{1}{2}\rho_A V_{WR}^2 C_{AA}(\psi_{WR})A_{XV} \tag{4.15}$$

using

$$C_{AA}(\psi_{WR}) = C_{AA0}K(\psi_{WR}) \tag{4.16}$$

Where

A_{XV} : Area of maximum transverse section exposed to the wind

$C_{AA}(\psi_{WR})$: Wind resistance coefficient

C_{AA0} : Wind resistance coefficient in head wind

$K(\psi_{WR})$: Directional coefficient of the wind resistance

V_{WR} : Relative wind velocity

ρ_A : Mass density of air

Wind resistance coefficient is mostly decided based on data derived from model test carried out in a wind tunnel. Many researchers make contributions in this field by carrying a wide range of model tests using various ships in wind tunnels. Such as Andersson (1978) who used a model of a 211m container ship with 19 different deck configurations; Blendermann (1997) did wind

tunnel tests of ten container configurations resembling random configurations on two ships. Other investigations have been carried out for more general ship types, for example Van Berlekom (1981), Aage (1968) and Chen (1995).

Wind tunnel tests are the most accurate procedure to estimate the wind forces on particular ships and offshore structures. However, these tests are time consuming and very expensive. So some numerical methods are generally used complementary or alternatively. For example, Isherwood (1972) proposed expressions for the forces and moment coefficients which are derived from multiple regression analysis of previously published experimental results; Blendermann (1993, 1994) derived expressions for the wind forces coefficients in the longitudinal and transverse directions and also the yaw and rolling moments. More research work was done by Gould (1982), Blendermann (1995) and others.

Natural boundary layer of the wind is formed when the air flows over the ocean surface. This means the wind speed at the sea surface is zero and increasing with the distance relative to the water surface. But if the wind is caused by the ship movement, then no boundary layer exists in this case and wind profile is homogenous (Andersen, 2012), see Fig. 4.1. The actual wind field encountered by the part of the ship above the waterline is a combination of the natural wind field with boundary layer and ship forward speed, see Fig. 4.2. Where φ describes the relative wind direction.
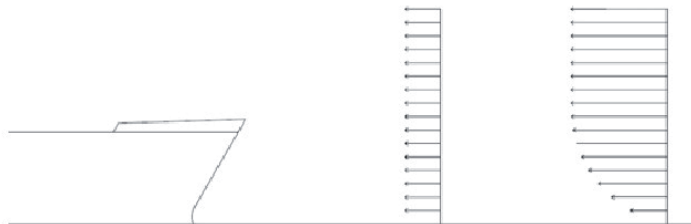

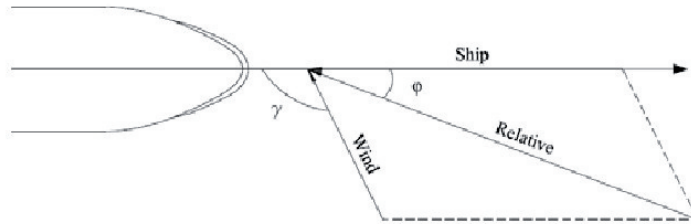Fig. 4.1 Local wind field caused by ship and the natural wind gradient at sea (Andersen, 2012)

Fig. 4.2 Relative wind direction (Andersen, 2012)

4.4.2 Speed loss due to wind resistance

With the methods described above, the additional resistance due to wind can be determined. Firstly, in speed loss tests, the wind force in head direction can then be included by modifying the applied tow rope force (fan speed). This method is considered to be the easiest and also an accurate way to do it. It is of course also possible to apply the effect of wind by using the same correction procedure as is outlined for correction of the lack of towrope, which is described earlier in this chapter and in Papers 1 and 2.

Secondly, when speed loss is found numerically, the wind resistance is added as a modification of the total resistance in the actual sea condition, and the rest of the calculation procedure is unaltered. This method to calculate speed loss due to wind effect is implemented in, *ShipX Ship Speed and Powering* (Berget, et al. 2009) and *Vessel Simulator* (Fathi et al., 2009). In *ShipX Ship Speed and Powering*, speed loss due to wind effect is calculated in the frequency domain. Definition of the ship transverse sectional area exposed to the wind and relationship between wind speed and sea states should go first. Then a wind coefficient is generated according to the results from wind tunnel tests carried out by Aage (1971). In the *Vessel Simulator*, speed loss due to wind effect is calculated in the time domain. More transient effects such as steering and changing of heading can be included. Wind resistance is calculated by the combination of wind transfer function and wind spectrum. This method is originally proposed by Fossen (2002). Static wind force and Harris and NPD wind gust spectrum are implemented in the *Vessel Simulator*.

Chapter 5 Conclusions and Recommendations for future work

5.1 Conclusions

Speed loss of an 8000 DWT tanker was studied both experimentally and numerically. The main purpose of the thesis is to find the physical reasons for speed reduction of a ship during seakeeping and maneuvering condition. The influences from environment, ship and propulsion system were all studied. Important conclusions are as follows.

Speed loss in head sea conditions

- Without using towrope force in the speed loss tests, speed reduction is underestimated, since the friction resistance coefficient is larger in model scale than in full scale, so that in model scale the added resistance due to waves is a smaller percentage of total resistance than in full scale.
- In order to make up for the discrepancy caused by lacking of towrope force, both a linear and a non-linear correction method is proposed in this thesis. These prediction methods improve the results significantly and show good correlation with the numerical results. The non-linear method performs better than the linear method.
- Reduction of speed loss in waves up to order of 10% can be gained by relatively minor changes to the bow shape of a vessel. The bulb had a positive influence on calm water resistance and negative effect on added wave resistance in the case studied. The latter one is more dominating. Therefore, model A with bulb reached the lowest attainable speeds in waves, while model C without bulb achieved the highest attainable speeds, when the propulsion power was the same for both models.
- Both time domain method and frequency domain method can give a good prediction of speed loss in head sea conditions.
- Added resistance predicted by the Gerritsma and Beukelman (G&B) method show better agreement with experimental data than the Direct Pressure Integration (DPI) method in this case. The DPI method is sensitive to the hull form, and doesn't properly predict how the added resistances change with bow shape.
- Without considering the loss of thrust due to in-and-out of water effect and ventilation, propulsive efficiency change in waves is mainly due to the change of propulsion point, for the moderate waves considered in this study. Speed reduction in waves is increasing

with the increase of added wave resistance. When wave length approaches ship length, speed loss reaches its peak value. Propulsive efficiency reaches its lowest point in this wave length range.

Speed loss in head sea conditions with zigzag maneuver

- The main reasons for the speed reduction for a vessel doing a zigzag maneuver in head sea can be attributed to added wave resistance, loss of thrust in the ship heading direction due to steering, and added resistance caused by yawing.
- The time-domain numerical simulations are in good agreement with the model tests for the straight-ahead conditions and for zigzag maneuvers in calm water. However, the numerical method underestimates speed reduction for a ship doing zigzag maneuver in heading waves.
- The magnitude of the stabilized overshoot angles are influenced by the converged speed results. The higher the attainable speed values get, the bigger stable overshoot angle is achieved. The lower the attainable speed value, the smaller stable overshoot angle is achieved.

Speed loss in oblique wave conditions

- Speed reduction of a vessel sailing along a straight line in oblique waves is due to added wave resistance and loss of thrust in the ship heading direction due to steering.
- In the model tests, due to the limitation of the ocean basin dimension, converged speed is not always available. A method is proposed in this thesis to predict the converged speed in waves. This method can give good prediction of the attainable speed. Thrust deduction factor gives a big influence on the converged speed values.
- When the power is kept constant in head sea and bow sea conditions, the higher the calm water speed, the less speed drop will be achieved in waves. The lower the calm water speed is, the bigger speed reduction will occur in waves.
- Speed reduction due to added resistance and due to steering are at almost the same level for head sea and bow sea conditions where with higher added wave resistance and very small rudder angle is needed; while with the increasing of heading angle to beam sea, speed loss due to steering plays a more important role than added wave resistance. This is because in order to keep the vessel sailing along the designed straight line course in waves, more rudder angle is needed which leads more thrust force deduction in the longitudinal direction.
- Propeller-rudder system has better ability to keep the vessel running at designed speed than azimuth thruster. Due to propeller thrust is not decomposed by the rudder angle and higher ratio of side force/longitudinal force is exist for the propeller-rudder system, so less steering angle and higher thrust is produced.

60

5.2 Recommendations for future work

- More advanced methods to predict added wave resistance, transverse sway drift force and mean yaw moment are needed. Since less satisfactory numerical results were observed for speed prediction in oblique waves than in head waves. More accurate prediction of wave forces seems to have the potential to improve the results.

- Generally speaking, the present numerical method can give good predictions of speed loss in regular waves without the existence of wind force. But in the environmental conditions with irregular seas and wind gusts coming from all directions the ship will have increased unsteady motions and the propulsion system will have more dynamic loads. Therefore, if the present numerical method can still give good predictions on speed loss in such a complicated environmental condition should be investigated.

- In this thesis, speed loss is studied using one selected tanker equipped with twin azimuth thrusters. In order to give more direct and practical instructions to the shipping industry about the relationship between vessel speed and environmental conditions, more categories of ocean going vessels equipped with their preferable propulsion systems should be studied for their speed keeping ability while sailing in the real sea environment.

- How the thrust deduction changes due to waves and steering should be further studied. Therefore, it is recommended to perform future propulsion tests in waves such that thrust deduction can be found, for instance by performing tests at two different propeller loadings in the same speed and wave condition.

References

Aage, C., *Vindkræfter på Skibe*, Institut for Skibs- og Havteknik, Danmarks Tekniske Højskole, 1968.

Aage, C., *Wind coefficients for nine ship models*, Hydro and Aerodynamisk laboratorium, Lyngby, Danmark, report no. A-3, May, 1971.

Aarsnes, J. V., Steen, S., *Experimental Methods in Marine Hydrodynamics*, Lecture Note for TMR 7, Department of Marine Technology, NTNU, 2008

Aertssen, G., *Service Performance and Trials at Sea.* App V Perf Committee, 12th, ITTC, 1969.

Alterskjær, S. *R&D phase 1, calm water tests with 3 different fore ships*. MARINTEK Report 530635.00.03, Trondheim, Norway, November, 2010.

Amini, H., *Azimuth Propulsors in Off-design Conditions*, Doctoral Theses at NTNU, 2011:186, ISBN 978-82-471-2921-0, 2011.

Andersson, G.O., *Untersuchung der Fahrtverluste durch Wind und Seegang bei einem schnellen Einschrauben-Containerschiff*. Bundesministerium für Forschung und Technologie, Meerestechnik, 1978.

Ayaz, Z., Spyrou, K. J., Vassalos, D., *An Improved Numerical Model for the Study of Controlled Ship Motions in Extreme Following and Quartering Seas*. The Proceedings of IFAC Conference on Control Applications in Marine Systems, Glasgow, UK, July, 2001.

Ayaz, Z., Turan, O., and Vassalos, D., *Manoeuvring and Seakeeping aspects of Pod-driven Ships*. Proc. IMechE vol. 219, Part M: J. Engineering for the Maritime Environment. 2005.

Ayaz, Z., Vassalos, D., Spyrou, K. J., *Manoeuvering Behaviour of Ships in Extreme Astern Seas*. Ocean Enigneering, Vol. 33, pp. 2381-2434, 2006.

Bailey, P. A., Hudson, D.A., Price, W. G., Temarel, P., *Time Simulation of Ship Manoeuvres in Waves*. HSVA's CPMC, International Workshop on Ship maneuverability, Hamburg, Germany, October, 2000.

Bailey, P. A., Price, W. G., Temarel, P., *A Unified Mathematical Model Describing the Manoeuvring of a Ship Travelling in a Seaway*. Trans. RINA, 140:131-149, 1997.

Belibassakis, K.A., *Effects of wave-induced ship motion on propeller-hull interaction with application to fouling estimation and propulsion optimization*. 13th Congress of Intl. Maritime Assoc. of Mediterranean, Turkey, 12-15, Oct. 2009.

Belibassakis, K.A., Polotis, G.K., *A non-linear velocity based boundary element method for the analysis of marine propellers in unsteady flow*. International Shipbuilding Progress, 45, pp.93-133, 1998.

Belibassakis, K.A., Polotis, G.K., *Unsteady performance of propellers with non-conventional blade geometry by a vorticity based panel method*. Pro. 10th Congress of International Maritime Association of the Mediterranean, IMAM, Rethymnon-Crete, 2002.

Berg, A., *Open water tests with Azipull*, MARINTEK Report 601973.00.01, Trondheim, Norway, June 2002.

Berget, K., Fathi, D. and Ringen, E. *ShipX Speed and Powering, Theory Manual*. MARINTEK, Trondheim, 2009.

Bhattacharyya, R., *Dynamics of Marine Vehicles*. Wiley Interscience, ISBN 0471072060, 1978.

Blendermann, W., *Estimation of wind loads on ships in wind with a strong gradient*. Proceedings of the 14th International Conference on Offshore Mechanics and Arctic Engineering (OMAE), New York: ASME, V1-A, p. 271-7, 1995.

Blendermann, W., *Messung der Windlast an zwei Containerschiffen in realem Ladezustand im Windkanal*, Institut für Schiffbau der Universität Hamburg, 1997.

Blendermann, W., *Parameter identification of wind loads on ships*. J. Wind Engng. Ind. Aerodyn, 51:339-51, 1994.

Blendermann, W., *Wind loads on moored and manoeuvring vessels*, Proceedings 12th International Conference on Offshore Mechanics and Arctic Engineering (OMAE), New York: ASME, Vol. 1, p. 183, 1993.

Buhaug, Ø., et al. *Second IMO GHG study 2009*. International Maritime Organization (IMO), London, UK 24, 2009.

Califano, A., Steen, S. *Identification of ventilation regimes of a marine propeller by means of dynamic-loads analysis.* Ocean Engineering 38 (14-15), pp. 1600-1610, October 2011(a).

Califano, A., Steen, S. *Numerical simulations of a fully-submerged propeller subject to ventilation.* 38, (14-15), Pages 1582-1599, October 2011(b).

Carrica, P.M., Paik, K.J., Hosseini, H.S. Stern, F., *URANS Analysis of a Broaching Event in Irregular Quartering Seas*. Journal of Marine Science and Technology. Volume 13, Issue 4, pp 395-407 November 2008.

Chen Q, Gu Z, Sun T, Song S., Wind environment over the Helideck of an offshore platform. J Wind Engng Ind Aerodyn, 54/55:621-31, 1995.

Chuang, Z. and Steen, S. *Prediction of speed loss of a ship in waves*. In Symp. Marine Propulsors (SMP'11), Hamburg, 2011.

Chuang, Z., Steen, S. *Experimental and Numerical Study of Stem Shape Influence on Speed Loss in Waves*. Ship Technology Research. VOL. 59, NO. 2, pp:4-17, April 2012 (a).

Chuang, Z., Steen, S., *Speed loss due to seakeeping and maneuvering in zigzag motion*. Ocean Engineering, Volume 48, pp. 38–46, January 2012 (b).

Clarke, D., *A two-dimensional strip method for surface ship hull derivatives: Comparison of theory with experiment on a segmented tanker model*. J. Mech. Eng. Sci. 14 (7), 1972.

Cummins, W. E., *The impulse response function and ship motions*. Schiffstechnik 9(47), pp. 101-109, 1962.

Faltinsen, O. M., Minsaas, K. J., Liapias, N. & Skjørdal, S.O. *Prediction of Resistance and Propulsion of a Ship in a Seaway*. Proceedings of 13th Symposium on Naval Hydrodynamics, Ed.T.Inui, The Shipbuilding Research Association, Japan. 1980.

Faltinsen, O.M., *Hydrodynamics of High-Speed Marine Vehicles*. Cambridge University Press, ISBN: 978-0-521-84568-7, 2005.

Faltinsen, O.M., *Modelling of Manoeuvring with Attention to Ship-ship Interaction and Wind Waves*, 2nd International conference on ship manoeuvring in shallow and confined water: ship to ship interaction, 2011.

Faltinsen, O.M., Zhao, R., *Numerical predictions of ship motions at high forward speed*. Philosophical Transactions of the Royal Society of London. Series A: Physical and Engineering Sciences 334.1634, 241-252, 1991.

Fang, M. C., Luo, J. H., and Lee, M. L., *A Nonlinear Mathematical Model for Ship Turning Circle Simulation in Waves*. Journal of Ship Research, Vol. 49, No. 2, pp. 69-79, June 2005.

Fang, M.C., Chen, G.R., *On the nonlinear hydrodynamic forces for a ship advancing in waves*, Ocean Engineering 33, pp. 2119-2124, 2006.

Fathi, D. et al. *ShipX Vessel Simulator, Theory Manual*. MARINTEK, 2009.

Fathi, D., Hoff, J.R., *ShipX Vessel Response, Theory Manual*. MARINTEK, Trondheim, 2008.

Fleischer, K.P., *Untersuchungen über das Zusammenwirken von Schiff und Propeller bei teilgetauchten Propellern (Investigations of the interaction between ship and propeller for partly submerged propellers)*. Bericht Nr. 35/73 Forschungszentrum des Deutschen Schiffbaus. Hamburg, Germany (in German). 1973.

Fossen, T.I., *Marine control systems: Guidance, navigation and control of ships, rigs and underwater vehicles*. Trondheim,, Norway: Marine Cybernetics, 2002.

Fujii, H. and Takahashi, T., *Experimental study on the resistance increase of a ship in regular oblique waves*. Proceeding of 14th ITTC, pp. 351-360, 1975.

Gerritsma, J., Beukelman, W., *Analysis of the resistance increase in waves of a fast cargo ship*. International Shipbuilding Progress, Vol.19, No.217, pp. 285-292, 1972.

Gould, R.W.F., *The estimation of wind loads on ship superstructures*. The Royal Institution of Naval Architects, monograph, No. 8, p. 34, 1982.

Grimstad, D. K., *Added resistance and Speed Loss Due to Steering*. Master Thesis at NTNU. 2009.

Guo, B. *Numerical and Experimental Investigation of Added Resistance in Waves*. PhD thesis, Norwegian University of Science and Technology, 2011.

Guo, B., Steen, S. *Evaluation of Added Resistance of KVLCC2 in Short Waves*, Journal of Hydrodynamics, 23(6) pp: 709-722, 2011.

Guo, B., Steen, S. *Experiment on added resistance in short waves*. 28th Symposium on Naval Hydrodynamics. Pasadena, California, California Institute of Technology, 2010.

Guo, B., Steen, S., Deng, G. B. *Seakeeping prediction of KVLCC2 in head waves with RANS*. Applied Ocean Research 35(0): 56-67, 2012.

Hansen, S. V. *Performance Monitoring of Ships*. PhD thesis, Technical University of Denmark, 2011

Havelock, T.H., *The Pressure of Water Waves Upon a Fixed Obstacle*. Proceedings of the Royal Society, London, England, 1940.

Hollenbach, K. U., *Estimating resistance and propulsion for single-screw and twin screw ships*. Ship Technology Research 45, 1998.

Holtrop, J. A., Statistical renanalysis of resistance and propulsion data. International Shipbuliding Progress 31, 1984.

Andersen, I. M. V., *Wind-Tunnel Investigation of Wind Loads on a Post-Panamax Container Ship as a Function of the Container Configuration on Deck,* 11th International Marine Design Conference, 2012.

Isherwood, R.M., *Wind resistance of merchant ships*, Trans. Roy. Inst. Naval Architects, 114:327-38, 1972.

ITTC-Recommended procedures and Guidelines, *Full Scale Measurements Speed and Power Trials Analysis of Speed/Power Trial Data*, 7.5-04-01-01.2, 2005.

ITTC-Recommended procedures and Guidelines, *Testing and Extrapolation Methods, Propulsion, Performance, Predictiong Powering Margins*, 7.5-02-03-01.5, 2008.

ITTC-Recommended procedures and Guidelines, *Testing and Extrapolation Methods, Propulsion, Performance, Predictiong Powering Margins*, 7.5-02-03-01.5, 2011.

ITTC-Recommended procedures and Guidelines, *Testing and Extrapolation Methods, Loads and Responses, Sea Keeping Prediction of Power Increase in Irregular Waves from Model Experiments in Regular Waves*, 7.5-02-07-02.2, 2008.

ITTC-Recommended procedures and Guidelines, *Testing and Extrapolation Methods, Loads and Responses, Sea Keeping Prediction of Power Increase in Irregular Waves from Model Experiments in Regular Waves*, 7.5-02-07-02.2, 2011.

Journee, J.M., *Motions and resistance of a ship in regular following waves*. Report 440, Delft University of Technology, Ship Hydromechanics Laboratory, The Netherlands, September, 1976(c).

Journée, J.M.J., *Motions, Resistance and Propulsion of a Ship in Regular Head Waves*. Report 0428, Delft University of Technology, Ship Hydromechanics, Laboratory, May 1976 (b).

Journée, J.M.J., *Prediction of Speed and Behaviour of a Ship in a Seaway*. International Shipbuilding Progress, Volume 23, No. 265, 1976 (a).

Kadoi, H., Takei, Y., et al., *Model tests on the propulsive performance of a pure car carrier in waves,* Papers Ship Res. Inst. (Japan), Vol. 23, 1986.

Kashiwagi, M., *Impact of hull design on added resistance in waves-Application of the enhanced unified theory*. Proceedings of the 10th International Marine Design conference, Trondheim, Norway, pp.521-535, 2009.

Kim, K.H. and Kim, Y., *Numerical analysis on added resistance of ships*, Proceedings of 20th ISOP, Beijing, China, 2010.

Koushan, K., *Dynamics of propeller blade and duct loadings on ventilated ducted thrusters operating at zero speed*. In: Proceedings of T-POD06–Second International Conference on Technological Advances in Podded Propulsion, Brest, France, 2006(a).

Koushan, K., *Dynamics of propeller blade and duct loadings on ventilated ducted thrusters due to forced periodic heave motion*. International Conference on Violent Flows (VF-2007), RIAM, Kyushu University, Fukuoka, Japan, 2007(a).

Koushan, K., *Dynamics of propeller blade and duct loadings on ventilated thrusters in dynamic positioning mode*. In: Dynamic Positioning Conference, Houston, TX, 2007(b).

Koushan, K., *Dynamics of ventilated propeller blade loading on thrusters*. In: World Maritime Technology Conference—WMTC'06, London, UK, 2006(b).

Koushan, K., *Dynamics of ventilated propeller blade loading on thrusters due to forced sinusoidal heave motion*. In: 26th Symposium on Naval Hydrodynamics, Rome, Italy, 2006(c).

Kumar, M., Anantha Subramanian, V., *A numerical and experimental study on tank wall influences in drag estimation*. Ocean engineering 34, no. 1, pp: 192-205, 2007.

Kwon, Y.J., *Speed Loss Due to Added Resistance in Wind and Waves*. The Naval Architect, March, 2008.

Lee, C.S. *Propeller in waves-State of the art*. The 2nd International symposium on Practical Design in Shipbuilding, Tokyo and Seoul, 1983.

Lee, S. K., *The calculation of zig-zag maneuver in regular waves with use of the impulse response functions*. Ocean engineering, 27, 87–96, 2000.

Liu, P., et al., *Some unsteady propulsive characteristics of a podded propeller unit under maneuvering operation*. First International Symposium on Marine Propulsors. Trondheim, Norway, June. 2009.

Liu, S., Papanikolaou, A., Zaraphonitis, G., *Prediction of added resistance of ships in waves*. Ocean Engineering 38(4): 641-650, 2011.

Loukakis, T. A., and Sclavounos, P. D., *Some Extensions of the Classical Approach to Strip Theory of Ship Motions, Including the Calculation of Mean Added Forces and Moments*. Journal of Ship Research, 22 (1), 1–19, 1978.

Martinussen, K., Ringen, E., *Maneuvering prediction during design stage*, HSVA's CPMC, Workshop, Hamburg, 2000.

Maruo, H., *On the Increase of the Resistance of a Ship in Rough Seas*. JSNAJ, Vol. 108, 1960.

Maruo, H., *Resistance in waves*. Research on Seakeeping Qualities of Ships in Japan, The Society of Naval Architects of Japan 8, pp: 67-102, 1963.

Maruo, H., *The Excess Resistance of a Ship in Rough seas*, International Shipbuilding Progress 4 (35), 1957.

Matsumoto, N., Suemitsu, K., *Interference Effects Between the Hull, Propeller and Rudder of a Hydrodynamic Mathematical Model in Manoeuvring Motion*. Naval Architecture and Ocean Engineering, vol. 22 (Society of Naval Architects of Japan), 1984.

McCarthy, J.H., Norley, W.H., Ober, G.L. *The Performance of a Submerged Propeller in Regular Waves*. Washington DC, USA, David Taylor Model Basin, 1961.

McCreight, W. R., *Ship Maneuvering In Waves*. 16th Symposium on Naval Hydrodynamics, 1986.

Minsaas, K., Faltinsen, O. M., Persson, B., *On the importance of added resistance, propeller immersion and propeller ventilation for large ships in a seaway*, The 2nd International Symposium on Practical Design in Shipbuilding, pp. 149-159, Tokyo and Seoul, 1983.

Minsaas, K., Sverre, S., *Lecture notes for TMR4220 Naval Hydrodynamics.* Department of Marine Technology, NTNU, March 2008.

Munif, A., Umeda, N., *Modeling Extreme Roll Motions and Capsizing of a Moderate-speed Ship in Astern waves*. Journal of the Society of Naval Architects of Japan, 187, pp. 51–58, 2000.

Nakamura, S. and Naito, S., *Propulsive performance of a container ship in waves*. The Society of Naval Architects of Japan. Naval Architecture and Ocean Engineering Vol. 15, 1977.

Norrbin, N.H., *On the added resistance due to steering on a straight course*. In: Proceedings of the 13th International Towing Tank Conference, Berlin, Hamburg, 1972.

Ogawa, A., Kasai, H., *On the Mathematical Model of Manoeuvring Motion of Ship*. International Shipbuilding Progress, 25, 306–319, 1978.

Ohkusu, M. *Prediction of Wave Forces on a Ship Running in Following Waves with Very Low Encountered Frequency*. Journal of the Society of Naval Architects of Japan, 159, pp. 129–138, 1986.

Perez Arribas, F. *Some methods to obtain the added resistance of a ship advancing in waves*. Ocean engineering 34.7, pp: 946-955, 2007.

Prpic-Orsic, J. and Faltinsen, O. M. *Speed loss calculation in a seaway*. The 13th Congress IMAM, pp. 393-400, 2009.

Prpic-Orsic, J., Faltinsen, O.M., *Estimation of Ship Speed Loss and Associated CO_2 Emissions in a Seaway*. Ocean Engineering, Volume 44, Pages 1–10, April 2012.

Rathje, H., Schellin, T. E. and Brehm, A., *Speed loss in waves and wave-induced torsion of a wide-breadth containership*. Proceedings of the Institution of Mechanical Engineers, Part M: Journal of Engineering for the Maritime Environment 225.4, pp: 387-401, 2011.

Reichel, M., *Manoeuvring forces on azimuthing podded propulsor model*. Polish Maritime Research 2(52), Vol. 14, pp. 3-8, 2007.

Ringen, E. *Vesim-Propulsion Model (pod), User Manual*. MARINTEK, Trondheim, 2010.

Ringen, E., *ShipX Manoeuvring Plug-In, theory manual*. MARINTEK, Trondheim, 2009.

Salvesen, N., Tuck, E. O. and Faltinsen, O. M., *Ship motions and sea loads*. SNAME (78) pp. 250-287, 1970.

Savio, L., Steen, S. *Identification and Analysis of Full Scale Ventilation Events*. International Journal of Rotating Machinery 2012 (2012).

Skejic, R., Berg, Tor T., *Combined Seakeeping and Maneuvering Analysis of A Two-ship Lightering Operations*. Proceedings of the ASME 2010 29th International Conference on Ocean, Offshore and Arctic Engineering (OMAE). June 6-11, Shanghai, China, 2010.

Skejic, R., Faltinsen, O.M., *A Unified Seakeeping and Maneuvering Analysis of Ships in Regular Waves*. Journal of Marine Science and Technology, Vol. 13, pp. 371-394, 2008.

Skejic, R., *Maneuvering and Seakeeping of a Single Ship and of Two Ships in Interaction*. Doctoral Thesis at NTNU, ISBN: 978-82-471-7037-3, 2008.

Smogeli, O.N., *Control of Marine Propellers–From Normal to Extreme Conditions*, Faculty of Engineering Science& Technology, Department of Marine Technology, Trondheim, PhD Thesis, p.187, 2006.

Søding, H., Influence of course control on propulsion power. Schiff & Hafen/Kommandobrucke 3, 63–68, 1984.

Steen, S. and Faltinsen, O. M., *Added resistance of a ship moving in small sea states*. Practical Design of ships and mobile units, Hague, Netherlands, 1998.

Strøm-Tejsen, J. and Porter, R. R. *Prediction of controllable-pitch propeller performance in off-design conditions*. Third Ship Control Systems Symposium, Paper VII B-1. Bath, UK. 1972.

Umeda, N., Hashimoto, H. *Qualitative Aspects of Nonlinear Ship Motions in Following and Quartering Seas with High Forward Velocity*. Journal of Marine Science and Technology, 6, pp. 111–121, 2002.

Van Berlekom, W. B., *Wind Forces on Modern Ship Forms - Effects on Performance*, Swedish Maritime Research Centre, 1981.

Van Berlekom, W. B., Tragardh, P. and Dellhag, A., *Large Tankers-Wind Coefficients and Speed Loss Due To Wind and Sea*. Naval Architect, Issue Number 1, pp. 41-58, 1975.

Van Berlekom, W. B., *Wind Forces on Modern Ship Forms-Effects on Performance*, Trans, Necies, Vol. 97, 1981.

Van Sluijs, M.F., *Performance and propeller load fluctuations of a ship in waves*, TNO Report No. 163 S, 1972.

Vartdal, L. *How to utilize data from HEMOS in "Performance in a Seaway".* In presentation at UTC Workshop, Ulsteinvik, Norway. Rolls-Royce Marine, 2008.

Woodward, M. D., Clarke, D. and Atlar., M. *On the manoeuvring prediction of pod driven ships*. In Proceedings of the International Conference on Marine Simulation and Ship Manoeuvrability, Kanazawa, Japan, paper RB-7(The Society of Naval Architects of Japan and Japan Institute of Navigation, Kanazawa). Vol. 2. 2003.

Yamazaki, R., Nakatake, K., Kino, S., Koguchi, K., *On the Propulsive Performance of a Ship in Regular Head Waves*. J.S.N.A. vol. 143, Japan, 1978.

Zhu, S., Wu, M., Moan, T., *Experimental and Numerical Study of Wave-Induced Load Effects of Open Ships in Oblique Seas,* Journal of Ship Research, Volume 55, Number 2, pp. 100-123 (24), June 2011.

Appendix A

Appended Papers

Paper 1:

Prediction of Speed Loss of a Ship in Waves

Paper 2:

Experimental and Numerical Study of Stem Shape Influence on Speed Loss in Waves

Paper 3:

Speed loss due to seakeeping and maneuvering in zigzag motion

Paper 4:

Speed loss of a vessel sailing in oblique waves

Paper 5:

Measurement of speed loss due to waves

Paper 1

Prediction of Speed Loss of a Ship in Waves

Zhenju Chuang, Sverre Steen

Prediction of Speed Loss of a Ship in Waves

Zhenju Chuang[1], Sverre Steen[2]

[1,2]Department of Marine Technology, Norwegian University of Science and Technology (NTNU), Trondheim, Norway

ABSTRACT

Prediction of speed loss of ocean-going vessels is important for ship design, fuel consumption and 'sea margin' evaluation. The main purpose of this paper is to investigate the speed loss of an 8000DWT tanker in moderate and severe sea states. The vessel is self-propelled by two Azipull thrusters. Different methods are used here to investigate speed loss in waves. A model test was done in Marintek, Trondheim, Norway. Attainable speeds in waves were all recorded as time series. Since the ship model in experiment has six degree of freedom, it is difficult to apply towrope force to correct for the difference in frictional resistance in model scale and full scale. Without using towrope force, the model tests will underestimate the speed loss values. A method to correct for the lack of towrope force is presented. Time domain and frequency domain numerical methods with full scale ship and propulsion system were also applied here to calculate speed loss values. From the comparison of the three methods, it is found that time-domain simulation results give the best correlation with corrected model test data in the whole range of wave conditions studied here, and the frequency-domain method overestimates speed loss values when wave length approaches ship length.

Keywords

Speed loss, seakeeping, time-domain, frequency-domain, towrope force

1 INTRODUCTION

The new framework of the global economy has stimulated and expanded the shipbuilding and shipping industry. Simultaneously, environmental concern and a constant increase in the price of fuels have put more pressure and demands on designers to minimize energy consumption. This increases the importance of the prediction of a ship speed and power in a seaway. Speed loss of a ship can be regarded as voluntary and involuntary (Faltinsen et al 1980). The former is to avoid slamming, propeller racing and excessive ship motion. The latter is due to added resistance from waves, wind, and current, as well as reduction of propulsive efficiency caused by waves and increased resistance.

This paper focuses on the involuntary speed loss. Both experiment and numerical methods are used here to predict attainable speed of a ship in moderate and severe sea states. The paper explores the use of time domain and frequency domain simulation in the prediction of speed loss, and discusses the importance of using tow rope force in self-propelled model tests used to determine speed loss.

2 EXPERIMENT

2.1 Seakeeping model test

In order to investigate speed loss due to waves, seakeeping model tests were carried out in the large towing tank (L/B/D=260/10/5) at MARINTEK, Trondheim, Norway. A model of an 8000 DWT tanker developed by Rolls-Royce Marine, Ship Technology - Merchant was tested in head sea waves and the hull was propelled by twin AZP120 model thrusters. The model had transom stern and conventional bow shape with bulb. The main dimensions of the ship and model are shown in Table 1, and the figure of the hull is shown in Fig 1.

Table 1: The main particulars of the 8000 DWT tanker

	UNIT	SHIP	Model
Sale		1	16.57
L_{OA}	[m]	118.336	7.142
Lpp	[m]	113.2	6.832
D	[m]	15	0.905
B	[m]	19	1.147
T	[m]	7.2	0.435

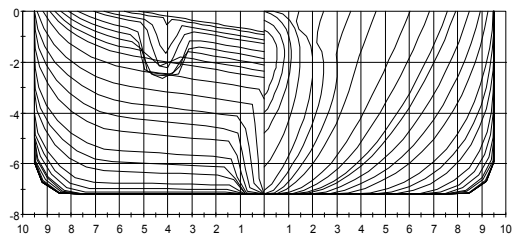
Fig. 1: Figure of the hull

Eight different regular head sea wave conditions were selected. Wave lengths ranges from 0.42Lpp to 2.15Lpp, and wave height changes from 0.06 to 0.24 meters in model scale. Details of the wave conditions are specified in Table 2.

Table 2: Wave conditions in model tests

	H(m)	T(s)	Fn	Lpp/λ
Regular waves	0.12	1.35	0.212	2.4
	0.12	1.84	0.212	1.29
	0.12	2.09	0.212	1
	0.06	2.38	0.212	0.77
	0.12	2.38	0.212	0.77
	0.24	2.38	0.212	0.77
	0.12	2.58	0.212	0.66
	0.12	3.07	0.212	0.46

The model was free to oscillate in six-degrees of freedom, with a track controller on the ship to keep the course and heading of the model during the whole process. The controller sets up a control point on the ship, which is typically a bit forward of forward perpendicular to ensure a stable controller. A track point which is located on the desired track at a specified distance in front of the control point is used by the controller to calculate the course to steer. The cross track error is calculated by finding the deviation of the ship control point from the track, and based on this, the course to steer can be calculated (in order to steer against the track point). The course to steer is then applied by an autopilot control system to calculate the commanded pod angle. Brake power was kept constant during the test to insure the speed loss value only due to added wave resistance.

Before the speed loss is measured when encountering waves, the model is running at Froude number equal to 0.212 in calm water. In this period, thrust is equal to the calm water resistance. Then the wave is coming and the speed drops due to the increase of wave resistance. Time series of vessel speed, propeller thrust, torque, RPM and six-degree of freedom motion at the center of gravity were all recorded. Fig 2 shows an example of speed loss in surge direction which is scaled to full scale from the model test.
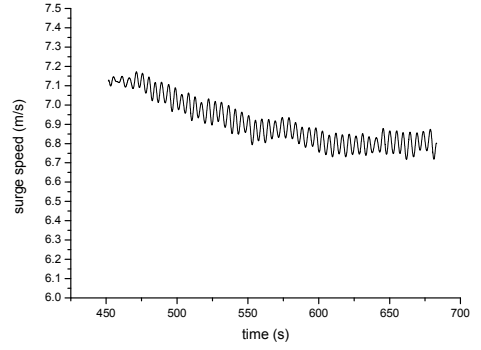

Fig. 2: Model test speed scaled to full scale

2.2 Importance of towrope force

The skin friction correction force, applied as an external tow force, is to achieve the theoretically correct propeller loads during the self-propulsion test. It takes into account the difference in skin friction coefficients between the model and the full scale ship (ITTC procedure). It also includes compensation for other effects such as correlation allowance, appendages, transom stern, etc. Towrope force can be calculated following the ITTC recommended procedure given as:

$$F_D = C_S \frac{\rho_m}{2} V_m^2 S_m \qquad (1)$$

Where

$$C_S = [C_{Fm} - (C_{FS} + \Delta C_F)](1+k_0) + (C_{BDm} - C_{BDs}) + (C_{Appm} - C_{Apps}) - C_A$$

$$(2)$$

In equation (1) and (2), F_D is towrope force; C_{Fm} and C_{FS} are friction resistance coefficients in model scale and in full scale; ΔC_F is roughness allowance; k_0 is form factor; C_{BDm} and C_{BDs} are transom stern drag coefficients in model scale and in full scale; C_{Appm} and C_{Apps} are appendage resistance coefficients in model scale and full scale; C_A is correlation coefficient.

In equation (2), the first term is the difference in friction resistance in full scale and in model scale, the second and third terms are the correction for difference in transom stern and the appendages, respectively. The last term is the correlation allowance which accounts for the systematic errors in scaling method.
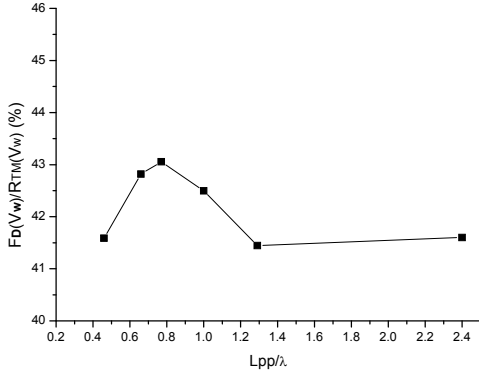
Fig. 3: Ratio between towrope force and model scale calm water resistance at attainable speeds in waves

Fig 3 shows the ratio between towrope force and calm water resistance of model scale at attainable speeds in waves. The reason for the non-constant value is that the attainable speed drops around $Lpp/\lambda=0.8$. It is seen from Fig.3 that the towrope force accounts for a large percent of the calm water resistance (over 40%).

Usually, towrope force can be applied by using a weight connected to a rope through a pulley system or connected the model to the carriage through a force transducer. However, in this seakeeping speed loss test, using towrope force is not practical. First consideration is that towrope is changing with vessel speed, and in this speed loss test, the model speed is decreasing all the time, so it is difficult to adjust towrope force value with the varying model speed all the time during this speed loss procedure. Since towrope force did not apply in model test, the experimental results have to be corrected before being used. A way of correcting model test data for lack of towrope force is specified in the following.

Since the power was kept constant both in calm water and in waves in the model tests discussed here, then the following equation exists:

$$\frac{R_{TC}V_C}{\eta_{DC}} = \frac{R_{TW}V_W}{\eta_{DW}} \qquad (3)$$

Where R_{TC} is calm water resistance; R_{TW} includes still water resistance and added resistance in waves; V_C is calm water attainable speed; V_W is attainable speed in waves; $\eta_D = \eta_H \eta_R \eta_0$ is propulsive efficiency. Here it is assumed that hull efficiency η_H and relative rotative efficiency η_R are equal in calm water and in waves, which means:

$$\eta_{HC} = \eta_{HW} \qquad (4)$$

$$\eta_{RC} = \eta_{RW} \qquad (5)$$

η_0 is the thruster open water efficiency and the corresponding open water efficiency in waves when towrope force is used or is not quite different, because the propulsion point is changed.
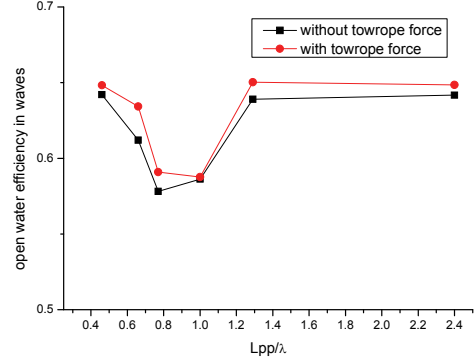

Fig. 4: Change of open water efficiency in waves

Fig 4 shows the change of open water efficiency in different sea states when towrope force is used and when it is not used. Inserting equations (4) and (5) into equation (3), yields:

$$\frac{R_{TC}V_C}{\eta_{0C}} = \frac{R_{TW}V_W}{\eta_{0W}} \qquad (6)$$

The added resistance in waves is found from a frequency domain calculation in our example.

To get an indication of the importance of using towrope when measuring speed loss, we can express R_{TW} as a function of speed in the following simplified way:

$$R_{TW} = R_{TC} + \Delta R_W - (\frac{dR_{TC}}{dV} + \frac{d\Delta R_W}{dV})(V_C - V_W) \qquad (7)$$

Where ΔR_W is added resistance in waves.

Inserting equation (7) into equation (6) and neglect second order terms, then the finally attainable speed in waves can be written as:

$$V_{W1} = V_C - V_C \frac{R_{TC} + \Delta R_W - R_{TC}\eta_{0W}/\eta_{0C}}{R_{TC} + \Delta R_W + (\frac{dR_{TC}}{dV} + \frac{d\Delta R_W}{dV})V_C}$$

$$(8)$$

If towrope force is not used in the model test, then R_{TC} in equation (8) should have the towrope force F_D added, which means:

$$V_{W2} = V_C - V_C \frac{(R_{TC}+F_D) + \Delta R_W - (R_{TC}+F_D)\eta_{0W}/\eta_{0C}}{(R_{TC}+F_D) + \Delta R_W + (\frac{d(R_{TC}+F_D)}{dV} + \frac{d\Delta R_W}{dV})V_C} \quad (9)$$

From comparison between equations (8) and (9), it can be seen that without using towrope force the speed loss values will be underestimated. The model test result should be corrected by the difference between the two expressions for velocity in waves:

$$\Delta V = V_{W2} - V_{W1} \quad (10)$$

3 TIME DOMAIN NUMERICAL MODEL

3.1 Mathematical model set up

The numerical model set up in order to solve equations of motion incorporates six degrees of freedom, and is solved in time domain.
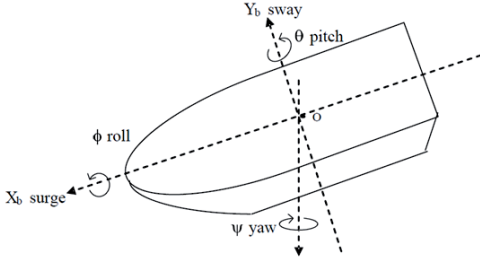
Fig. 5: B-frame

All the hydrodynamic forces are given in a body fixed coordinate system. Neglecting hydroelastic effects and assuming that the vessel is moving as a rigid body, the motion of any point on the hull may be obtained by combinations of the motion responses in the six basic degrees of freedom denoted as η_j where j=1…6 is the degree of freedom (surge, sway, heave, roll, pitch and yaw).

The classical model is derived from Newton's second law as:

$$(M + A_{jk})\ddot{\eta}_j = \sum F_k \quad (11)$$

where M is the 6 x 6 inertia matrix and A_{kj} is added mass. $\ddot{\eta}_j$ is the generalized acceleration vector in j-direction. F_k is a vector of linearly superimposed forces and moments in k-direction.

By a change of notation, this equation may be written as:

$$(M + A_{jk})\dot{v}_j = \sum F_k \quad (12)$$

where $\dot{v}$ is the generalized acceleration vector. v =[u,v,w,p,q,r]^T is the generalized velocity vector. Here $(u,v,w) = (\dot{\eta}_1, \dot{\eta}_2, \dot{\eta}_3)$ are linear velocities in surge, sway and heave; $(p,q,r) = (\dot{\eta}_4, \dot{\eta}_5, \dot{\eta}_6)$ are the angular velocities in roll, pitch and yaw. $\sum F_k$ is the sum of all the external forces. In this analysis, the external forces from calm water resistance, incoming wave resistance and thrust from propulsion system are considered. The accelerations can be expressed as:

$$\dot{v}_j = (M + A_{jk})^{-1} \sum F_k \quad (13)$$

This equation is solved at each time step to get the vessel speed as time series.

3.2 Retardation function

Added mass and damping are frequency dependent. However, in the real time domain calculation, especially in the irregular sea state, there are many excitation frequencies. When the transient response happens, the radiation forces are calculated by means of a convolution integral using retardation (kernel) functions, or the so-called 'memory effects'. Following the work by Cummins (1962), the radiation force in time domain is written as:

$$F = \int_0^t h(t-\tau)\dot{\eta}(\tau)d\tau \quad (14)$$

Where $h_{jk}(t)$ is retardation function, which can be evaluated by:

$$h_{jk}(t) = -\frac{2}{\pi}\int_0^\infty w(A_{jk}(w) - A_{jk}(\infty))\sin wt \, dw \quad (15)$$

$$h_{jk}(t) = \frac{2}{\pi}\int_0^\infty (B_{jk}(w) - B_{jk}(\infty))\cos wt \, dw \quad (16)$$

where $A_{jk}(\infty)$ and $B_{jk}(\infty)$ are added mass and damping matrix at infinite frequency.

Calculation of $h_{jk}(t)$ requires information on the behavior of either A_{jk} or B_{jk} at all frequencies.

3.3 Calm water resistance

The total calm water resistance of the vessel is the sum of viscous resistance, residual resistance, appendage resistance and transom stern resistance. In the literature, there are ways to calculate the calm water resistance, such as empirical resistance calculation methods: Holtrop (1984) and Hollenbach (1998) methods. These methods are based on a regression

analysis of many previous models tests with similar models, and mainly depends on the ship main dimensions, such as length, draught and block coefficients, and so on. They can hardly cover the effect of important details of the hull shape such as bulb design and the transom stern.

This analysis uses the resistance model test to get calm water resistance curve of the ship. The model test was done in the towing tank in MARINTEK, Trondheim, Norway. Froude scaling is used to get the full scale ship resistance from model test results:

$$\frac{U_M}{\sqrt{gL_M}} = \frac{U_S}{\sqrt{gL_S}} \qquad (17)$$

The model is tested at equal Froude number as the ship. Total resistance of the model is assumed to be composed of the following parts (Minsaas & Steen, 2008):

$$C_{Tm} = C_{Rm} + (1+k)C_{Fm} + C_{BDm} + C_{Appm} \quad (18)$$

where C_{Tm} is total model resistance coefficient; C_{Rm} is model residual resistance coefficient; k is form factor; C_{Fm} is frictional resistance coefficient; C_{BDm} is transom stern resistance coefficient; C_{Appm} is appendages resistance coefficient.

Strictly speaking, air resistance should be included; however, it is a small part compared to others, so here we neglect it. Residual resistance is Froude scaled, which means that:

$$C_{Rm} = C_{Rs} \qquad (19)$$

The full scale total resistance coefficient could be written as:

$$C_{Ts} = C_{Rs} + (C_{Fs} + \Delta C_F)(1+k) + C_{BDs} + C_{Apps} + C_A \quad (20)$$

where ΔC_F is the roughness correction and C_A is correlation coefficient, which is an empirical constant to account for systematic errors in the scaling method.

In the resistance model test, seventeen speeds were chosen with the corresponding Froude number range from 0.152 to 0.273.

With this resistance curve, the resistance at any speed in this range can be found from the polynomial curve:

$$R_{TS} = a_1 * V^3 + a_2 * V^2 + a_3 * V + a_4 \qquad (21)$$

Where a_1-a_4 are regression coefficients. Fig 6 shows the percentage of maximum calm water resistance based on the model tests and the fitted curve according to equation (21).
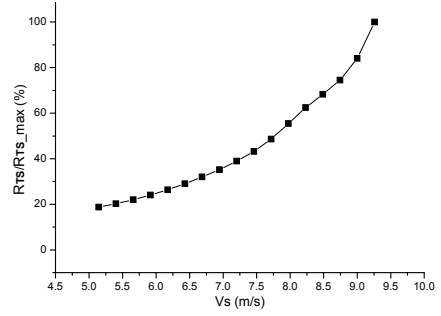

Fig. 6: Full scale calm water resistance percentage

3.4 WAVE FORCES

Wave forces here are composed of first order wave excitation force, second order wave drift forces which are pre-calculated before the time domain simulation started for different vessel speeds, headings and wave frequencies. When the simulation starts, both of the two forces from the waves at each time step are calculated by interpolation on the input dataset of the speed, heading and frequency. Ship motion at each wave frequency is calculated by strip theory (Salvesen et al 1970).

The first order wave excitation force is described by transfer function and the wave elevation and can be expressed as:

$$F_{wave}^{(1)} = H^{(1)}(\omega, \theta)\zeta(\omega, \theta, x, y) \qquad (22)$$

Where $H^{(1)}(\omega, \theta)$ is first order transfer function. It depends on wave frequency ω and propagation direction θ. $\zeta(\omega, \theta, x, y)$ is wave elevation, which is a function of wave frequency, propagation direction and position in space.

The second order wave drift force can be divided into added resistance, transverse drift force and mean yaw moment in surge, sway and yaw direction respectively. This paper only considers head sea conditions, so only added resistance is included. Added resistance is calculated by G&B method (Gerritsma & Beukelman 1972) which is based on the energy principle under the assumption that radiated energy is equal to the work of added resistance done and the energy contained in the damping waves. Added resistance can be written as:

$$R_{AW} = \frac{k}{2\omega_e} \int_0^L b' V_{za}^2 dx_b \qquad (23)$$

Where k is wave number; ω_e is encounter frequency; b' is sectional damping coefficient; V_{za} is the amplitude of vertical relative velocity; x_b is the coordinate of cross section.

3.5 PROPULSION SYSTEMS

The propulsion system is composed of two Azipull thrusters working at the stern. The thrusters are controlled by a track controller similar to the experiment. Outputs are the commanded rudder angle to the two Azipull propulsors.

In a purely head sea condition, course track error is controlled in less than 0.1, which means the ship is going straight line along the course. The output pod angle is controlled within the range of less than 0.5 degrees in regular sea. So the thrust forces in surge direction are much more important than in other directions and can be written as:

$$T = 2(1-t)n^2 D^4 K_T \qquad (24)$$

$$Q = 2\rho n^2 D^5 K_Q \qquad (25)$$

Where t is thrust deduction, for which the value is taken from the calm water performance model tests. Thrust and torque gotten from equation (24) and (25) include the effect of wake fraction. Wake fraction values in waves were assumed to be the same value as in calm water, which was taken from model test.

When the simulation starts after a few seconds of transient machinery response, the power reaches its constant value, as shown in Fig. 7. Fig. 8 and Fig. 9 show that it takes longer before thrust and torque reach steady values. It should be noted that the ship was initiated with the speed to be obtained in calm water. Fig. 10 shows how the propeller RPM is controlled to obtain constant power.
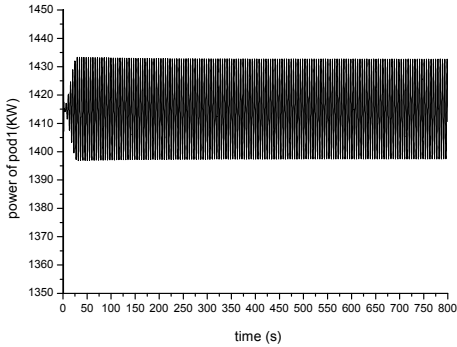
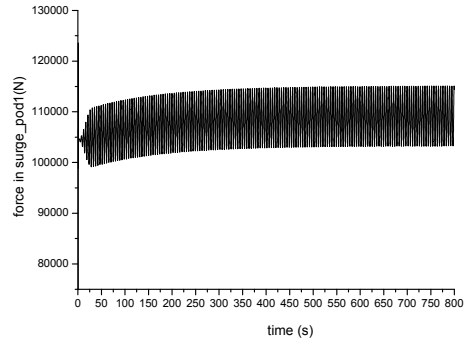Fig. 7: Power during the time simulation

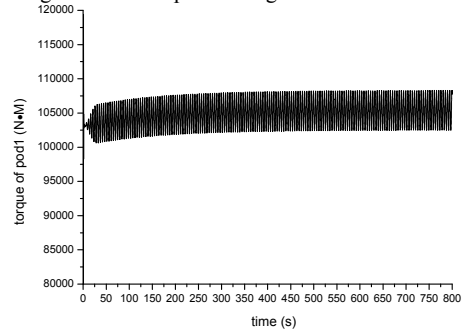Fig. 8: Thrust of pod1during the time simulation

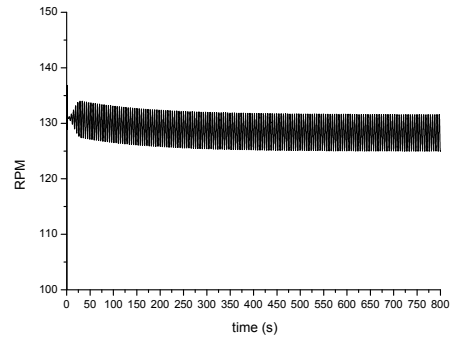Fig. 9: Torque of pod1 during the time simulation

Fig. 10: RPM of pod1 during the time simulation

4 Frequency Domain method

Speed loss calculated in frequency domain is considered to be a result of change of equilibrium between the total ship resistance and propeller thrust, which happens when the resistance increases due to waves. The main procedure is based on the computational algorithm (Fathi et al 2009), shown in Fig. 11:
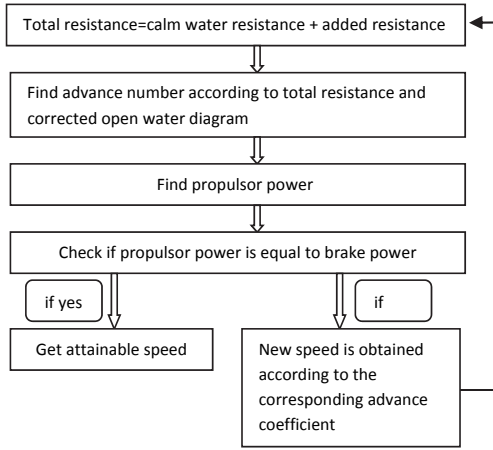
Fig. 11: Computational algorithm

First, total resistance, which includes the calm water resistance and the added resistance, is calculated at the initial vessel speed; then the open water diagram according to the total resistance to find the torque and advance number is used; after which the delivered propulsor power is calculated according to the equation:

$$P_D(kw) = \frac{2\pi}{1000} \bullet \rho \bullet D^5 \bullet n^3 \bullet \frac{K_Q}{\eta_R} \qquad (26)$$

where η_R is relative rotative efficiency, and K_Q is the torque coefficient.

Lastly, one should check if the required propulsion power equals the power specified to be delivered to the propeller. If they are equal, then the final attainable speed is obtained. Otherwise, one should calculate the new speed according to the corresponding advance number and recalculate the total resistance again until the equilibrium point occurs.

5 VERIFICATION OF NUMERICAL MODEL

Comparisons of the results from model test, time domain and frequency domain in different sea states are given in this section. Here, 'EXP' means the model test data scaled directly to full scale data (without correcting for tow rope force),;'EXP_corrected' represents the model test data after being corrected according to equation (10) and scaled to full scale; 'TD' and 'FD' denote the results obtained separately from time domain simulation and frequency domain, where ship motion is calculated by strip theory (Salvesen et al 1970) and added resistance is calculated by Gerritsma & Beukelman (1972), which is based on the energy conservation.

Fig. 12 gives one example of speeds in time domain with and without towrope force, both for time domain simulation and for the experimental results. As can be seen from Fig. 12, when towrope force is not applied, the speed loss value will be underestimated. With respect to the effect of tow rope, principally the same results are found in all the eight different regular sea states.
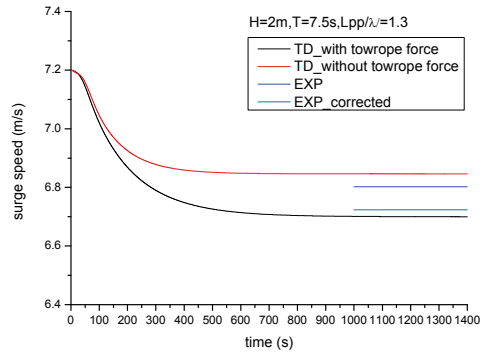

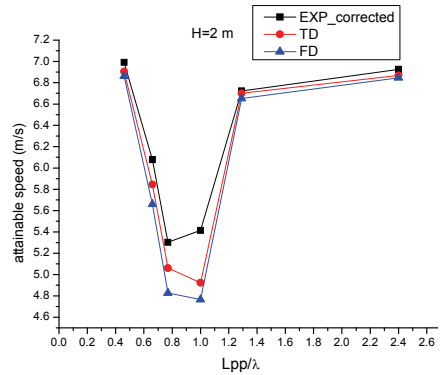Fig. 12: Difference between surge speeds for towrope force

Fig. 13: Mean attainable speed at different sea states

The corresponding numerical values and the relative error with respect to the corrected experimental results are reported in Table 3.

Table 3: Mean attainable speed and the relative error

Lpp/λ	EXP_correct	TD	Error (%)	FD	Error (%)
2.4	6.9257	6.8682	0.8302	6.84648	1.1431
1.3	6.7233	6.7002	0.34342	6.65116	1.0728
1.0	5.4150	4.9227	9.0915	4.76478	12.008
0.8	5.3028	5.0604	4.5717	4.82646	8.9831
0.7	6.0781	5.8438	3.8549	5.65914	6.8926
0.5	6.9915	6.9039	1.2535	6.8619	1.8542

Fig. 13 shows the relationship between mean attainable speed and wave length when wave height is equal to 2 meters. Generally speaking, these three methods are in a good correlation to predict speed loss in regular waves. However, it is observed from Table 3 that the error between corrected experimental data and the simulated data with time domain method is less than that between corrected experimental data and the simulated data in the frequency domain for all wave conditions considered. One of the most important reasons for this is in time domain; the real thrust values were taken into consideration, which includes the oscillation of thrust force at each time step, but in frequency domain calculation, only mean thrust values were taken into account by applying the open water character curve. So speed loss calculation in time domain is better than frequency domain results. Also, a large error between experimental result and the other two numerical results (9.0915%, 12.008% respectively) is observed in the case when Lpp/λ gets close to 1, where the lowest attainable speed occurs. Due to the limitations of the length of towing tank, the attainable speed from model test is not so converged, which means that speed loss value in this case was underestimated in model test.
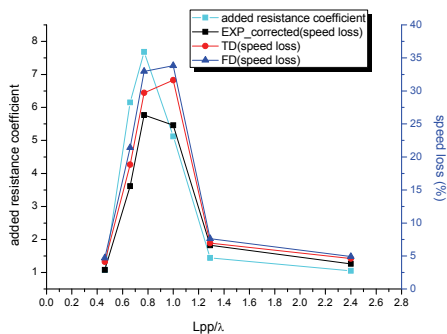

Fig 14: Added resistance and speed loss (%)

Fig. 14 shows the same trends of speed loss and added resistance. Added resistance reaches its peak value when wave length approaches ship length, where the most severe speed loss is observed.
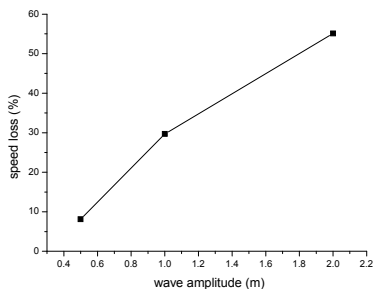

Fig 15: Relation of speed loss and wave elevation

Fig. 15 shows the relationship between wave elevation and speed loss in time domain calculation. In the long wave, sea states with λ/Lpp=1.3 and wave elevations are equal to 0.5m, 1m and 2m, respectively. Speed loss is observed increasing linearly with increased wave elevation in this long wave case study.

6 CONCLUSIONS AND REMARKS

In this paper, a method of correcting the model test result in order to include the effect of towrope in the prediction of speed loss is presented. Numerical simulations for speed loss in both time domain and frequency domain are presented. The corrected speed loss from model tests was compared with the numerical simulations in both time and frequency domain. Then the most important findings in the study are given as follows:

Without considering the loss of thrust, the speed loss of a vessel will increase with the increasing of added resistance. When wave length approaches ship length, speed loss reaches its peak value. Speed loss is observed to increase linearly with increasing wave elevation in the long wave range.

When model tests are performed without using a tow rope force to correct for the relatively larger frictional resistance in model scale, the results will underestimate speed loss values when the power is kept constant. A way for correction of experimental data is suggested here.

The time domain simulation of the speed loss gives better prediction than frequency domain simulation for the whole range of wave conditions tested here.

The time domain simulation results agree reasonably well with the model test data corrected by the method suggested by this paper. And more verification of this correction method for lack of towrope force needs further research work before it is widely used.

REFERENCES
Cummins, W. E. (1962). 'The impulse response function and ship motions'. Schiffstechnik **9**(47), pp. 101-109.

Fathi, D. et al. (2008). ShipX Vessel Simulator, Theory Manual. MARINTEK.

Fathi, D. et al. (2009). ShipX Speed and Powering, Theory Manual. MARINTEK.

Faltinsen, O., Minsaas, K., Liapias, N. & Skjørdal, S.O. (1980). 'Prediction of Resistance and Propulsion of a Ship in a Seaway'. Proceedings of 13th Symposium on Naval Hydrodynamics, The Shipbuilding Research Association, Japan.

Gerritsma, J. B. (1972). 'Analysis of the resistance increase in waves of a fast cargo ship'. International Shipbuilding Progress **19**(217), pp. 285-292.

Hollenbach, K. U. (1998). 'Estimating resistance and propulsion for single-screw and twin screw ships'. Ship Technology Research **45**.

Holtrop, J. A. (1984). 'Statistical renanalysis of resistance and propulsion data'. International Shipbuiliding Progress **31**.

Minsaas, K. & Sverre, S. (2008). 'Lecture notes for TMR4220'. Naval Hydrodynamics. March 2008.

Salvesen, N., Tuck, E. O. & Faltinsen, O. M. (1970). 'Ship motions and sea loads'. SNAME (**78**) pp. 250-287.

Paper 2

Experimental and Numerical Study of Stem Shape Influence on Speed Loss in Waves

Zhenju Chuang, Sverre Steen

Experimental and Numerical Study of Stem Shape Influence on Speed Loss in Waves

By Zhenju Chuang[1],[*] & Sverre Steen[1]

ABSTRACT

This paper addresses prediction of ship motion and propulsion system behaviour to demonstrate the effect of waves in real sea states. For a *8000* t deadweight tanker, three different stem shapes are studied experimentally and numerically. Numerical simulations of speed loss were performed in time and frequency domain, generally agreeing well with experimental results. While a conventional bow with bulb and flare gave least calm water resistance, a bow without bulb and flare gave least total resistance in severe wave conditions.

Key words: Added Resistance, Seakeeping, Speed

1 Introduction

　　Usually, the performance evaluation of a ship during the design stage is primarily done for calm water without consideration of the weather conditions prevailing on the operation route, *Prpic-Orsic and Faltinsen* (2009). The effect of weather is included by adding a certain percentage to the power requirement in calm water (sea margin). The sea margin is determined using the hydrodynamic knowledge of the model testing institution together with operational information from the ship operator, *ITTC* (2008). Ship routing requires reliable prediction of speed loss in waves as a function of wave height and direction. *Journee* (1976) calculated the speed and behaviour of a single-screw ship in waves. Only pitch and heave motions were considered, with added mass and damping calculated by Lewis transformation. Propeller performance was considered by applying open-water curves. *Faltinsen et al.* (1980) developed a procedure to calculate the influence of wave-induced motions on the wake, open-water propeller characteristics, thrust deduction and relative rotative efficiency. The authors pointed out that it may be physically wrong to apply fully submerged propeller characteristics in waves due to the change of shaft immersion and induced loss of thrust and torque. They also proposed an asymptotic formula for added resistance in short waves, and a pressure integration method to calculate the added wave resistance in longer waves. *Prpic-Orsic and Faltinsen* (2009) studied the speed loss in actual sea states in the time domain by implementing a thrust loss model

---

[1] Norwegian University of Science and Technology, Trondheim, Norway

[*] *Corresponding author*. Present address: chuang.zhenju@ntnu.no

based on experimental data by *Smogeli* (2006). Calm-water resistance was obtained by applying an empirical method; added resistance was obtained using direct pressure integration, *Faltinsen et al.* (1980).

Rathje et al. (2010) studied a wide-bodied container ship in waves using a RANS (Reynolds averaged Navier-Stokes) equation solver to simulate the ship motion in calm water as well as in head waves, assuming constant thrust.

Experience gained from experiments at MARINTEK indicates that reduction of power of the order of *20%* may be gained by relatively small changes of the bow and stern on a vessel, *Buhaug et al.* (2009). One of the aims of this paper is to explore the potential benefits of reducing the speed loss by changing the bow design. The speed loss of three different bow shapes is compared. Another aim is to gain more insight into speed loss theories applying model tests and numerical studies. The real propulsion system properties in waves are taken into consideration. Nomenclature in this paper follows ITTC standard, unless specified otherwise.

2 Model tests

Speed loss seakeeping model tests were carried out in a large towing tank of the length *260* m, breadth *10* m and depth *5* m at MARINTEK. A model of a *8000* t deadweight tanker was used, Table 1.

Tab. 1: Principal particulars of the *8000* t deadweight tanker (model A), scale *1 : 16.57*.

	full scale	model scale
L_{OA} [m]	*118.3*	*7.142*
L_{pp} [m]	*113.2*	*6.832*
D [m]	*15.0*	*0.905*
B [m]	*19.0*	*1.147*
T [m]	*7.2*	*0.435*

2.1 Experimental set-up

The ship has a wide transom stern. It is self-propelled by twin AZP120 model thrusters. Three different bow shapes were used in the experiment to investigate the stem shape influence on added resistance, Fig. 1. Model A has conventional bow with flare and bulb, model B has vertical stem with very little flare and bulb, and model C has vertical stem with very little flare and without bulb. All three models have the same waterline contour at the design loading condition.

Fig. 1: Stem shapes of models A (left), B (centre) and C (right).

In short waves with $\lambda/L_{pp} < 0.5$, added wave resistance is mainly caused by wave reflection at the bow; in long waves with $0.7 < \lambda/L_{pp} < 1.5$, the main source of added resistance are ship motions. In the tests, both wave ranges were considered. The tests were carried out in regular head

waves of the height *0.12* m for the ratios L_{pp}/λ of *0.46*, *0.66*, *0.77*, *1.0*, *1.29* and *2.4*. All models were tested at the same initial speed, corresponding to Froude number $F_n = 0.22$.

The accuracy of the wave amplitude is very important, since the added wave resistance is generally proportional to wave amplitude squared. All waves selected were calibrated before the model tests. Three wave probes were used, located in the middle of the tank, on the carriage and in front of the model bow.

The model was self-propelled and free to oscillate in six degrees of freedom. A track controller kept the model running along the centerline of the towing tank. The track controller set up a control point on the ship slightly ahead of the forward perpendicular. A track point, located on the desired track at a distance of *20* m forward of the centre of gravity in front of the control point, was used to calculate the course to steer. The cross track error was calculated by finding the deviation of the ship control point from the track. The course to steer was calculated based on this error. Another control system was applied to the propulsion system to keep the power constant during wave-ship interaction to obtain the speed loss only due to added wave resistance and loss of propulsive efficiency.

The model was tested in calm water with each of the three bow shapes before performing the tests in waves. The three bow shapes have slightly different calm-water resistance. The propulsion power in calm water was adjusted for each bow so that the speed in calm water was the same for all versions of the model, corresponding to $F_n = 0.22$. For the tests in waves, the model was accelerated to calm-water speed and then encountered the train of regular waves. Upon encountering the waves, the model speed dropped gradually due to additional resistance due to waves. Time series of vessel speed, propeller thrust, torque, RPM and six-degree of freedom motions at the centre of gravity were recorded. Figure 2 shows the calibrated wave elevation measured on the carriage for a wave with full scale period *7.5* s and height *2.0* m. Figure 3 gives an example of the recorded full-scale surge speed of model A in the wave shown in Fig. 2.
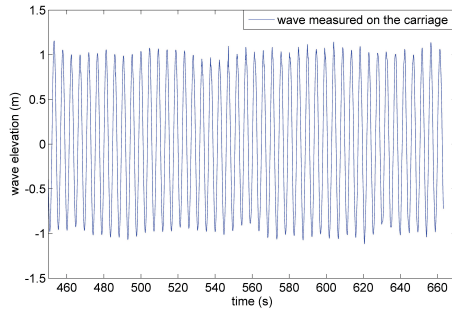

Fig. 2: Wave elevation measured during model test with full scale period *7.5* s and height *2.0* m.
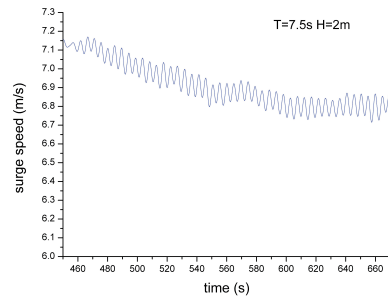
Fig. 3: Surge speed of the model, scaled to full scale.

2.2 Tow-rope force

The frictional resistance coefficient in model scale is larger than in full scale, since the Reynolds number is larger in full scale than in model scale. Usually, the model propeller is required to operate at the same relative loading as the ship propeller. In order to achieve this, a friction correction force (often called tow-rope force) should be used, which can also correct for some other effects such as correlation allowance, scale effect on appendages and transom stern.

Constant tow-rope force can be applied in two ways. In the *Continental method*, a weight is applied, connected to the rope through a pulley system. Propeller revolutions are adjusted so that the model moves with the same speed as the carriage, with a pre-determined tow-rope force, Fig. 4 (left). In the *British method*, the model is connected to the carriage through a force transducer that measures the resistance force, Fig. 4 (right). The model speed is determined by the carriage speed.

The pre-calculated towing force is obtained by adjusting the propeller speed; alternatively, two or three different propeller speeds are tested and the correct propulsion point is found by interpolation.
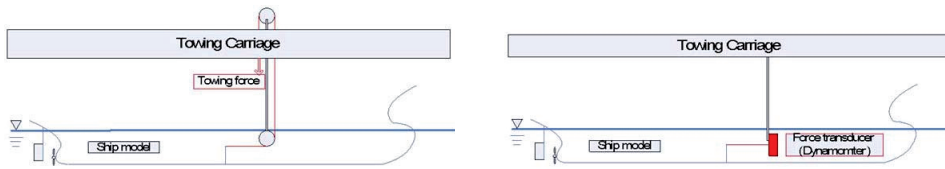

Fig. 4: Test set-up for propulsion test in the Continental (left) and British (right) methods.

The tow-rope force can be expressed as

$$F_D = C_S \rho_m V_m^2 S_m / 2$$

The tow-rope force coefficient C_S should be equal to the difference between model and full scale total resistance coefficient. It depends on details of the resistance scaling method. This work applies the standard method used at MARINTEK,

$$C_S = [C_{Fm} - (C_{Fs} + \Delta C_F)](1 + k_0) + (C_{BDm} - C_{BDs}) + (C_{Appm} - C_{Apps}) - C_A \qquad (1)$$

The first term in eq. (1) is the difference in friction resistance between the full and model scales. The second and third terms correct for the differences in resistance related to transom stern and appendages, respectively. The last term is the correlation allowance which accounts for systematic errors in the scaling method and model test set-up.
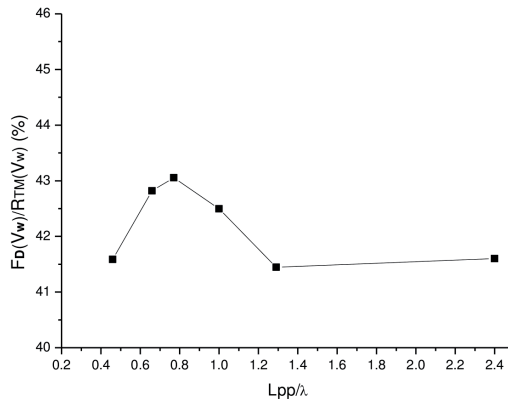

Fig. 5: Ratio between tow-rope force and model scale calm water resistance at attainable speeds in waves.

Figure 5 shows the ratio between tow-rope force and calm-water resistance at the model scale for attainable speeds in waves for model A. The tow-rope force accounts for a large percentage of the calm-water resistance (over *40%*). However, in the seakeeping tests, the tow-rope force was not included due to the practical difficulty of applying a tow-rope force on a freely running model. So the model test results have to be corrected before comparison with full-scale data. An approach for this correction was suggested by *Chuang and Steen* (2011). However, that approach neglected the nonlinear change of the total resistance in waves. An improved approach is specified below.

The delivered power was kept constant in time in the model tests, and had the same value in calm water and in waves. When no tow-rope force is used, resistance and thrust should be balanced

for converged speed. The resistance in waves is separated into calm-water resistance R_{TC} and added resistance due to waves R_{AW}, then the power equality can be expressed as:

$$R_{TC}V_C/\eta_{DC} = [R_{TC}(V_{W1}) + R_{AW}(V_{W1})]\,V_{W1}/\eta_{DW} \qquad (2)$$

V_{W1} is the converged speed in waves without tow-rope, and $\eta_D = \eta_0\eta_H\eta_R$ is the propulsive efficiency. Index c denotes calm water, index w 'in waves'. The change of propulsive efficiency in waves is taken into account by changing the propulsion point, i.e. by changing open-water efficiency coefficient η_0. Relative rotative efficiency η_R and hull efficiency η_H are assumed to be constant. When tow-rope force is used, the resistance less the tow-rope force value should be equal to the thrust from the propulsion system when attainable speed is achieved both in calm water and in waves. The power equality becomes:

$$[R_{TC}(V_C) - F_D(V_C)]\,V_C/\eta_{DC} = [R_{TC}(V_{W2}) + R_{AW}(V_{W2}) - F_D(V_{W2})]\,V_{W2}/\eta_{DW} \qquad (3)$$

V_{W2} is the converged speed in waves with tow-rope.

In equations (2) and (3), calm-water resistance, tow-rope force and added wave resistance can be expressed by the only unknown variable V_W. Then insert each polynomial resistance and force curve into these two equations and solve them for the converged speed in different wave conditions. The model test result should be corrected by the difference between the two expressions for velocity in waves, i.e. $\Delta V = V_{W1} - V_{W2}$.

3 Numerical methods to calculate speed loss

3.1 Time-domain model

For the time-domain simulations, the *ShipX Vessel Simulator* (*Vesim*) was applied, *Ringen and Fathi* (2008). The theory implemented in *Vesim* is outlined in the following. The equations of motion in six degrees of freedom are solved in a body-fixed coordinate system in full scale.

$$(M + A_{jk})\,\ddot{\eta}_j = \sum F_k$$

This equation is solved at each time step to get the vessel speed as time series. $\sum F_k$ is the sum of all the external forces. In this analysis, external forces from calm-water resistance, incoming wave resistance and thrust from propulsion system are considered. In the following, we focus on the forces in surge direction,

$$\sum F_1 = F_{calm} + F_{wave} + F_{thrust}$$

Each term of the total force will be described in Section 4.

Added mass and damping are frequency dependent. However, in time-domain calculations, there are many excitation frequencies. Thus, the radiation forces are calculated by means of a convolution integral, using retardation (kernel) functions to include the memory effects. Following *Cummins* (1962), the radiation force is written as

$$F = \int_0^t h(t - \tau)\dot{\eta}(\tau)\,\mathrm{d}\tau$$

The retardation function $h_{jk}(t)$ can be evaluated by

$$h_{jk}(t) = -\frac{2}{\pi}\int_0^\infty w[A_{jk}(w) - A_{jk}(\infty)]\sin wt\,\mathrm{d}w$$

$$h_{jk}(t) = \frac{2}{\pi}\int_0^\infty [B_{jk}(w) - B_{jk}(\infty)]\cos wt\,\mathrm{d}w$$

$A_{jk}(\infty)$ and $B_{jk}(\infty)$ are added mass and damping matrix at infinite frequency. Calculation of $h_{jk}(t)$ requires information on the behaviour of either A_{jk} or B_{jk} at all frequencies.

3.2 Frequency-domain model

Speed loss was also calculated in the frequency domain in order to find the forward speed that gives equilibrium between thrust and resistance. An iterative procedure is used. The procedure is based on *Berget et al.* (2009), Fig. 6.
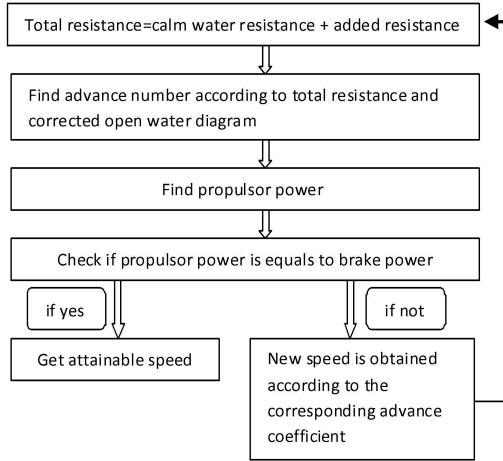

Fig. 6: Speed loss algorithm in the frequency domain.

Based on the initial vessel speed input, the total resistance including the calm-water resistance and the added resistance are calculated. Then based on calculated total resistance, the open-water diagram is applied to find the corresponding torque and advance number. After that the delivered propulsion power is calculated as

$$P_D = 2\pi\rho D^5 n^3 K_Q / \eta_R$$

Finally, the delivered propulsion power is compared with the power delivered to the propeller. If they are equal the final attainable speed is obtained. Otherwise, new speed is calculated according to the known corresponding advance number, and the total resistance is updated until the equilibrium point is found.

4 Calculation of forces

4.1 Calm-water resistance

The resistance model tests were performed in the towing tank. Seventeen speeds covered a Froude number range from *0.152* to *0.273*. Full-scale ship resistance was determined from model test results according to a slightly modified version of the ITTC'78 method as

$$C_{Tm} = C_{Rm} + (1 + k)C_{Fm} + C_{BDm} + C_{Appm}$$

Strictly speaking, air resistance should be included. However, it comprises only a small part in the total resistance, therefore it is neglected in this study. Residual resistance is Froude scaled, i.e. $C_{Rm} = C_{Rs}$. The total full-scale resistance coefficient can be written as

$$C_{Ts} = C_{Rs} + (C_{Fs} + \Delta C_F)(1 + k) + C_{BDs} + C_{Apps} + C_A$$

and the total calm-water resistance can be calculated as

$$R_{Ts} = \frac{1}{2}\rho V^2 S C_{Ts}$$

The resistance at any speed within the range of interest can be found from approximating the resistance curve by the polynomial

$$R_{Ts} = a_1 V^3 + a_2 V^2 + a_3 V + a_4 \tag{4}$$

a_1 to a_4 are regression coefficients. Figure 7 shows the calm-water resistance of the three different models in percentage of maximum calm water resistance of model A. The results show that resistance values for model A and model B are quite similar. Model A is somewhat better at speeds below $V_s = 7.2$ m/s, while model B is slightly better above 7.2 m/s. Model C has significantly higher resistance at speeds above 6.0 m/s, due to the missing wave cancellation effect set up by the bulb for the other two designs.
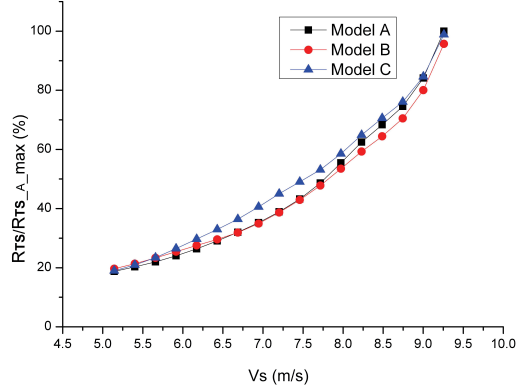

Fig. 7: Full-scale calm-water resistance for three models.

4.2 Added resistance in waves

Added resistance by Gerritsma & Beukelman's method

Added resistance is calculated by the method of *Gerritsma and Beukelman* (1972), based on the assumption that the energy in the radiated waves caused by the wave-induced ship motions is equal to the work of added resistance. We consider regular head waves. The energy radiated during one wave encounter period T can be obtained by

$$P = \int_0^T \int_L b_{33} V_Z^2 \, \mathrm{d}x_b \, \mathrm{d}t$$

L is the ship length, b_{33} the sectional damping coefficient of the vertical motion of a section x_b, V_z is the average vertical relative velocity of water in heave. The damping coefficient can be defined as

$$b_{33} = N' - V \mathrm{d}m'/\mathrm{d}x_b$$

N' is the 2D cross-sectional heave damping coefficient, and m' is the cross-sectional added mass. The vertical relative velocity can be approximated by

$$V_Z = \dot{Z} - x_b\dot{\theta} + U\theta - \dot{\zeta}' \tag{5}$$

$\dot{Z}$ is the vessel vertical velocity, U the ship forward speed, θ the pitch angle, ζ' the effective wave displacement for a cross-section. The value of ζ' is a correction to the Froude-Krylov hypothesis, which assumes that the water pressure on the ship hull and the wave field is not disturbed by the

ship. This correction affects the amplitude of the incident wave. For deep water, it can be calculated as

$$\zeta' = \zeta \left(1 - \frac{k}{y_w} \int_{-T}^{0} y_b e^{k z_b} \, \mathrm{d}z_b \right) \tag{6}$$

k is the wave number, y_w is the half width of the design waterline at section x_b, and ζ is the wave amplitude without modification. y_b and z_b are the lateral and vertical coordinates, respectively, of section at x_b.

V_Z is a harmonic function of time with amplitude V_{Za} and frequency ω_e. The mean value of power can be written as

$$P = \frac{\pi}{\omega_e} \int_L b_{33} V_Z^2 \, \mathrm{d}x_b$$

The work done by the added resistance R_{AW} is given by

$$P = R_{AW}(V + c)T_e = R_{AW}\lambda$$

Thus, added resistance can be expressed as

$$R_{AW} = \frac{\pi}{\omega_e \lambda} \int_L b_{33} V_Z^2 \, \mathrm{d}x_b \tag{7}$$

This method works well when the relative vertical motion with respect to the water is important, as shown by equations (5) and (6). Thus this method is intended to predict added wave resistance in long waves. In short waves, when the ship oscillatory motion can be neglected, eq. (7) cannot predict resistance satisfactorily. For a motionless ship at a high speed, this method will underestimate the diffraction force and also fail to include the influence of viscous effects when the encounter frequency is high.

Added resistance by direct pressure integration

The second theory used here to calculate added resistance is direct pressure integration (DPI), *Faltinsen et al.* (1980). This theory assumes that the incident wave length is large relative to the cross-section dimensions. The diffraction potential is solved by the 'relative motion method', which implies that the wave length is large, three-dimensional effects can be neglected and the diffraction potential can be found from a two-dimensional Laplace equation. This method expands the Laplace equation to second order taking instantaneous ship motion and wetted hull surface into consideration and integrates the longitudinal component of the oscillating pressure over the wetted surface of the hull. Added resistance can be written as

$$\begin{aligned}
R_{AW} = &-\frac{\rho g}{2} \int_c \overline{\zeta_r^2}\, n_1 \mathrm{d}s - \omega_e^2 M\overline{\eta_3 \eta_5} + \omega_e^2 M\overline{(\eta_2 - Z_G \eta_4)\eta_6} + \\
&\rho \int_{S_B} \overline{(\eta_2 + x\eta_6 - z\eta_4)\tfrac{\partial}{\partial y}\left(\partial\phi/\partial t + U\partial\phi/\partial x\right)_m n_1}\mathrm{d}s + \\
&\rho \int_{S_B} \overline{(\eta_3 - x\eta_5 + y\eta_4)\tfrac{\partial}{\partial z}\left(\partial\phi/\partial t + U\partial\phi/\partial x\right)_m n_1}\mathrm{d}s + \\
&\tfrac{1}{2}\rho \int_{S_B} \overline{\left[(\partial\phi/\partial x)^2 + (\partial\phi/\partial y)^2 + (\partial\phi/\partial z)^2\right]n_1}\mathrm{d}s
\end{aligned}$$

$\zeta_r = \zeta - (\eta_3 - x\eta_5 + y\eta_4)$ is the relative wave amplitude along the ship, ω_e is the encounter frequency, ϕ is the first-order velocity potential, c is the waterline, and ζ_i ($i = 1, 2, ..., 6$) are the vessel displacement amplitudes in six degrees of freedom.

Accurate calculation of ship motion plays an important role in added resistance prediction. The Salvesen-Tuck-Faltinsen (STF) strip theory *Salvesen et al.* (1970) is used to find the ship motions.

4.3 Propulsion system

Azipull thruster model

In the time-domain simulations, thrusters were controlled by an autopilot system to keep the power constant. This is analogous to the experiment. A track controller was also applied in the simulations. The present implementation assumes that the track is going straight north. Therefore, only the east position of the track is specified to define the ship's track. Output is the rudder angle commanded to the two Azipull propulsors.

The propeller model is based on *Strøm-Tejsen and Porter* (1972). A general analytical expression was developed for the performance of an arbitrary propeller as function of blade-area ratio, pitch, propeller rate, direction of revolution, ship speed and direction of motion. Thus, propeller thrust and torque are calculated based on a four-quadrant numerical model. The first step in calculating the thrust and torque from the propeller is to calculate the advance velocity, ship drift angle and azimuth angle at the propeller position. Based on the revolutions and diameter, the hydrodynamic angle of advance can be obtained as

$$\beta_i = tan^{-1}\left(\frac{V_a}{0.7\pi nD}\right)$$

β_i is the hydrodynamic angle of advance, V_a is the advance velocity, n is the propeller revolutions, and D is the propeller diameter. The propeller thrust and torque coefficients are applied as functions of hydrodynamic angle of advance in four quadrants. The effect of the pod is included as a calculated drag force, based on the total ship velocity at propeller position, pod area and the drag coefficient. The pod drag coefficient, based on model tests data, is applied as a function of pod angle and ship heading angle, *Ringen* (2010). Interaction effects between propeller race and pod are neglected. Thrust deductions are obtained from calm-water model tests and assumed to be constant and independent of waves and propeller loading.

One example of power and thrust simulated using this model in regular head waves with period *7.5* s and height *2.0* m are shown in Fig. 8. The power was kept constant in the entire time window. Thrust was observed oscillating around an increasing value during the initial stage and later around a constant value. This can be explained by the speed change: the vessel speed decreased at the beginning and then converged.
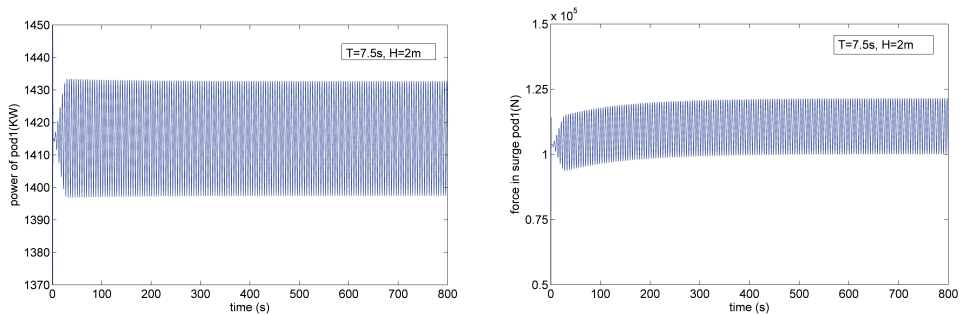

Fig. 8: Power (left) and thrust (right) in time-domain simulation in regular head waves with period *7.5* s and height *2.0* m.

In the frequency domain, ignoring the thrust fluctuations, only first-quadrant open-water characteristics obtained from open-water model tests, Fig. 9, were used to evaluate the mean thrust and torque values.

Change of propulsive efficiency in waves

The propulsive efficiency expresses the ratio between the effective towing power required to overcome the resistance and the power supplied to the propeller,

$$\eta_D = \eta_0 \eta_H \eta_R = \frac{V T_m (1 - t)}{2\pi n Q_m}$$

In a seaway, propulsive efficiency might be reduced due to the following effects:

– loss of effective propeller disc area
– propeller disturbing the free surface and creating a wave system
– Wagner effect, related to blades emerging from the water
– change of propulsion point

The first three effects can be accounted for by adopting a thrust loss factor, *Faltinsen et al.* (1980), but they are only important for high sea states – higher than the waves studied here. In this paper, the first three effects are not taken into consideration. The changing propulsive efficiency due to change of propulsion point in waves from the time-domain study of model A is shown in Fig. 10. Also in the frequency-domain calculation, the propulsive efficiency changes with resistance due to the changing propulsion point.
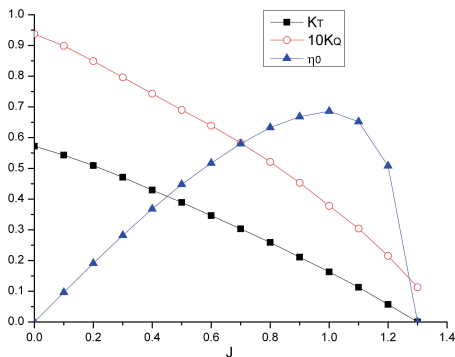

Fig. 9: Open-water propeller curves applied in the fre-quency domain.
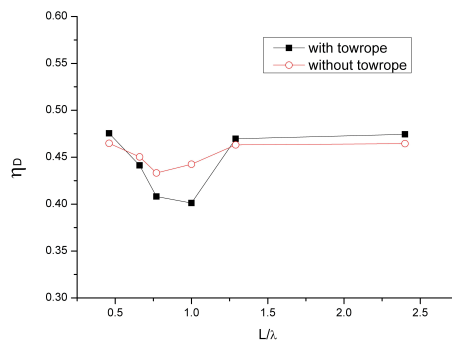

Fig. 10: Propulsive efficiency change due to tow-rope force in waves for model A in the time-domain study.

Since the calm-water propulsion point (when tow-rope force is used) and $F_n = 0.22$ is located at $J = 0.9$, it is easily found from the propeller open-water curves in Fig. 9 that an increase in resistance will lead to a shift in the propulsion point to the left in Fig. 9, leading to a reduced open-water efficiency, and thereby reduced propulsive efficiency. Thus, the change in propulsion efficiency in Fig. 10 reflects the change in added resistance due to waves.

5 Comparison between model tests and simulations

In this section, speed loss results obtained from model tests and simulations are compared. Simulations were carried out in full scale, and model test results were scaled to full scale according to the direct Froude scaling method. In the following figures, 'EXP without towrope' means the model test data scaled directly to full scale, without correcting for lack of tow rope force, 'EXP corrected, new method' represents the model test data after being corrected according to the method given in Section 2.2, 'TD' denotes time domain and 'FD' frequency domain.

5.1 Importance of tow-rope force correction

Figure 11 gives an example of the speed loss of model A, showing different attainable surge speeds under the scenarios that the tow-rope force is corrected or not, in time-domain simulation and model test. The time evolution is shown for the simulation and converged speed is indicated for the model test. Results from time-domain simulation without tow-rope force coincide fairly well with experimental results without correction ('EXP without towrope'). The model test results with correction for tow-rope by the method suggested in this paper ('EXP corrected, new method') agree well with the time-domain simulation result with tow-rope force. The model test data corrected by the method by *Chuang and Steen* (2011) are shown as 'EXP corrected (linear)'. The correction method for the tow-rope force proposed in this paper improves the result, but it slightly underestimates the difference in speed in this case. The simulation without tow-rope force was performed by direct scaling the model resistance as $R_{Ts} = R_{Tm}(L_s/L_m)^3(\rho_s/\rho_m)$. For the case with tow-rope force, the calm-water resistance curve is applied according to eq. (4). Thus the speed loss found from seakeeping model tests is underestimated if no correction of the tow-rope force is applied. The proposed correction method can be regarded as a useful tool for this purpose.

6 Model test results

The model tests covered the range of wave lengths given by $0.46 < L/\lambda < 2.4$. Figure 12 shows the experimental speed loss for the three models after the correction for tow-rope force. The speed loss change as a function of L/λ is similar for all three models. This is expected since the large speed loss around $L/\lambda = 1$ is caused by heave and pitch motions, which are not much influenced by the bow shape. However, there are significant differences of the level of speed loss between the three models. Model A has a conventional bow and bulb and experiences the largest speed loss. Model C, which has a vertical stem without bulb, gets the lowest speed loss at most wave lengths. The difference between models A and C reaches up to *10%*: for $L/\lambda = 0.8$, speed loss for model A is *32%* and for model C *23%*, and for $L/\lambda = 1.0$, speed loss for model A is *36%* and for model C *27%*.
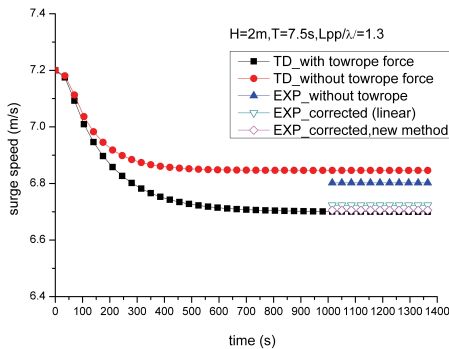

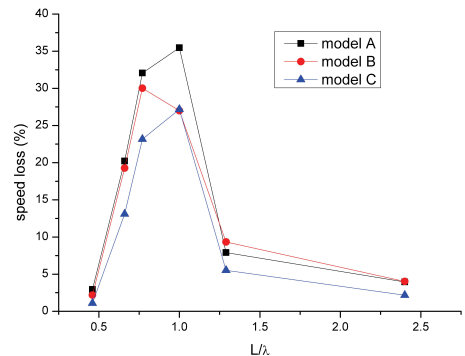Fig. 11: Attainable surge speed for model A with and without tow rope.

Fig. 12: Model test data for speed loss for three models.

6.1 Numerical results in time domain and frequency domain

Figure 13 compares results derived from model tests and simulations in both time and frequency domain computations. For this comparison, the added resistance was calculated by the *Gerritsma and Beukelman* (1972) method. For $\lambda \approx L$, added resistance reaches a peak value. The same speed loss trends were observed. Speed decreases as added wave resistance increases. When added resistance achieves a peak at $L/\lambda \approx 1$, the most severe speed loss occurs. Both the time-
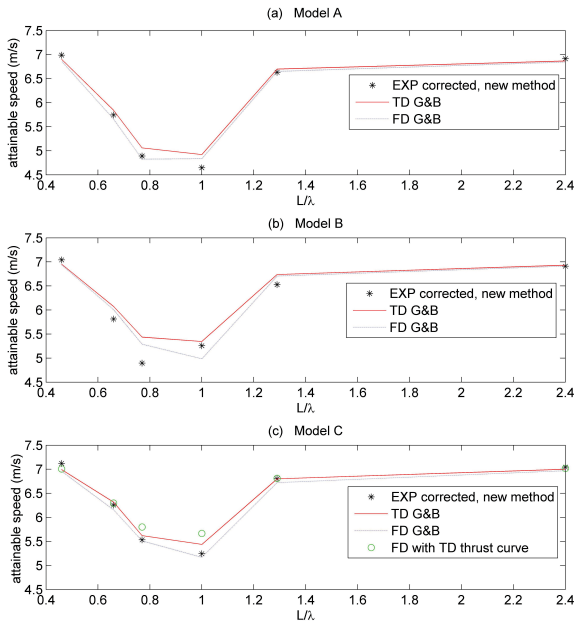
Fig. 13: Mean attainable speeds obtained in TD and FD computations for three models in different sea states.

domain method and the frequency-domain method predict the attainable speed in waves well. The small difference between the two methods is mainly caused by the two different thruster models used. The four-quadrant numerical model used in the time domain produces slightly higher thrust than the open-water curve used in the frequency-domain calculations. This deviation increases slightly when the advance coefficient decreases. To illustrate the effect of the thrust curve on the results, Fig. 13(c) includes an additional curve labelled 'FD with TD thrust curve', which shows the results from frequency-domain computations using the four-quadrant thrust curve. Most of the difference between time domain and frequency domain results vanishes.

Speed loss for model B is less than for model A, and speed loss for model C is less than for model B. This is due to the difference in the total resistance. The calm-water resistance of model C is slightly higher, while its added resistance in waves is smaller than for the other two models. Figure 14 shows an example of the non-dimensional added resistance coefficients $\sigma_{aw} = R_{aw}/(\rho g \zeta_a^2 B^2/L_{pp})$ obtained from the *Gerritsma and Beukelman* (1972) method. The added resistance coefficients of model A with conventional bow are the largest, and model C indicates the smallest values; model B is in between. The same trends were observed in all wave conditions studied in this paper. Thus, even though a bulb usually will reduce the calm-water resistance of a vessel, it may cause larger added resistance in waves.

Figure 15 shows the full-scale brake power for the three models as percentage of the maximum brake power of model A, based on the model tests in calm water. Model C has significantly higher brake power at speeds between *6.0* and *8.5* m/s, due to its higher calm-water resistance. The brake power is similar for models A and B. At the design speed *7.2* m/s, the brake power for model A is slightly higher than for model B, and at the speed of *6.7* m/s it is slightly lower. Table 2 lists the time-domain speed loss results for the three models in waves with different power settings. Power setting *1* means that the three models were running with different power and each power is used to balance the different calm-water resistance in order to obtain the same initial speeds, corresponding to *Fn = 0.22*. This is the same procedure as in the model test. The corresponding speed reduction values are found according to the time-domain converged attainable speeds in Fig. 13. Power setting *2* means that all the three models were running with the same power value. This power is the power
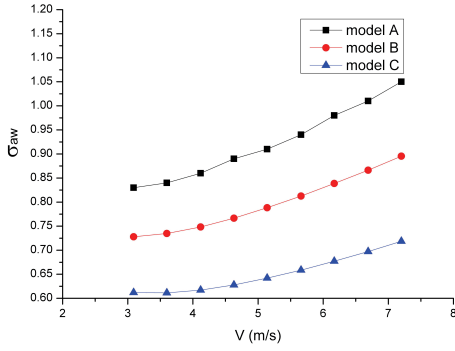
Fig. 14: Added resistance coefficients of three models in head waves with period *5.5* s and height *2.0* m.
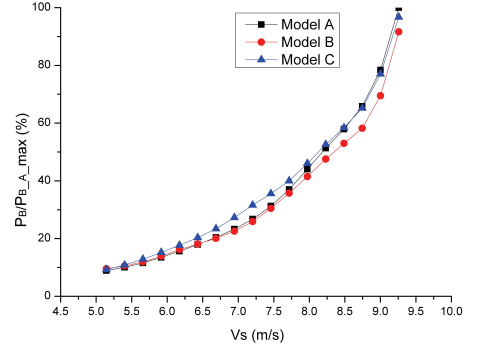

Fig. 15: Full-scale brake power for three models.

Tab. 2: Attainable speeds [m/s] from time-domain simulations for three models with different power settings.

	Power setting *1*			Power setting *2*		
	A	B	C	A	B	C
Power [kW]	*2380*	*2310*	*2680*	*2380*	*2380*	*2380*
Calm water	*7.20*	*7.20*	*7.20*	*7.20*	*7.24*	*6.95*
$L/\lambda = 2.4$	*6.87*	*6.93*	*7.00*	*6.87*	*6.94*	*6.73*
$L/\lambda = 1.3$	*6.70*	*6.74*	*6.80*	*6.70*	*6.71*	*6.45*
$L/\lambda = 1.0$	*4.92*	*5.35*	*5.74*	*4.92*	*4.83*	*5.16*
$L/\lambda = 0.77$	*5.06*	*5.44*	*5.83*	*5.06*	*5.15*	*5.41*
$L/\lambda = 0.66$	*5.84*	*6.07*	*6.32*	*5.84*	*5.94*	*5.98*
$L/\lambda = 0.46$	*6.90*	*6.96*	*6.99*	*6.90*	*6.97*	*6.73*

required for model A to reach the speed of *7.2* m/s in calm water. In this case, model B and model C indicate lower calm-water speeds. For power setting *2*, model C achieves the highest speed in waves in the range of wave lengths giving the largest speed loss, L/λ from *0.66* to *1.0*.

6.2 Influence of added resistance prediction method on the speed loss

Figure 16 shows the speed losses and non-dimensional added resistance coefficients from model tests and time-domain simulations, where added resistance due to waves was calculated by the methods of *Gerritsma and Beukelman* (1972) and direct pressure integration (DPI). Both methods predict the added resistance well in most cases, with the *Gerritsma and Beukelman* (1972) method being slightly better than DPI. For wave lengths near the ship length, DPI overestimates added resistance for the ship with a conventional bulbous bow. The DPI method was found sensitive to the ship hull shape. When the wave length is close to the ship length, the DPI method overestimates added resistance, leading to the deviation of the estimated speed loss from the model test results. Especially for model A, which has a conventional bow with bulb, the deviation is much larger than for the other two models. For model C, with a rather simple vertical stem shape, the DPI method produces a very good prediction. Figure 16 shows that the DPI method provides in general larger added resistance than the method of *Gerritsma and Beukelman* (1972) and the experimental results.

Model tests and simulations show that model C with simple vertical stem shape is more efficient in reducing the added resistance in waves than the other models.
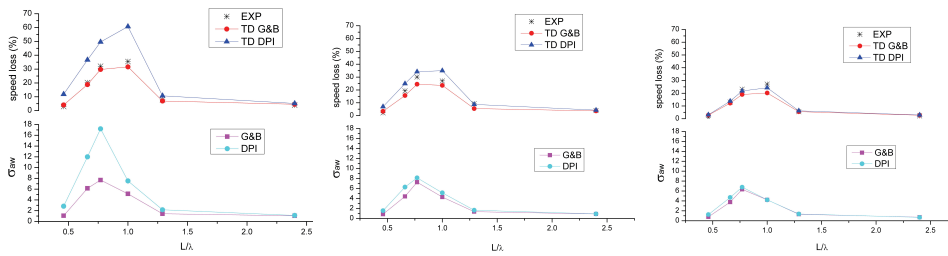
Fig. 16: Speed loss (top) and added resistance due to waves (bottom) for model *A* (left), *B* (middle) and *C* (right).

7 Conclusions

The results of this study show that the speed loss is strongly underestimated in self-propelled seakeeping model tests, unless a tow-rope force corrects for the relatively larger frictional resistance in model scale. The proposed correction method improves the prediction. Second, if the loss of thrust is not considered, propulsive efficiency in waves changes only due to the change of propulsion point. For wave lengths near ship length, speed loss reaches its peak value and propulsive efficiency its lowest point. Third, speed loss in waves can be reduced by up to 10% by relatively small changes to the bow shape of a vessel. A bulbous bow may decrease calm-water resistance, but increase added wave resistance and lead to increased total resistance. Fourth, both the time-domain and frequency-domain methods used in this paper predicted speed loss in head sea well. Further studies in oblique waves are needed to generalise this conclusion. Finally, added resistance in waves predicted by the *Gerritsma and Beukelman* (1972) method agrees better with experimental data than direct pressure integration method.

References

Berget, K., Fathi, D. and Ringen, E. *(2009).* ShipX Speed and Powering, Theory Manual. *MARINTEK, Trondheim*

Buhaug, Ø., Corbett, J. J., Endresen, Ø., Eyring, V., Faber, J., Hanayama, S., Lee, D. S., Lindstad, H., Markowska, H., Mjelde, A. Z., Nelissen, D., Nilsen, J., Pålsson, C., Winebrake, J. J., Wu, W. Q. and Yoshida, K. *(2009).* Second IMO GHG study *2009*. *Int. Maritime Organization (IMO), London*

Chuang, Z. and Steen, S. *(2011).* Prediction of speed loss of a ship in waves. *In Symp. Marine Propulsors (SMP'11), Hamburg*

Cummins, W. E. *(1962).* The impulse response function and ship motions. *Schiffstechnik, 9:101–109*

Faltinsen, O. M., Minsaas, K. J., Liapias, N. and Skjørdal, S. O. *(1980).* Prediction of resistance and propulsion of a ship in a seaway. *In 13-th Symp. Naval Hydrodynamics, Tokyo*

Gerritsma, J. and Beukelman, W. *(1972).* Analysis of the resistance increase in waves of a fast cargo ship. *Int. Shipbuilding Progress, 19:285–292*

ITTC *(2008).* Testing and extrapolation methods, propulsion, performance, predicting powering margins. *Int. Towing Tank Conf.*

Journee, J. M. J. *(1976).* Prediction of ship and behaviour of ship in a seaway. *Int. Shipbuilding Progress, 23*

Prpic-Orsic, J. and Faltinsen, O. M. *(2009).* Speed loss calculation in a seaway. *In IMAM Conf., Istanbul*

Rathje, H., Schellin, T. E. and Brehm, A. *(2010).* Speed loss in waves and wave-induced torsion of a wide-breadth containership. *In 11-th Int. Symp. Practical Design of Ships and Other Floating Structures (PRADS), Rio de Janeiro*

Ringen, E. *(2010).* Vesim-Propulsion Model (pod), User Manual. *MARINTEK, Trondheim*

Ringen, E. and Fathi, D. *(2008).* ShipX Vessel Simulator Plug-In, Theory Manual. *MARINTEK, Trondheim*

Salvesen, N., Tuck, E. O. and Faltinsen, O. M. *(1970).* Ship motions and sea loads. *SNAME Trans., 78:250–287*

Smogeli, O. N. *(2006). Control of marine propellers – From normal to extreme conditions. Ph.D. thesis, NTNU, Trondheim*

Strøm-Tejsen, J. and Porter, R. R. *(1972).* Prediction of controllable-pitch propeller performance in off-design conditions. *In 3-rd Ship Control System Symp., Bath*

Paper 3

Speed loss due to seakeeping and maneuvering in zigzag motion

Zhenju Chuang, Sverre Steen

Speed loss due to seakeeping and maneuvering in zigzag motion

Zhenju Chuang*, Sverre Steen

Department of Marine Technology, Norwegian University of Science and Technology (NTNU), Trondheim, Norway

ABSTRACT

Ships are prone to experience a slight zigzag motion due to the interaction between steering, waves and other external disturbances. The zigzag motion will induce an added resistance and hence speed loss. This paper aims at addressing an effective tool to predict a ship's zigzag motion and azimuth propulsion system behavior in calm water and different sea conditions, and the resulting speed loss. Both model tests and numerical simulations have been carried out. Model tests with a freely running model were done in MARINTEK, Trondheim, Norway. The propulsion system was composed of two azipull thrusters, with autopilot control system to keep the power constant during the test process. Model speeds and the propulsion system behavior were recorded as time series when the models were freely running in calm water and regular head sea waves. Numerical simulations with simplified modular maneuvering model were conducted to verify the model test data. Good agreement between simulations and experimental results was found. The results also showed that when wave added resistance reach its peak value, the vessel has the most severe speed loss.

1. Introduction

Recent development of the maritime transportation has highlighted the importance of the precise maneuverability of a ship both for designer and operator. With the increasing awareness of the environmental protection, more attention was paid to the efficient hull form design. Also larger ships increasingly tend to use azimuth propulsion instead of traditional propeller and rudder system, due to its better maneuverability. However, especially for full ship forms, the use of azimuth propulsion instead of conventional propeller and rudder tends to make the ship more course–unstable. A course–unstable ship tends to experience a slight zigzag motion during transit (Grimstad, 2009). The zigzagging leads to added resistance, and the steering of the azimuth propulsors leads to thrust loss. Both effects contribute to the speed loss. This paper is addressing an effective tool to predict speed loss of an ocean-going vessel during zigzag motion in both calm water and wave conditions.

In recent years, there have been a number of publications on maneuvering in waves. Lee (2000) developed linear integro-differential sway-yaw equations with rudder deflection in regular waves. The maneuvering motion of Todd's series 60 model was calculated with impulse response functions to consider the wave exciting force in zigzag 10–10 maneuver in waves. However, only linear maneuvering derivatives were taken into account in his

model. He pointed out that more calculations must be carried out for directionally unstable ship with nonlinear derivatives included. Fang et al. (2005) developed a simplified six degrees of freedom mathematical model to present the two container ship' behavior during turning circle maneuver in waves. All hydrodynamic coefficients are time varying with encounter frequency and calculated by strip theory. He showed that the effect of nonlinear terms for maneuvering derivatives is significant and cannot be neglected. Skejic (2008) applied a two time scale concept to solve the combined seakeeping and maneuvering problem. Ship maneuverability in waves was analyzed by using a two time scale formulation in which the linear wave induced motions of a ship are assumed to occur on a more rapidly varying time scale than the maneuvering. The wave frequency problem is affected by the slowly varying maneuvering. On the other hand, the effect of the seakeeping on the maneuvering analysis is in term of slowly varying mean second order wave loads that occur for the changing ship speed and wave heading. However, this method is challenged when the encounter frequency is low, for example in following sea condition.

However, the knowledge of the prediction of performance of azimuth (or pod) propulsor driven ship during seakeeping and maneuvering is limited. Ayaz et al. (2005) took advantage of an existing coupled non-linear six-degree-of-freedom model to simulate the maneuvering and seakeeping behavior of an azimuthing pod-driven vessel. His attention was paid to roll and pitch motion of the vessel in different sea states without addressing any speed trends. Reichel (2007) focused on the maneuvering in calm water of a gas carrier model with an azimuthing podded propulsor. Steering forces were measured with the different range

* Corresponding author. Tel.: +47 96807451; fax: +47 73595528.
  E-mail address: chuang.zhenju@ntnu.no (Z. Chuang).

Fig. 1. Experimental set up.

Fig. 2. Thrusters arrangement at the stern.

Table 1
Principal dimensions of model hull.

	UNIT	Model
L_{OA}	[m]	7.142
Lpp	[m]	6.832
D	[m]	0.905
B	[m]	1.147
T	[m]	0.435

Table 2
Waves Setting.

Vm (m/s)	H (m)	T (s)	λ/L_{pp}
1.77	0.12	1.351	0.417
	0.12	1.597	0.57
	0.12	1.842	0.775
	0.12	2.088	0.996
	0.12	2.579	1.52

Table 3
Variables measured in the model tests.

Ship model	Six degrees freedom of motion; yaw rate;
Propulsion characters	Unit thrust, power; propeller thrust, torque, shaft speed; rudder feedback angle;
Wave	Wave elevation relative to the tank; Wave elevation in front of the ship model;

of advance coefficients and deflection angles, where fixed vessel speed was set in each single test without taking wave effect into account. Liu et al. (2009) investigated propulsive dynamics of a podded propulsor unit in steering motion at fixed azimuth angles numerically, ignoring the influence of the hull effect on the thruster.

Analysis of ship maneuvering requires knowledge about resistance, propulsion, ship machinery, seakeeping, steering and automatic control (Faltinsen, 2011). In this paper, both experimental and numerical work was done taking all these factors into consideration Fig. 1.

2. Model test procedure

Seakeeping and maneuvering model tests were carried out in the large towing tank ($L \times B \times D = 260\,\text{m} \times 10\,\text{m} \times 5\,\text{m}$) at MARINTEK, Trondheim, Norway. Recording and control equipment were installed on the towing carriage. A model of a new 8000 DWT tanker was used in the model test, which was developed by Rolls-Royce Marine, Ship Technology – Merchant. During the tests, the ship model was self-propelled and self-steered by scale-models of twin AZP120 thrusters (with the model scale propeller diameter of 0.199 m), as shown in Fig. 2. No tow rope force was applied, so that the model operated at the model self-propulsion point. The only connection between the model and carriage are cables to relay the measurements and provide power to the propulsion motors. Zigzag 10/2 (10 deg for rudder angle, 2 deg for ship heading) maneuvers were carried out in both calm water and head regular waves.

The ship model has a wide transom and conventional bow with bulb. The main dimensions of the model hull are listed in Table 1.

Five regular head waves were carefully selected, covering the range of both short and long waves. All waves were calibrated before the tests. The wave data from the calibration is shown in Table 2 in model scale.

Four test types were carried out to quantify the performance of speed loss due to yawing, loss of thrust and added wave resistance. Power settings were kept the same during these four steps.

Straight line course in calm water was tested first as a basic reference. In this case, the vessel was running with constant initial

speed with the pre-designed thruster power. A track controller was used in order to keep the model running along the centerline of the towing tank. Secondly, zigzag motion in calm water was considered. Speed loss caused by added resistance due to yawing and loss of thrust will be apparent by comparing the speeds from this run and the basic run. After that, straight line course in waves was tested. Head sea conditions were modeled with the wave setting as specified in Table 3, and the track controller was used in this case. Comparing the measured data obtained from this step and the reference, speed reduction caused by added wave resistance is found. The results and discussion of the model test results and simulation of performance in waves in straight ahead condition is found in Section 5, and is not shown here. Finally, zigzag motion in waves was considered. Speed drop in this case includes all the effects including added resistance

due to yawing and loss of thrust as well as added wave resistance. By testing all the five different wave conditions, the relation between speed loss and added wave resistance in the same zigzag maneuver can be seen.

The most important variables measured during the model tests are listed in Table 3.

3. Numerical simulations

For the numerical time domain simulations, the Vesim ship simulator (Ringen and Fathi, 2008) combined with ShipX Vessel Response Plug-In (Fathi and Hoff, 2008) ShipX maneuvering Plug-In (Ringen, 2009) was applied to solve the coupled six degrees of freedom maneuvering equations of motion. Wave effects were considered by updating the hydrodynamic coefficients at each time step and the retardation function was used to consider the memory effect. Maneuvering equations of motion were established based on the simplified modular maneuvering model concept which was proposed by the Japanese research group named Maneuvering Mathematical Modeling Group (MMG) (Ogawa and Kasai, 1978). The MMG model represents total system forces and moments through a set of interactively connected modules with each module programmed as a separate unit. The complete maneuvering model can be expressed by linearly superimposing each module together. Herein, three modules were considered, namely: maneuvering forces module, wave resistance module and propulsion system module. Each of them will be specified in the following.

3.1. Maneuvering forces

Added mass coefficients were obtained by STF strip theory of Salvesen et al., (1970) and high speed strip theory of Faltinsen and Zhao (1991). Linear damping coefficients in sway and yaw are based on the slender body theory. Some linear damping derivatives such as linear damping in sway caused by sway and yaw, and linear yaw damping moment caused by sway and yaw are obtained with the combination of the added mass coefficients CH, as described in Clarke (1972).

The longitudinal resistance R_{TM} was found from ordinary towing tests in the towing tank. Since we compare the simulations with model tests without tow rope force correction, we have used the model scale resistance curve in the simulations, directly scaled to full scale using the scale relation:

$$R_{TS} = R_{TM}\lambda^3 \rho_S/\rho_M \qquad (1)$$

Where λ is the geometric scale ratio, ρ is the water density, and subscripts M and S means model and full scale respectively. Seventeen speeds were chosen with the corresponding Froude number range from 0.152 to 0.273, and a polynomial fit to the scaled resistance was made. The resistance of any speed within the range of interest can be found from the polynomial curve:

$$R_{TS} = a_1*V^3 + a_2*V^2 + a_3*V + a_4 \qquad (2)$$

where a_1-a_4 are regression coefficients. Non-linear damping in sway and yaw is of quadratic form and obtained according to the cross-flow principle. The cross flow principle assumes that the flow separates at the lee side of a structure. This separation will cause a drag force in the opposite direction of hull motion and a lift force in the perpendicular direction of the hull motion. The drag force is called cross flow drag and it is a non-linear force by nature. To evaluate the cross flow drag force in sway and yaw, an empirical formula for the 2-D drag coefficient was applied, and integrated over the length of the vessel to obtain the total

coefficients, as shown in Eqs. (3) and (4).

$$F_D^2(\theta) = \frac{1}{2}\rho \int_L C_D(\theta,x)D(x)u_D(\theta,x)|u_D(\theta,x)|dx \qquad (3)$$

$$F_D^6(\theta) = \frac{1}{2}\rho \int_L C_D(\theta,x)D(x)xu_D(\theta,x)|u_D(\theta,x)|dx \qquad (4)$$

L is length of the vessel; $D(x)$ is sectional draught at longitudinal coordinate x. C_D is sectional cross flow drag, which was obtained in this paper by adopting the method proposed by Martinussen and Ringen (2000). In the calculation, it is assumed that flow separation will take place at a certain cross-section in the after-body. At small drift angles, this cross section is located at the position of the maximum curvature of the after-body hull lines. It is assumed that forward of this cross section there is no non-linear transverse force. The cross sectional drag coefficients were set for forebody hull sections, midbody sections and after body sections, and applied as functions of breadth-to-draught ratio B/T. All the data were obtained from tests with free running models and ship trials.

Non-linear damping in ship heading direction was calculated by a semi-empirical formula listed in Matsumoto and Suemitsu (1984). Introduction of this derivative was aimed at improving the calculation of speed loss in maneuvers involving the effect of large drift angle on the longitudinal force.

3.2. Wave forces

Wave forces are mainly composed of first order wave excitation forces and second order wave drift forces. In the current calculations, they are pre-calculated for different vessel speeds, headings and wave frequencies before the time domain simulation started. When the simulation started, both first and second order forces from the waves were calculated by interpolation in the input dataset at each time step. Radiation forces are calculated by means of a convolution integral using retardation functions to account for the memory effects.

3.2.1. First order wave exciting force

The first order wave excitation force is described by transfer function and the wave elevation.

$$F_{wave}^{(1)} = H^{(1)}(\omega,\theta)\zeta(\omega,\theta,x,y) \qquad (5)$$

where $H^{(1)}(\omega,\theta)$ is first order transfer function. It depends on wave frequency ω and propagation direction θ. $\zeta(\omega,\theta,x,y)$ is wave elevation which is the function of wave frequency, propagation direction and position in space.

3.2.2. Second order wave drift force

The second order wave drift force in oblique regular sea condition is mainly considered as added wave resistance; transverse drift force and mean yaw moment in surge, sway and yaw respectively. These forces are calculated by the method proposed by Loukakis and Sclavounos (1978). This method is based on the extension of the method proposed by Gerritsma and Beukelman (1972) which is originally only for head waves. The G&B method is based on the energy principle under the assumption that radiated energy is equal to the work of added resistance done and the energy contained in the damping waves. And this energy relationship can be expressed by the Eq. (6).

$$(-R_x)(U-c)T = \frac{\pi}{\omega}\int_0^L (b_{33} - U\frac{da_{33}}{d\xi})|U_{RZ}|^2 d\xi \qquad (6)$$

where R_x is added resistance, U is ship forward speed, c is the speed of wave propagation, ω and T the frequency and period of encounter, U_{RZ} is the vertical relative velocity of each ship section,

a_{33} and b_{33} are two dimensional sectional added mass and damping coefficients.

The left part of Eq. (6) corresponds to the work done on the fluid plus the amount of energy taken away from the direction of propagation of the incident wave and radiated all around the ship.

This approach can be extended to calculate the added resistance and drift force in oblique regular waves. It is known that if one considers a control surface fixed in space and surrounding the ship, the energy influx and efflux through it are equal when the contribution of the diffracted waves and ship generated waves are taken into consideration. The velocity of the ship relative to the fixed control surface is $U_R = U - c$ and can be resolved into U_{RH} and U_{RT} which are along and vertical to c respectively. The motion of the ship with U_{RT} does not make contribution to the mean horizontal force R_T, which consequently has the direction of the incident wave propagation. Then $(-R_T)U_{RH}$ shall represent the net energy given by the ship to the fluid $((-R_x)U)$ and the energy radiated all around the ship ($R_T c$). Then the left part of Eq. (6) can be rewritten as:

$$P = (-R_T)U_{RH} = (-R_T)(-c - U\cos\beta) \quad (7)$$

β is the wave propagation angle.

The final expressions which allow us to calculate the added resistance and drift force in oblique waves are:

$$(-R_T)(-c - U\cos\beta) = P_{35} + P_{26} + P_4 + 2P_{24} \quad (8)$$

$$|R_T| = \frac{k}{\omega}(P_{35} + P_{26} + P_4) + \frac{2k}{\omega}P_{24} \quad (9)$$

$$|R_x| = |R_T\cos\beta| \quad (10)$$

$$|R_y| = |R_T\sin\beta| \quad (11)$$

Where P_{35}, P_{26}, P_4, and P_{24} are energy radiated by ship heave-pitch motion, sway-yaw motion, roll motion and sway-roll motion during one encounter period.

3.3. Thrust forces

The propulsion system consists of two Azipull thrusters. A four-quadrant numerical propeller model was used here for maneuvering studies. The propeller model is based on the work described by Tejsen and Porter (1972). General analytical expression has been developed for the performance of an arbitrary propeller as functions of blade–area ratio, blade pitch setting and any combination of propeller rate and direction of revolution and ship speed and direction of motion. The first step in calculating the thrust and torque from the propeller is to calculate the advance velocity, ship drift angle and rudder angle at the propeller position. Based on the revolutions and diameter, the hydrodynamic angle of advance can be obtained, as shown in Eq. (12).

$$\beta_i = \tan^{-1}\left(\frac{V_a}{0.7\pi nD}\right) \quad (12)$$

where β_i is hydrodynamic angle of advance, V_a is advance velocity, n is propeller revolutions, D is propeller blade diameter. The propeller thrust and torque coefficients are applied as function of hydrodynamic angle of advance in four quadrants. The effect of the pod is included as a calculated drag force, based on the total ship velocity at propeller position, pod area and the drag coefficient. The Pod drag coefficient, which is based on the model tests data, is applied as a function of pod angle and ship heading angle (Ringen, 2010). Interaction effects between propeller race and pod are neglected.

An electric engine model was selected here for the two thrusters. Gear ratio and shaft loss were included by editing engine–propeller gear ratio and mechanical efficiency. Also the total moment of inertia of the engine and propeller were considered in order to give the correct rate of change of engine revolutions.

Thrusters were controlled by an autopilot system to keep the power constant, in the same way as in the experiment. Interaction between thruster and the ship hull was considered by including steady wake fraction ω and thrust deduction factor t, which are acquired from model tests.

It should be noted that also in the simulation, the model propulsion point was considered. This means that thrust forces are significantly larger, relative to the ship mass, than in full scale, since the thrust must overcome the larger frictional resistance of the hull in model scale. In turns, this means that the ship becomes more maneuverable when the model self-propulsion point is applied.

4. Speed loss due to yawing and loss of thrust

4.1. Speed loss due to loss of thrust

Calculation of hydrodynamic forces on the azimuth thruster due to steering is based on Fig. 3.

As shown in Fig. 3, the thruster has a steering angle α relative to the ship fixed coordinate system Os-$XsYs$, where T is the total thrust force along the propeller shaft. The thruster is rotated according to the rudder angle demand. Then the force in the longitudinal direction and the transverse direction relative to the ship can be expressed by Eqs. (13) and (14):

$$F_{longitudinal} = T \cdot \cos\alpha \quad (13)$$

$$F_{transverse} = T \cdot \sin\alpha \quad (14)$$

It can be seen that there will be a reduced force in the longitudinal direction of the ship if the azimuth unit has a rudder angle. The thrust T will also change when the inflow angle α change, as given by the four-quadrant propeller model explained in Section 3.3. As a result of the changing thrust force in long-itudinal direction $F_{longitudinal}$, the balance between thrust and resistance will change so that vessel speed drops until a new equilibrium point is established at a lower speed value.

4.2. Added resistance increase due to yawing

Here the added resistance increase due to yawing will be derived without considering the effect of waves. If a vessel suffers yaw motion, added resistance will be induced on the ship. The viscous resistance is increasing since the flow incidence towards the hull increases. However, it is difficult to split this component from the whole resistance, and therefore it is neglected in this paper. Also, a centrifugal force will be created on the ship when it
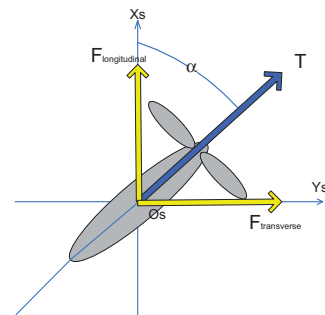

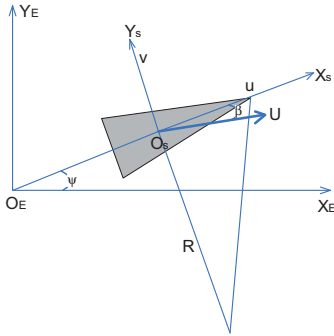**Fig. 3.** Azimuth thruster with steering angle.

Fig. 4. Maneuvering coordinate system.

is moving in a turn. This force will give a contribution to the longitudinal response of the ship. This is the added resistance due to yawing defined here. Norrbin (1972) developed a method to find the added resistance due to yawing using centrifugal force. This method is explained in the following.

Fig. 4 shows the in-plane earth fixed coordinate system O_E-$X_E Y_E$ and the body-fixed coordinate system O_S-$X_S Y_S$. The ship is turning with forward speed U, drift angle β, yaw angle ψ and turning radius R. The u and v are the ship mean speed in X_S and Y_S direction respectively.

Søding (1984) formulated the longitudinal component of Newton's second law in the body-fixed coordinate system as:

$$(M - X_{\dot u})\dot u = Mvr + X_{vr}vr - R_T + (1-t)T(u,n) + X_{vv}v^2 + X_{rr}r^2 + X_{\delta\delta}\delta^2 \tag{15}$$

where the notations are consistent with Fig. 4. The derivative term such as $X_{\dot u}, X_{vr}\ldots$ are used to express longitudinal hydrodynamic forces on the hull and the rudder. Further, R_T is ship resistance, in this section only calm water resistance included, t is thrust deduction, T is propeller thrust based on open-water characteristics, n is number of propeller revolutions per second, δ is rudder angle.

The main reason for added resistance increase in a turning motion is the terms Mvr and $X_{vr}vr$ and their linear dependency of the yaw rate. Other terms such as R_T and T are assumed to be independent of the turning motion. The second order maneuvering term $X_{vv}v^2$ is zero due to the symmetry of the ship (Faltinsen, 2005). $X_{rr}r^2, X_{\delta\delta}\delta^2$ are small compared to the other terms and can be neglected. Based on the relationship established as the following:

$$u = R\dot\psi \tag{16}$$

$$v = -u\beta \tag{17}$$

The two terms turn into:

$$Mvr + X_{vr}vr = -(M + X_{vr})\frac{u^2}{R}\beta \tag{18}$$

where β is always positive since the bow is always pointing inwards in a steady turn. So the right side of Eq. (18) is the added resistance term created during yaw motion.

5. Discussion of results

Speed loss behavior of a vessel equipped with two Azipull thrusters during zigzag (10/2, 10 deg for rudder angle and 2 deg for ship heading control) motion in both calm water and waves is of interest. Speed reduction and propulsion system behavior

obtained from model tests and numerical simulations are compared and verified in this section. Note that simulations were performed in full scale, and then scaled back to model scale in order to allow comparison with the model test results.

Fig. 5 shows the speed obtained in calm water during a zigzag maneuver. The green line represents the converged speed in calm water when the vessel was running along a straight line course, and serves as a reference. The blue line denotes the obtained speed of the model during the zigzag motion in calm water in the model tests, while the red line shows the speed obtained simulating the same maneuver. The rudder angle was set to 10 deg to port at first and reversed to starboard 10 deg when the vessel heading had turned 2 deg off the original heading. Then the ship would continue turning to port with decreasing rate and successively turn to starboard. These steps were repeated until the model reached the end of the tank or came too close to the tank walls. The recorded heading angle and rudder angle trends are shown in Figs. 6 and 7. In the tests of zigzag motion, converged speed was not achieved as shown by the blue line due to the towing tank length and width limits. Only three overshoot angles were captured during the test. It is clear from Fig. 5 that speed loss in numerical simulation coincides fairly well with the corresponding model test data, although the deviation might seem to be increasing during the last overshoot both in speed and heading.

When the test was repeated with the first rudder execute setting to starboard, a similar deviation in speed and heading were also observed in the final overshoot. The main reason for the deviation is believed to be the closeness to the tank wall, which is not included in the numerical simulation. Kumar and Subramanian (2007) pointed out that tank wall effects taper off at half tank width
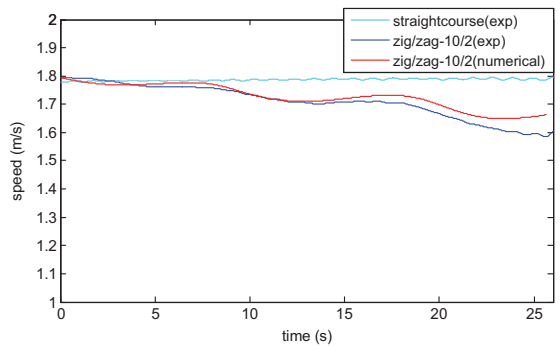

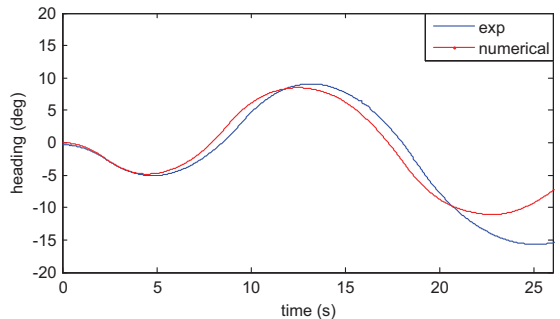**Fig. 5.** Speeds obtained during 10-2 zigzag in calm water condition.

Fig. 6. Headings obtained during 10-2 zigzag in calm water condition.

divided by model width ratio in excess of 5. In the third and final overshoot in the test reported in Figs. 5–8, the distance from ship's forward perpendicular to tank wall divided by ship width is 2.34 (the model had about 15 deg heading in this condition). In this case, it was observed that the bow waves were reflected by the tank wall and hit the stern, which will cause more heading deviation. Also there will be a suction force on the ship model, mainly on the bow, since this is closest. This 'wall effect' was observed in all the tests results from zigzag in calm water.

Fig. 8 shows the average unit side-force (y-axis in the ship fixed coordinate system) from the thruster units during the zigzag motion in calm water. In general, the magnitude is well predicted. The oscillations of the unit side force measured in the model test are mainly with three frequencies. The lowest one is around 1.8 Hz which is with the ship pitch period in calm water. The second one is about 10 Hz, which corresponds to the propeller shaft frequency and the third frequency which around 19 Hz is the thruster natural frequency. A 20 Hz low pass filter was applied in the model test, so for instance the blade passing frequency will not be found in the results. The oscillation in the numerical simulation is mainly caused by the ship's pitch motion. Also change of inflow to the propeller blade will change the thrust in magnitude and direction. When the ship is heading towards starboard or port, change of the sway force will induce a change of the inflow to the propeller and also the change of azimuth angle will affect the incoming flow to the propeller.

Based on the good agreement achieved in calm water condition, we proceeded to include wave effects in the simulations and experiments. The waves selected here were shown in Table 3,

including one short wave and four long waves. The same zigzag maneuver 10/2 was conducted in waves.

Fig. 9 shows speed loss during straight course motion in the only short wave condition selected here with period $T=1.351$ s, wave height $H=0.12$ m (in model scale), and wave length divided by ship length $\lambda/L=0.42$. Without yawing and loss of thrust in this case, the slight speed reduction of 3.1% was due to added wave resistance in surge direction. Numerical model result agrees well with model test data.

Fig. 10 shows speed loss in zigzag motion in the same short wave condition as Fig. 9. In the model test, the model was accelerated by an additional towing force, and by increasing the propeller speed during the acceleration phase. When a specified threshold-speed was reached, the towing rope was slackened and the propeller speed reduced to match the specified power setting. The selection of threshold speed had some importance for the results. Ideally, one would set the threshold speed equal to the calm water speed, but to increase the convergence, the threshold speed was set to a value just above the expected converged speed in the actual test condition. This is the reason why the speed plots might start at different velocity values—the propulsion power is the same in all cases. In Fig. 10, the blue line is the speed reduction trend recorded in the model test while the red line is the corresponding numerical result. It is observed that the general speed trends are captured, but that the speed loss is under predicted by the numerical simulation. Both speed lines are oscillating with two frequencies. The high frequency visible in Fig. 10 is the first order wave encounter frequency, and the low frequency (roughly six cycles shown in Fig. 10) is caused by the
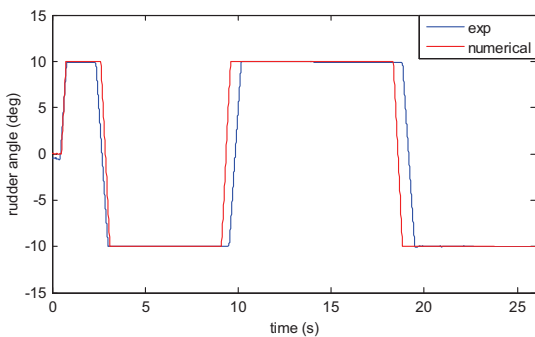

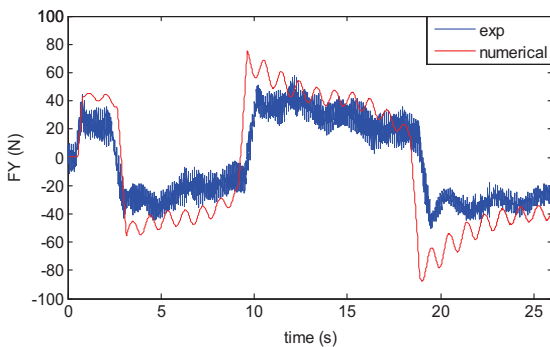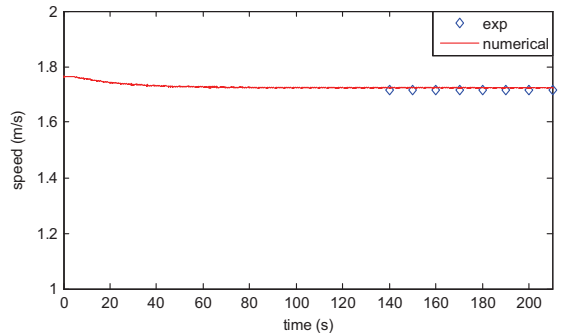**Fig. 7.** Rudder angles obtained during 10-2 zigzag in calm water condition.

Fig. 9. Speeds obtained during straight course motion in a regular head wave with period $T=1.351$ s and height $H=0.12$ m.

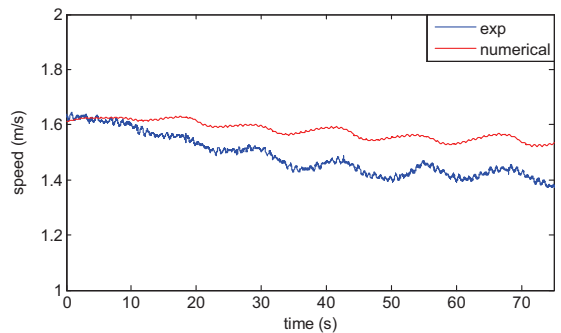**Fig. 8.** Average unit-side force obtained during 10-2 zigzag in calm water condition.

Fig. 10. Speeds obtained during 10-2 zigzag in a regular wave with period $T=1.351$ s and height $H=0.12$ m.

heading change frequency. During each heading change period, when the heading approaches its maximum or minimum, the corresponding surge velocity reaches its minimum value; and when the heading angle turns to zero degree, the speed comes up with its local maximum value. Thus within this zigzag motion, the low frequency speed change is two times the heading oscillation frequency. By comparing the two speed trends, it can be seen that the numerical simulation underestimates the speed loss observed in the model tests, and that the deviation is increasing with time.

The same speed varying trends can also be seen in Figs. 14 and 15. Fig. 14 shows the speed loss in straight course motion in head regular waves with wave period $T=1.842$ s, wave height $H=0.12$ m and wave length divided by ship length $\lambda/L=0.78$. Good agreement between simulations and experiment was achieved for the straight ahead condition. Fig. 15 presents the speed trends in zigzag motion in the same wave condition. Also for this wave, the numerical simulation underestimated the speed reduction, and this discrepancy was increasing with time. Since the current numerical simulation gives good prediction of the speed in waves in straight ahead condition, and of the speed during zigzag in calm water, the most likely reason for the speed deviation during zigzag in waves seems to be that the transverse added wave resistance is underestimated in this numerical model. So with the same power setting, speed obtained in numerical simulation is higher than in model tests. Also, all the hydrodynamic coefficients were derived from Salvesen-Tuck-Faltinsen (STF) method (Salvesen et al., 1970) which includes the terms caused by the presence of the stern. But the terms due to the interaction of oscillatory flow with the body steady forward motion at the aftermost section as mentioned by Loukakis and Sclavounos (1978) was neglected in this numerical simulation. These interaction terms became more important when the ship is doing zigzag motion in waves with increasing roll amplitude up to 3 deg.

By comparing Fig. 10 with Fig. 5, it can be seen that the time window obtained in waves is longer than in calm water. The first reason is that the transverse wave resistance increased in waves, which will restrained the ship's sway motion. So the model can have more zigzag motion time before it is stopped to avoid touching the tank wall. The other one is that more speed reduction occurs in waves than that in calm water, which leads to increasing steering forces and decreasing inertia forces during maneuvering. Both reasons make the model become more controllable in waves than in calm water.

Figs. 11 and 12 give comparisons of vessel heading and rudder angle. Good agreement is achieved in this wave condition. The vessel heading were increasing during the initial stage and then became stabilized around 12 deg. Fig. 13 shows a comparison of the average unit-side force of the thruster units. The side force is also well predicted Figs. 14 and 15.
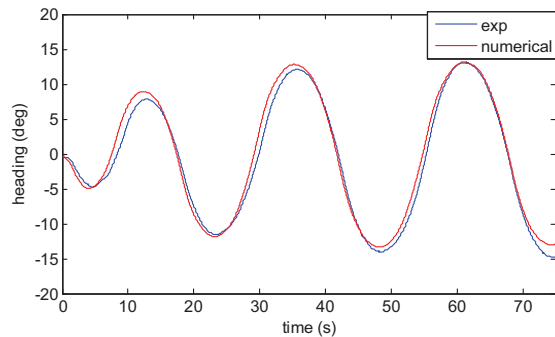

Fig. 11. Headings obtained during 10-2 zigzag in a regular wave with period $T=1.351$ s and height $H=0.12$ m.
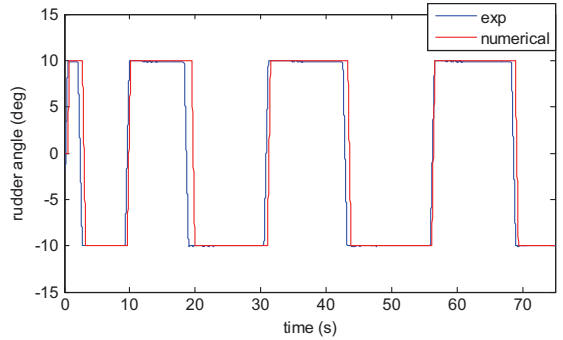

Fig. 12. Rudder angles obtained during 10-2 zigzag in a regular wave with period $T=1.351$ s and height $H=0.12$ m.
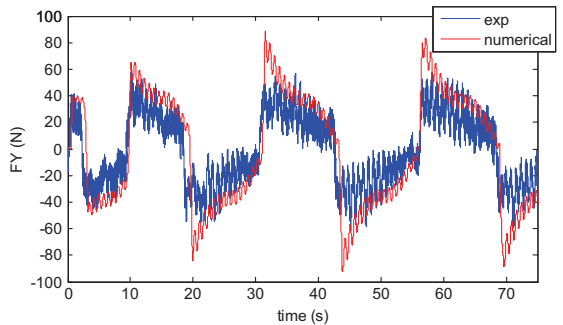

Fig. 13. Average unit-side forces obtained during 10-2 zigzag in a regular wave with period $T=1.351$ s and height $H=0.12$ m.
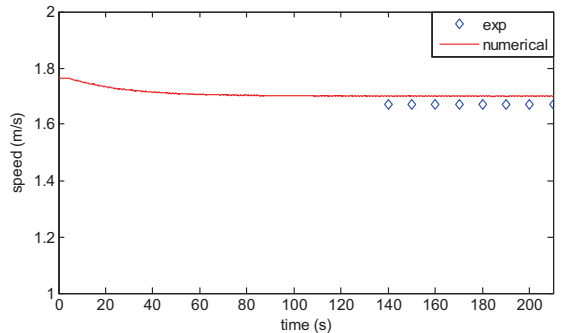

Fig. 14. Speeds obtained during straight course motion in a regular head wave with period $T=1.842$ s and height $H=0.12$ m.

In Figs. 16 and 17 heading and rudder angle in the numerical simulations were observed gradually forward of the model test results in this long wave case study, something that is believed to be a direct result of the difference in speed between model tests and simulations. The simulated speed is higher than that in model test, as shown in Fig. 15, which means that it needs shorter rudder execute time to achieve the desired heading angle. The change in heading angle will also give feedback to the rudder performance.

Due to the limitations of the towing tank condition, we can't get converged speed loss results neither in calm water nor in wave conditions. However, based on the agreement between the
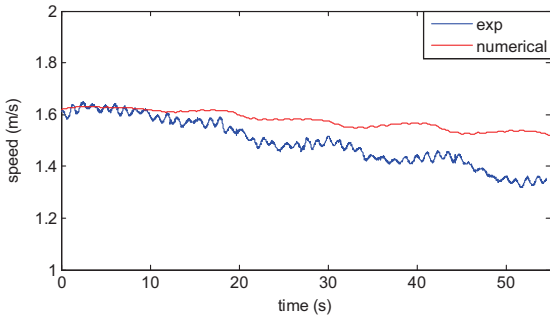
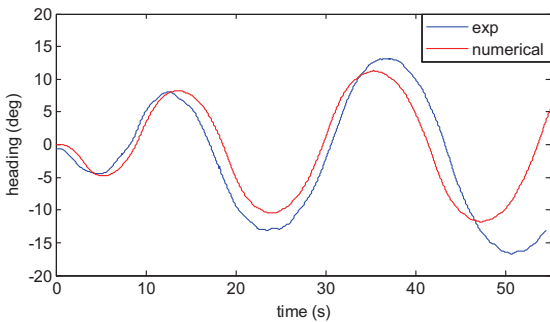**Fig. 15.** Speeds obtained during 10-2 zigzag in a regular wave with period $T=1.842$ s and height $H=0.12$ m.

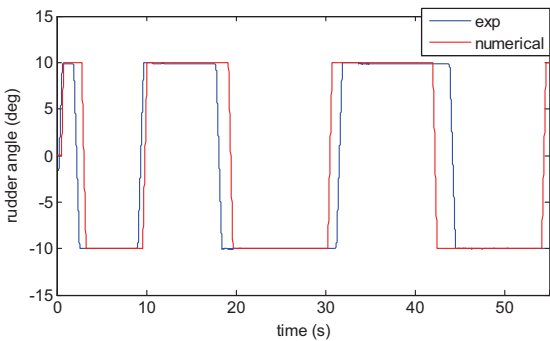**Fig. 16.** Headings obtained during 10-2 zigzag in a regular wave with period $T=1.842$ s and height $H=0.12$ m.

Fig. 17. Rudder angles obtained during 10-2 zigzag in a regular wave with period $T=1.842$ s and height $H=0.12$ m.

Fig. 18. Numerical speed deduction trends during 10-2 zigzag in different wave conditions.
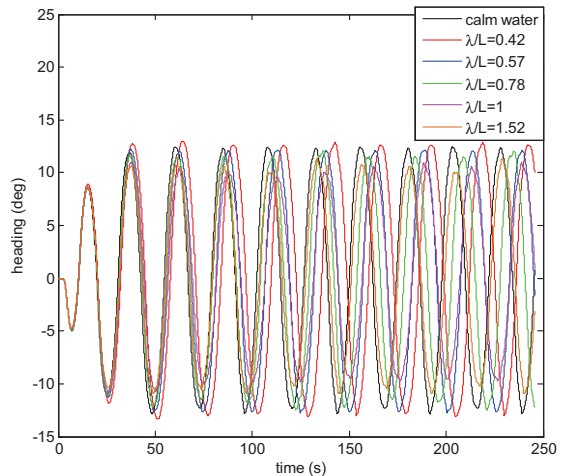
Fig. 19. Numerical Headings during 10-2 zigzag in different wave conditions.

numerical simulations and model test results in the transient phase, one might draw conclusions regarding the reliability of the simulation model. Furthermore, the simulation can then be run for a time which is sufficient to reach stable conditions. Figs. 18–20 show the converged speed, heading and rudder angle trends both in calm water and in different sea conditions. It is found that stable conditions are obtained after about two minutes in model scale.

Fig. 18 shows the surge speed trends from time domain numerical simulation in calm water and five different regular head sea conditions with wave length λ divided by ship length L from 0.42 to 1.52 in the same zigzag maneuver execute 10/2,
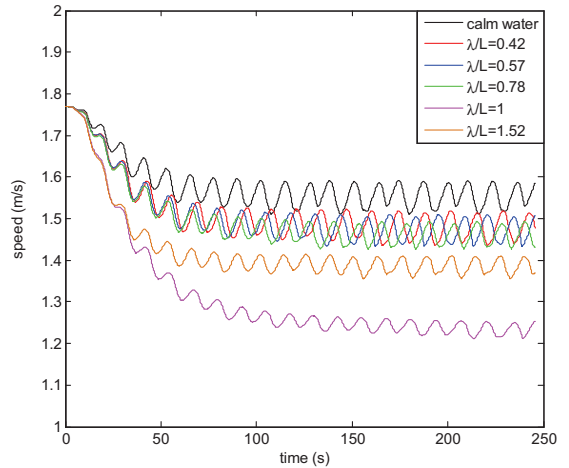
where the frequencies higher than the first order wave encounter frequency components were filtered out. The ship model started at the same initial speed 1.77 m/s, and the speed was decreasing during the steering period. Minimum speed loss was shown in calm water, due to loss of thrust and added resistance caused by yawing. In waves, the speed reduction was larger. When added wave resistance gets its peak value for wave lengths of $\lambda/L=1$, the largest speed loss was obtained. Less speed loss is achieved as the added wave resistance decreases. The converged speed loss is listed in Table 4.

Fig. 19 shows the heading in both calm water and waves during the numerically simulated zigzag motion. It can be seen that the overshoot angles are increasing during the first four turnings and then become stabilized around 12 degrees. Fig. 20 shows the heading variations in 25 s during stable conditions. The higher the attainable speed, the larger overshoot angle amplitude; the lower the attainable speed, the smaller overshoot angle amplitude. This is mainly due to the fact that the propeller power

Fig. 20. Heading magnitude with the influence of wave condition.

Table 4
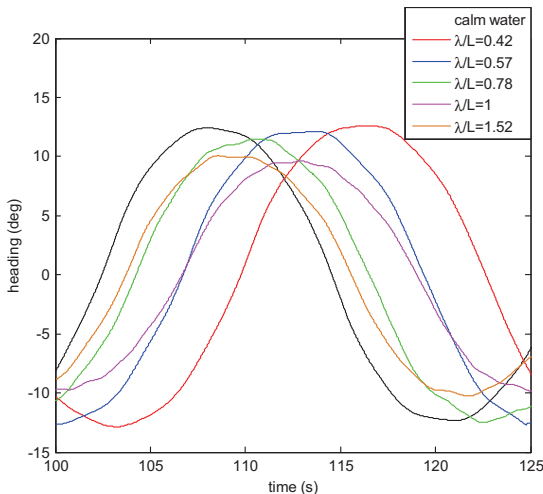Speed loss in different conditions.

	Speed loss (%)
Calm water	12.11
$\lambda/L = 0.42$	16.32
$\lambda/L = 0.57$	16.80
$\lambda/L = 0.78$	17.40
$\lambda/L = 1$	30.15
$\lambda/L = 1.52$	21.64

is constant between the different wave conditions, so that then the speed drops due to added wave resistance, the thrust force increases, both in absolute terms and relative to the maneuvering forces. This means in calm water where the least speed loss percentage happened (12.11%), and the biggest overshoot angle obtained; and when in the wave condition with $\lambda/L = 1$ where the biggest speed reduction percentage (30.15%) happened, the least overshoot angle achieved in the same case. The other wave conditions fall in between, both in terms of speed loss and overshoot angles.

6. Conclusions

A new 8000 DWT tanker has been selected for the investigation of zigzag maneuvering motion in waves. Both model tests and numerical simulations have been performed. Comparisons on the ship and propulsion system behavior are shown and discussed. Some conclusions can be drawn as follows:

The speed loss in a 10-2 zigzag maneuver in calm water obtained from the numerical simulation is in good agreement with the experimental results. This indicates that the Norrbin-model for added resistance due to yawing and the applied model of the azimuth thruster performance is reliable for the current ship.

Very good agreement is also obtained between simulation and experiment for straight-ahead running in various regular waves. When the wave length approaches ship length and added wave

resistance reach its peak value, the largest amount of speed loss was observed.

However, when the vessel is doing zigzag maneuvers in waves, the simulated speed is significantly higher than the speed obtained in the experiments. Thus, it seems that the numerical model under predicts the transverse added wave resistance.

The magnitude of the stabilized overshoot angles are influenced by the converged speed results. The higher the attainable speed values get, the bigger stable overshoot angle is achieved. The lower the attainable speed value obtained, the smaller stable overshoot angle is achieved.

The current numerical model can give good prediction of speed loss during maneuvering in calm water, and of speed loss in straight-ahead running in waves. However, it underestimates the speed reduction values during maneuvering in waves. Further investigation is needed to clarify the causes and improve the simulation model on this point.

References

Ayza, Z, Turan, O, Vassalos, D, 2005. Maneuvering and Seakeeping Aspects of Pod-Driven Ships'. Proc. IMechE vol. 219 Part M: J. Engineering for the Maritime Environment.

Clarke, D., 1972. A two-dimensional strip method for surface ship hull derivatives: Comparison of theory with experiment on a segmented tanker model. J. Mech. Eng. Sci. 14 (7).

Faltinsen, O.M., 2005. Hydrodynamics of High-Speed Marine Vehicles. Cambridge University Press, ISBN: 978-0-521-84568-7.

Faltinsen, O.M., 2011. Modeling of maneuvering with attention to ship–ship interaction and wind waves. 2nd International conference on ship maneuvering in shallow and confined water: ship to ship interaction.

Faltinsen, O.M., Zhao, R., 1991. Numerical predictions of ship motions at high forward speed. Phil. Trans. R. Soc. London. A 334, 241–252.

Fang, Ming-Chung, et al., 2005. A nonlinear mathematical model for ship turning circle simulation in waves. J. Ship Res. 49 (2), 69–79pp., 69–79.

Fathi, D., Hoff, J.R., 2008. ShipX Vessel Response, Theory Manual. MARINTEK.

Gerritsma, J.Beukelman, 1972. Analysis of the resistance increase in waves of a fast cargo ship. Int. Shipbuild. Prog. 19 (217), 285–292.

Grimstad, Dagny Kristine, 2009. Added resistance and speed loss due to steering. Master Thesis at NTNU.

Kumar, Manoj, Subramanian, V. Anantha, 2007. A numerical and experimental study on tankwall influences in drag estimation. Ocean Eng. 34 (1), 192–205.

Loukakis, Sclavounos, 1978. Some Extensions of the Classical Approach to Strip Theory of Ship Motions, Including the Calculation of Mean Added Forces and Moments. J. Ship Res. 22 (1), 1–19.

Lee, Seung-keon, 2000. The calculation of zig-zag maneuver in regular waves with use of the impulse response functions. Ocean Eng. 27, 87–96.

Liu, P., et al., 2009. Some unsteady propulsive characteristics of a podded propeller unit under maneuvering operation. Smp09. Trondheim, Norway, June.

Martinussen, K., Ringen, E., 2000. Maneuvering prediction during design stage, HSVA's CPMC, Workshop, Hamburg.

Matsumoto, N., Suemitsu, K., 1984. Interference Effects Between the Hull, Propeller and Rudder of a Hydrodynamic Mathematical Model in Manoeuvring Motion. Naval Architecture and Ocean Engineering, vol. 22 (Society of Naval Architects of Japan).

Norrbin, N.H., 1972. On the added resistance due to steering on a straight course. **In:** Proceedings of the 13th International Towing Tank Conference, Berlin, Hamburg.

Ogawa, A., Kasai, H., 1978. On the Mathematical Model of Manoeuvring Motion of Ship. Int. Shipbuild. Prog. 25, 306–319.

Reichel, M., 2007. Manoeuvring forces on azimuthing podded propulsor model. Pol. Marit. Res. 14, 3–8.

Ringen, Edvard,.2009. ShipX Manoeuvring Plug-In, theory manual. MARINTEK.

Ringen, Edvard, 2010. Vesim-Propulsion Model (pod), user manual. MARINTEK.

Ringen, E., Fathi, D., 2008. ShipX Vessel Simulator, Theory Manual. MARINTEK.

Salvesen, N., Tuck, E.O., Faltinsen, O.M., 1970. Ship motion and sea loads. Soc. Nav. Archit. Mar. Eng. 78 (6), 1–30.

Skejic, Renato, 2008. Maneuvering and Seakeeping of a Single Ship and of Two Ships in Interaction. Doctoral Thesis at NTNU.

Stoøm Tejsen, J. and Porter, R.R., 1972. Prediction of Controllable-Pitch Propeller Performance in Off-Design Conditions, Paper VII B-1, Third ship control system symposium, Bath.

Søding, H., 1984. Influence of course control on propulsion power. Schiff & Hafen/ Kommandobrucke 3, 63–68.

Paper 4

Speed loss of a vessel sailing in oblique waves

Zhenju Chuang, Sverre Steen

Speed loss of a vessel sailing in oblique waves

Zhenju Chuang *, Sverre Steen

Norwegian University of Science and Technology, Department of Marine Technology, NO-7491 Trondheim, Norway

ABSTRACT

In order to demonstrate the effect of oblique waves on ocean-going vessel behavior in realistic sea states, this paper addresses an effective and useful tool to predict the ship's motion and propulsion system behavior with sufficient accuracy, considering the wave conditions on the operating route. Seakeeping model test was carried out with a freely running model in oblique waves in the ocean basin at the Marine Technology Centre, Trondheim, Norway. A time domain numerical simulation study was performed, and the results of the simulation are compared with the model test data.

Due to the length limitation of the ocean basin, converged speed in waves cannot be achieved in all runs. A correction method is proposed in this paper to determine the converged speed from non-converged runs. The correction method is based on the condition that the converged speed in waves is dependent on the balance between resistance and propulsion force.

© 2013 Elsevier Ltd. All rights reserved.

1. Introduction

The ship behavior in actual weather condition is currently one of the major concerns for designers and ship owners as well as for ship officers (Prpic-Orsic and Faltinsen, 2012). Speed loss of an ocean-going vessel can be categorized as voluntary or involuntary (Faltinsen et al., 1980). The former is to avoid slamming, propeller racing and excessive ship motion. The latter is due to added resistance from waves, wind, and current, as well as reduction of propulsive efficiency caused by waves and increased resistance. This paper focuses on the involuntary speed reduction. A reliable speed loss prediction requires integrated knowledge about resistance, propulsion, ship machinery, seakeeping, steering and automatic control. In order to get a better understanding and insight into the nature of the ship speed drop process, the research reported in this paper is based on model tests and numerical simulations.

In recent years, there has been some research on speed loss, fuel consumption and GHG emissions. Prpic-Orsic and Faltinsen (2012) developed a numerical model to predict the speed loss of a vessel in irregular sea and implemented the ventilating propeller model by Smogeli (2006). Their work also covered the estimation of CO_2 emission from a containership on the Northern North Atlantic route, which was based on the mean speed drop, constant engine power and fuel consumption. But their model lacks verification. Chuang and Steen (2012) used model tests and a time domain numerical modal to study the speed loss due to

zig-zag motion in waves. They pointed out that the reasons for speed reduction for a ship doing zig-zag maneuvering in waves are due to yawing, loss of thrust due to steering and added wave resistance. However, most of this work was focused on head sea conditions.

Based on the literature study, research on the speed loss of a vessel sailing in oblique waves is limited. Carrica et al. (2008) applied URANS analysis to study the speed variation during broaching event of a ship in irregular quartering seas. But they implemented a significantly simplified propeller model. A more advanced propeller model is needed to achieve more accurate results. However, several researchers have made great contributions on how to predict added wave resistance in oblique waves. Fujii and Takahashi (1975) provided a semi-empirical formula to calculate the wave resistance in regular oblique waves. The formula gives a good consideration of added wave resistance components both due to ship motions and due to bow reflection, which is based on the contribution from Maruo (1963) and Havelock (1940). Gerritsma and Beukelman (1972) evaluated the added resistance in longitudinal waves by equating the work of added resistance to the energy contained in the waves radiated away from the ship. Their work has later been tested by Journee (1976) in following waves. His results shows that the method of Gerritsma and Beukelman gives a considerable negative added resistance obtained in different wave and speed ranges which gives a significant deviation from experiments. Therefore, Gerritsma and Beukelman method needs modification in order to be applied on other than head sea.

The purpose of this paper is to put emphasis on the speed loss of an ocean-going vessel in head sea, bow sea, beam sea and quartering sea conditions. Calm water resistance, azimuth

* Tel.: +47 96807451; fax: +47 73595528.
E-mail address: chuang.zhenju@ntnu.no (Z. Chuang).

propulsion system, ship machinery, seakeeping, steering and automatic control are all included both in model test and time domain numerical simulations. Due to the limitation of the experimental environment, converged speed in waves cannot be achieved in all runs. A correction method is also proposed in this paper to find converged speed from non-converged model tests.

2. Model test

2.1. Model test set up

Model tests to obtain speed loss in oblique waves have been carried out in the Ocean basin laboratory at the Marine Technology Center in Trondheim, Norway. The ocean basin laboratory has an effective length of 65 m, width of 50 m and during the tests the movable bottom was set to a depth of 4 m. A double-flap wave maker (BM2) along the 50-meter side is generating long crested waves. Along the 65-meter side, there is a multi-flap wave maker (BM3) consisting of 144 individually controlled flaps. Wave absorption beaches are installed on the two opposite sides to reduce the problems of wave reflection. A carriage is available to follow models with forward speed. The carriage carries power and signal cables to the model, and can be used to assist the model during acceleration and deceleration phases. The model applied during the tests was a 1:16.57 scale model of an 8000DWT tanker developed by Rolls-Royce Marine, Ship Technology—Merchant. The model is built by MARINTEK. The ship model has a wide transom and conventional bow with bulb. The main dimensions of the ship model and body plan are listed in Table 1 and Fig. 1. The model is self-propelled with two models of AZP120 azimuth thruster propellers. The main particulars of the propeller models are listed in Table 2.

In order to compensate for the relatively higher frictional resistance of the model, towrope force is applied by an air fan mounted on the model. The towrope force is obtained by controlling the speed of the fan. The fan was mounted on a load cell so that the thrust of the fan could be measured. However, due to thrust loss of the fan, the effective fan force is only 0.67 times the fan force measured directly. This has been verified by

Table 1
Principal dimensions of model hull.

	UNIT	Model
L_{OA}	[m]	7.142
Lpp	[m]	6.832
D	[m]	0.905
B	[m]	1.147
T	[m]	0.435
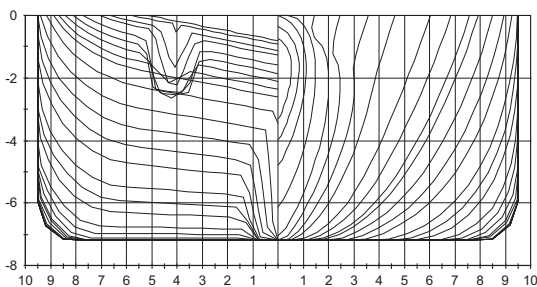
Fig. 1. Body plan of the model (below-water part only).

Table 2
Principal dimensions of model propellers.

	UNIT	Model
Propeller diameter D	[m]	0.199
Pitch ratio at $P/D=0.7$	[·····]	1.2
Blade area ratio	[·····]	0.435
Number of blades	[·····]	4

Table 3
Calibrated waves in model scale.

Wave No.	Wave maker	Wave type	H(m)	T(s)	λ/Lpp
1	BM2	REG	0.121	1.351	0.42
2	BM2	REG	0.121	1.842	0.78
3	BM2	REG	0.121	2.088	1
4	BM2	REG	0.121	2.383	1.3
5	BM2	REG	0.061	2.383	1.3
6	BM2	REG	0.242	2.383	1.3
7	BM2	REG	0.121	2.579	1.52
8	BM2	REG	0.121	3.071	2.15
9	BM3	REG	0.121	1.351	0.42
10	BM3	REG	0.121	1.842	0.78
11	BM3	REG	0.121	2.088	1
12	BM3	REG	0.121	2.383	1.3
13	BM3	REG	0.121	2.579	1.52

Table 4
Test conditions for all the runs.

Vm (m/s)	Direction (deg)	Wave no.
1.769	30	1,2,3,4,5,6,7,8
	60	1,2,3,4,5,7,8
	90	9,10,11,13
	150	1,2,3,4,7,8
1.191	30	2,3,4,6,7
	60	2,3,4,7
	150	2,4

additional tests which compare the force measured by the load cell and the net force accelerating the model. A control system kept the propulsion power constant during the tests, equal to the power required to reach design speed in calm water. So the speed reductions recorded are only due to added wave resistance, steering, and reduction of propulsive efficiency. An autopilot heading controller is used on the vessel in order to keep the designed heading during the tests. The model is free and self-propelled during tests. The only connection between the model and carriage are cables to relay the measurements and provide power to the propulsion motors. The cables are handled so the forces from the cables on the model are small. An optical tracking system is used to the instantaneous position of the model. Velocities are derived from the measured positions.

2.2. Test conditions and procedures

The aim of the tests is to measure the speed loss in oblique waves. Since added resistance is proportional to the square of the wave amplitude, the quality of the waves are really important for the results. All the waves are carefully calibrated prior to the testing, without the ship model in the ocean basin. Thirteen waves combined with four headings and two vessel speeds are tested. The waves used are listed in Table 3 and the combination of speed, heading and wave conditions are specified in Table 4.

Heading angle is defined as the angle between wave propagation directions and the *x*-axis which is in a body fixed coordinate system pointing from fore perpendicular towards aft perpendicular. The scenarios of the heading angles in the ocean basin are shown in Fig. 2. Four angles are tested, they are 30 deg, 60 deg, 90 deg and 150 deg.

The motor power is adjusted so that a speed of $V_m=1.769$ m/s ($Fn=0.22$) is reached on a straight line course in calm water. All subsequent tests marked with this speed in Table 4 are performed at this power setting. The same procedure is used for the other speed, which is $V_m=1.191$ m/s ($Fn=0.15$). A controller is controlling the fan used to produce the tow rope force, so that the fan gives the specified force according to the speed obtained in the actual condition. However, due to a thrust deduction effect

of the fan that was discovered after the tests, the effective tow rope force applied is only 67% of the correct value. A heading controller is used in order to keep the model running at the designed heading in the ocean basin. Outputs are commanded rudder angles to the twin azimuth propulsors.

The test procedure is as follows: First, the model is towed to the corner of the basin and set up with the correct heading direction as shown in Fig. 2. Then, the propellers are started initially with a high power level to accelerate the model. When a pre-defined speed is reached, the power is reduced automatically to the correct level. When the model is getting close to the end of the basin, the propellers are stopped and the model is stopped by tightening a rope from the carriage, connected to the stern of the model. The value of the pre-defined speed threshold is important
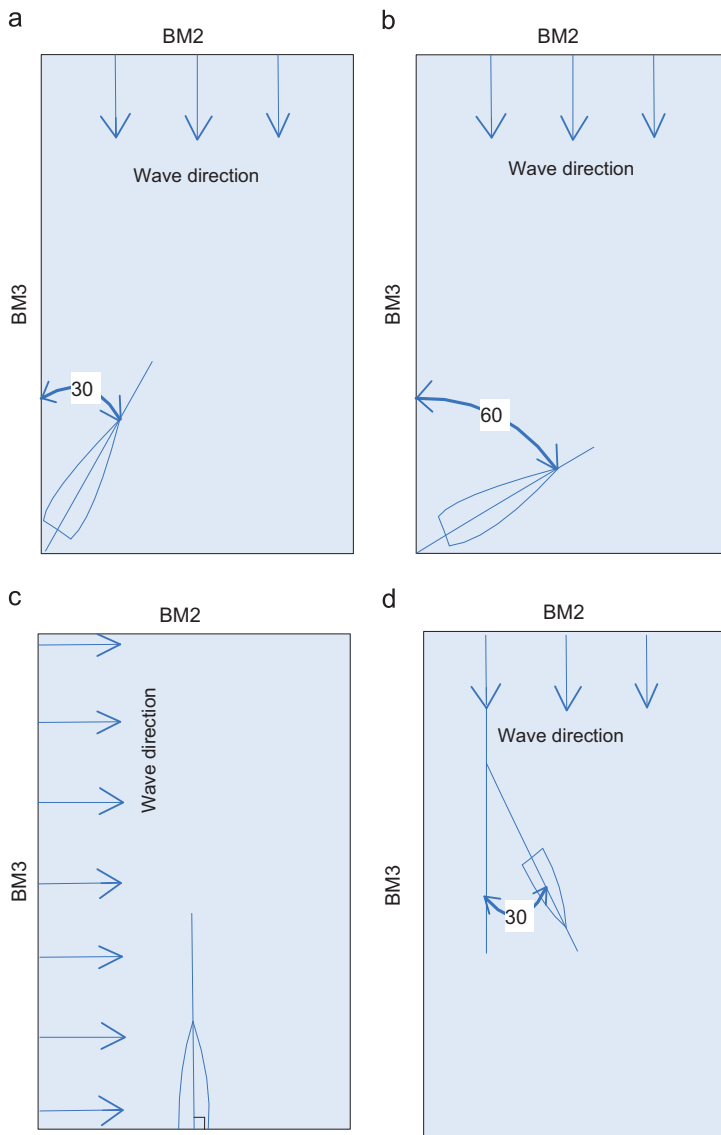

Fig. 2. Scenarios of the model test setting for each vessel-wave direction relationship. (a) head sea (30 deg), (b) head sea (60 deg), (c) beam sea (90 deg) and (d) quartering sea (150 deg).

for the ability to reach a converged speed. Some trial and error was used to find the right threshold speed for different test conditions. Still, converged speed was not reached in all cases. The reason for the relatively slow speed convergence is the low resistance/weight-ratio of such a displacement ship model, so that the residual thrust-resistance imbalance results in relatively low acceleration/deceleration.

During the tests the following variables are recorded: vessel motions in six degrees of freedom, vessel yaw acceleration (in terms of a rate gyro), propeller thrust, RPS, torque, unit thrust, revolutions of the fan, fan force, and wave elevation in the basin and relative wave elevation at the thruster position. Sampling frequency for model positions is 25 Hz and all the other measurements are sampled at 200 Hz. A rate limiter was set equal to 30 deg/s to limit the maximum rate of azimuth angle response.

After all the waves were finished with the first heading, the model position for the next heading was rearranged as shown in Fig. 1(b)–(d). When all the work was finished with the first model speed, all the procedures were repeated for the next calm water vessel speed $V_m = 1.191$ m/s.

2.3. Analysis of model test data

When converged speed is achieved in the model test, the time series of the recorded speed is oscillating around a constant mean value. In this case, the measured vessel speed can be taken directly by averaging the data within the corresponding time period. While, for non-converged runs, the vessel speed kept decreasing or increasing within the time window. Table 5 shows the acceleration of the model of the two above cases. The acceleration here is the average acceleration which was found by derivation of the low-pass filtered velocity, so that the wave encounter frequency variations are excluded.

In order to decide in a systematic and orderly manner if the model's speed is converged or not, we established a criterion based on the acceleration: If $a < 0.001$ m/s^2, then the speed is regarded as converged speed; If $a \geq 0.001$ m/s^2, then the speed is treated as non-converged speed. Applying this criterion, there are seven out of 36 runs where the speed is not sufficiently converged, with increasing or decreasing trend till the end of the tests. In Table 5, all the seven cases with non-converged speeds and several cases with sufficiently converged speed are listed. Fig. 3 shows two examples of the seven cases with non-converged speeds.

As shown in Fig. 3, the model speed is still changing throughout the entire test. For this case, the attainable speed in this wave

Table 5
Overview of runs with non-converged speed, compared with a few samples with converged speed.

H (m)	T (s)	Heading (deg)	V_0 (m/s)	a (m/s^2)	$(m \times a/T_{\text{thrust + towrope}}) \times 100\%$
Converged					
0.121	2.383	30	1.769	0.0008	2.1871
0.121	3.071	30	1.769	0.0000	0.0000
0.121	2.383	60	1.769	−0.0007	−1.9206
0.121	2.579	60	1.769	0.0008	2.2588
0.121	2.088	90	1.769	−0.0008	−2.1303
Non-converged					
0.121	1.842	30	1.769	−0.0016	−4.3918
0.121	1.351	60	1.769	0.0013	3.6941
0.121	1.842	60	1.769	−0.001	−2.6767
0.121	2.088	60	1.769	0.0025	6.5907
0.061	2.383	60	1.769	0.0048	11.7753
0.121	1.351	90	1.769	−0.0030	−8.6945
0.121	2.579	90	1.769	−0.0036	−10.30

condition cannot be taken directly from the measurement. So the model test results have to be corrected before they can be compared with the numerical calculation results. A methodology for correction is outlined in the following.

Converged speed is based on the balance between net thrust force, towrope force and the sum of the calm water resistance and added wave resistance. Eq. (1) shows how the acceleration of the model is related to the force balance in the direction of travel. In this force balance, we know the calm water resistance R_{calm} from calm water model tests performed earlier with some modifications which will be specified clearly in Section 2.1. R_{calm} and R_{aw} is calculated using the average velocity of the effective time window. The average values used to present the speed loss and other results are computed from an effective time window of between 20 to 30 s for different conditions. The effective time windows are chosen as close as to the end of the test as possible, but before the propellers were stopped and the model was towed to stop, so that the speed with the smallest acceleration is captured. The thrust T_{thrust} is measured during the tests, as is also the tow rope force $T_{\text{towrope\_effective}} = 0.67 T_{\text{towrope\_measure}}$.

$$m \times a = R_{\text{calm}} + R_{aw} - T_{\text{thrust}} \times (1-t) - T_{\text{towrope\_effective}} \qquad (1)$$

It is then necessary to decide the thrust deduction factor of the propulsion system in waves. If we know the added resistance due to waves, R_{aw} we can easily determine the thrust deduction fraction in waves $(1-t)$. Ideally, $R_{\text{calm}} + R_{aw}$ should be determined from towing the model in waves and measuring the resistance. In lack of such measurements we have computed R_{aw} by the method of Loukakis and Sclavounos (1978) outlined in Section 2.2.2.

Nakamura and Naito (1977), Yamazaki et al. (1978) and Bhattacharyya (1978) arrived at the consistent conclusion that the thrust deduction factor in waves is slightly lower than in calm water. This small deviation is changing with different wave conditions and Froude number. With our data, we can either use the computed added resistance and then find the thrust deduction fraction from the measurements, or we can make an assumption about the thrust deduction fraction and find the added resistance from the measurements. If nothing is known about the thrust deduction fraction in waves, the best assumption is to use the calm water value. Since the results are quite sensitive to the change of propulsion factors, we apply both methods and compare the results.

Fig. 4(a) shows the thrust deduction in regular waves of different wave lengths in heading direction of 30, 60 and 90 deg. The differences between thrust deduction in calm water and in waves are evident in the range of L/λ from 0.4 to 1.3. In very long and very short waves, thrust deduction in waves is fairly close to the one in calm water. The reason for this is probably that in the intermediate wave lengths, the ship experience large motions and added resistance, so that flow conditions in the propeller area become quite different from the calm water condition. The changing of wake fraction in different wave conditions is shown in Fig. 4(b). This is similar to results by Nakamura and Naito (1977), but the variation in the thrust deduction and wake fraction seen in Fig. 4 is larger than what is shown by Nakamura and Naito (1977). The reason for that is probably the inaccuracy of the calculated added wave resistance, which is clearly a short-coming of our method. Another source of difference is of course that the hull forms and type of propulsion system differs quite strongly between our case and Nakamura and Naito (1977). Nakamura and Naito studied a single-screw container vessel with a conventional propeller, while we study a tanker with twin azimuth propulsors. Also thrust deduction variation due to steering will probably contribute to the large difference.
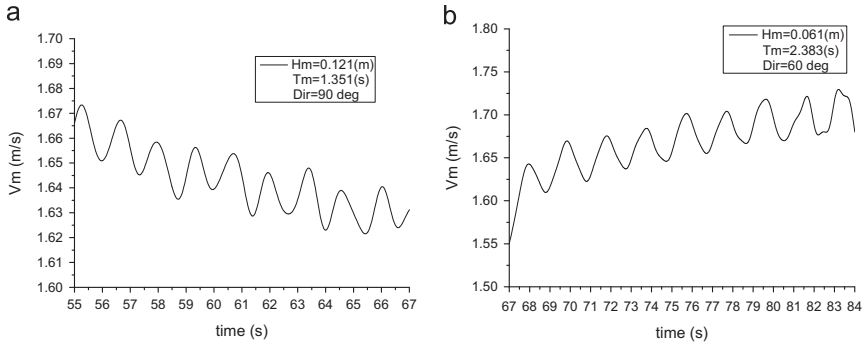
Fig. 3. Two examples of not converged speeds from model tests with initial speed 1.769 m/s. (a) Beam sea, $H=0.121$ m, $T=1.315$ and (b) wave direction 60 deg, $H=0.061$ m, $T=2.383$ s.
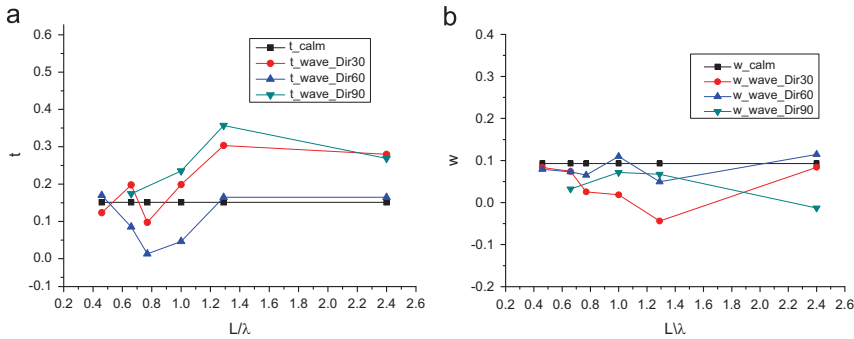

Fig. 4. Thrust deduction and wake factor in waves. (a) Thrust deduction t and (b) wake fraction w.

The converged speed is found by requiring the acceleration term in Eq. (1) to be zero. We then arrive at the following equation:

$$R_{calm}(V) + R_{aw}(V) - T_{thrust}(V) \times (1-t) - T_{towrope\_effective}(V) = 0 \qquad (2)$$

All terms are speed dependent, except the thrust deduction, which we assume to be constant. $R_{calm}(V)$ is known from modified resistance tests. $R_{aw}(V)$ is computed according to the method of Loukakis and Sclavounos (1978). $T_{towrope\_effective}(V)$ is also a known function of the speed, when experimental uncertainty is neglected.

In order to obtain the speed dependent longitudinal thrust force $T_{thrust}(V)$, the following method is used. Since the power P is controlled to be constant during the whole test, we can assume that the power is also constant in the ship heading direction within this small speed variation range, which means: $T_{thrust}(V_1) \times V_1 \times \eta_{D1} = T_{thrust}(V) \times V \times \eta_D$, where V_1 is the measured non-converged speed at the end of the test; η_D is propulsive efficiency, which is assumed to be constant within the small range of speed change. For larger velocity variations, with significant change of propulsion point, the change of propulsive efficiency must be included. So the speed dependent longitudinal thrust force in Eq. (2) can be written as $T_{thrust}(V) = T_{thrust}(V_1) \times V_1/V$, Where $T_{thrust}(V_1)$ is known from the measurements.

The results of this correction method are presented in Section 3.

3. Theoretical calculations

Ship motions were calculated in ShipX Vessel Response (Fathi and Hoff, 2008) by the simple but powerful Salvesen–Tuck–Faltinsen (STF) strip theory (Salvesen et al., 1970). Wave effects were

considered by updating the first order and second order wave excitation forces at each time step and the retardation function was used to consider the memory effect. Linear and nonlinear maneuvering hydrodynamic forces were obtained through ShipX maneuvering Plug-In (Ringen, 2009). Thrust forces were applied by implementing a four-quadrant propeller model. When all the modules were ready, seakeeping combined with maneuvering equations were solved at each time step in the Vessel simulator Vesim (Ringen and Fathi, 2008). Some of the theory behind these calculations is given in the following sections.

The numerical simulation is performed for full scale. All the results are then scaled to model scale for comparisons.

3.1. Calm water resistance

Calm water resistance is obtained from the resistance test in the towing tank in MARINTEK (Alterskjær, 2010). For full scale speed range 0–6 kn, calm water resistance is obtained based on assuming that the wave making resistance is negligible, so that the residual resistance coefficient C_R is effectively zero. For 10–18 knots, the value of the residual resistance coefficient is found from calm water towing tests. The resistance scaling method in use here follows the standard method in use at MARINTEK, which is a variation of the ITTC'78 method. The method used to find the total resistance from model tests, valid for the speed range 10–18 knots is outlined first.

The relation between model total resistance R_{Tm} and the model total resistance coefficient C_{Tm} is:

$$R_{Tm} = \frac{1}{2}\rho_m V_m^2 S_m \times C_{Tm} \qquad (3)$$

where ρ_m is model test water density, S_m is the area of ship model wetted surface.

The total resistance coefficient can be computed using a friction line and form factor:

$$C_{Tm} = C_R + C_{Fm} \times (1+k) + C_{BDm} + C_{Appm} \tag{4}$$

$C_{Fm} = (0.075/(\log_{10} R_N - 2)^2)$ is the friction resistance coefficient in model scale, where R_N is Reynolds number;

k is form factor which is calculated using the empirical the equation $k = 0.6\,\varphi + 145\,\varphi^{3.5}$ with $\varphi = (C_B/L_{WL})\sqrt{B \times (T_A + T_F)}$, where C_B is block coefficient, L_{WL} is length of the waterline, T_A is draught at aft perpendicular, T_F is draught at forward perpendicular;

$C_{BD} = 0.29\sqrt{(S_B/S/C_F)}$ is the transom stern resistance coefficient, where S_B is transom stern area and S is wetted hull surface in front of the transom;

C_{Appm} is model scale appendage resistance coefficient, $C_{Appm} = 0$ in this case study;

How full scale ship resistance is determined from model test results is briefly outlined below. The residual resistance is Froude scaled, which means that the residual resistance coefficient is equal in model and full scale:

$$C_{Rm} = C_{Rs} \tag{5}$$

The full scale total resistance coefficient can be written as:

$$C_{TS1} = C_{Rs} + (C_{Fs} + \Delta C_F)(1+k) + C_{BDs} + C_{Apps} + C_A \tag{6}$$

$\Delta C_F = (110(H \times V_s)^{0.21} - 403) \times C_{FS}^2$ is a roughness correction. $H = 150(10^{-3}\,\text{mm})$ is used as a standard value.

C_A is the correlation allowance which accounts for systematic errors in the scaling method and model test set-up.

For the low speed range 0–6 knots, the residual resistance coefficient is zero, so that Eq. (6) is simplified to

$$C_{TS2} = (C_{Fs} + \Delta C_F)(1+k) + C_{BDs} + C_{Apps} + C_A \tag{7}$$

Since the original calm water tests in towing tank happened in 2010, the model had bilge keels added for the test in this paper, and a larger superstructure which leads to increased air resistance. Also, experience is that the model resistance generally increases with time, mainly because of surface finish deterioration. Resulting calm water resistance curve was corrected for the runs in the ocean basin, according to a comparison of the thrust measured in calm water in the ocean basin and the original calm water test results. Considering the changes to the model, an increase of model resistance of 3.89 N at $V_0 = 1.769$ m/s is used to correct the original calm water resistance curve. The increase of resistance amounts to 5.6% of the original calm water resistance at this speed. An additional model resistance coefficient is computed for this speed, and resistances at other speeds are corrected by assuming that the additional model resistance coefficient varies linearly with speed:

$$\Delta C_{Tm} = \frac{3.89}{\frac{1}{2}\rho_m V_0^2 S_m} \times \frac{V_m}{V_0} \tag{8}$$

where $V_0 = 1.769$ m/s. The modified full scale calm water resistance coefficient that we apply in the numerical simulations is then obtained by Eq. (9):

$$C_{Ts\_modified} = (C_{Tm} + \Delta C_{Tm}) - 0.67 \times C_s \tag{9}$$

The tow rope force coefficient C_s is expressed as the difference between the model and full scale total resistance coefficients $C_s = C_{Tm} - C_{Ts}$. Due to the previously mentioned thrust loss of the fan used to apply the tow rope force, effective towrope force is only 0.67 times the fan force measured directly.

Modified full scale calm water resistance is calculated as $R_{Ts\_modified} = C_{Ts\_modified} \times (1/2)\rho V^2 S$.

Finally, the polynomial expression for modified resistance in the entire speed range from 0 to 18 knots is established.

$$R_{TS} = a_1 \times V^3 + a_2 \times V^2 + a_3 \times V + a_4 \tag{10}$$

where $a_1 - a_4$ are regression coefficients. The resulting full scale calm water resistance applied in numerical study is shown as Fig. 5.

For the simulations, we have adopted the thrust deduction fraction from the original calm water propulsion tests ($t = 0.151$). The thrust deduction obtained from the calm water runs in the ocean basin, using the corrected resistance curve of Fig. 5, was slightly higher. The difference is found to be caused mainly by steering, and since this effect is inherently included in the simulation, the thrust deduction fraction without this effect is applied.

3.2. Added resistance due to waves

Wave forces in regular waves are mainly composed of first order wave excitation forces and second order wave drift forces in surge, sway and yaw directions. In the current calculations, they are pre-calculated for different vessel speeds, headings and wave frequencies before the time domain simulation started. When the simulation started, both first and second order forces from the waves were calculated by interpolation in the input dataset at each time step. Radiation forces are calculated by means of a convolution integral using retardation functions to account for the memory effects.

3.2.1. First order wave exciting force
The first order wave excitation force is described by transfer function and the wave elevation.

$$F_{wave}^{(1)} = H^{(1)}(\omega, \theta) \zeta(\omega, \theta, x, y) \tag{11}$$

where $H^{(1)}(\omega, \theta)$ is first order transfer function. It depends on wave frequency ω and propagation direction θ. $\zeta(\omega, \theta, x, y)$ is wave elevation which is the function of wave frequency, propagation direction and position in space.

3.2.2. Second order wave drift force on a ship in oblique waves
As shown in fig. 6, the ship is moving along a predetermined direction along its x-axis with speed V. The waves are coming from a direction at angle β with propagating speed c_-. Added wave resistance R_{-x}, transverse drift force R_{-y} and mean yaw moment in surge, sway and yaw directions are composed of the mean second order wave force on a ship in oblique waves. These forces are calculated by the method proposed by Loukakis and
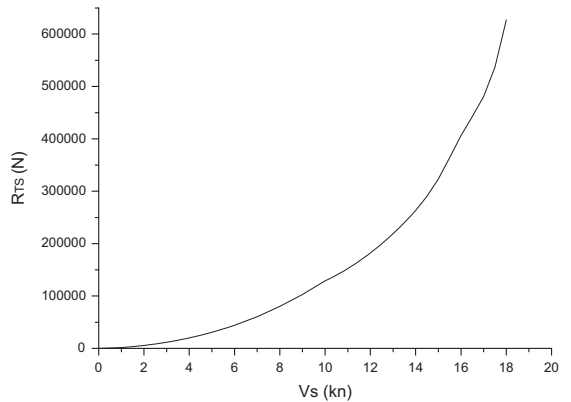
Fig. 5. Calm water resistance used in numerical simulation.

Sclavounos (1978). This method is based on the extension of the method proposed by Gerritsma and Beukelman (1972) which is originally only for head waves.

The Gerritsma and Beukelman method is based on the energy principle under the assumption that radiated energy is equal to the work of added resistance done and the energy contained in the damping waves. And this energy relationship can be expressed by Eq. (12).

$$(-R_x)(V-c)T = \frac{\pi}{\omega}\int_0^L \left(b_{33}-V\frac{da_{33}}{d\xi}\right)|V_{RZ}|^2 d\xi \tag{12}$$

where ω and T are encounter frequency and encounter period of the wave, V_{RZ} is the vertical relative velocity of each ship section, a_{33} and b_{33} are two-dimensional sectional added mass and damping coefficients.

The left part of Eq. (12) corresponds to the work transferred to the fluid plus the amount of energy transfer from the incident waves due to their direction of propagation plus radiated waves all around the ship.

This approach can be extended to calculate the added resistance and drift force in oblique regular waves. It is known that if one considers a control surface fixed in space and surrounding the ship, the energy influx and efflux through it are equal when the contribution of the diffracted waves and ship generated waves are taken into consideration. The velocity of the ship relative to the fixed control surface is $V_R = V - c$ and can be resolved into V_{RH} and V_{RT} which are parallel and normal to c respectively. The motion of the ship with V_{RT} does not make contribution to the mean horizontal force R_T, which consequently has the direction of the incident wave propagation. Then $(-R_T)V_{RH}$ shall represent the net energy given by the ship to the fluid $((-R_x)V)$ and the energy radiated all around the ship ($R_T c$). Then the left part of Eq. (16) can be rewritten as:

$$P = (-R_T)V_{RH} = (-R_T)(-c-V\cos\beta) \tag{13}$$

The final expressions which allow us to calculate the added resistance and drift force in oblique waves are:

$$(-R_T)(-c-V\cos\beta) = P_{35}+P_{26}+P_4+2P_{24} \tag{14}$$

$$|R_T| = \frac{k}{\omega}(P_{35}+P_{26}+P_4)+\frac{2k}{\omega}P_{24} \tag{15}$$
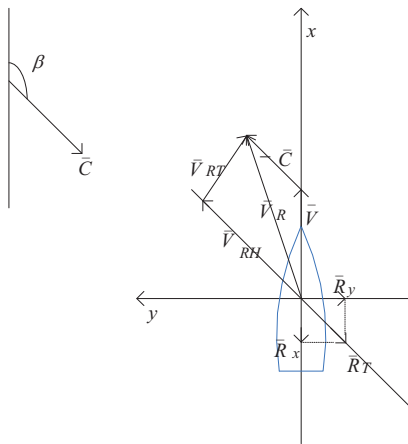
$$|R_x| = |R_T\cos\beta| \tag{16}$$

Fig. 6. Definition of heading direction and mean second order force.

$$|R_y| = |R_T\sin\beta| \tag{17}$$

where P_{35}, P_{26}, P_4, and P_{24} are energy radiated by ship heave-pitch motion, sway-yaw motion, roll motion and sway-roll motion during one encounter period.

3.3. Thrust force

The model was equipped with models of Rolls-Royce Azipull pulling azimuthing thrusters. In the time-domain simulations, an empirically based propulsion model is applied to represent the forces from the thrusters. The simulation model is based on a systematic series of open water tests with a model of the Azipull thruster (Berg, 2002), where advance number, azimuth angle and propeller pitch was varied systematically. The model tests reported by Berg (2002) were performed by MARINTEK, while the implementation of the propulsion model was done by Rolls-Royce Marine. The empirical propulsion model is interpolating in the model tests in tabular form to produce propeller open water curve for the instantaneous value of pitch and azimuth angle. The propulsion model also contains a correction term to account for the flow straightening effect of the hull when the ship is turning, but this correction is without importance for the cases studied here.

An electric engine model is selected here for the two thrusters. An azimuth rate limiter with maximum rate limit allowed for signal 7.5 deg/s (in full scale) is applied to get rid of the high frequency oscillations. Gear ratio and shaft loss are included by editing engine-propeller gear ratio and mechanical efficiency. Also the total moment of inertia of the engine and propeller are considered in order to give the correct rate of change of engine revolutions. A heading controller is used to keep the desired heading and keep the power constant. This is the same way as done in the model tests.

3.4. Speed loss due to loss of thrust

Thrust loss in waves during maneuvering can mainly be attributed to ventilation and steering. Ventilation typically occurs in rough wave conditions, when large relative motions between sea surface and ship occur at the propeller positions. Ventilation leads to a significant drop in thrust, accompanied by a slightly lower drop in the propeller torque. Ventilation is not detected in the reported tests.

Calculation of hydrodynamic forces on the azimuth thruster due to steering is illustrated Fig. 7. As shown in Fig. 7, the thruster has a steering angle α relative to the ship fixed coordinate system Os-XsYs, where T is the total thrust force along the propeller shaft. The thruster is rotated according to the rudder angle demand. Then the force in the longitudinal direction and the transverse direction relative to the ship can be expressed by Eqs. (18) and (19):

$$F_{\text{longitudinal}} = T \times \cos\alpha \tag{18}$$

$$F_{\text{transverse}} = T \times \sin\alpha \tag{19}$$

It can be seen that there will be a reduced force in the longitudinal direction of the ship if the azimuth unit has an azimuth angle other than zero. The thrust T will also change when the azimuth angle α change. As a result of the changing thrust force in longitudinal direction $F_{\text{longitudinal}}$, the balance between thrust and resistance will change so that vessel speed drops until a new equilibrium point is established at a lower speed value.

4. Discussion of the results

Speed reduction of a vessel in oblique waves due to added wave resistance and steering is studied. Results obtained from model tests and numerical simulations are compared in this section. Numerical simulations are carried out in full scale, so the data are scaled to model scale in order to make comparison with the experimental data. In the numerical simulations, thrust deduction and wake fraction are always set equal to the calm water values, since the calm water values are much closer to the reality than the calculated values. Calculated thrust deductions are only used when applying the attainable speed prediction method.

4.1. Testing the attainable speed prediction method

The attainable speed prediction method as explained in Section 1.3 has to be tested. The testing can be based on cases where we have both converged and non-converged runs in the same condition. Table 6 lists the error between the attainable speed which were measured directly from the converged test and the predicted speed found from the non-converged test using both calculated and calm water thrust deduction factor in the correction procedure.

It can be seen from Table 6 that attainable speed can be well predicted, and that the method is sensitive to the thrust deduction factor applied. Using the calculated thrust deduction gives better prediction than calm water thrust deduction in the first three cases. The reason is probably that the calculated thrust deduction already includes the error of the calculated added wave resistance. Using the calculated thrust deduction in Eq. (2) to predict the converged speed will partly cancel the error of

Fig. 7. Azimuth thruster with steering angle.

calculated added resistance. The dependence of the choice of thrust deduction fraction on the converged speed prediction method is further demonstrated in the following section.

4.2. Comparison of experimental and theoretical results

In this section, model tests and numerical results are compared. In the numerical simulations, thrust deduction is always set equal to the calm water thrust deduction value 0.151. Fig. 8 compares the attainable speed in a heading of 30 deg and a speed of 1.769 m/s. It is found that numerical results agree well with the experimental data. In the case with ship length divided by wave length equal to 1.29, the model speed is still decreasing during the test. So the correction method suggested in Section 1.3 was applied on this point, both with thrust deduction from calm water ($t\_calm=0.151$) and found using calculated R_{aw} ($t\_calculated=0.304$). It can be seen that the predicted speed is sensitive to the different thrust deduction factors applied. Fig. 9 shows propeller revolutions per second for the same runs as reported in Fig. 8. Computed and measured propeller speed generally agree well with each other, which is on the basis that for calm water condition $RPS\_exp/RPS\_numerical=1.0283$. Fig. 10 compares the unit thruster force in longitudinal direction in waves. It can be seen that numerical thrust has a good correspondence with experimental thrust in all wave conditions. In still water condition, the unit thrust measured from the model propulsors and the effective fan force is equal to 1.0466 times of the unit thrust force found in the numerical simulations. This small deviation in calm water could be due to inaccuracy in the net fan force, or in the calm water resistance, where for instance the neglecting of air resistance will introduce a small error. Since power control was applied, when the model speed reach its lowest point at $L/\lambda=1$, the highest corresponding thrust force were obtained. This trend is well captured both in model tests and in numerical simulations.

Figs. 11–13 presents the comparisons between model test and numerical simulation results in terms of speed, RPS and longitudinal thrust force in 60 deg heading angle with an initial speed of 1.769 m/s. Attainable speed method were applied in the wave condition with $L/\lambda=1$ ($t\_calculated=0.0461$), 1.29 ($t\_calculated=0.1646$) and 2.4 ($t\_calculated=0.1646$).

Figs. 14–16 compares the speed, propeller revolution and unit thrust in the longitudinal direction between model test and numerical simulation results in the case with calm water speed 1.769 m/s and heading angle 90 deg. The correction procedure described in Section 1.3 is used for the cases when ship length divided by wave length is equal to 0.66 ($t\_calculated=0.174$) and 2.4 ($t\_calculated=0.2686$). Generally good agreement is achieved between model test and numerical simulations. It can be seen from Figs. 11 and 14 that the numerically calculated attainable speeds are always slightly lower than the experimental values. The most likely reason to cause this is that the numerical thrust value is always lower than the experimental values, which can be seen from Figs. 13 and 16. Also applying more accurate method to predict wave resistance might have the potential to improve the results.
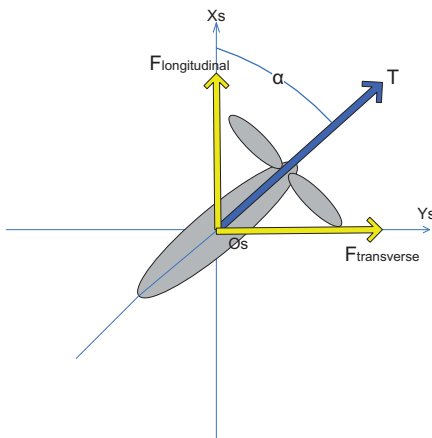
Table 6
Testing attainable speed prediction method.

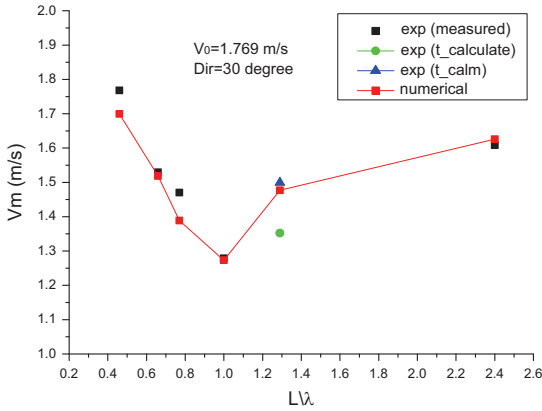| H (m)	T (s)	Heading (deg)	V_0 (m/s)	V_measured (m/s)	V_test ($t\_calculate$)	Error1 (%)	V_test (t_calm)	Error2 (%)
0.121	2.383	30	1.769	1.4702	1.4658	−0.3027	1.4326	−2.5557
0.121	3.071	30	1.769	1.7681	1.7898	1.2298	1.7722	0.2328
0.121	2.579	60	1.769	1.6927	1.6803	−0.7324	1.6374	−3.2693
0.121	2.088	90	1.769	1.7523	1.7571	0.2745	1.8123	3.4222

Fig. 8. Attainable speed in waves with initial speed 1.769 m/s, heading 30 deg.
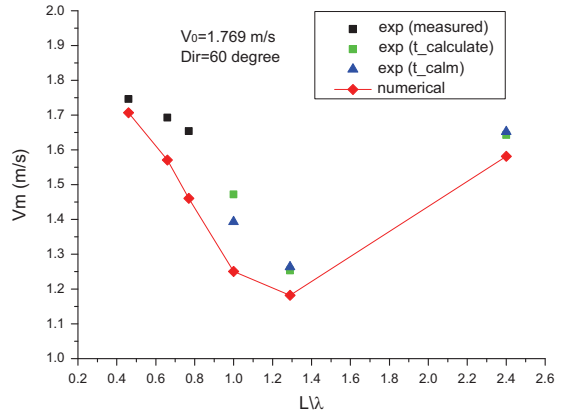

Fig. 11. Attainable speed in waves with initial speed 1.769 m/s, heading 60 deg.

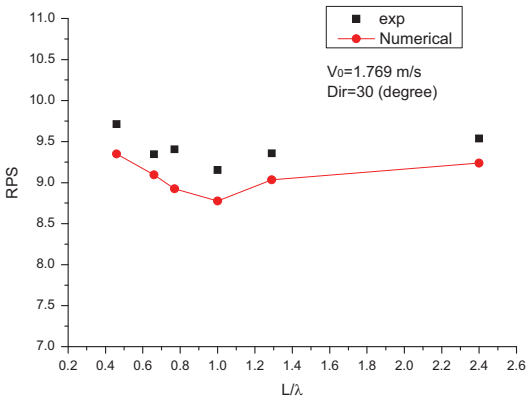**Fig. 9.** Propeller revolutions per second in waves with initial speed 1.769 m/s, heading 30 deg.
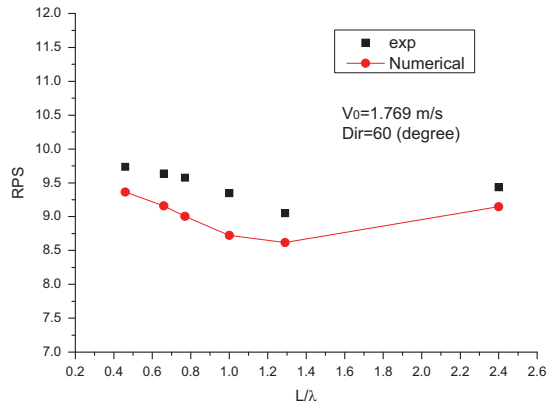

Fig. 12. Propeller revolutions per second in waves with initial speed 1.769 m/s, heading 60 deg.
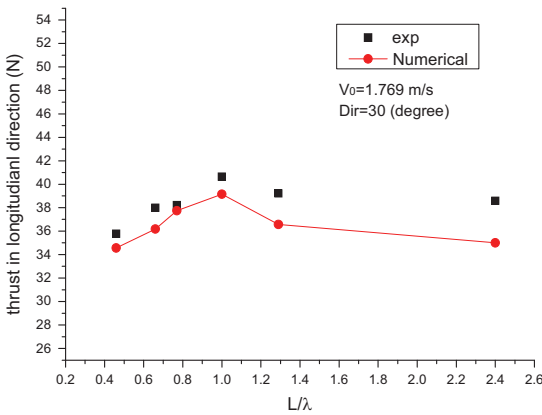

Fig. 10. Unit thrust in longitudinal direction in waves with initial speed 1.769 m/s, heading 30 deg.
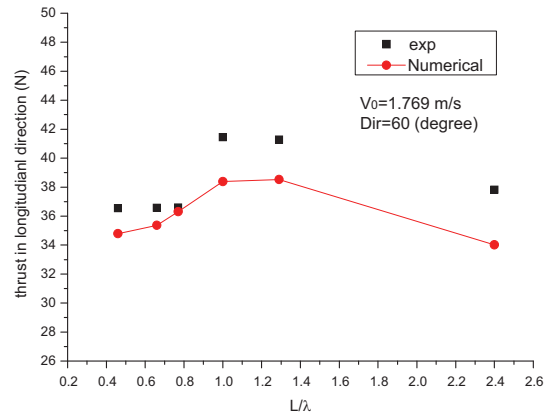

Fig. 13. Unit thrust in longitudinal direction in waves with initial speed 1.769 m/s, heading 60 deg.
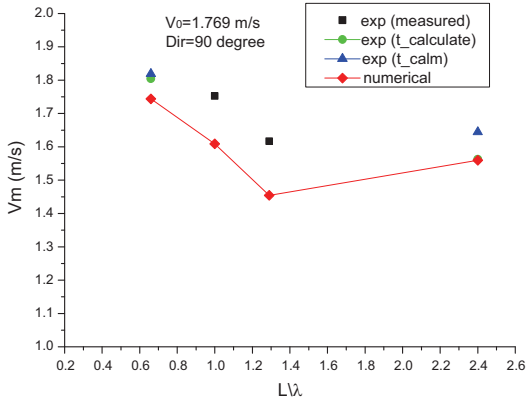
Fig. 14. Attainable speed in waves with initial speed 1.769 m/s in Beam Sea.
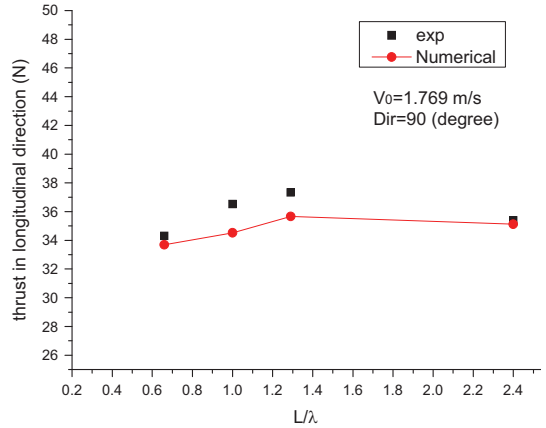

Fig. 16. Unit thrust in longitudinal direction in waves with initial speed 1.769 m/s in Beam Sea.
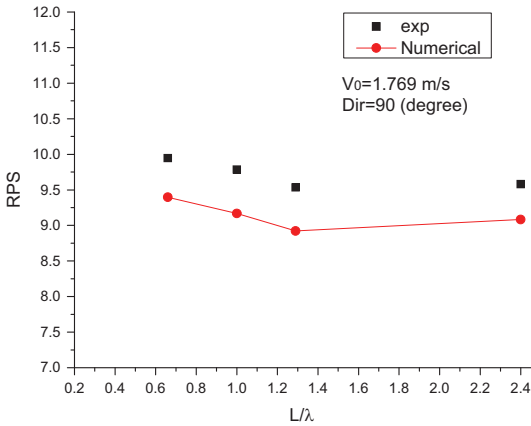

Fig. 15. Propeller revolutions per second in waves with initial speed 1.769 m/s in Beam Sea.
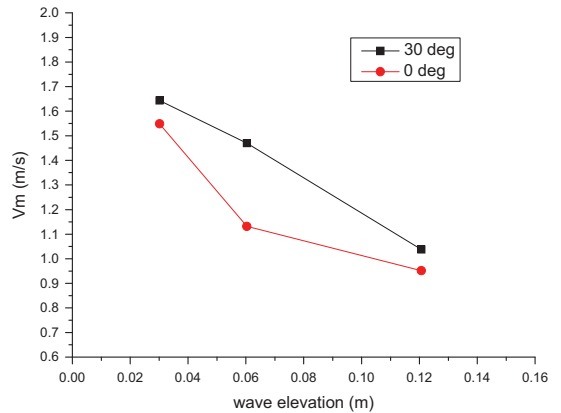

Fig. 17. Attainable speed with varying wave elevations in 0 deg, 30 deg heading conditions in waves with period 2.383 s.

4.3. Relation between attainable speed, wave condition and heading angles

Fig. 17 shows the relation between attainable speeds and wave elevation in 0 and 30 deg wave heading at a power corresponding to calm water speed of 1.769 m/s. Wave elevations (amplitudes) were 0.0302 m, 0.0604 m and 0.1207 m. Speed loss data for 0 deg heading is obtained from Chuang and Steen (2011). It has to be pointed out that the original experimental data for 0 deg heading in Chuang and Steen (2011) was obtained without including tow rope force in the model test. The data were corrected using the method proposed in the paper considering the effect of towrope force. Speed is dropping with the increase of wave elevation, since added wave resistance is proportional to wave elevation squared. Also, when heading increase the drop in speed is reduced.

Figs. 18 and 19 present the model test speed loss in percentage in waves with corresponding calm water speed V_0 equal to 1.769 m/s and heading angles 30, 60, 90 and 150 deg. Thrust deduction factor based on calculated added resistance was used in Fig. 18 and calm water thrust deduction factor was applied in

Fig. 19 when making prediction for the attainable speed at the encircled data points.

Fig. 20 represents the speed loss in percentage in waves with corresponding calm water speed $V_0 = 1.191$ m/s with 30 deg and 60 deg headings. It can be concluded that within head and bow sea conditions increasing the heading angle can greatly reduce speed reduction.

By comparing Figs. 18–20, it is shown that the speed loss in percentage is increasing with the decreasing of the corresponding calm water speed in the same sea conditions.

4.4. Contribution to total speed loss from added wave resistance and from steering

Speed drop for a ship sailing in oblique waves is due to added wave resistance (R_{aw}) and due to loss of thrust in the longitudinal direction (($T - F_{\text{longitudinal}}) \times (1 - t)$, where $T = \sqrt{F_{\text{longitudinal}}^2 + F_{\text{transverse}}^2}$ as shown in Fig. 7) for steering. How much each of them contributes to speed loss in our tests is figured out in this section.
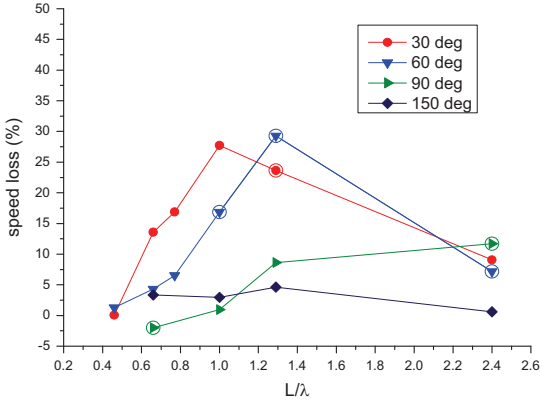
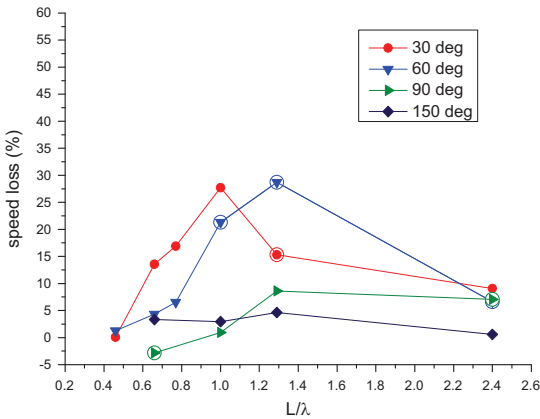**Fig. 18.** Experimental Speed loss in waves for $V_0 = 1.769$ m/s, with calculated t for non-converged runs.

Fig. 19. Experimental Speed loss in waves for $V_0 = 1.769$ m/s, with calm water t for non-converged runs.
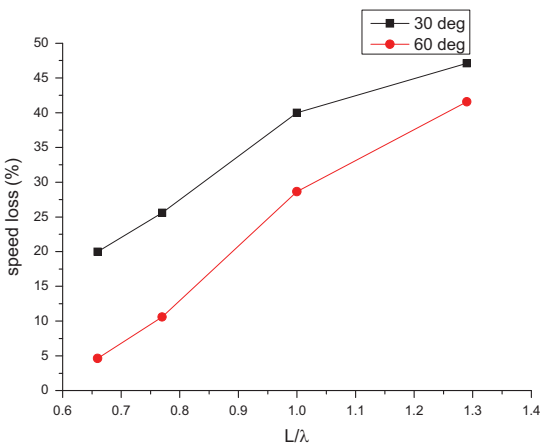

Fig. 20. Speed loss in waves for $V_0 = 1.191$ m/s.

Speed loss in percentage due to added wave resistance is calculated by Eq. (20):

$$\Delta V_{\text{added}} = \frac{V_0 - V}{V_0} \frac{R_{aw}}{R_{aw} + (T - F_{\text{longitudinal}}) \times (1-t)} \times 100\% \qquad (20)$$

Speed loss in percentage due to steering is calculated by Eq. (21):

$$\Delta V_{\text{steering}} = \frac{V_0 - V}{V_0} \frac{(T - F_{\text{longitudinal}}) \times (1-t)}{R_{aw} + (T - F_{\text{longitudinal}}) \times (1-t)} \times 100\% \qquad (21)$$

where V_0 is calm water speed; t is calm water thrust deduction factor. In Eqs. (20) and (21) we use measured attainable speed V (for non-converged runs, V is predicted by the method proposed in Section 1.3, with calculated thrust deduction factor), thrust T and longitudinal thrust force component $F_{\text{longitudinal}}$, but the added wave resistance R_{aw} unfortunately has to be taken as the calculated value.

Fig. 21 shows the experimental speed loss components in different wave lengths with different headings and different initial speeds. It can be seen that for head sea and bow sea conditions (Fig. 21(a) (b) (d)), speed loss due to added resistance and due to steering are of almost the same magnitude with speed loss due to steering slightly higher than due to added wave resistance. For beam sea condition (Fig. 21(c)), speed drop due to steering is much larger than the speed drop due to added wave resistance in most of the cases, since the added resistance is low and because the increasing sway drift force need more steering force to keep the heading. At the point with $L/\lambda = 0.66$ in Fig. 21(c), negative speed loss due to steering is caused by the predicted attainable speed in wave is higher than calm water speed in this case.

5. Conclusions

Model tests and numerical simulations were carried out to investigate the speed loss effects of a ship sailing in oblique waves. In the experiment, due to the limited length of the ocean basin, converged speed cannot be achieved in every run. A method proposed in this paper was used to predict the attainable speed from non-converged runs. Applying the correct thrust deduction factor in waves is important, since thrust force plays an important role for the finally converged speed and thrust deduction factor is varying with different thruster loading and vessel motion conditions. In lack of properly measured thrust deduction fraction in waves, two alternative approaches were tested; using the calm water thrust deduction fraction also in waves, and using computed added resistance due to waves to find the thrust deduction fraction in waves. Using computed added resistance gave the best agreement in the cases where the correction method could be verified. In the test case described in this paper, the method gives generally good prediction of the attainable speed in waves based on non-converged runs.

In oblique waves, the speed loss increase with the added wave resistance. When wave length approaches ship length, the speed loss reaches its peak value. For a fixed heading angle, speed loss is increasing roughly linearly with increasing wave elevation for our tests with constant propulsive power. This is also expected since added resistance is proportional to wave elevation squared.

When the power is kept constant in head sea and bow sea conditions and the higher the initial calm water speed, the less will the speed drop in waves and vice versa; The lower the initial calm water speed, larger speed reductions are experienced in waves.

Speed reduction due to added resistance and due to steering are at almost the same level for head sea and bow sea conditions for this tanker with twin azimuth propulsors; while increasing
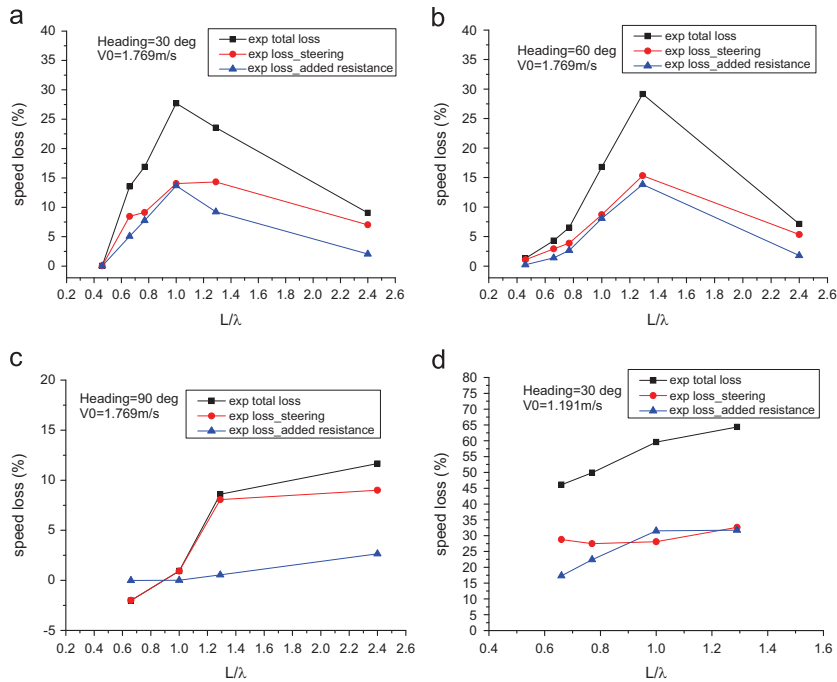
Fig. 21. Speed loss components for different conditions. (a) 30 deg heading with $V_0 = 1.769$ m/s, (b) 60 deg heading with $V_0 = 1.769$ m/s, (c) 90 deg heading with $V_0 = 1.769$ m/s and (d) 30 deg heading with $V_0 = 1.191$ m/s.

the heading angle to beam sea, speed loss due to steering plays a more important role than added wave resistance. This is because the added resistance decrease with increasing heading angle, and because more frequent and higher rudder (or azimuth) angle adjustments are required in order to keeps the vessel sailing along the designed straight line course in waves. This leads to increased thrust force deductions in the longitudinal direction.

References

Alterskjær, S. R&D Phase I, Calm Water Tests With 3 Different Fore Ships. MARINTEK Report 530635.00.03. Trondheim, Norway, November, 2010.

Berg, A.A., Open Water Tests with Azipull. MARINTEK Report 601973.00.01. Trondheim, Norway, June 2002.

Bhattacharyya, R., 1978. Dynamics of Marine Vehicles. Wiley Interscience, ISBN: 0471072060.

Carrica, P.M., Paik, K., et al., 2008. URANS analysis of a broaching event in irregular quartering seas. J. Mar. Sci. Technol., 395–407.

Chuang, Z., Steen, S. Prediction of Speed Loss of a Ship in Waves. SMP'11, Hamburg, Germany, 2011.

Chuang, Z., Steen, S., 2012. Speed loss due to seakeeping and maneuvering in zigzag motion. Ocean Eng. 48, 38–46, January.

Faltinsen, O.M., Minsaas, K.J., Liapias, N. &Skjørdal, S.O. 'Prediction of resistance and propulsion of a ship in a seaway. In: Inui, T. (Ed.), Proceedings of 13th Symposium on Naval Hydrodynamics. The Shipbuilding Research Association, Japan. 1980.

Fathi, D., Hoff, J.R., 2008. ShipX vessel response. Theory Manual. Marintek.

Fujii H., Takahashi T., Experimental study on the resistance increase of a ship in regular oblique waves. In: Proceeding of 14th ITTC, vol. 4, pp. 351–60. 1975.

Gerritsma, J., Beukelman, W., 1972. Analysis of the resistance increase in waves of a fast cargo ship. International Shipbuilding Progress 19 (217), 285–292.

Havelock, T.H., 1940. The pressure of water waves upon a fixed obstacle. P.R.S. Series A 175 (963).

Journee, J.M., Motions and Resistance of a Ship in Regular Following Waves. Report 440, Delft University of Technology, Ship Hydromechanics Laboratory, The Netherlands, September, 1976.

Loukakis, Sclavounos, 1978. Some extensions of the classical approach to strip theory of ship motions, including the calculation of mean added forces and moments. J. Ship Res. 22 (1), 1–19.

Maruo, H., 1963. Resistance in waves. 60th anniversary series. The society of Naval Architects of Japan.

Nakamura, S., Naito, S., 1977. Propulsive performance of a container ship in waves. The Society of Naval Architects of Japan. Naval Archit. Ocean Eng. 15.

Prpic-Orsic, J., Faltinsen, O.M., 2012. Estimation of ship speed loss and associated CO_2 emissions in a seaway. Ocean Eng. 44, 1–10, April.

Ringen, E., Fathi, D., ShipX Vessel Simulator, Theory Manual. MARINTEK. 2008.

Ringen, Edvard, ShipXManoeuvring Plug-In, Theory Manual. MARINTEK. 2009.

Salvesen, N., Tuck, E.O., Faltinsen, O.M., 1970. Ship motions and sea loads. SNAME 78, 250–287.

Smogeli, O.N.,2006. Control of Marine Propellers–From Normal to Extreme Conditions. Ph.D. Thesis. p. 187, Faculty of Engineering Science & Technology, Department of Marine Technology, Trondheim.

Yamazaki, R., Nakatake, K., Kino, S., Koguchi, K., 1978. On the propulsive performance of a ship in regular head waves. J.S.N.A. Japan 1978 (143), 95.

Paper 5

Measurement of speed loss due to waves

Sverre Steen, Zhenju Chuang

Measurement of speed loss due to waves

Sverre Steen[1] and Zhenju Chuang[1]

[1]Department of Marine Technology, Norwegian University of Science and Technology (NTNU), Trondheim, Norway

ABSTRACT

Knowledge of the speed loss of ships due to waves is important in ship design and in planing ship operations. Added resistance due to waves is an important contribution, but only a part of the problem. The thrust and propulsive efficiency is also changing due to operation in waves, and the changes must be included in an accurate manner. The complexity of the problem means that CFD is at the moment not suited for practical predictions of speed loss due to waves. The conventional powering prediction approach also has severe shortcomings when it comes to prediction of speed loss due to waves. The use of non-linear time-domain simulations shows promising results. Model testing is still considered to be the most accurate method for prediction of speed loss. This paper demonstrates the importance of properly accounting for the friction correction in model tests. The importance of contributions from steering is shown, and a method to find the speed loss from short model test runs is given.

Keywords

Speed loss, added resistance, model testing, propulsion.

1 INTRODUCTION

On the background of increasing focus on reducing fuel consumption of ships, there is increasing awareness of the importance of the speed and power performance of ships travelling in realistic sea states, compared to the ideal calm water, no wind condition considered in standard speed-power predictions. A lot of attention is, quite rightfully, given to the prediction of added resistance due to waves, but this is only a part of the problem. What is really needed is knowledge of speed loss due to waves, or alternatively, required added power to maintain the speed in a seaway.

This paper initially discusses the factors contributing to speed loss. Then, alternative methods to predict the speed loss are discussed. Finally, how the speed loss in waves might be determined from model tests is discussed in detail. The importance of properly accounting for the larger frictional resistance in model scale is pointed out, and a method for correcting model test results is given. The effect of steering is discussed. A method to find the speed loss from tests where converged speed wasn't reached is demonstrated.

2 SPEED LOSS DUE TO WAVES

In this chapter we give an overview of the physical effects contributing to speed loss, before we discuss how speed loss can be predicted.

2.1 Factors contributing to speed loss

Added resistance

The added resistance is frequently the most important contribution to speed loss. The added resistance of a ship advancing at constant speed in a straight course in waves has been studied by many authors, for many years. Pérez Arribas (2007) gives an overview of the different methods. The overview given in the introduction to the recent paper by Liu et al. (2011) is also worth a read. The largest added resistance is experienced in head seas, when the length of the encountered waves is of the same order of magnitude as the ship length. Thus, most methods focus on this case. To deal with the special case of short waves, special methods have been derived, such as the one given in Faltinsen et al. (1980). Successful combinations of methods for short and long waves are reported by Guo and Steen (2010) and Prpić-Oršić and Faltinsen (2012). CFD methods based on RANS and Volume of Fluid (VoF) surface capturing is found to be capable of predicting added resistance with reasonable accuracy in both long and short waves Guo (2011), but computational cost of such methods is still prohibitive for practical use. Guo (2011) also confirmed that added frictional resistance has a negligible influence on the total resistance.

In other than head seas, ships will experience yawing motions of varying magnitude, depending on wave length and the course stability of the ship. The yawing motions influence the added resistance, but this is often not accounted for. Chuang and Steen (2012) showed results of experiments in small amplitude zig-zag tests, and showed how the added resistance was influenced by the zig-zagging.

Thrust loss

There are several factors contributing to loss (or change) of thrust when the ship travels in waves:

- Ventilation and out-of-water

- Wave-making by the propeller due to closeness to free surface

- Change of propulsive factors (mainly thrust deduction and wake fraction)

- Change of propulsion point

Ventilation and propeller out-of-water can lead to large thrust loss, but is only occurring in quite high sea states. Faltinsen et al. (1980) gives a good summary of how these effects can be estimated in a simple manner. Prpić-Oršić and Faltinsen (2012) show that a non-linear time-domain simulation is required to properly account for the effect of propeller ventilation on the speed loss. In the cases studied in this paper, the propellers are not ventilating or getting out of the water.

When the propeller is getting close to the free surface, but not sufficiently to cause ventilation, the pressure field surrounding the propeller will disturb the free surface. This will reduce the pressure differential over the propeller, since the free surface will partly allow the pressure differential to escape. Faltinsen et al. (1980) give a method to include this effect based on empirical data.

It is known that wake fraction and thrust deduction will change due to waves and ship motions, but there is surprisingly little knowledge in open literature about the magnitude of change and how to compute it. Usually, model tests are either performed with towed or with self-propelled model, while the determination of change of thrust deduction generally requires the model to be tested both towed and self-propeller in otherwise identical conditions. One of the few such published datasets are given in Naito and Nakamura (1977). This publication also includes one of the very few measurements of change of wake distribution, which shows that the wake is reduced in waves, especially close to the propeller hub. Guo et al. (2012) studied the change of nominal 3-D wake in waves in the propeller plane of the KVLCC2 using RANS and found that the change was largest where the calm water wake was largest, so that the wake field in waves appeared to be more uniform, with the characteristic "hook-shape" of the wake of this full-bodied tanker almost entirely vanished when travelling in a wave with a length similar to the ship length.

When the resistance changes, the propulsion point will change, since the thrust has to balance the resistance. Both the speed and the thrust will change. How much each of them will change depend on how the engine is responding. If a constant power control is applied, the speed will be more reduced than if for example a constant RPM control is used. Thus, the characteristics of the motor, including the effect of its control, must be taken into account in the speed loss calculation.

2.2 Methods for prediction of speed loss

Here we will discuss which methods which are available to predict the speed loss. Methods might be classified in different ways. Here we have chosen the following division of methods:

- The classical powering prediction approach
- Time-domain simulations
- Direct CFD approach
- Model testing of a self-propelled model

- Full scale testing

The classical powering prediction approach

In this approach, a modified resistance curve is created by adding resistance increase due to wind, waves, steering, yawing and other effects to the calm water resistance. Then, thrust deduction and wake fraction in waves are estimated, or taken to be equal to their calm water values, if other information is not available. Then, a powering prediction is performed in exactly the same way as for the calm water situation. In such a calculation, non-linear effect, like for instance propeller ventilation, can't be taken into account in a proper manner. Only the zeroth-order added resistance due to waves is included. Furthermore, effects of steering and yawing can hardly be included.

Time-domain simulations

In time-domain simulations, it is in principle straight forward to include non-linear effects. A ship simulation model that combines seakeeping and manoeuvring is required. Several such simulation models have been developed over the later years.

Direct CFD approach

In the direct CFD approach, the ship sailing in waves is simulated in a time-accurate CFD simulation. The propeller forces are simulated by including the rotating propeller in the simulation, for instance in a sliding mesh arrangement, or by using a simplified propeller model that takes the instantaneous inflow conditions to the propeller from the CFD simulation. A simplified propeller treatment will have difficulties in properly representing the unsteady working conditions of the propeller and the resulting dynamic propeller wake. By including the propeller, this problem is avoided, but resulting in a rather hefty increase in the computational cost. To properly represent the nonlinear effects included in the speed loss problem, the simulation should be performed in a realistic irregular wave train, resulting in a need for excessively long computational times. One of the few reports of such a calculation in the literature is Carrica et al. (2008). CFD in general holds great promise in marine hydrodynamics, but speed loss due to waves seems to be one of the most difficult problems to solve with this method, due to the huge computational effort required.

Model testing of a self-propelled model

When model testing a self-propelled model to determine the speed loss, the ship hull, propeller and rudder are all modeled, and all physical effects of importance should be included, except for cavitation. Thus, outside of the expense of such model tests, problems are related to scale effects, limited length of runs, and issues related to modeling of engine characteristics, auto-pilot and steering and so forth. These issues are discussed in detail in the remaining parts of this paper.

Full scale testing

Although one can say that full scale tests are not a prediction method, but a method to verify a prediction, we will still make a few notes on the quantification of speed

loss from full scale measurements. There is currently rapid progress in technology for monitoring ship performance, and remote monitoring systems are rapidly implemented. Savio and Steen (2012) reports how the remote monitoring system Hemos can be used to identify propeller ventilation, while Hansen (2011) reports how another remote monitoring system is used to monitor the speed-power performance of a container vessel in service. This technical progress means that full scale measurements will play a more important role in hydrodynamics research in the future, but some major problems concerning the measurement of speed loss remain: The measurement of the wave condition, and the accurate measurement of speed through water. Together, this means that obtaining accurate speed loss results from full scale measurements is difficult.

3 MODEL TESTS TO MEASURE SPEED LOSS

Model testing is still considered the most accurate way of predicting the speed loss of a ship in waves. It enables inclusion of most important effects in a realistic way. Tests might be performed in a towing tank or seakeeping basin. Tests in long-crested head sea waves in a towing tank is most widespread, both because such facility is most common, and because speed loss is often largest in head seas. However, by limiting the testing to long-crested head seas, important effects due to steering and yawing are lost. This chapter discusses techniques for performing model tests of speed loss, and how such tests can be analysed and corrected. To exemplify, we use model test results of a recent series of tests with a 1:16.57 scale model of a 118 m long tanker, performed in the towing tank and ocean basin at the Marine Technology Centre in Trondheim, Norway. The main dimensions of the model are given in Table 1 below. The model was equipped with scale models of two Rolls-Royce Azipull azimuthing thrusters as main propulsors. The propellers had a diameter of 0.199 m and a pitch ratio $P/D_{0.7}=1.2$.

Table 1 Main dimensions of model

| L_{OA}	[m]	7.142
Lpp	[m]	6.832
D	[m]	0.905
B	[m]	1.147
T	[m]	0.435

3.1 Model test set-up

For testing in a towing tank, different set-ups are possible:

1. Model connected to the carriage in the same way as for an ordinary propulsion test – fixed in sway and yaw.

2. Model connected to the carriage with wires and springs.

3. Free-running model.

The set-up 1 used for ordinary propulsion tests is limited with respect to the wave height and wave length, since only small motions are usually allowable in both surge and vertical plane motions. The set-up 2 is normally used for towing a model in waves. It is illustrated in Figure 1. In this set-up a beam is fixed transversely to the model at the longitudinal position of the centre of pitch. To each end of the beam, wires are connected in a crow-foot arrangement. Force transducers are mounted between the beam and the wires so that the longitudinal force from the wires on the model can be measured. The wires are pre-tensioned sufficiently to ensure that the wires won't get slack at any time during testing. In this way, the heading of the model is quite precisely maintained. The wires are connected to the carriage through springs. The springs have a stiffness which shall allow some freedom in surge. The spring stiffness must be such that resonant surge motions are avoided. The arrangement can be used for testing speed loss by adjusting the carriage speed so that the towing force measured at the points where the wire is connected to the beam on average equals the correct friction correction force. This might be a severe control problem, especially in irregular waves. Benefits of this type of set-up are that an actively controlled rudder is not required, and that the wires allow for a method of applying tow rope force.
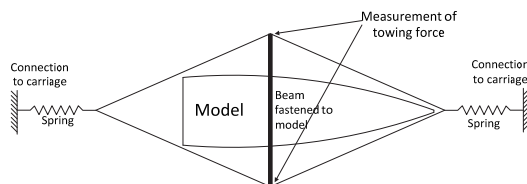
Figure 1 Towing arrangement for seakeeping tests (set-up type 2)

Model tests with a free-running, self-propelled model require use of a controlled rudder, with an auto-pilot to keep the model on course and on a track in the centre of the towing tank. Thus, not only vertical position needs to be measured, but also the horizontal position, effectively requiring the use of an optical position measurement system. Application of the tow rope force (see next section) is also challenging. The recommended way is to use an air fan which gives a thrust force in the direction of travel. By varying the fan speed, the thrust force can be controlled to give the specified tow rope force.

3.1 Friction correction force

In order to obtain correctly scaled propeller loading, a friction correction force has to be applied on the model. This force is often called tow rope force, named after the way this force was traditionally applied during a propulsion test. The tow rope force is given as:

$$F_D = \tfrac{1}{2}\rho V_M^2 S_M C_s \qquad (1)$$

Where subscript M means model scale and subscript S means full scale. V is velocity, S is wetted surface, ρ is water density and C_s is the tow rope force coefficient. C_s is in principle expressed as the difference in total resistance coefficient between model and full scale:

$$C_s = C_{TM} - C_{TS} \qquad (2)$$

The main difference between model and full scale total resistance coefficient is the magnitude of the frictional coefficient, but also effect of roughness, transom stern drag, difference in air resistance and appendages, and the correlation allowance should be taken into account. Then, we arrive at the following expression for the tow rope force coefficient:

$$C_s = [C_{FM} - (C_{FS} + \Delta C_F)](1+k) + (C_{BDM} - C_{BDS}) \\ + (C_{AppM} - C_{AppM}) - C_A \qquad (3)$$

Where ΔC_F is the roughness allowance, C_{BD} is the transom stern resistance and C_{App} is the appendage resistance coefficient. As an example, for a 1:16:57 scale model of a 118 m long tanker at F_N=0.212 the tow rope force amounts to 41.5% of the calm water resistance. Data for this model is found in Chuang and Steen (2011). If a speed loss test is performed without applying tow rope force, the added resistance due to waves becomes a smaller relative increase of the total resistance, so the predicted speed loss will be less. We will now look at how much less, and start with the condition of the model tests reported in Chuang and Steen (2011), where the power to the propeller was kept constant. Therefore, the following equality holds:

$$\frac{R_{TC} \cdot V_C}{\eta_{DC}} = \frac{R_{TW} \cdot V_W}{\eta_{DW}} \qquad (4)$$

Where R_T is the total resistance, subscript C means calm water and subscript W means in the studied wave condition. η_D means quasi-propulsive efficiency, $\eta_D = \eta_H \cdot \eta_R \cdot \eta_0$. We assume here that hull efficiency η_H and relative rotative efficiency η_R are the same in calm water and in waves, so that we can replace η_D with the open water efficiency η_0 in equation (4). The total resistance in waves can be approximated by the following expression:

$$R_{TW} = R_{TC} + \Delta R_W - (\frac{dR_{TC}}{dV} + \frac{d\Delta R_W}{dV}) \cdot \Delta V \qquad (5)$$

where the speed loss $\Delta V = V_C - V_W$ and ΔR_W is the added resistance due to waves, evaluated at the calm water speed V_C. If we insert (4) in (5) and neglect the term proportional to ΔV^2 we get:

$$\Delta V = V_C \frac{R_{TC} + \Delta R_W - R_{TC} \cdot \eta_{0W} / \eta_{0C}}{R_{TC} + \Delta R_W + (\frac{dR_{TC}}{dV} + \frac{d\Delta R_W}{dV})V_C} \qquad (6)$$

This is actually an expression for the speed loss due to waves when the power is kept constant. If R_{TC} is taken as the resistance corrected for tow rope force (which means the full scale resistance directly Froude-scaled to model scale), then the speed loss when tow rope force is not

applied can be found by replacing R_{TC} in equations (5) and (6) by $R_{TC}+F_D$, equation (6) becomes:

$$\Delta V_{F_D} = V_C \frac{R_{TC} + F_D + \Delta R_W - (R_{TC} + F_D) \cdot \eta_{0W} / \eta_{0C}}{R_{TC} + F_D + \Delta R_W + (\frac{dR_{TC}}{dV} + \frac{dF_D}{dV} + \frac{d\Delta R_W}{dV})V_C} \qquad (7)$$

Usually η_{0W} / η_{0C} is not too far from one, and if we temporarily assume $\eta_{0W} / \eta_{0C} = 1$, just to see the effect of the tow rope more clearly, then (7) becomes:

$$\Delta V_{F_D} = V_C \frac{\Delta R_W}{R_{TC} + F_D + \Delta R_W + (\frac{dR_{TC}}{dV} + \frac{dF_D}{dV} + \frac{d\Delta R_W}{dV})V_C} \qquad (8)$$

So it is clear that neglecting tow rope means that ΔV becomes smaller.

The correction for lack of tow rope force in the experiment is $\Delta V - \Delta V_{F_D}$, so that corrected attainable speed is computed as:

$$V_{corrected} = V_{measured} - (\Delta V - \Delta V_{F_D}) \qquad (9)$$

Later, Chuang and Steen (2012) updated the method to include higher order terms. In this method, R_{TC} and R_{TW} in equation (4) are represented by polynomials, and the equation solved by iteration for the attainable speed in waves V_W, both with and without towrope. Then the difference is used to correct the measured speed in waves according to equation (9). Results of a test in regular head waves of the previously mentioned tanker model are shown in Table 2. Unfortunately, the model tests were only performed without tow rope force, so a proof of the method is not available. In order to provide a partial validation, the table includes results of time-domain simulations with and without tow rope.

Table 2 Predicted full scale speed based on model tests of a tanker in calm water and regular head wave of height 2 m and period T=7.5 s (L_{PP}/λ=1.3)

Condition:	Speed [m/s]
Calm water	7.20
Without tow rope	6.80
Corrected (linear)	6.72
Corrected non-linear	6.71
Simulation, without tow rope	6.85
Simulation, with tow rope	6.70

Figure 2 shows the attainable speed of the same ship as Table 4 for a number of different wave lengths. Values corrected with the linear and the non-linear methods are shown, as well as the uncorrected measured value and the predicted speed using equation (7). It is seen that when the speed loss is large, it is important to correct for tow rope force, and that this should preferably be done with the fully non-linear method. However, that said, it is surprising that the speed loss predicted using the linear

prediction method gives so good agreement with the measured value.

In the calculations, the calm water resistance is taken from model tests and the added resistance is computed using the method of Gerritsma and Beukelman (1972).
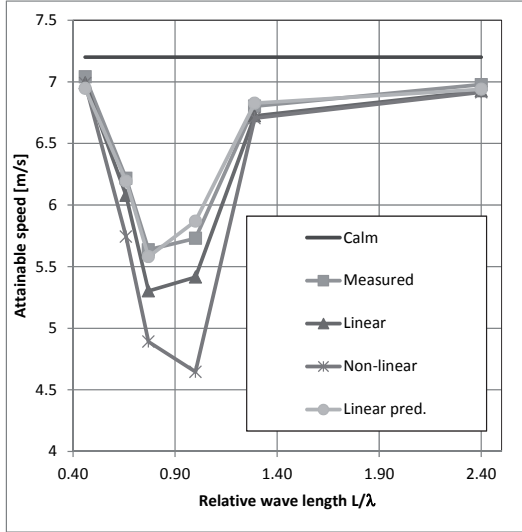
Figure 2 Attainable speed of tanker from model tests in regular head waves of height H=2 m.

3.2 Importance of steering

As indicated in the previous chapter, the speed loss can be predicted quite well in head seas if the added resistance due to waves is known, and as long as the waves don't cause the propeller to get out of the water or ventilate. However, in other than head seas, the waves will cause the vessel to yaw, and steering will often be applied to counteract the yawing and keeping the vessel on the wanted course. If yawing and steering are important for the speed loss, testing with a propelled, free model is required. Tests with the 1:16.57 scale model of the 118 m tanker, were performed in the ocean basin at the Marine Technology Centre at different headings relative to the waves. Since the model was free-running, self-propelled and controlled by an auto-pilot, we can use the results to exemplify the importance of steering on the speed loss. The speed loss is split into added resistance and steering using the following equations:

$$\Delta V_{added} = \frac{V_0 - V}{V_0} \frac{R_{aw}}{R_{aw} + (T - F_x) \cdot (1-t)} \cdot 100\% \quad (10)$$

$$\Delta V_{steering} = \frac{V_0 - V}{V_0} \frac{(T - F_x) \cdot (1-t)}{R_{aw} + (T - F_x) \cdot (1-t)} \cdot 100\% \quad (11)$$

where V_0 is calm water speed; t is calm water thrust deduction factor, V is attainable speed, T is thrust and F_x is longitudinal thrust force component. All these variables are measured in the experiment. However, the added wave resistance R_{aw} unfortunately has to be taken as the calculated value, which is a weakness of this method. To be able to separate speed loss due to steering from added resistance without depending on the computed added wave resistance, one would have to do extra tests with restrained heading, which would certainly be a challenge in our ocean basin. Results of using equations (10) and (11) to decompose the results of the tests with the tanker model in 30, 60 and 90 degrees heading are shown in Figure 3, Figure 4, and Figure 5. It is seen that in 30 and 60 degrees heading, speed loss due to added resistance and steering are of almost equal magnitude for this vessel, while in 90 degrees heading, speed loss due to steering dominates. Thus, it seems clear that to determine the speed loss in other than head seas, the steering should be properly included.
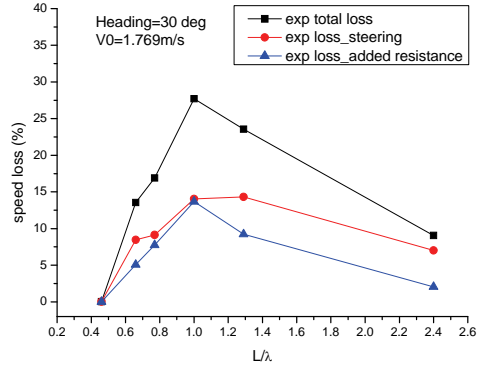
Figure 3 Speed loss due to steering and added resistance in regular waves at a heading of 30 degrees.
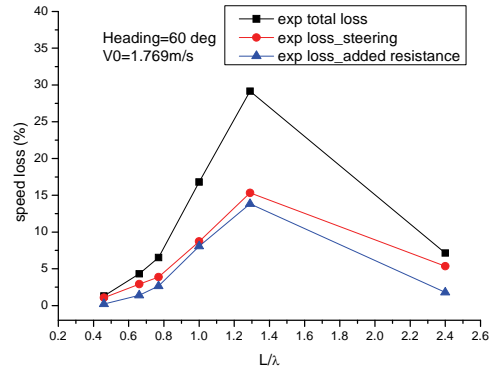
Figure 4 Speed loss due to steering and added resistance in regular waves at a heading of 60 degrees.

Figure 5 Speed loss due to steering and added resistance in regular waves at a heading of 90 degrees.
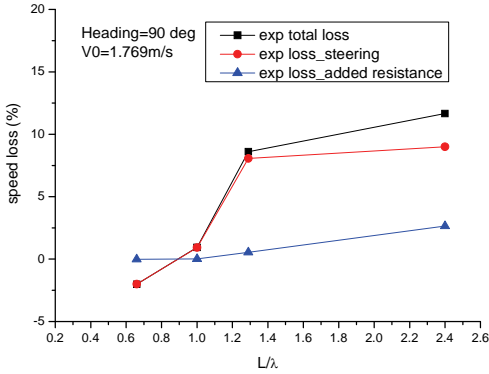
3.3 Correction of non-converged runs

Especially when large, heavy models are tested in model basins with limited length, it will often be difficult to get a converged speed in a speed loss test, since the acceleration resulting from an imbalance between thrust and resistance will be small, due to the large mass. The inertia force is expressed as:

$$m \cdot a = R_{TC} + \Delta R_W - T(1-t) - F_D \qquad (12)$$

Here R_{TC} is the model resistance, T is the total thrust, t is thrust deduction fraction and F_D is the tow rope force, so here we assume that the tow rope is properly enforced on the model. An example of a non-converged run is shown in Figure 6.
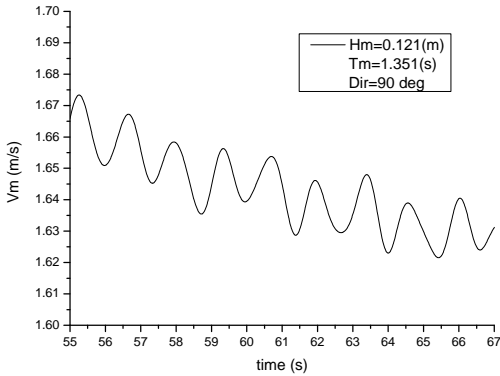
Figure 6 Example of non-converged speed loss run in beam seas.

Chuang and Steen (2012) applied the criterion $a \geq 0.001 \, \text{m/s}^2$ to decide when the speed is treated as non-converged. To find the converged speed, we require that the acceleration shall be zero, so equation (12) becomes:

$$R_{TC} + \Delta R_W - T(1-t) - F_D = 0 \qquad (13)$$

All terms in this equation is considered as speed-dependent, except for the thrust deduction fraction t. Polynomial approximations to R_{TC}, F_D and ΔR_W can be easily established. The thrust T is known from

measurements at the non-converged speed V_{nc}. Then, by neglecting the change of efficiency and assuming that tests are performed at constant power we can find the thrust for a new speed V as:

$$T(V) = T(V_{nc})V_{nc}/V \qquad (14)$$

Using (14), we can now solve equation (13) iteratively to find the converged speed. The method was applied to oblique wave tests with the same model as reported in section 3.1.

Table 3 Validation of method to correct runs with non-converged speed. Wave height H=0.121 m, calm water speed 1.769 m/s

L/λ	Heading (deg)	V$_{measured}$ (m/s)	V$_{corrected}$ (m/s)	Error (%)
0.77	30	1.470	1.471	0.079
0.46	30	1.768	1.766	-0.108
0.66	60	1.693	1.745	3.091
1.00	90	1.752	1.811	3.366

Further details of the method are shown in Chuang and Steen (2012).

3.4 Model tests to determine propulsive factors

The change of propulsive factors in waves is often overlooked. The classic study by Naito and Nakamura (1977) shows that for their single screw container vessel, the thrust deduction fraction at F_N=0.15 varies about ±0.04, while the wake fraction varies ±0.03, as can be seen from Table 4. It is worth noting that the propulsion tests in waves by Naito and Nakamura (1977) were performed at model propulsion point (that means without tow rope force).

Table 4 Values of thrust deduction and wake fraction in calm water and waves for a container ship. Values extracted from Fig. 18 of Naito and Nakamura (1977)

F$_N$=0.15	Calm	λ/L=1.2	λ/L=1.7
1-t	0.83	0.87	0.79
1-w	0.70	0.73	0.67

In order to properly measure the thrust deduction fraction in a model test, two different methods are suggested:

1. Perform both resistance and propulsion test at same speed in the same wave conditions

2. Perform the propulsion test at (at least) two different tow rope forces for the same speed and wave condition.

The first method is similar to the conventional ITTC'78 approach used in calm water. The problem with this approach is that it is time-consuming and that conditions might be different during resistance and propulsion tests if the propulsion test in waves is carried out with a free running model (method 3 of section 3.1). To do the

propulsion test with a free model, the propulsion test must be performed first, and the resistance test performed afterwards at the same speed as was achieved in the propulsion test. The resistance test will necessarily have to be performed with a (partly) restrained model in a set-up somewhat similar to Figure 1. Then, differences between thrust and resistance might not only be the classical thrust deduction, but also be due to steering and yawing during propulsion.

In the second method, the thrust deduction is found from the results of tests 1 and 2 by solving the system of two ordinary equations:

$$T_1(1-t) = R_T - F_{D1}$$
$$T_2(1-t) = R_T - F_{D2}$$
(15)

where R_T is the total resistance in the actual wave condition, including added wave resistance, T is the total thrust and F_D is the applied tow rope force. Both T and F_D are measured. For this approach to work, we have to assume that $(1-t)$ is independent of propeller loading, and both tests must be performed at the same speed and wave condition, so that we can justify the assumption of R_T being the same in both measurements. The variation in propeller loading can be obtained by varying the air fan thrust in a free model set-up, but in that case it will be difficult to obtain the same speed. Dividing both equations in (15) with $\frac{1}{2}\rho v^2$ will reduce the sensitivity to small differences in velocity between the two runs. If the model is mounted in the spring and wire system shown in Figure 1, the test can performed at constant speed and the variation in tow rope force obtained simply by varying the propeller speed. However, this method is only recommended in head and following waves. Therefore, it can be concluded that determining thrust deduction in other than head and following waves is not straight forward and that it is difficult to give a general recommendation for method to be used.

To find the wake fraction in waves, we need data from a propeller open water test. According to Naito and Nakamura (1977) and McCarthy et al. (1961) the propeller open water characteristics don't change in waves. That is a reasonable assumption according to our experience, as long as the propeller is well submerged, so ventilation and out-of-water effects can be excluded. Thus, to find the change of wake in moderate sea states, a calm water open water test can be applied. If the analysis is based on a load-varied propulsion test, according to method 2 above, we can separate the effect of propeller loading on the wake fraction.

4   CONCLUSIONS

Through analyses of a series of model tests with a 1:16.57 scale model of a 118 long tanker propelled by twin azimuthing thrusters, the importance of including tow rope force in model tests to determine speed loss is demonstrated. Furthermore, a method to correct results for the lack of tow rope force is demonstrated.

To find the speed loss in other than head seas, model tests should be performed with a free-running, auto-pilot controlled model, so that the effects of both added resistance and steering are included. For the model of the 118 m long tanker, it was demonstrated that steering and added resistance contributed equally much to the speed loss in 30 and 60 degrees heading in regular waves.

When performing speed loss model tests in an ocean basin, obtaining converged speed is a frequent problem, due to slow convergence and limited length of the basin. A correction method to obtain the value of converged speed from non-converged runs is demonstrated, and good results are found.

To determine the thrust deduction in waves, we need results from both resistance and propulsion test at the same speed in the same waves, or we can use two propulsion tests at different tow rope force. Both methods can be performed by testing at a pre-determined speed with a partially restrained model. However, in oblique waves, testing the model in free-running condition is recommended, so it is not clear what is the best method for obtaining the thrust deduction in oblique waves.

REFERENCES

Carrica, P., K.-J. Paik, Hosseini, H. S., Stern, F. (2008). "URANS analysis of a broaching event in irregular quartering seas." Journal of Marine Science and Technology **13**(4): 395-407.

Chuang, Z., Steen, S. (2011). Prediction of Speed Loss of a Ship in Waves. The Second International Symposium on Marine Propulsors. M. Abdel-Maksoud. Hamburg, Germany. **1**: 8.

Chuang, Z., Steen, S. (2012). "Experimental and Numerical Study of Stem Shape Influence on Speed Loss in Waves." Ship Technology Research **59**(2): 13.

Chuang, Z., Steen, S. (2012). "Speed loss due to seakeeping and maneuvering in zigzag motion." Ocean Engineering **48**(0): 38-46.

Faltinsen, O., Minsaas, K. J. Liapis, N., Skjørdal, S. O. (1980). Prediction of Resistance and Propulsion of a Ship in a Seaway. <u>13th Symposium on Naval Hydrodynamics</u>. T. Inui. Tokyo, Japan, The Shipbuilding Research Association of Japan.

Gerritsma, J., W. Beukelman (1972). "Analysis of the Resistance Increase in Waves of a Fast Cargo Ship." <u>International Shipbuilding Progress</u> **19**(217): 8.

Guo, B. (2011). <u>Numerical and Experimental Investigation of Added Resistance in Waves</u>. PhD PhD, Norwegian University of Science and Technology.

Guo, B., Steen, S. (2010). Experiment on added resistance in short waves. <u>28th Symposium on Naval Hydrodynamics</u>. Pasadena, California, California Institute of Technology.

Guo, B., Steen, S., Deng, G. B. (2012). "Seakeeping prediction of KVLCC2 in head waves with RANS." <u>Applied Ocean Research</u> **35**(0): 56-67.

Hansen, S. V. (2011). <u>Performance Monitoring of Ships</u>. PhD PhD, Technical University of Denmark.

Liu, S., A. Papanikolaou, Zaraphonitis, G. (2011). "Prediction of added resistance of ships in waves." <u>Ocean Engineering</u> **38**(4): 641-650.

McCarthy, J. H., W. H. Norley, Ober, G.L. (1961). The Performance of a Submerged Propeller in Regular Waves. Washington DC, USA, David Taylor Model Basin.

Naito, S. and S. Nakamura (1977). "Propulsive Performance of a Container Ship in Waves." <u>The Society of Naval Architects of Japan. Naval Architecture and Ocean Engineering</u> **15**.

Pérez Arribas, F. (2007). "Some methods to obtain the added resistance of a ship advancing in waves." <u>Ocean Engineering</u> **34**(7): 946-955.

Prpić-Oršić, J., O. M. Faltinsen (2012). "Estimation of ship speed loss and associated CO2 emissions in a seaway." <u>Ocean Engineering</u> **44**(0): 1-10.

Savio, L., Steen, S. (2012). "Identification and Analysis of Full Scale Ventilation Events." <u>International Journal of Rotating Machinery</u> **2012**: 19.

Appendix B Comparisons between conventional propeller-rudder system and azimuth thruster on the ability to keep the vessel on its speed

The propulsion system plays a key role in the vessel's ability to keep speed when sailing under seakeeping and maneuvering conditions. Conventional propeller-rudder system tends to make the ship more course-stable due to larger rudder area. On the other side, azimuth and podded propulsors are always preferred for better low-speed maneuverability. In this section, we compare the speed loss of our case vessel equipped with the azimuth thrusters with the case when the same ship is equipped with twin propellers and conventional rudders. The predictions are done using Vesim, and the comparisons between Vesim results and model tests as presented in papers 1-4 serve as validation of this calculation method. The azimuth thruster used here is the pod model described in section 3.3.1 in Chapter 3. The same propeller was applied for the propeller-rudder system and the azimuth. The dimension for the rudder is specified in Fig. B1 where D is full scale propeller diameter (D=3.3m).
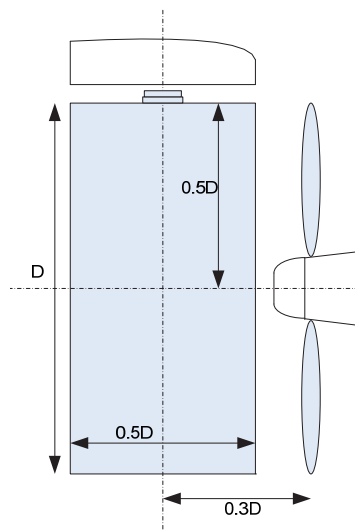
Fig. B1 Sketch of the rudder

The same resistance and propulsive factors are applied for the ship with conventional propeller-rudder arrangement and azimuth thruster. This is to ensure comparable results when it comes to the speed loss. The two propulsion systems were tested in the same oblique wave conditions with sailing headings to be 30 degrees, 60 degrees and 90 degrees with initial speed to be the design speed of 14 knots (1.769 m/s model scale). Comparisons between the performance of the two propulsion systems with respect to attainable speed, steering angle and thrust force in waves are given in Fig. B2-Fig. B4 in model scale values.
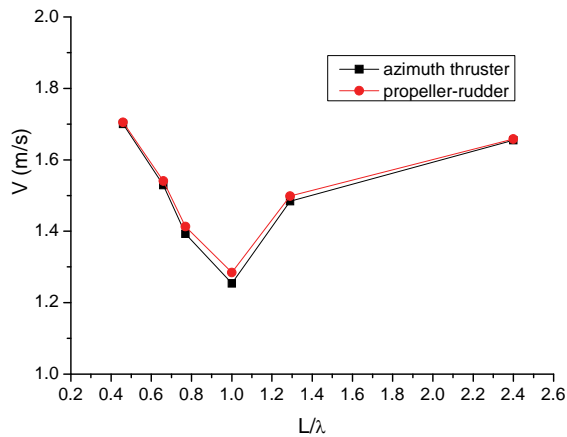
Fig. B2 (a) Attainable speed comparisons
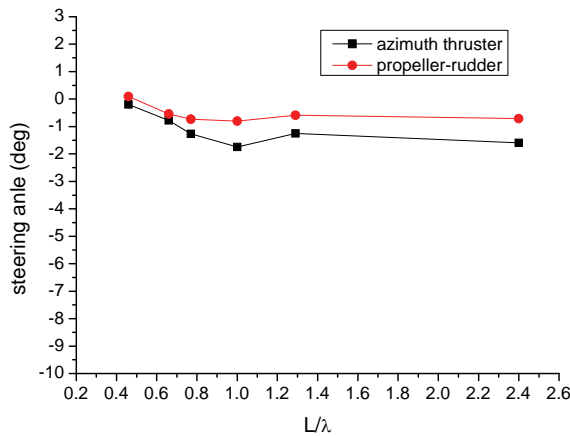
Fig. B2 (b) Average steering angle comparisons
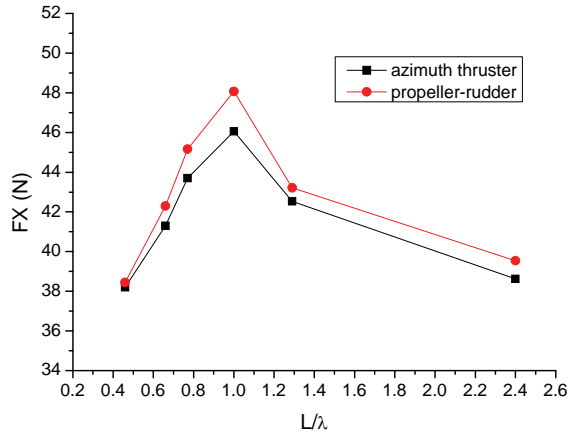
Fig. B2 (c) Longitudinal thrust force comparisons

Fig. B2 Comparisons between azimuth thruster and propeller-rudder system in 30 degrees head sea, with V_0=1.769m/s
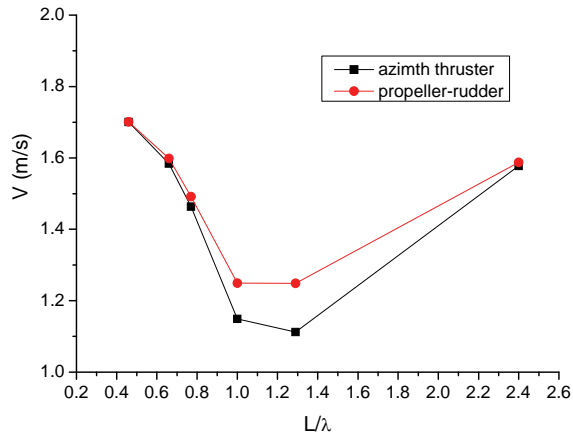
Fig. B3 (a) Attainable speed comparisons
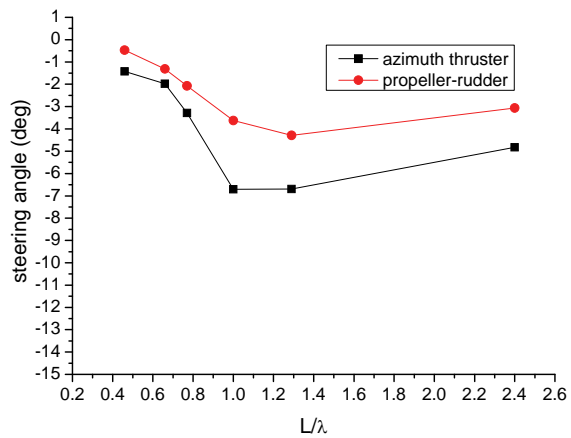
Fig. B3 (b) Average steering angle comparisons
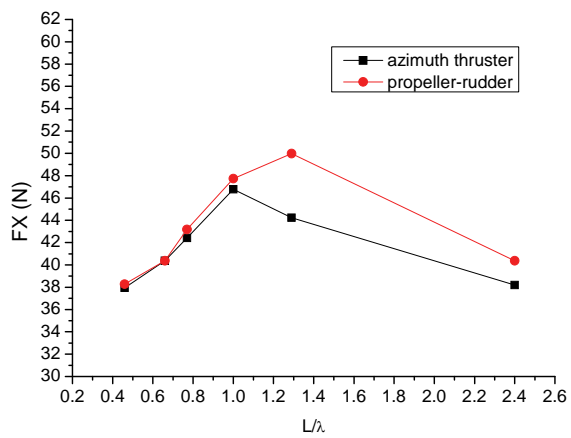
Fig. B3 (c) Longitudinal thrust force comparisons

Fig. B3 Comparisons between azimuth thruster and propeller-rudder system in 60 degrees bow sea, with V_0=1.769m/s
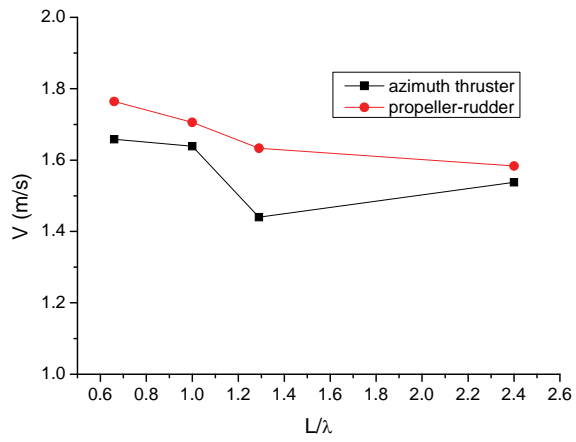
Fig. B4 (a) Attainable speed comparisons
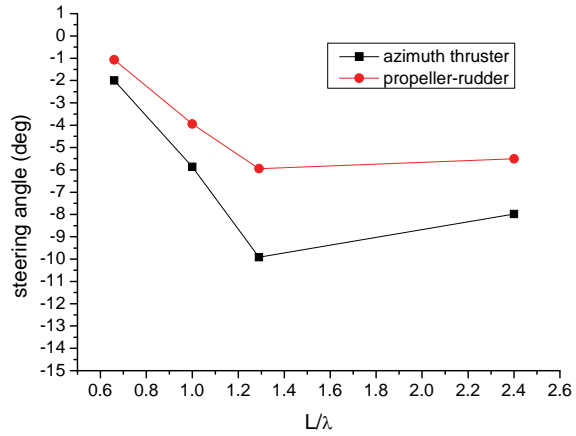
Fig. B4 (b) Average steering angle comparisons
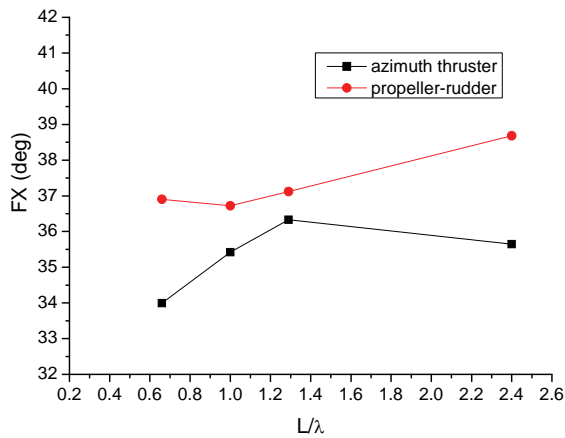
Fig. B4 (c) Longitudinal thrust force comparisons

Fig. B4 Comparisons between azimuth thruster and propeller-rudder system in 90 degrees beam sea, with V_0=1.769m/s

The results in Fig. B2- Fig. B4 show that the conventional rudder-propeller system is better than the azimuth thruster from the aspect of speed loss. The rudder-propeller system can always provide larger thrust with smaller steering angle so that higher attainable speed is achieved. The reason is specified as follows.

(a) Azimuth thruster
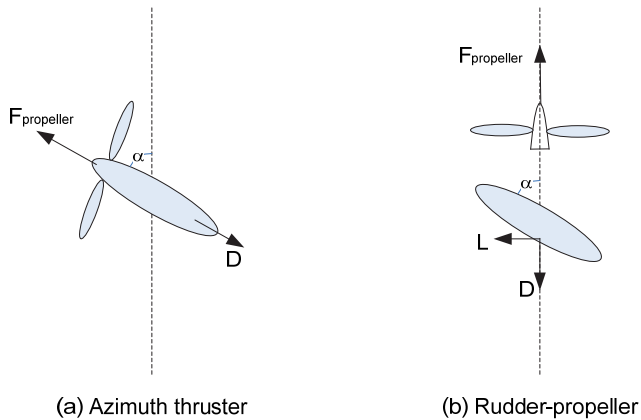
(b) Rudder-propeller

Fig. B5 Sketch of azimuth and rudder-propeller thrusters

Fig. B5 shows the sketch of the azimuth (a) and rudder-propeller (b) system with the same steering angle α. $F_{propeller}$ is the thrust from the propeller; D is pod drag force.

For the azimuth thruster, the force balance in ship longitudinal direction is specified as:

$$R_{aw} + R_{calm} = (F_{propeller} - D_{pod})\cos\alpha \qquad (B1)$$

For the rudder-propeller, the force balance in ship longitudinal direction is specified as:

$$R_{aw} + R_{calm} = F_{propeller} - D_{rudder} \qquad (B2)$$

From these equations it is clear that the rudder-propeller system can be expected to produce higher thrust than the azimuth thruster since the propeller thrust is unaltered by the rudder angle in this simplified model. However, the drag component is different for the two systems, and it is known that for really large rudder angles the reduction of net thrust due to rudder drag might be large.

To see the actual thrust and side force characteristics of the two propulsion systems, some special simulations were performed. In these simulations, the ship was fixed with designed speed (V_1=1.26m/s and V_2=1.52m/s) and heading (0 degree) by using a *simple speed/heading controller* (Fathi, 2009) which apply external forces and moments directly on the ship. Thrusters were supplied with the power setting which can keep the ship running with designed speed (V_1 and V_2) in calm water. For each speed, thruster force in longitudinal direction (FX) and transverse direction (FY) were obtained for the azimuth/rudder angles to be -20, -15, -8, -5, -3, -1, 0, 1, 3, 5, 8, 15, 20 degrees respectively. Results are shown in Fig. B5, Fig. B6 and Fig. B7.
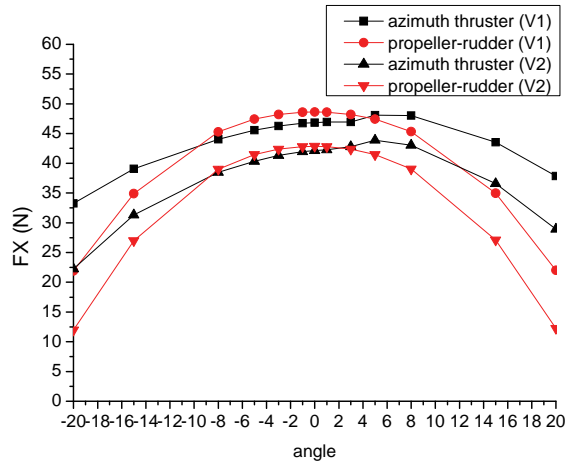
Fig. B5 FX comparisons between azimuth and propeller-rudder for V_1=1.26m/s and V_2=1.52m/s
in different steering angle condition
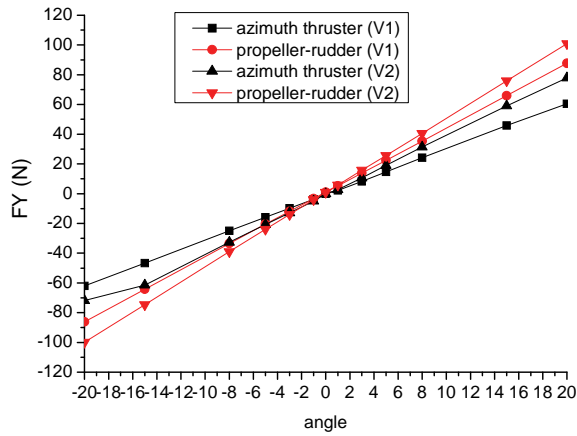
Fig. B6 FY comparisons between azimuth and propeller-rudder for V1=1.26m/s and V2=1.52m/s
in different steering angle condition
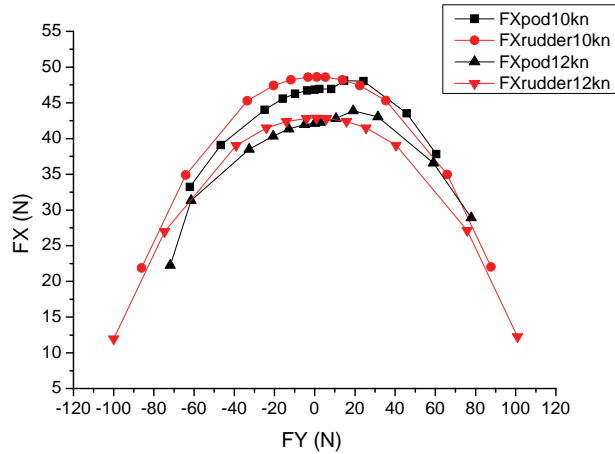
Fig. B7 FX and FY relationships between azimuth and propeller-rudder for V_1=1.26m/s and V_2=1.52m/s in different steering angle condition

It is shown clearly in Fig. B5 that within the mainly thruster working range around -10 degrees to 0 degree, the propeller-rudder produces higher thrust than the azimuth thruster at the same speed with the same angle . For the positive working angles between 3 to 10 degrees for azimuth thruster, an unexpected peak in longitudinal thrust force was shown. This could be caused by the deficiency of implementing this empirical thruster model based on systematic open water tests (make reference to Paper 4). Fig. B7 gives another way of presenting Fig. B5 and Fig. B6 to show the difference in F_x values for a fixed F_Y value for the two propulsion systems. Still higher FX is shown in the propeller-rudder system than azimuth thruster with the working range of the cases studied here. This is further confirmed that smaller steering angle is needed for the rudder to balance the transverse resistance.

So it can be concluded that propeller-rudder has better ability to keep the vessel running at designed speed than azimuth thruster. However, there are other important factors influencing the choice of propulsion system, which we have not investigated in this study, such as the low speed maneuverability.

Previous PhD theses published at the Departement of Marine Technology
(earlier: Faculty of Marine Technology)
NORWEGIAN UNIVERSITY OF SCIENCE AND TECHNOLOGY

Report No.	Author	Title
	Kavlie, Dag	Optimization of Plane Elastic Grillages, 1967
	Hansen, Hans R.	Man-Machine Communication and Data-Storage Methods in Ship Structural Design, 1971
	Gisvold, Kaare M.	A Method for non-linear mixed -integer programming and its Application to Design Problems, 1971
	Lund, Sverre	Tanker Frame Optimalization by means of SUMT-Transformation and Behaviour Models, 1971
	Vinje, Tor	On Vibration of Spherical Shells Interacting with Fluid, 1972
	Lorentz, Jan D.	Tank Arrangement for Crude Oil Carriers in Accordance with the new Anti-Pollution Regulations, 1975
	Carlsen, Carl A.	Computer-Aided Design of Tanker Structures, 1975
	Larsen, Carl M.	Static and Dynamic Analysis of Offshore Pipelines during Installation, 1976
UR-79-01	Brigt Hatlestad, MK	The finite element method used in a fatigue evaluation of fixed offshore platforms. (Dr.Ing. Thesis)
UR-79-02	Erik Pettersen, MK	Analysis and design of cellular structures. (Dr.Ing. Thesis)
UR-79-03	Sverre Valsgård, MK	Finite difference and finite element methods applied to nonlinear analysis of plated structures. (Dr.Ing. Thesis)
UR-79-04	Nils T. Nordsve, MK	Finite element collapse analysis of structural members considering imperfections and stresses due to fabrication. (Dr.Ing. Thesis)
UR-79-05	Ivar J. Fylling, MK	Analysis of towline forces in ocean towing systems. (Dr.Ing. Thesis)
UR-80-06	Nils Sandsmark, MM	Analysis of Stationary and Transient Heat Conduction by the Use of the Finite Element Method. (Dr.Ing. Thesis)
UR-80-09	Sverre Haver, MK	Analysis of uncertainties related to the stochastic modeling of ocean waves. (Dr.Ing. Thesis)
UR-81-15	Odland, Jonas	On the Strength of welded Ring stiffened cylindrical Shells primarily subjected to axial Compression
UR-82-17	Engesvik, Knut	Analysis of Uncertainties in the fatigue Capacity of

Welded Joints

UR-82-18	Rye, Henrik	Ocean wave groups
UR-83-30	Eide, Oddvar Inge	On Cumulative Fatigue Damage in Steel Welded Joints
UR-83-33	Mo, Olav	Stochastic Time Domain Analysis of Slender Offshore Structures
UR-83-34	Amdahl, Jørgen	Energy absorption in Ship-platform impacts
UR-84-37	Mørch, Morten	Motions and mooring forces of semi submersibles as determined by full-scale measurements and theoretical analysis
UR-84-38	Soares, C. Guedes	Probabilistic models for load effects in ship structures
UR-84-39	Aarsnes, Jan V.	Current forces on ships
UR-84-40	Czujko, Jerzy	Collapse Analysis of Plates subjected to Biaxial Compression and Lateral Load
UR-85-46	Alf G. Engseth, MK	Finite element collapse analysis of tubular steel offshore structures. (Dr.Ing. Thesis)
UR-86-47	Dengody Sheshappa, MP	A Computer Design Model for Optimizing Fishing Vessel Designs Based on Techno-Economic Analysis. (Dr.Ing. Thesis)
UR-86-48	Vidar Aanesland, MH	A Theoretical and Numerical Study of Ship Wave Resistance. (Dr.Ing. Thesis)
UR-86-49	Heinz-Joachim Wessel, MK	Fracture Mechanics Analysis of Crack Growth in Plate Girders. (Dr.Ing. Thesis)
UR-86-50	Jon Taby, MK	Ultimate and Post-ultimate Strength of Dented Tubular Members. (Dr.Ing. Thesis)
UR-86-51	Walter Lian, MH	A Numerical Study of Two-Dimensional Separated Flow Past Bluff Bodies at Moderate KC-Numbers. (Dr.Ing. Thesis)
UR-86-52	Bjørn Sortland, MH	Force Measurements in Oscillating Flow on Ship Sections and Circular Cylinders in a U-Tube Water Tank. (Dr.Ing. Thesis)
UR-86-53	Kurt Strand, MM	A System Dynamic Approach to One-dimensional Fluid Flow. (Dr.Ing. Thesis)
UR-86-54	Arne Edvin Løken, MH	Three Dimensional Second Order Hydrodynamic Effects on Ocean Structures in Waves. (Dr.Ing. Thesis)
UR-86-55	Sigurd Falch, MH	A Numerical Study of Slamming of Two-Dimensional Bodies. (Dr.Ing. Thesis)
UR-87-56	Arne Braathen, MH	Application of a Vortex Tracking Method to the Prediction of Roll Damping of a Two-Dimension Floating Body. (Dr.Ing. Thesis)

UR-87-57	Bernt Leira, MK	Gaussian Vector Processes for Reliability Analysis involving Wave-Induced Load Effects. (Dr.Ing. Thesis)
UR-87-58	Magnus Småvik, MM	Thermal Load and Process Characteristics in a Two-Stroke Diesel Engine with Thermal Barriers (in Norwegian). (Dr.Ing. Thesis)
MTA-88-59	Bernt Arild Bremdal, MP	An Investigation of Marine Installation Processes – A Knowledge - Based Planning Approach. (Dr.Ing. Thesis)
MTA-88-60	Xu Jun, MK	Non-linear Dynamic Analysis of Space-framed Offshore Structures. (Dr.Ing. Thesis)
MTA-89-61	Gang Miao, MH	Hydrodynamic Forces and Dynamic Responses of Circular Cylinders in Wave Zones. (Dr.Ing. Thesis)
MTA-89-62	Martin Greenhow, MH	Linear and Non-Linear Studies of Waves and Floating Bodies. Part I and Part II. (Dr.Techn. Thesis)
MTA-89-63	Chang Li, MH	Force Coefficients of Spheres and Cubes in Oscillatory Flow with and without Current. (Dr.Ing. Thesis
MTA-89-64	Hu Ying, MP	A Study of Marketing and Design in Development of Marine Transport Systems. (Dr.Ing. Thesis)
MTA-89-65	Arild Jæger, MH	Seakeeping, Dynamic Stability and Performance of a Wedge Shaped Planing Hull. (Dr.Ing. Thesis)
MTA-89-66	Chan Siu Hung, MM	The dynamic characteristics of tilting-pad bearings
MTA-89-67	Kim Wikstrøm, MP	Analysis av projekteringen for ett offshore projekt. (Licenciat-avhandling)
MTA-89-68	Jiao Guoyang, MK	Reliability Analysis of Crack Growth under Random Loading, considering Model Updating. (Dr.Ing. Thesis)
MTA-89-69	Arnt Olufsen, MK	Uncertainty and Reliability Analysis of Fixed Offshore Structures. (Dr.Ing. Thesis)
MTA-89-70	Wu Yu-Lin, MR	System Reliability Analyses of Offshore Structures using improved Truss and Beam Models. (Dr.Ing. Thesis)
MTA-90-71	Jan Roger Hoff, MH	Three-dimensional Green function of a vessel with forward speed in waves. (Dr.Ing. Thesis)
MTA-90-72	Rong Zhao, MH	Slow-Drift Motions of a Moored Two-Dimensional Body in Irregular Waves. (Dr.Ing. Thesis)
MTA-90-73	Atle Minsaas, MP	Economical Risk Analysis. (Dr.Ing. Thesis)
MTA-90-74	Knut-Aril Farnes, MK	Long-term Statistics of Response in Non-linear Marine Structures. (Dr.Ing. Thesis)
MTA-90-75	Torbjørn Sotberg, MK	Application of Reliability Methods for Safety Assessment of Submarine Pipelines. (Dr.Ing.

Thesis)

| MTA-90-76 | Zeuthen, Steffen, MP | SEAMAID. A computational model of the design process in a constraint-based logic programming environment. An example from the offshore domain. (Dr.Ing. Thesis) |

MTA-91-77   Haagensen, Sven, MM   Fuel Dependant Cyclic Variability in a Spark Ignition Engine - An Optical Approach. (Dr.Ing. Thesis)

MTA-91-78   Løland, Geir, MH   Current forces on and flow through fish farms. (Dr.Ing. Thesis)

MTA-91-79   Hoen, Christopher, MK   System Identification of Structures Excited by Stochastic Load Processes. (Dr.Ing. Thesis)

MTA-91-80   Haugen, Stein, MK   Probabilistic Evaluation of Frequency of Collision between Ships and Offshore Platforms. (Dr.Ing. Thesis)

MTA-91-81   Sødahl, Nils, MK   Methods for Design and Analysis of Flexible Risers. (Dr.Ing. Thesis)

MTA-91-82   Ormberg, Harald, MK   Non-linear Response Analysis of Floating Fish Farm Systems. (Dr.Ing. Thesis)

MTA-91-83   Marley, Mark J., MK   Time Variant Reliability under Fatigue Degradation. (Dr.Ing. Thesis)

MTA-91-84   Krokstad, Jørgen R., MH   Second-order Loads in Multidirectional Seas. (Dr.Ing. Thesis)

MTA-91-85   Molteberg, Gunnar A., MM   The Application of System Identification Techniques to Performance Monitoring of Four Stroke Turbocharged Diesel Engines. (Dr.Ing. Thesis)

MTA-92-86   Mørch, Hans Jørgen Bjelke, MH   Aspects of Hydrofoil Design: with Emphasis on Hydrofoil Interaction in Calm Water. (Dr.Ing. Thesis)

MTA-92-87   Chan Siu Hung, MM   Nonlinear Analysis of Rotordynamic Instabilities in Highspeed Turbomachinery. (Dr.Ing. Thesis)

MTA-92-88   Bessason, Bjarni, MK   Assessment of Earthquake Loading and Response of Seismically Isolated Bridges. (Dr.Ing. Thesis)

MTA-92-89   Langli, Geir, MP   Improving Operational Safety through exploitation of Design Knowledge - an investigation of offshore platform safety. (Dr.Ing. Thesis)

MTA-92-90   Sævik, Svein, MK   On Stresses and Fatigue in Flexible Pipes. (Dr.Ing. Thesis)

MTA-92-91   Ask, Tor Ø., MM   Ignition and Flame Growth in Lean Gas-Air Mixtures. An Experimental Study with a Schlieren System. (Dr.Ing. Thesis)

MTA-86-92   Hessen, Gunnar, MK   Fracture Mechanics Analysis of Stiffened Tubular Members. (Dr.Ing. Thesis)

MTA-93-93	Steinebach, Christian, MM	Knowledge Based Systems for Diagnosis of Rotating Machinery. (Dr.Ing. Thesis)
MTA-93-94	Dalane, Jan Inge, MK	System Reliability in Design and Maintenance of Fixed Offshore Structures. (Dr.Ing. Thesis)
MTA-93-95	Steen, Sverre, MH	Cobblestone Effect on SES. (Dr.Ing. Thesis)
MTA-93-96	Karunakaran, Daniel, MK	Nonlinear Dynamic Response and Reliability Analysis of Drag-dominated Offshore Platforms. (Dr.Ing. Thesis)
MTA-93-97	Hagen, Arnulf, MP	The Framework of a Design Process Language. (Dr.Ing. Thesis)
MTA-93-98	Nordrik, Rune, MM	Investigation of Spark Ignition and Autoignition in Methane and Air Using Computational Fluid Dynamics and Chemical Reaction Kinetics. A Numerical Study of Ignition Processes in Internal Combustion Engines. (Dr.Ing. Thesis)
MTA-94-99	Passano, Elizabeth, MK	Efficient Analysis of Nonlinear Slender Marine Structures. (Dr.Ing. Thesis)
MTA-94-100	Kvålsvold, Jan, MH	Hydroelastic Modelling of Wetdeck Slamming on Multihull Vessels. (Dr.Ing. Thesis)
MTA-94-102	Bech, Sidsel M., MK	Experimental and Numerical Determination of Stiffness and Strength of GRP/PVC Sandwich Structures. (Dr.Ing. Thesis)
MTA-95-103	Paulsen, Hallvard, MM	A Study of Transient Jet and Spray using a Schlieren Method and Digital Image Processing. (Dr.Ing. Thesis)
MTA-95-104	Hovde, Geir Olav, MK	Fatigue and Overload Reliability of Offshore Structural Systems, Considering the Effect of Inspection and Repair. (Dr.Ing. Thesis)
MTA-95-105	Wang, Xiaozhi, MK	Reliability Analysis of Production Ships with Emphasis on Load Combination and Ultimate Strength. (Dr.Ing. Thesis)
MTA-95-106	Ulstein, Tore, MH	Nonlinear Effects of a Flexible Stern Seal Bag on Cobblestone Oscillations of an SES. (Dr.Ing. Thesis)
MTA-95-107	Solaas, Frøydis, MH	Analytical and Numerical Studies of Sloshing in Tanks. (Dr.Ing. Thesis)
MTA-95-108	Hellan, Øyvind, MK	Nonlinear Pushover and Cyclic Analyses in Ultimate Limit State Design and Reassessment of Tubular Steel Offshore Structures. (Dr.Ing. Thesis)
MTA-95-109	Hermundstad, Ole A., MK	Theoretical and Experimental Hydroelastic Analysis of High Speed Vessels. (Dr.Ing. Thesis)
MTA-96-110	Bratland, Anne K., MH	Wave-Current Interaction Effects on Large-Volume Bodies in Water of Finite Depth. (Dr.Ing. Thesis)
MTA-96-111	Herfjord, Kjell, MH	A Study of Two-dimensional Separated Flow by a Combination of the Finite Element Method and

Navier-Stokes Equations. (Dr.Ing. Thesis)

MTA-96-112	Æsøy, Vilmar, MM	Hot Surface Assisted Compression Ignition in a Direct Injection Natural Gas Engine. (Dr.Ing. Thesis)
MTA-96-113	Eknes, Monika L., MK	Escalation Scenarios Initiated by Gas Explosions on Offshore Installations. (Dr.Ing. Thesis)
MTA-96-114	Erikstad, Stein O., MP	A Decision Support Model for Preliminary Ship Design. (Dr.Ing. Thesis)
MTA-96-115	Pedersen, Egil, MH	A Nautical Study of Towed Marine Seismic Streamer Cable Configurations. (Dr.Ing. Thesis)
MTA-97-116	Moksnes, Paul O., MM	Modelling Two-Phase Thermo-Fluid Systems Using Bond Graphs. (Dr.Ing. Thesis)
MTA-97-117	Halse, Karl H., MK	On Vortex Shedding and Prediction of Vortex-Induced Vibrations of Circular Cylinders. (Dr.Ing. Thesis)
MTA-97-118	Igland, Ragnar T., MK	Reliability Analysis of Pipelines during Laying, considering Ultimate Strength under Combined Loads. (Dr.Ing. Thesis)
MTA-97-119	Pedersen, Hans-P., MP	Levendefiskteknologi for fiskefartøy. (Dr.Ing. Thesis)
MTA-98-120	Vikestad, Kyrre, MK	Multi-Frequency Response of a Cylinder Subjected to Vortex Shedding and Support Motions. (Dr.Ing. Thesis)
MTA-98-121	Azadi, Mohammad R. E., MK	Analysis of Static and Dynamic Pile-Soil-Jacket Behaviour. (Dr.Ing. Thesis)
MTA-98-122	Ulltang, Terje, MP	A Communication Model for Product Information. (Dr.Ing. Thesis)
MTA-98-123	Torbergsen, Erik, MM	Impeller/Diffuser Interaction Forces in Centrifugal Pumps. (Dr.Ing. Thesis)
MTA-98-124	Hansen, Edmond, MH	A Discrete Element Model to Study Marginal Ice Zone Dynamics and the Behaviour of Vessels Moored in Broken Ice. (Dr.Ing. Thesis)
MTA-98-125	Videiro, Paulo M., MK	Reliability Based Design of Marine Structures. (Dr.Ing. Thesis)
MTA-99-126	Mainçon, Philippe, MK	Fatigue Reliability of Long Welds Application to Titanium Risers. (Dr.Ing. Thesis)
MTA-99-127	Haugen, Elin M., MH	Hydroelastic Analysis of Slamming on Stiffened Plates with Application to Catamaran Wetdecks. (Dr.Ing. Thesis)
MTA-99-128	Langhelle, Nina K., MK	Experimental Validation and Calibration of Nonlinear Finite Element Models for Use in Design of Aluminium Structures Exposed to Fire. (Dr.Ing. Thesis)
MTA-99-	Berstad, Are J., MK	Calculation of Fatigue Damage in Ship Structures.

129		(Dr.Ing. Thesis)
MTA-99-130	Andersen, Trond M., MM	Short Term Maintenance Planning. (Dr.Ing. Thesis)
MTA-99-131	Tveiten, Bård Wathne, MK	Fatigue Assessment of Welded Aluminium Ship Details. (Dr.Ing. Thesis)
MTA-99-132	Søreide, Fredrik, MP	Applications of underwater technology in deep water archaeology. Principles and practice. (Dr.Ing. Thesis)
MTA-99-133	Tønnessen, Rune, MH	A Finite Element Method Applied to Unsteady Viscous Flow Around 2D Blunt Bodies With Sharp Corners. (Dr.Ing. Thesis)
MTA-99-134	Elvekrok, Dag R., MP	Engineering Integration in Field Development Projects in the Norwegian Oil and Gas Industry. The Supplier Management of Norne. (Dr.Ing. Thesis)
MTA-99-135	Fagerholt, Kjetil, MP	Optimeringsbaserte Metoder for Ruteplanlegging innen skipsfart. (Dr.Ing. Thesis)
MTA-99-136	Bysveen, Marie, MM	Visualization in Two Directions on a Dynamic Combustion Rig for Studies of Fuel Quality. (Dr.Ing. Thesis)
MTA-2000-137	Storteig, Eskild, MM	Dynamic characteristics and leakage performance of liquid annular seals in centrifugal pumps. (Dr.Ing. Thesis)
MTA-2000-138	Sagli, Gro, MK	Model uncertainty and simplified estimates of long term extremes of hull girder loads in ships. (Dr.Ing. Thesis)
MTA-2000-139	Tronstad, Harald, MK	Nonlinear analysis and design of cable net structures like fishing gear based on the finite element method. (Dr.Ing. Thesis)
MTA-2000-140	Kroneberg, André, MP	Innovation in shipping by using scenarios. (Dr.Ing. Thesis)
MTA-2000-141	Haslum, Herbjørn Alf, MH	Simplified methods applied to nonlinear motion of spar platforms. (Dr.Ing. Thesis)
MTA-2001-142	Samdal, Ole Johan, MM	Modelling of Degradation Mechanisms and Stressor Interaction on Static Mechanical Equipment Residual Lifetime. (Dr.Ing. Thesis)
MTA-2001-143	Baarholm, Rolf Jarle, MH	Theoretical and experimental studies of wave impact underneath decks of offshore platforms. (Dr.Ing. Thesis)
MTA-2001-144	Wang, Lihua, MK	Probabilistic Analysis of Nonlinear Wave-induced Loads on Ships. (Dr.Ing. Thesis)
MTA-2001-145	Kristensen, Odd H. Holt, MK	Ultimate Capacity of Aluminium Plates under Multiple Loads, Considering HAZ Properties. (Dr.Ing. Thesis)
MTA-2001-146	Greco, Marilena, MH	A Two-Dimensional Study of Green-Water Loading. (Dr.Ing. Thesis)

MTA-2001-147	Heggelund, Svein E., MK	Calculation of Global Design Loads and Load Effects in Large High Speed Catamarans. (Dr.Ing. Thesis)
MTA-2001-148	Babalola, Olusegun T., MK	Fatigue Strength of Titanium Risers – Defect Sensitivity. (Dr.Ing. Thesis)
MTA-2001-149	Mohammed, Abuu K., MK	Nonlinear Shell Finite Elements for Ultimate Strength and Collapse Analysis of Ship Structures. (Dr.Ing. Thesis)
MTA-2002-150	Holmedal, Lars E., MH	Wave-current interactions in the vicinity of the sea bed. (Dr.Ing. Thesis)
MTA-2002-151	Rognebakke, Olav F., MH	Sloshing in rectangular tanks and interaction with ship motions. (Dr.Ing. Thesis)
MTA-2002-152	Lader, Pål Furset, MH	Geometry and Kinematics of Breaking Waves. (Dr.Ing. Thesis)
MTA-2002-153	Yang, Qinzheng, MH	Wash and wave resistance of ships in finite water depth. (Dr.Ing. Thesis)
MTA-2002-154	Melhus, Øyvin, MM	Utilization of VOC in Diesel Engines. Ignition and combustion of VOC released by crude oil tankers. (Dr.Ing. Thesis)
MTA-2002-155	Ronæss, Marit, MH	Wave Induced Motions of Two Ships Advancing on Parallel Course. (Dr.Ing. Thesis)
MTA-2002-156	Økland, Ole D., MK	Numerical and experimental investigation of whipping in twin hull vessels exposed to severe wet deck slamming. (Dr.Ing. Thesis)
MTA-2002-157	Ge, Chunhua, MK	Global Hydroelastic Response of Catamarans due to Wet Deck Slamming. (Dr.Ing. Thesis)
MTA-2002-158	Byklum, Eirik, MK	Nonlinear Shell Finite Elements for Ultimate Strength and Collapse Analysis of Ship Structures. (Dr.Ing. Thesis)
IMT-2003-1	Chen, Haibo, MK	Probabilistic Evaluation of FPSO-Tanker Collision in Tandem Offloading Operation. (Dr.Ing. Thesis)
IMT-2003-2	Skaugset, Kjetil Bjørn, MK	On the Suppression of Vortex Induced Vibrations of Circular Cylinders by Radial Water Jets. (Dr.Ing. Thesis)
IMT-2003-3	Chezhian, Muthu	Three-Dimensional Analysis of Slamming. (Dr.Ing. Thesis)
IMT-2003-4	Buhaug, Øyvind	Deposit Formation on Cylinder Liner Surfaces in Medium Speed Engines. (Dr.Ing. Thesis)
IMT-2003-5	Tregde, Vidar	Aspects of Ship Design: Optimization of Aft Hull with Inverse Geometry Design. (Dr.Ing. Thesis)
IMT-2003-6	Wist, Hanne Therese	Statistical Properties of Successive Ocean Wave Parameters. (Dr.Ing. Thesis)

IMT-2004-7	Ransau, Samuel	Numerical Methods for Flows with Evolving Interfaces. (Dr.Ing. Thesis)
IMT-2004-8	Soma, Torkel	Blue-Chip or Sub-Standard. A data interrogation approach of identity safety characteristics of shipping organization. (Dr.Ing. Thesis)
IMT-2004-9	Ersdal, Svein	An experimental study of hydrodynamic forces on cylinders and cables in near axial flow. (Dr.Ing. Thesis)
IMT-2005-10	Brodtkorb, Per Andreas	The Probability of Occurrence of Dangerous Wave Situations at Sea. (Dr.Ing. Thesis)
IMT-2005-11	Yttervik, Rune	Ocean current variability in relation to offshore engineering. (Dr.Ing. Thesis)
IMT-2005-12	Fredheim, Arne	Current Forces on Net-Structures. (Dr.Ing. Thesis)
IMT-2005-13	Heggernes, Kjetil	Flow around marine structures. (Dr.Ing. Thesis
IMT-2005-14	Fouques, Sebastien	Lagrangian Modelling of Ocean Surface Waves and Synthetic Aperture Radar Wave Measurements. (Dr.Ing. Thesis)
IMT-2006-15	Holm, Håvard	Numerical calculation of viscous free surface flow around marine structures. (Dr.Ing. Thesis)
IMT-2006-16	Bjørheim, Lars G.	Failure Assessment of Long Through Thickness Fatigue Cracks in Ship Hulls. (Dr.Ing. Thesis)
IMT-2006-17	Hansson, Lisbeth	Safety Management for Prevention of Occupational Accidents. (Dr.Ing. Thesis)
IMT-2006-18	Zhu, Xinying	Application of the CIP Method to Strongly Nonlinear Wave-Body Interaction Problems. (Dr.Ing. Thesis)
IMT-2006-19	Reite, Karl Johan	Modelling and Control of Trawl Systems. (Dr.Ing. Thesis)
IMT-2006-20	Smogeli, Øyvind Notland	Control of Marine Propellers. From Normal to Extreme Conditions. (Dr.Ing. Thesis)
IMT-2007-21	Storhaug, Gaute	Experimental Investigation of Wave Induced Vibrations and Their Effect on the Fatigue Loading of Ships. (Dr.Ing. Thesis)
IMT-2007-22	Sun, Hui	A Boundary Element Method Applied to Strongly Nonlinear Wave-Body Interaction Problems. (PhD Thesis, CeSOS)
IMT-2007-23	Rustad, Anne Marthine	Modelling and Control of Top Tensioned Risers. (PhD Thesis, CeSOS)
IMT-2007-24	Johansen, Vegar	Modelling flexible slender system for real-time simulations and control applications
IMT-2007-25	Wroldsen, Anders Sunde	Modelling and control of tensegrity structures. (PhD Thesis, CeSOS)
IMT-	Aronsen, Kristoffer Høye	An experimental investigation of in-line and

2007-26		combined inline and cross flow vortex induced vibrations. (Dr. avhandling, IMT)
IMT-2007-27	Gao, Zhen	Stochastic Response Analysis of Mooring Systems with Emphasis on Frequency-domain Analysis of Fatigue due to Wide-band Response Processes (PhD Thesis, CeSOS)
IMT-2007-28	Thorstensen, Tom Anders	Lifetime Profit Modelling of Ageing Systems Utilizing Information about Technical Condition. (Dr.ing. thesis, IMT)
IMT-2008-29	Berntsen, Per Ivar B.	Structural Reliability Based Position Mooring. (PhD-Thesis, IMT)
IMT-2008-30	Ye, Naiquan	Fatigue Assessment of Aluminium Welded Box-stiffener Joints in Ships (Dr.ing. thesis, IMT)
IMT-2008-31	Radan, Damir	Integrated Control of Marine Electrical Power Systems. (PhD-Thesis, IMT)
IMT-2008-32	Thomassen, Paul	Methods for Dynamic Response Analysis and Fatigue Life Estimation of Floating Fish Cages. (Dr.ing. thesis, IMT)
IMT-2008-33	Pákozdi, Csaba	A Smoothed Particle Hydrodynamics Study of Two-dimensional Nonlinear Sloshing in Rectangular Tanks. (Dr.ing.thesis, IMT/ CeSOS)
IMT-2007-34	Grytøyr, Guttorm	A Higher-Order Boundary Element Method and Applications to Marine Hydrodynamics. (Dr.ing.thesis, IMT)
IMT-2008-35	Drummen, Ingo	Experimental and Numerical Investigation of Nonlinear Wave-Induced Load Effects in Containerships considering Hydroelasticity. (PhD thesis, CeSOS)
IMT-2008-36	Skejic, Renato	Maneuvering and Seakeeping of a Singel Ship and of Two Ships in Interaction. (PhD-Thesis, CeSOS)
IMT-2008-37	Harlem, Alf	An Age-Based Replacement Model for Repairable Systems with Attention to High-Speed Marine Diesel Engines. (PhD-Thesis, IMT)
IMT-2008-38	Alsos, Hagbart S.	Ship Grounding. Analysis of Ductile Fracture, Bottom Damage and Hull Girder Response. (PhD-thesis, IMT)
IMT-2008-39	Graczyk, Mateusz	Experimental Investigation of Sloshing Loading and Load Effects in Membrane LNG Tanks Subjected to Random Excitation. (PhD-thesis, CeSOS)
IMT-2008-40	Taghipour, Reza	Efficient Prediction of Dynamic Response for Flexible amd Multi-body Marine Structures. (PhD-thesis, CeSOS)
IMT-2008-41	Ruth, Eivind	Propulsion control and thrust allocation on marine vessels. (PhD thesis, CeSOS)
IMT-2008-42	Nystad, Bent Helge	Technical Condition Indexes and Remaining Useful Life of Aggregated Systems. PhD thesis, IMT

IMT-2008-43	Soni, Prashant Kumar	Hydrodynamic Coefficients for Vortex Induced Vibrations of Flexible Beams, PhD thesis, CeSOS
IMT-2009-43	Amlashi, Hadi K.K.	Ultimate Strength and Reliability-based Design of Ship Hulls with Emphasis on Combined Global and Local Loads. PhD Thesis, IMT
IMT-2009-44	Pedersen, Tom Arne	Bond Graph Modelling of Marine Power Systems. PhD Thesis, IMT
IMT-2009-45	Kristiansen, Trygve	Two-Dimensional Numerical and Experimental Studies of Piston-Mode Resonance. PhD-Thesis, CeSOS
IMT-2009-46	Ong, Muk Chen	Applications of a Standard High Reynolds Number Model and a Stochastic Scour Prediction Model for Marine Structures. PhD-thesis, IMT
IMT-2009-47	Hong, Lin	Simplified Analysis and Design of Ships subjected to Collision and Grounding. PhD-thesis, IMT
IMT-2009-48	Koushan, Kamran	Vortex Induced Vibrations of Free Span Pipelines, PhD thesis, IMT
IMT-2009-49	Korsvik, Jarl Eirik	Heuristic Methods for Ship Routing and Scheduling. PhD-thesis, IMT
IMT-2009-50	Lee, Jihoon	Experimental Investigation and Numerical in Analyzing the Ocean Current Displacement of Longlines. Ph.d.-Thesis, IMT.
IMT-2009-51	Vestbøstad, Tone Gran	A Numerical Study of Wave-in-Deck Impact usin a Two-Dimensional Constrained Interpolation Profile Method, Ph.d.thesis, CeSOS.
IMT-2009-52	Bruun, Kristine	Bond Graph Modelling of Fuel Cells for Marine Power Plants. Ph.d.-thesis, IMT
IMT 2009-53	Holstad, Anders	Numerical Investigation of Turbulence in a Sekwed Three-Dimensional Channel Flow, Ph.d.-thesis, IMT.
IMT 2009-54	Ayala-Uraga, Efren	Reliability-Based Assessment of Deteriorating Ship-shaped Offshore Structures, Ph.d.-thesis, IMT
IMT 2009-55	Kong, Xiangjun	A Numerical Study of a Damaged Ship in Beam Sea Waves. Ph.d.-thesis, IMT/CeSOS.
IMT 2010-56	Kristiansen, David	Wave Induced Effects on Floaters of Aquaculture Plants, Ph.d.-thesis, CeSOS.
IMT 2010-57	Ludvigsen, Martin	An ROV-Toolbox for Optical and Acoustic Scientific Seabed Investigation. Ph.d.-thesis IMT.
IMT 2010-58	Hals, Jørgen	Modelling and Phase Control of Wave-Energy Converters. Ph.d.thesis, CeSOS.
IMT 2010- 59	Shu, Zhi	Uncertainty Assessment of Wave Loads and Ultimate Strength of Tankers and Bulk Carriers in a

IMT 2010-60	Shao, Yanlin	Reliability Framework. Ph.d. Thesis, IMT/ CeSOS Numerical Potential-Flow Studies on Weakly-Nonlinear Wave-Body Interactions with/without Small Forward Speed, Ph.d.thesis,CeSOS.
IMT 2010-61	Califano, Andrea	Dynamic Loads on Marine Propellers due to Intermittent Ventilation. Ph.d.thesis, IMT.
IMT 2010-62	El Khoury, George	Numerical Simulations of Massively Separated Turbulent Flows, Ph.d.-thesis, IMT
IMT 2010-63	Seim, Knut Sponheim	Mixing Process in Dense Overflows with Emphasis on the Faroe Bank Channel Overflow. Ph.d.thesis, IMT
IMT 2010-64	Jia, Huirong	Structural Analysis of Intect and Damaged Ships in a Collission Risk Analysis Perspective. Ph.d.thesis CeSoS.
IMT 2010-65	Jiao, Linlin	Wave-Induced Effects on a Pontoon-type Very Large Floating Structures (VLFS). Ph.D.-thesis, CeSOS.
IMT 2010-66	Abrahamsen, Bjørn Christian	Sloshing Induced Tank Roof with Entrapped Air Pocket. Ph.d.thesis, CeSOS.
IMT 2011-67	Karimirad, Madjid	Stochastic Dynamic Response Analysis of Spar-Type Wind Turbines with Catenary or Taut Mooring Systems. Ph.d.-thesis, CeSOS.
IMT - 2011-68	Erlend Meland	Condition Monitoring of Safety Critical Valves. Ph.d.-thesis, IMT.
IMT – 2011-69	Yang, Limin	Stochastic Dynamic System Analysis of Wave Energy Converter with Hydraulic Power Take-Off, with Particular Reference to Wear Damage Analysis, Ph.d. Thesis, CeSOS.
IMT – 2011-70	Visscher, Jan	Application of Particla Image Velocimetry on Turbulent Marine Flows, Ph.d.Thesis, IMT.
IMT – 2011-71	Su, Biao	Numerical Predictions of Global and Local Ice Loads on Ships. Ph.d.Thesis, CeSOS.
IMT – 2011-72	Liu, Zhenhui	Analytical and Numerical Analysis of Iceberg Collision with Ship Structures. Ph.d.Thesis, IMT.
IMT – 2011-73	Aarsæther, Karl Gunnar	Modeling and Analysis of Ship Traffic by Observation and Numerical Simulation. Ph.d.Thesis, IMT.
Imt – 2011-74	Wu, Jie	Hydrodynamic Force Identification from Stochastic Vortex Induced Vibration Experiments with Slender Beams. Ph.d.Thesis, IMT.
Imt – 2011-75	Amini, Hamid	Azimuth Propulsors in Off-design Conditions. Ph.d.Thesis, IMT.
IMT – 2011-76	Nguyen, Tan-Hoi	Toward a System of Real-Time Prediction and Monitoring of Bottom Damage Conditions During

Ship Grounding. Ph.d.thesis, IMT.

IMT-2011-77	Tavakoli, Mohammad T.	Assessment of Oil Spill in Ship Collision and Grounding, Ph.d.thesis, IMT.
IMT-2011-78	Guo, Bingjie	Numerical and Experimental Investigation of Added Resistance in Waves. Ph.d.Thesis, IMT.
IMT-2011-79	Chen, Qiaofeng	Ultimate Strength of Aluminium Panels, considering HAZ Effects, IMT
IMT-2012-80	Kota, Ravikiran S.	Wave Loads on Decks of Offshore Structures in Random Seas. Ph.d.thesis, CeSOS.
IMT-2012-81	Sten, Ronny	Dynamic Simulation of Deep Water Drilling Risers with Heave Compensating Sysetm, IMT.
IMT-2012-82	Berle, Øyvind	Risk and resilience in global maritime supply chains, IMT.
IMT-2012-83	Fang, Shaoji	Fault Tolerant Position Mooring Control Based on Structural Reliability, CeSOS.
IMT-2012-84	You, Jikun	Numerical studies on wave forces and moored ship motions in intermediate and shallow water, CeSOS.
IMT-2012-85	Xiang ,Xu	Maneuvering of two interacting ships in waves, CeSOS
IMT-2012-86	Dong, Wenbin	Time-domain fatigueresponse and reliability analysis of offshore wind turbines with emphasis on wlded tubular joints and gear components, CeSOS
IMT-2012-87	Zhu, Suji	Investigation of Wave-Induced Nonlinear Load Effects in Open Ships considering Hull Girder Vibrations in Bending and Torsion, CeSOS
IMT-2012-88	Zhou, Li	Numerical and Experimental Investigation of Station-keeping in Level Ice, CeSOS
IMT-2012-90	Ushakov, Sergey	Particulate matter emission characteristics from diesel enignes operating on conventional and alternative marine fuels, IMT
IMT-2013-1	Yin, Decao	Experimental and Numerical Analysis of Combined In-line and Cross-flow Vortex Induced Vibrations, CeSOS
IMT-2013-2	Kurniawan, Adi	Modelling & geometry optimisation of wave energy converters, CeSOS
IMT-2013-3	Al Ryati, Nabil	Technical condition indexes doe auxiliary marine diesel engines, IMT
IMT-2013-4	Firoozkoohi, Reza	Experimental, numerical and analytical investigation of the effect of screens on sloshing, CeSOS
IMT-2013-5	Ommani, Babak	Potential-Flow Predictions of a Semi-Displacement Vessel Including Applications to Calm Water Broaching, CeSOS

IMT-2013-6	Xing, Yihan	Modelling and analysis of the gearbox in a floating spar-type wind turbine, CeSOS
IMT-7-2013	Balland, Océane	Optimization models for reducing air emissions from ships, IMT
IMT-8-2013	Yang, Dan	Transitional wake flow behind an inclined flat plate---Computation and analysis, IMT
IMT-9-2013	Abdillah, Suyuthi	Prediction of Extreme Loads and Fatigue Damage for a Ship Hull due to Ice Action, IMT
IMT-10-2013	Ramìrez, Pedro Agustìn Pèrez	Ageing management and life extension of technical systems- Concepts and methods applied to oil and gas facilities, IMT
IMT-11-2013	Chuang, Zhenju	Experimental and Numerical Investigation of Speed Loss due to Seakeeping and Maneuvering. IMT
IMT-12-2013	Etemaddar, Mahmoud	Load and Response Analysis of Wind Turbines under Atmospheric Icing and Controller System Faults with Emphasis on Spar Type Floating Wind Turbines, IMT